Sedimentology of the southern Karoo Ripon Formation and the southwestern Karoo Vischkuil/Laingsburg formations of the Ecca Group: Implications for basin and palaeoenvironmental reconstruction

By

Schalk Willem Walters

Thesis presented in fulfillment of the requirements for the degree of Master of Science in the Faculty of Science at University of Stellenbosch

Department of Earth Science

Primary Supervisor: Dr. Ryan T. Tucker

Secondary Supervisor: Prof. Bruce S. Rubidge

December 2017

Declaration

By submitting this thesis electronically, I declare that the entirety of the work contained herein is my own, original work, that I am the sole author thereof (save to the extent explicitly otherwise stated), that reproduction and publication thereof by Stellenbosch University will not infringe any third party rights and that I have not previously in its entirety or in part submitted it for obtaining any qualification.

December 2017

Abstract

Between the towns of Prince Albert (Western Cape) and Willowmore (Eastern Cape) the well-known Laingsburg depocenter and less-known Ripon depocenter of the southern Main Karoo Basin (South Africa) meet and exhibit an interfingering relationship involving the Laingsburg and Vischkuil formations (Laingsburg depocenter) on the one side and the Ripon Formation (Ripon depocenter) on the other. Studies regarding the link between these two submarine fan-dominated depocenters have been avoided to date due to the complex sedimentology and stratigraphic relationships involved. New sedimentologic and stratigraphic analysis presented in this thesis suggests that the Ripon depocenter is much more widespread than initially suggested. Channelized sandstones in the Pluto's Vale Member, as well as in the upper Wonderfontein Member, also suggest that up-dip feeders for the Ripon depocenter are more widespread than previously thought. Through detailed facies and architectural analysis, this study provides a basin reconstruction model, suggesting that the lower Vischkuil Formation is the distal equivalent of the lower Pluto's Vale Member submarine fan complex. Sedimentary petrology, including sandstone petrology and U-Pb detrital zircon geochronology, indicates that the two depocenters have slightly different source regions. Specifically, sandstones of the Laingsburg depocenter are characterized by feldspathic litharenites, whereas sandstones from the Ripon depocenter are characterized as ultralithofeldspathic. Zircon ages indicate that submarine fan development in the Laingsburg depocenter only initiated after deposition of the Pluto's Vale Member in the Ripon depocenter. The zircon populations and U/Th ratios further indicate that zircon grains were derived from South American as well as a source in the soutwestern part of Antarctica, known as the Dyer arc.

Opsomming

Tussen die dorpe Prince Albert (Wes-Kaap) en Willowmore (Oos-Kaap) ontmoet die welbekende Laingsburg subkom en die minderbekende Ripon subkom van die suidelike Hoof Karookom (Suid-Afrika) mekaar en toon ‘n oorvleulende verhouding tussen die Laingsburg en Vischkuil formasies (Laingsburg subkom) aan die een kant en die Ripon Formasie (Ripon subkom) aan die ander kant. Navorsing oor die verband tussen hierdie twee diep-mariene waaiergedomineerde subkomme is tot dusver vermy weens die komplekse sedimentologie en stratigrafiese verhoudings wat daarby betrokke is. In hierdie tesis word ‘n nuwe sedimentologiese en stratigrafiese analise aangebied wat bewys dat die Ripon subkom meer wydverspreid as wat oorspronklik gesuggereer is. Kanaalsandstene in die Pluto’s Vale Lid, sowel as in die hoër Wonderfontein Lid, suggereer ook dat die aanvoer sisteme van die Ripon subkom meer wydverspreid is as wat aanvanklik vermoed is. Deur middel van gedetailleerde fasies en argitektoniese analise bied hierdie studie ‘n kom-herkonstruksiemodel wat suggereer dat die laer Vischkuil Formasie die distale ekwivalent van die laer Pluto’s Vale Lid diep-water waaierkompleks is. Sedimentêre petrologie, insluitend sandsteenpetrologie en U-Pb detritale sirkoon geochronologie, dui daarop dat die brongebied van die twee subkomme effens van mekaar verskil. Dit word spesifiek aangedui deurdat sandsteenlae van die Laingsburg subkom deur veldspaatryke litiese areniet gekenmerk word, terwyl sandstene van die Ripon subkom deur ultra-hoë litiese en veldspaat eienskappe gekenmerk word. Sirkoon-ouderdomme dui ook daarop dat diep-water waaierontwikkeling in die Laingsburg subkom eers ontstaan het ná afsetting van die Pluto’s Vale Lid in die Ripon subkom. Die sirkoon-populasies en U/Th-verhoudings toon verder aan dat die sirkoon-korrels van Suid-Amerika afkomstig is, sowel as van ‘n bron bekend as die Dyer eilandboog in die suidweste van Antarktika.

Acknowledgments

A huge amount of gratitude goes to my supervisor, Dr. Ryan T. Tucker as well as my co-supervisor, Prof. Bruce S. Rubidge. This has been quite a journey and both of you have gone beyond limits to provide support, knowledge and patience. Ryan, no number of rusks or wine could express how grateful I am. I would also like to thank Prof. Bruce Rubidge and the DST-NRF (African origins) as well as Prof. George Henry (CIMERA) for providing funding for this project. A special thanks to Dr. De Ville Wickens for proposing this project and for providing endless guidance and support.

Then I would like to thank my fellow Masters student LW Jonk for supporting me in multiple thesis related breakdowns and for just being awesome. A special thanks to Tannie Loxie and George Olivier for supporting in the logistic side of the project.

I would like to thank the amazing people of Prince Albert and surrounding farms. Thanks to Di and Mark Steyn for making me feel at home and feel part of the family during my stay in Prince Albert. I would also like to thank Lapidaria Guesthouse for my stay in Willowmore. Thanks to the farmers that opened their farms for research and making me feel welcome. A special thanks to Alwo and Daan Dercksen, Migau Nortje, Johan Senekal and Barries Snyman.

I am endlessly grateful for my friends who always understood and supported me through this thesis. A special thanks to Johannes and Zabby. Then, I would not have been able to get this far if it weren't for my parents. Their unconditional love and support is more than words can explain.

Lastly, thanks be to God, for giving me the honor and the amazing opportunity of exploring Your creation. All the glory goes to Him.

Index

List of Figures

List of Tables

Chapter 1:
Introduction

Chapter 1: Introduction

The Main Karoo Basin in South Africa has been the focal point of geological research since it was first described by Dunn (1879, 1886), Schwarz (1897), Rogers & Du Toit (1903) and Rogers (1910) in the late eighteen hundreds to early nineteen hundreds. Since then, scientific investigations into the Karoo Basins and its stratigraphy have provided context for a crucial period in Earth's history; the termination of convergence and subsequent separation of Gondwana, along with the initial isolation of the African continent (Du Toit, 1937; Stollhofen et al., 1998; Catuneanu et al., 2005). The Karoo is renowned for its fossil record, which records the emergence of terrestrial vertebrate life (Rubidge, 1995; Botha et al., 2005; Nicolas & Rubidge, 2010; Bordy et al., 2011; Hancox et. al., 2013), as well as the radiation of the mammalian forerunners (Rubidge, 2013), the appearance of early archosaurmorphs (Botha-Brink & Smith, 2011; Ezcurra & Butler, 2015), and the end-Permian and end-Triassic mass extinctions (Barret, 2009). Along with this, the Karoo is also of great economic importance, which includes: the voluminous, high-grade coal seams in the northern Karoo (Cairncross & Cadle, 1988; Roberts, 1988; Cairncross et al., 1990), uranium deposits in the south central Karoo (Turner, 1985; Van Rooyen, 2010) and the possibility of shale gas in the lower stratigraphic units (Geel et al., 2013; Warren, 2013; Wait & Rossouw, 2014; Ingle & Atkinson, 2015; Götz et al., 2016; Lochner et al., 2016).

The 700 000 km^2 Karoo Basin, believed to be much more widespread during the Permian, provides the World's most complete and well-exposed stratigraphic record of the terrestrial realm across the Permian-Triassic boundary (Catuneanu et al., 2005). It forms part of several Gondwanan basins that were developed along the southern extent of the Gondwana supercontinent, including the Paraná Basin (South America), Bowen Basin (Australia), Beacon Basin (Antarctica) and the Karoo Basin (South Africa) (Fig 1.1 A). The Karoo Basin is regionally bound by the Cape Fold Belt to the south and the west of the basin while the northern margin of the basin thins out over the Kaapvaal Craton (Cole, 1992; Catuneanu et al., 2002). Currently, the most widely-accepted origin for the Karoo Basin is based on a retro-arc foreland basin model (Dickenson, 1974; Catuneanu, 2004) (Fig 1.1 B). Stratigraphic records,

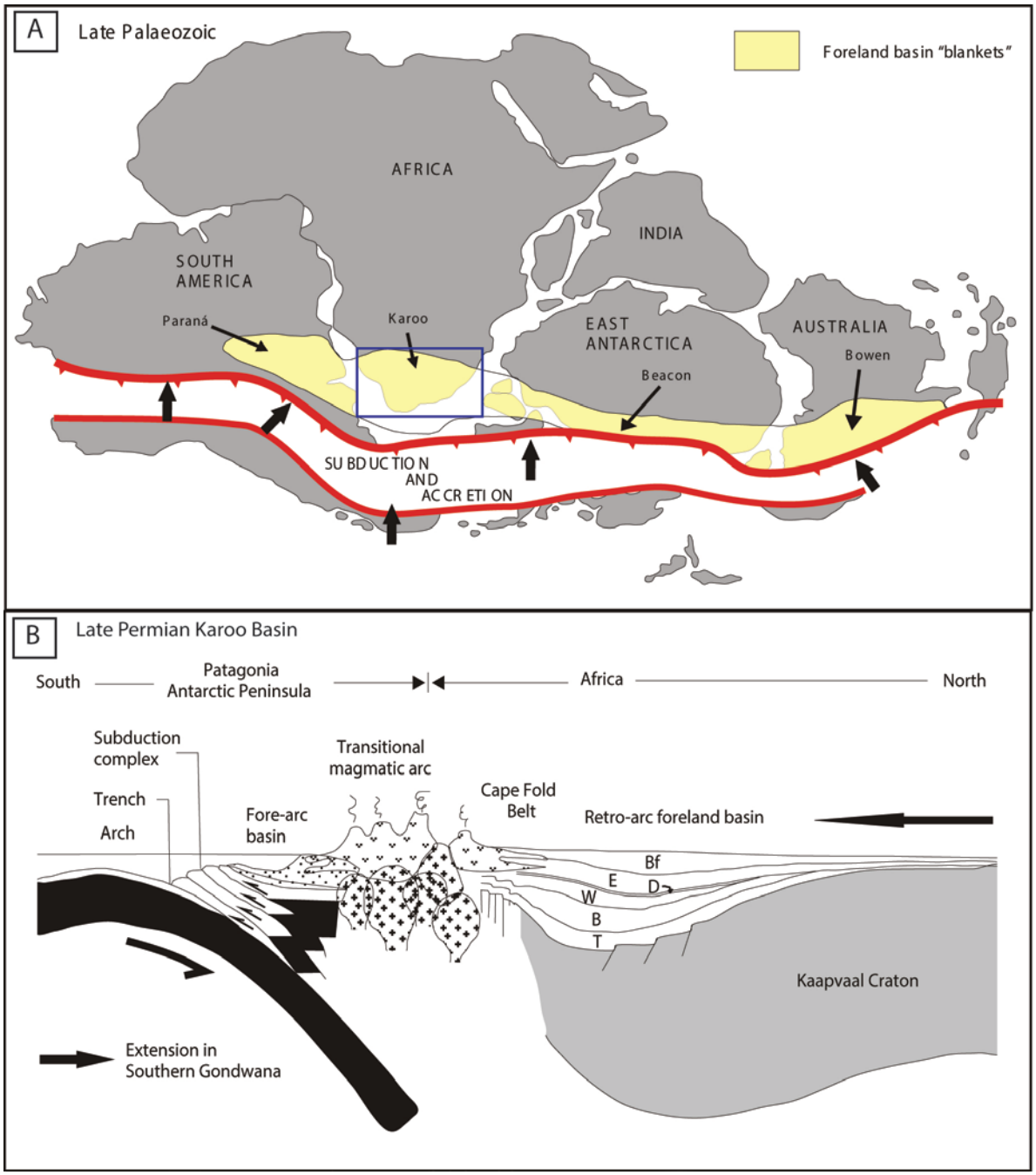

Figure 1.1: A) Schematic of Gondwana during the Late Palaeozoic showing the distribution of Gondwanan foreland basins which formed due to subduction of the Palaeo-Pacific plate towards the North. The Karoo Basin is situated at the tip of the post-Gondwana African Plate (After De Wit & Ransome (1992)). B) Schematic cross-sectional view of subduction tectonics in the southern margin of Gondwana during the Late Permian showing the evolution of the Karoo retro-arc foreland basin and subsequent influence of the Cape Fold Belt. T-Table Mountain Group, B-Bokkeveld Group, W-Witteberg Group, D-Dwyka Group, E-Ecca Group, Bf-Beaufort Group. After Van Lente (2004) (Modified from Johnson (1991)).

spanning from the Carboniferous to Triassic, within the entire Main Karoo Basin exhibit the thickest succession (~10.0 km) of sedimentation in the southern margin of the basin and thins towards the north to ~1000.0 m (Veevers et al., 1994; Pysklywec & Mitrovica, 1999).

The expansive stratigraphic record in the Karoo Basin can be subdivided into the Dwyka Group (glacio-marine), Ecca Group (deep-marine to marginal-marine), Beaufort Group (terrestrial fluvial) and finally to the Molteno, Elliot and Clarens formations (semi-arid/arid) (Turner, 1983; Smith, 1990; Bordy et al., 2004a, 2004b; Catuneanu et al., 2005; Johnson et al., 2006; Fildani et al., 2007; Bordy & Abrahams, 2016). Broad scale studies by Kingsley (1981), Johnson (1991), Wickens (1994), Sixsmith et al. (2004), Hodgson et al. (2006), van der Merwe et al. (2009) and Flint et al. (2011) focused on elucidating palaeoenvironmental context and developmental history for the Ecca Group along the southern margin of the basin, which forms a crucial part of the lower Karoo Supergroup. Whereas many of these seminal studies resolve much of the southern Karoo Basin's stratigraphy for the Ecca Group, locally cryptic stratigraphic correlation and problematic temporal relationships still result in unresolved sections of the Karoo succession (Visser, 1993; Catuneanu et al., 2002; Johnson et al., 2006; Fildani et al., 2009; Tankard et al., 2009). Lateral facies changes in the stratigraphic record of the Ecca Group are likely a reflection of large local variability across micro depocenters.

Three subbasins have been identified in the southwestern Karoo Basin namely the Tanqua subbasin (west of the Cape Syntaxis), the Laingsburg subbasin (east of the Cape Syntaxis) the Grahamstown/Southern subbasin (Eastern Cape) (Kingsley, 1981; Wickens, 1994; Catuneanu et al., 2002) (Fig 1.2). This study will be referring to these subbasins as depocenters, where the Grahamstown subbasin is referred to as the Ripon depocenter. Both the Tanqua (Fig 1.3) and Laingsburg (Fig 1.4) depocenters have been extensively studied and detailed stratigraphic correlations have been achieved between these depocenters (Wickens, 1994; Johnson et al., 2001; Catuneanu et al., 2002; Grecula et al., 2003; Andersson et al., 2004; Figueiredo et al., 2010; Spychala et al., 2015). Conversely, very little research has been undertaken on the Ripon depocenter and its lateral stratigraphic relationship with

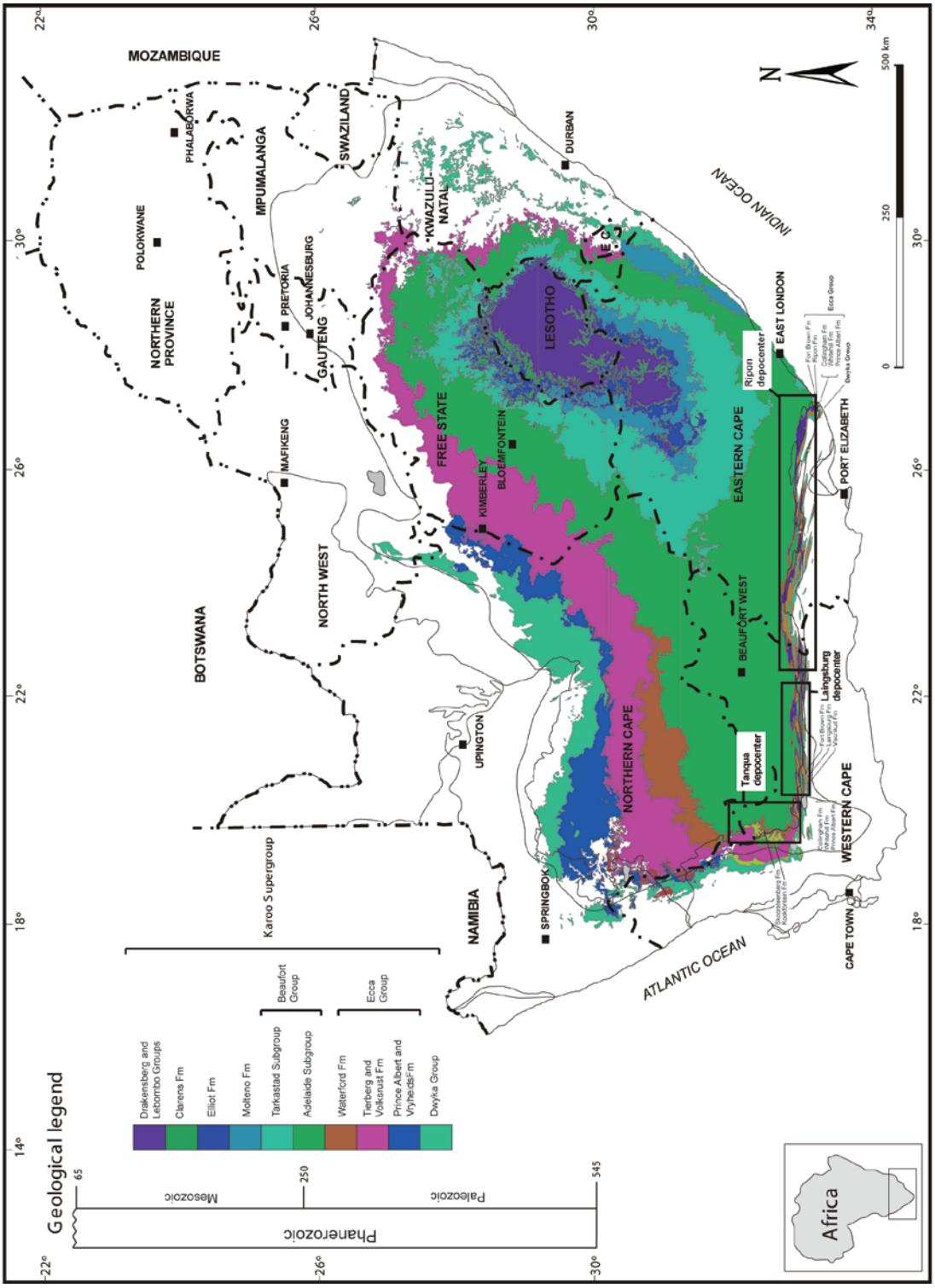

Figure 1.2: Geological map of the Karoo Supergroup in South Africa published by the Council of Geoscience, South Africa, and modified after Johnson et al. (1996). The three depocenters are shown along the southern margin of the Main Karoo Basin.

the southwestern Laingsburg depocenter (Kingsley, 1981; Johnson, 1991).

The 1:250 000 geological maps of Oudtshoorn 3322 (1979) and Ladismith 3320 (1991), published by the Council for Geoscience of South Africa, amplifies this stratigraphic uncertainty with individual lithological units mapped as different formations across the two geological maps (Fig 1.5). The Ladismith 3320 geological map shows a stratigraphic progression from the lower Ecca Group formations to the Vischkuil, Laingsburg and overlying Fort Brown formations. However, the Laingsburg Formation is abruptly terminated on the edge of the Ladismith 3320 geological map and continues as the Ripon Formation on the Oudtshoorn 3322 map, also indicating an interfingering relationship with the Vischkuil Formation. A few studies have attempted to correlate the Laingsburg and Ripon depocenters (Catuneanu et al., 2002; van der Merwe et al., 2009; McKay et al., 2016), but this problem currently lacks resolution.

The study area is situated from the town of Prince Albert (Western Cape, South Africa) and extends eastwards along strike of the Cape Fold Belt to a few km east of the N12 towards the town of Willowmore (Eastern Cape, South Africa) (Fig 1.6). Because of the regional nature of this project, the study area was designated to cover a large extent of the lateral morphology between the Vischkuil/Laingsburg formations and the Ripon Formation. Outcrop is limited, but seven key sites were recognized and used to provide sufficient data for this study. These key sites were selected due to outcrop availability and accessibility through either road cuttings or natural erosional processes.

This study ultimately seeks to provide insight and clarity on this localized cryptic stratigraphy. To provide crucial sedimentological and stratigraphic context between the Vischkuil/Laingsburg formations (Laingsburg depocenter) and the Ripon Formation (Ripon depocenter) a number of objectives were determined. These include utilizing facies and architectural analysis in the study area to determine facies variations within outcrop and regional scale. This aided in identifying key facies associations to enclose unique characteristics for each formation involved and therefore accurately define formation boundaries. It was also important to construct vertical profiles and correlations at

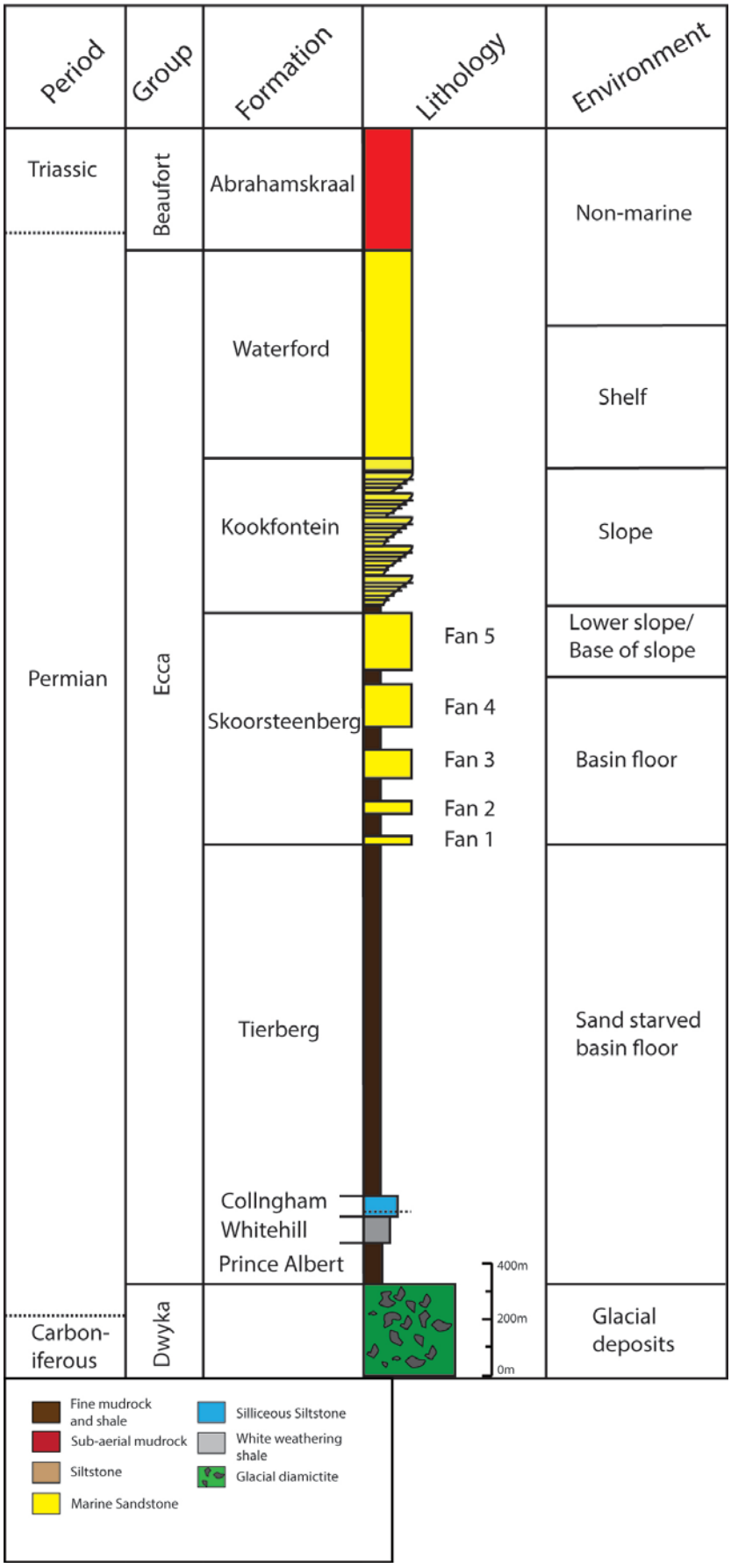

Figure 1.3: Simplified stratigraphic column of the Tanqua depocenter. Modified from Prélat et al. (2009).

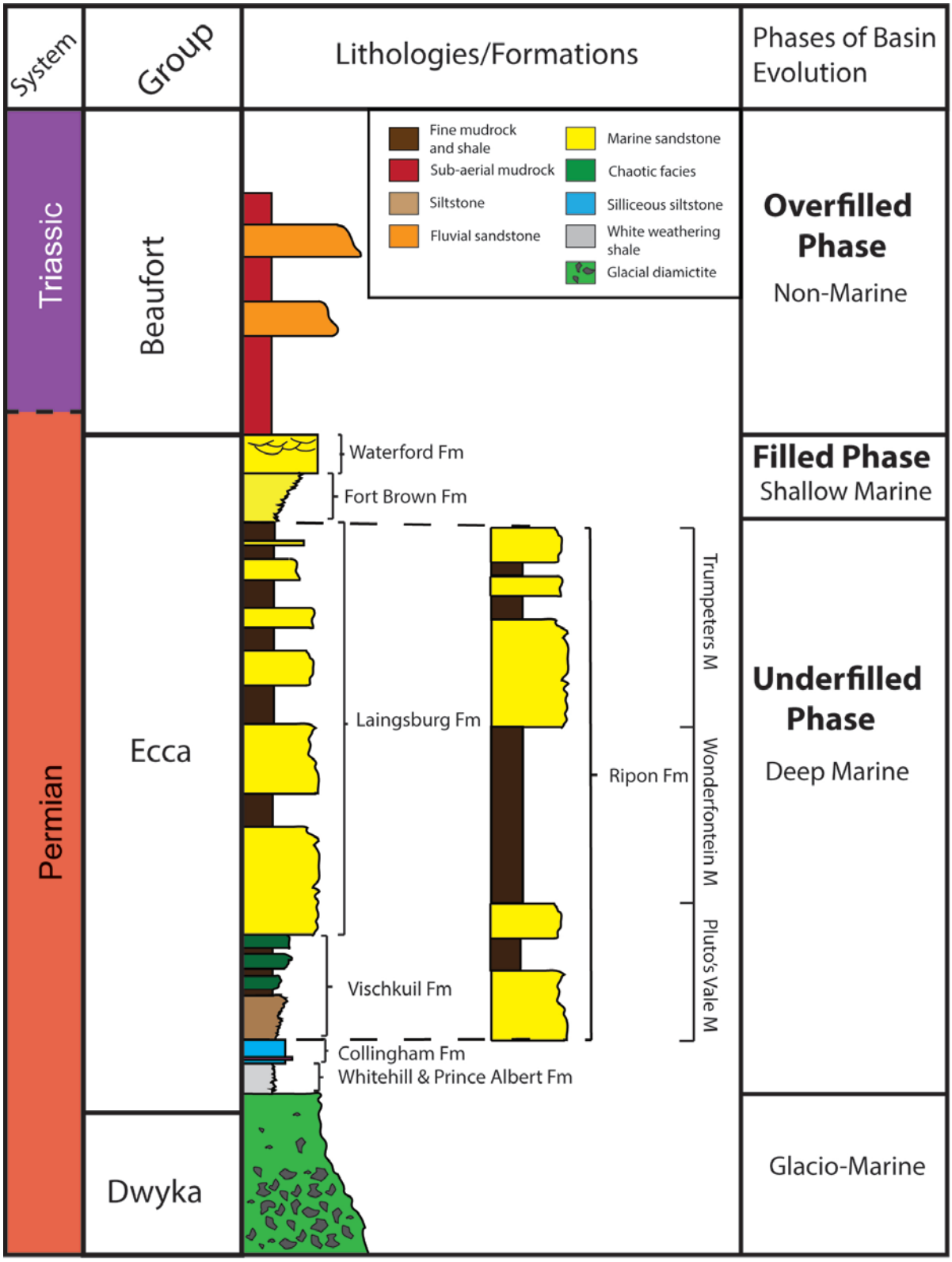

Figure 1.4: Simplified stratigraphic column of the Laingsburg and Ripon depocenters. Modified from Van der Merwe et al. (2009) and Johnson & Kingsley (1993).

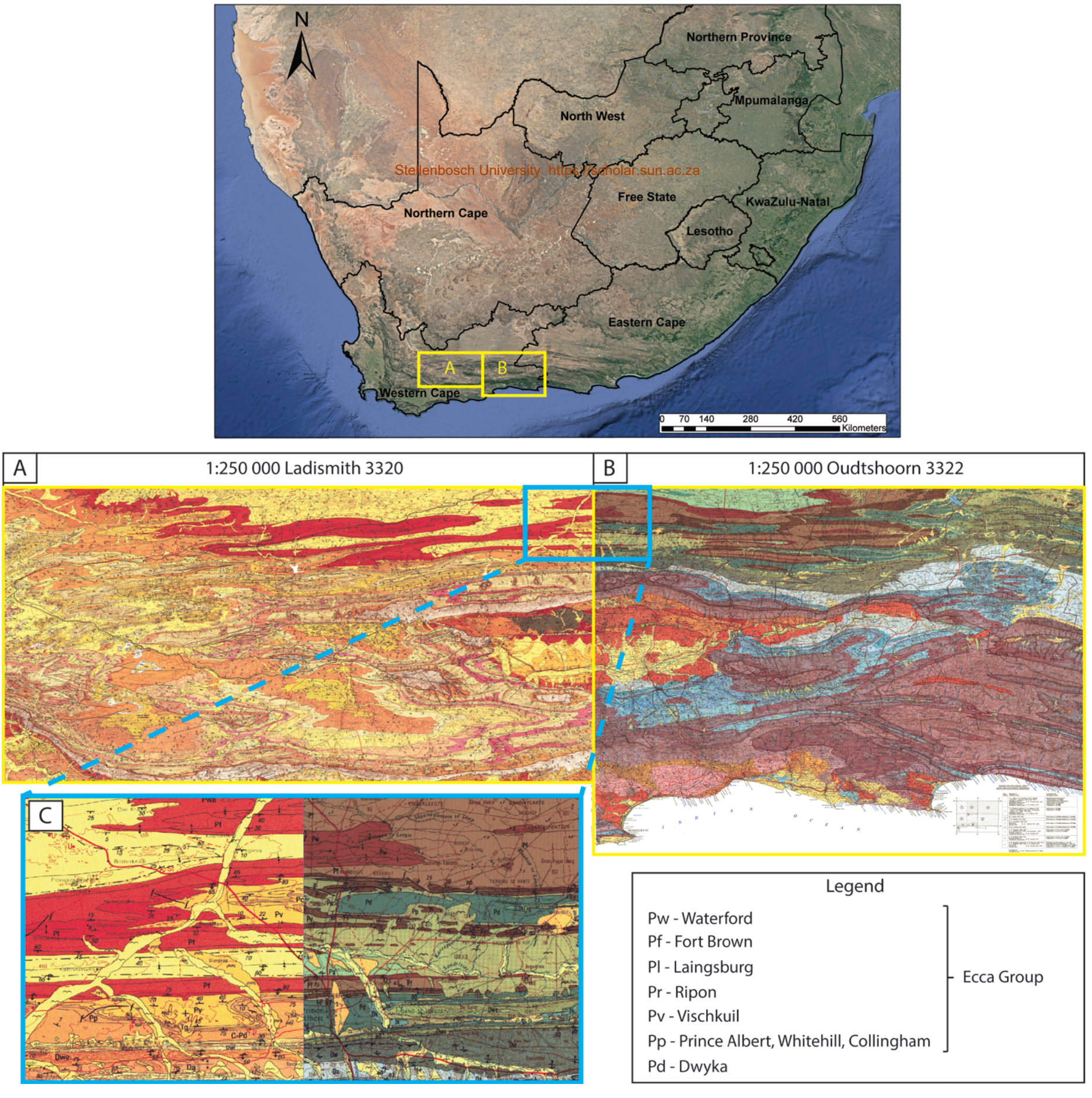

Figure 1.5: Geological map series provided by the Council for Geoscience of South Africa, with discrepancies on the lateral extent of certain Ecca formations. A) 1:250 000 geological map of Ladismith. B) 1:250 000 geological map of Oudtshoorn. C) The Laingsburg and Ripon formations change abruptly where the two maps meet.

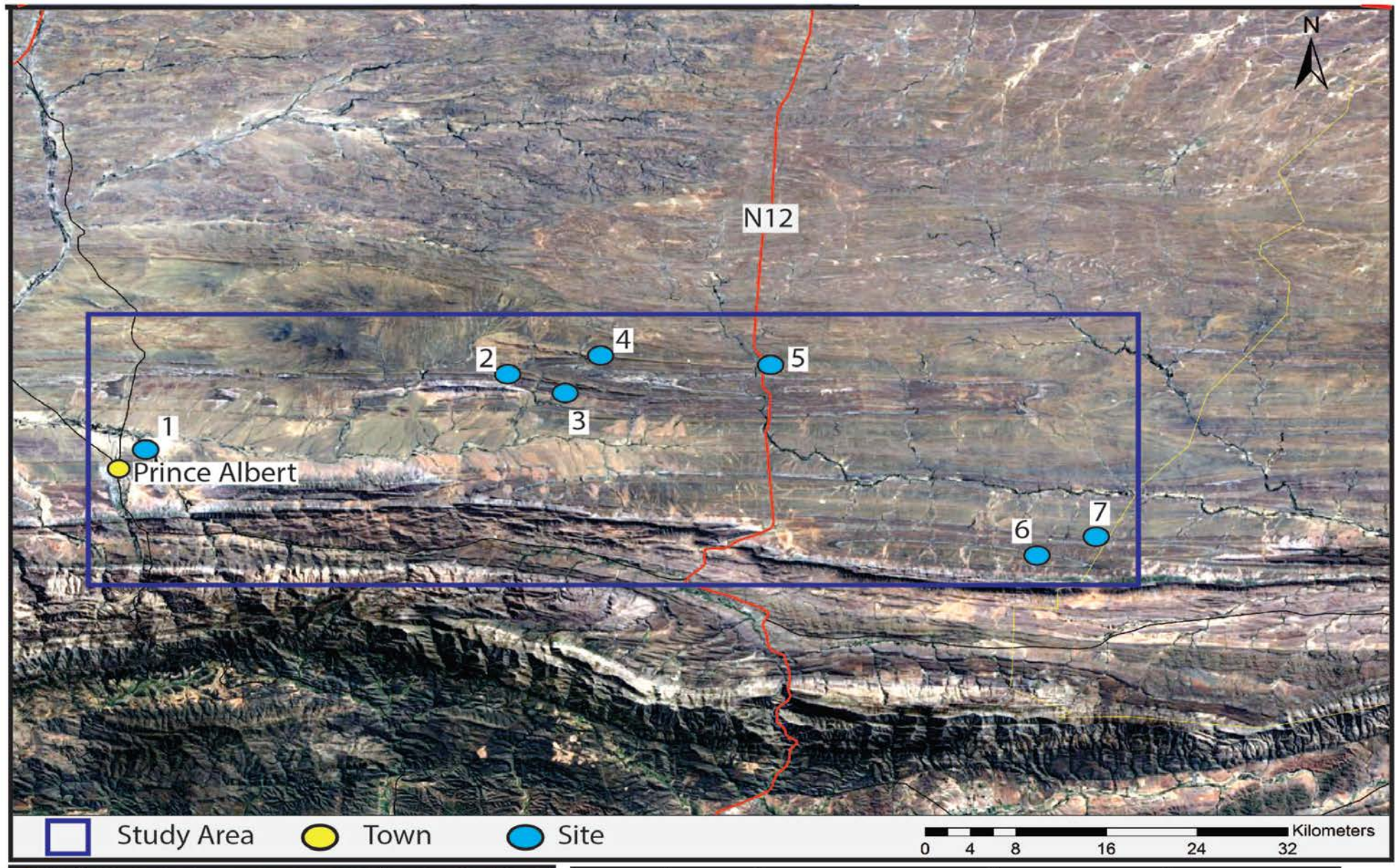

Site	Code	Farm Name	Latitude	Longitude
1	WK	Zacharias Fontein 135	S 33.211320°	E 22.055130°
2	KG	Groot Tygerberg 102	S 33.113500°	E 22.351340°
3	GS	Klein Sleutelfontein 127	S 33.137682°	E 22.386495°
4	BK	Jansenskraal 104	S 33.116990°	E 22.403490°
5	N12	N12 Road Cutting	S 33.122877°	E 22.539521°
6	OM	Klipfontein 174	S 33.281730°	E 22.779140°
7	MK	Minnies Kraal 112	S 33.218020°	E 22.826890°

Figure 1.6: Location of study area from the town of Prince Albert to about 25 km east of the N12 highway. 1- Zacharias Fontein 135, 2- Groot Tygerberg 102, 3- Jansenskraal 104, 4- Klein Sleutelfontein 127, 5- N12, 6- Klipfontein 174, 7- Minnies Kraal 112. Table shows geographic coordinates as well as code given to each site.

decimetre scale. These stratigraphic profiles utilized facies analysis to construct stratigraphic transects based on the occurrence of facies associations.

Clastic sediment petrography as well as U-Pb detrital Zircon dating using LA-ICPMS was conducted to provide insight into sediment provenance and transport history. U-Pb detrital zircon analysis was also used for basin development studies and depositional history with regards to sediment source and maximum depositional age. This, coupled with palaeocurrent data, provided insight into the sediment source and input as well as identifying different depocenters. The outcome of this research provided context on early basin development, depositional conditions, and clarified the lithostratigraphic subdivision and interrelationship of the formations involved. Therefore, this project provided crucial sedimentological evidence to decipher the depositional conditions and palaeoenvironmental setting that generated these stratigraphic relationships.

Chapter 2:
Geological Background

Chapter 2: Geological background

2.1 Tectonic History

Multiple models have been proposed over the years on the development of the Karoo Basin which includes a model by Hälbich (1983) suggesting an orogeny without subduction as well as continent-continent collision with a southward subduction as proposed by Winter (1984). Tankard et al. (2009) suggested tectonic subsidence through rigid basement block movement (Fig 2.1 A). As the result of extensive studies done by Visser (1985, 1989, 1991, 1992) and later De Wit & Ransome (1992); Johnson et al. (1997); Pysklywec & Mitrovica (1999); as well as Catuneanu (2004), a well-defined retro-arc foreland basin model was developed based on the suggested placement of the basin with regards to the northward subduction of the Panthalassan Palaeo-Pacific Plate south of Gondwana and the magmatic arc that formed as a result of subduction during the Late Carboniferous to Early Triassic (De Wit et al., 1988; Pysklywec & Mitrovica, 1999; Catuneanu, 2004; Catuneanu et al., 2005; Johnson et al., 2006; Tankard et al., 2009) (Fig 2.1 B, C; Fig 2.2 A).

Onset of the Karoo Basin subsidence was introduced after regional uplift caused by the assembly of Pangea during the middle Carboniferous. This uplift is recognized by the 30 my hiatus in deposition between the Carboniferous upper Cape Supergroup and the lower glacial-derived sediments of the Karoo Supergroup (Visser, 1990; Catuneanu et al., 2005; Tankard et al., 2009). During the initiation of subduction tectonics to the south of Gondwana, magmatic arc development heralded the change from a stable passive margin to an active margin (Pysklywec & Mitrovica, 1999).

Permo-Triassic thin-skinned thrusting of the overlying plate in a compressional regime resulted in a fold and thrust belt that caused subsidence of the late Karoo Basin through orogenic loading. Remnants of this fold and thrust belt is preserved in South Africa as the Cape Fold Belt (Johnson et al., 2006). The Cape Fold Belt consists of three sections; a north-trending Cederberg branch, an east-trending Swartberg branch and a central intersection zone of the two branches (Cape Syntaxis)

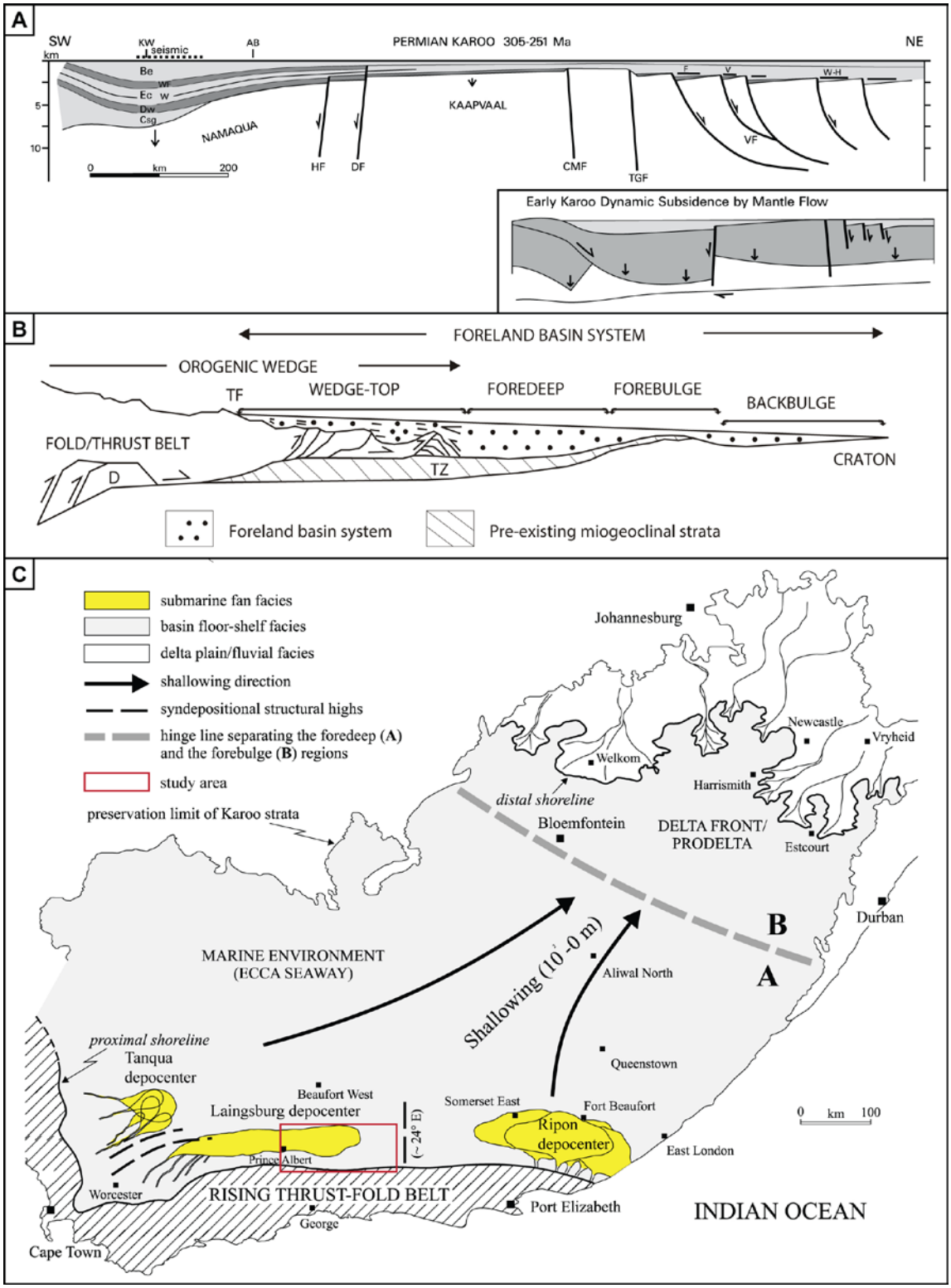

Figure 2.1: A) Basic subsidence model suggesting rigid basement block moving as the main driver behind Karoo Basin subsidence. Mantel convection caused the Namaqua block to subside with the Kaapvaal Craton still providing a thick lithospheric highland. Be, Beaufort Group; CMF, Colesberg Fault; Csg, Cape Supergroup; DF, Doringberg Fault; Dw, Dwyka Group; Ec, Ecca Group; F, Freestate Coalfield; HF, Hartbees Fault; TGF, Trompsburg Fault; V, Vereeniging Coalfield; VF, Virginia Fault; W, Whitehill Formation; Wf, Waterford Formation; W-H, Witbank (N) and Highveld (S) Coalfield. After Tankard et al. (2009). B) Basic revised foreland basin model showing a more realistic fold and thrust belt with a wedge-top, foredeep, forebuldge and backbuldge. D, schematic duplex; TF, Topographic front; TZ, frontal triangle zone. After Van Lente (2004), DeCelles & Gills, (1996). C) Palaeo-geography of foredeep and forebuldge placement in the Karoo Basin showing deposition of the three depocenters proposed by Catuneanu et al. (2002). Notice the strong boundaries of these depocenters. After Catuneanu et al. (2002)

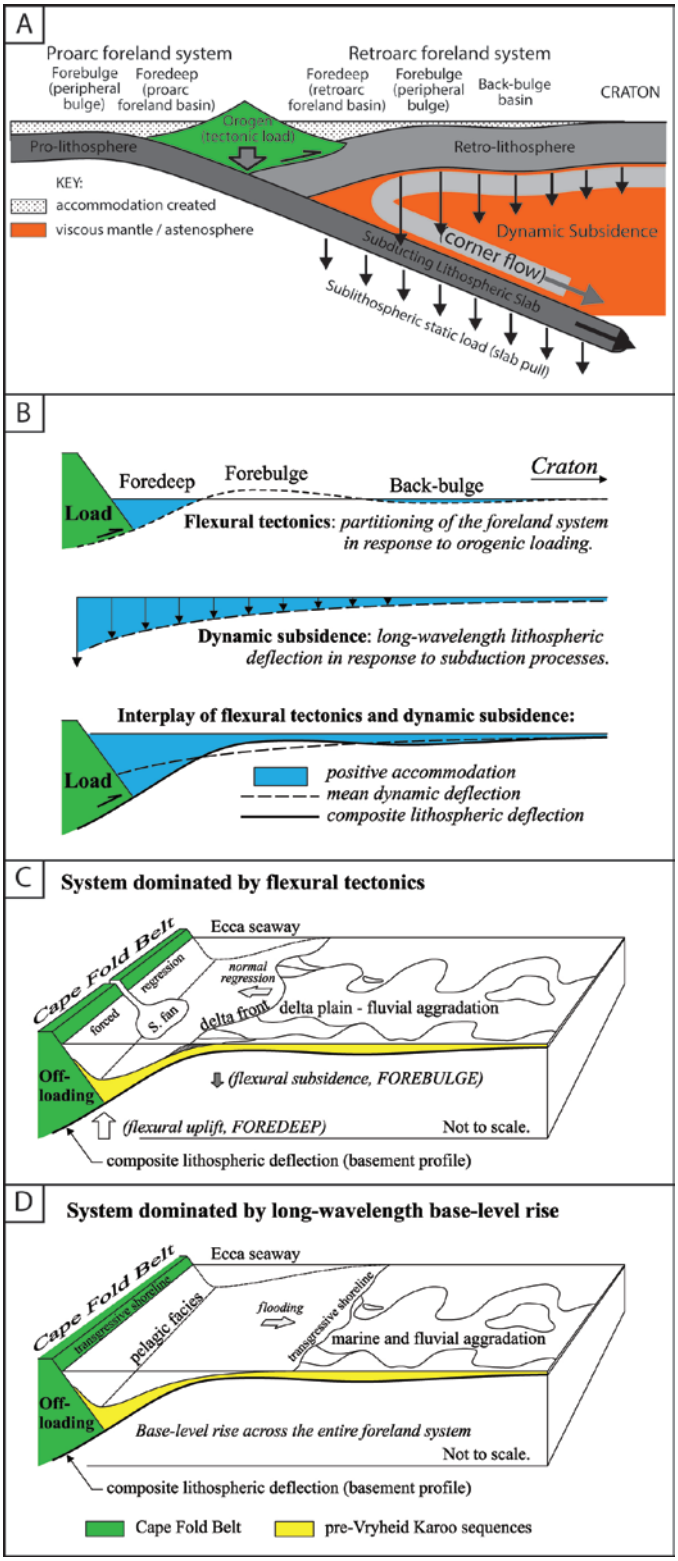

Figure 2.2: A) Cross-sectional view of subduction tectonics and orogenic loading in the formation of a pro-arc and retro-arc foreland system. Slab pull from the subducting slab and corner flow of the asthenosphere provide subsidence of the retro-lithosphere. B) Schematic indicating the combined effect of flexural tectonics and dynamic subsidence. Flexural tectonics is a response to orogenic loading caused by the compression of lithosphere while dynamic subsidence is a response to subduction processes as seen in Figure 2.2 A. After Catuneanu (2004). C-D) The effect of flexural tectonics and dynamic subsidence on depositional sequences during orogenic off-loading. A system temporarily dominated by flexural tectonics would cause a forced regression close to the orogenic hinterland and a normal regression towards the forebulge. A system temporarily dominated by longwave base level rise would cause transgression which creates period of pelagic settling in the foredeep. After Catuneanu et al. (2002).

(Hälbich, 1983; De Beer, 1989) (Fig 2.3). It incorporates most of the Cape Supergroup as well as adjacent lower Karoo stratigraphy.

The subduction tectonic setting introduced the formation of a foredeep, forebulge and back-bulge flexural system which constituted a large part of the basin subsidence (Catuneanu et al., 1998; Pysklywec & Mitrovica, 1999; Catuneanu et al., 2002; Catuneanu et al., 2005) (Fig 2.2 B). Flexural tectonics is one of the biggest basin-scale controls on the evolution of this retroarc foreland system. In the Karoo foreland system, deposition of the foreland stretches up to 1000.0 km north due to sedimentation across the forebulge into the backbulge region (Fig 2.2 C). This can be achieved by dynamic subsidence (Pysklywec & Mitrovica, 1999; Catuneanu, 2004; Tankard et al., 2009) where loading of the foredeep region can cause the retro-lithosphere to independently subside. When the rate of dynamic subsidence exceeds the rate of forebulge uplift the base level can create accomodation across the entire foreland system resulting in the preservation of wide-spread basin deposition (Catuneanu, 2004) (Fig 2.2 D). Other minor controls on foreland basin development can include basement tectonics through the reactivation of crustal faults as well as rate of sedimentation and compaction (Tankard et al., 2009).

The foredeep, which includes the southern section of the Main Karoo Basin, contains a more complete preservation of the depositional history than the forebulge or back-bulge since no erosional reworking took place in the foredeep.

The foredeep stratigraphically comprises an underfilled phase (deep-marine), a filled phase (deltaic shallow-marine) and an overfilled phase (terrestrial fluvial). The early underfilled phase occurred where dynamic subsidence was less than flexural uplift and deposition occurred mostly in the foredeep. The late underfilled phase towards the filled phase occurred when dynamic subsidence exceeded flexural uplift and deep and shallow marine sediments were deposited across the entire foreland basin (Pysklywec & Mitrovica, 1999; Catuneanu, 2004) (Fig 1.4). The subducting slab is proposed to have detached from the lithosphere around the P-T boundary which caused uplift to

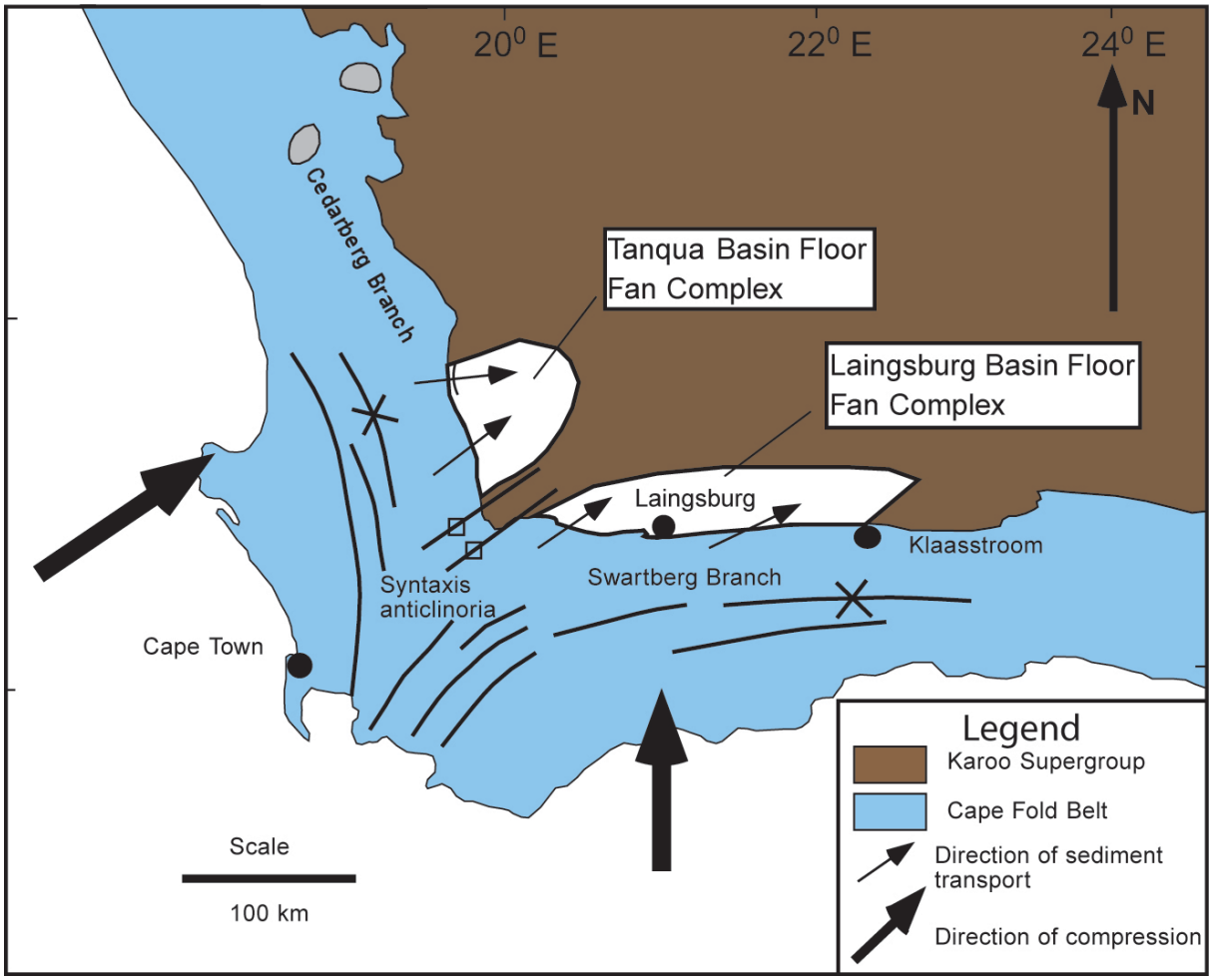

Figure 2.3: Depositional separation of the Tanqua and Laingsburg depo-centres due to the influences of compressional tectonics during the evolution of the Cape Fold Belt. After Wickens (1994).

occur up to 20 My later (Pysklywec & Mitrovica, 1999).

2.2 Basin Sedimentation

2.2.1 Dwyka Group

Early stages of sediment emplacement into the Karoo is preserved as rocks of the Dwyka Group. These Carboniferous to early Permian (~300.0 Ma) rocks largely consist of clast-rich massive diamictite, stratified diamictite, carbonate rich diamictite, conglomerates, mudrock with stones and clast-poor facies such as sandstone and mudrock (Johnson et al., 2006). For the most part, much of the Dwyka is considered to have been emplaced within glacially influenced depocenters, with distinct northern terrestial ice sheet facies (Mbizane Formation), and a marginal marine glaciomarine southern facies containing dropstones (Elandsvlei Formation) (Visser, 1986). The southern facies show about seven sequences caused by successive fluctuations of the ice-front introduced to the basin from the north over time (Visser, 1983, 1989, 1997).

Preserved interbedded ash fall tuffs in the lower Dwyka provides evidence for arc volcanism, interpreted to be the early onset of subduction related tectonics to the south of Gondwana caused by the Panthalassan oceanic slab subducting northward underneath southern Gondwana. Paleaocurrent data indicates that the ice sheets moved towards the south. The upper units of the Dwyka Group indicate a gradual change to marine depocenters lacking glacial detritus (Visser, 1983; Johnson et al., 2006).

2.2.2 Ecca Group

The Permian Ecca Group was first named by Rubidge (1858) after strata exposed in the Ecca Pass near Grahamstown (Eastern Cape, South Africa). Initial subdivision of the Ecca Group was conducted by Rogers & Du Toit (1903) who suggested a lower shale unit, middle Laingsburg sandstone beds as well as an upper sandstone and shale unit. It was later documented by Blignaut et al. (1948) and Rossouw

et al. (1964) that the area east of Laingsburg can be subdivided into the Lower Ecca sandstone and shales, Middle Ecca shales and the Upper Ecca sandstone and shales. Studies by Du Toit (1954) and Ryan (1967) recognized four separate facies of the Ecca Group; Southern, Western, Northern and Central Facies.

Environmental interpretation through facies descriptions was first applied to the Ecca Group by Hobday (1973) on the Vryheid Formation in the northern part of the Karoo Basin. This method of facies analysis for defining deep marine settings was later widely applied to the southwestern part of the basin (Wickens, 1994; Grecula et al., 2003; Sixsmith et al., 2004; Hodgson et al., 2006; van der Merwe et al., 2009).

Keunen (1963) was the first to recognize that the sandstone beds of the Laingsburg Formation were deposited by turbidite processes. This concept was refined by Theron (1967) on the Ecca close to the town of Laingsburg, who suggested a progradation from distal to proximal turbidites. In the Eastern Cape Provence, stratigraphic research was undertaken by Johnson (1976) and Kingsley (1977).

The first comparative study done on the Tanqua and Laingsburg depocenters was conducted by Wickens (1994). Since then many studies have focused on providing high-resolution stratigraphy and correlation between these two depocenters (Grecula, 2000; Sixsmith, 2000; Johnson et al., 2001; Hodgson et al., 2006). Petrographic and geochemical studies (Scott, 1997; Adelmann & Fiedler, 1998; Van Lente, 2004) confirmed that the rocks of both the Tanqua and Laingsburg depocenters came from a single source which distributed sediment into the separate depocenters (Anderson et al., 2003; Van Lente, 2004).

More than a decade ago it was commonly considered that the main sediment source of the Laingsburg and Tanqua depocenters were the uplifted and eroded Cape Supergroup (Lock, 1980; Cole, 1992; Veevers et al., 1994). Earlier studies did suggest a source region further south of the Cape Fold Belt (Elliot & Johnson, 1972; Elliot & Watts, 1974; Visser, 1979), but recent studies provided substantial

evidence against a Cape Supergroup source and supports sediments derived from a magmatic arc south of the Cape Fold Belt (Van Lente, 2004; Nguema-Mve, 2005; McKay et al., 2015). The Ripon depocenter exhibits similar results from petrographic studies supporting a transitional magmatic arc source (Johnson, 1991).

The southern Ecca Group presents a unique Permian regressive succession from basin floor to shelf sedimentation. The Ecca Group represents the under-saturated basin fill from a deep marine to deltaic environment and most of the Lower Ecca formations (Prince Albert, Whitehill and Collingham) extend across the entire southwestern Karoo Basin (Fig 1.4). Deposition of the Ecca Group in the southern depocenters of the Main Karoo Basin represents a prograding basin-fill with influences of eustatic sea-level rise and fall (Visser, 1993; Pysklywec & Mitrovica, 1999; Figueiredo et al., 2010).

After the glaciation period (Dwyka Group), initiation of the Ecca was characterized by deep-marine hemi-pelagic shales and silts. (Visser, 1990; Catuneanu et al., 2005; Johnson et al., 2006). These are represented by the basal Prince Albert and the Whitehill formations. The largely argillaceous Collingham Formation, which regionally forms a conformable contact with the underlying Whitehill Formation, is overlain by the Vischkuil and Tierberg formations in the Laingsburg and Tanqua depocenters respectively. These formations are mudrock- and siltstone-rich deposits with sub-ordinate fine-grained sandstone beds, and in places exhibit chaotic syn-depositionally deformed strata (Andersson & Worden, 2004; van der Merwe et al., 2009; van der Merwe et al., 2010; van der Merwe et al., 2011). In the southeastern part of the basin the sandstone-rich Ripon Formation directly overlies the Collingham Formation (Kingsley, 1981; Johnson, 1991) (Fig 1.4). In the Laingsburg depocenter the Collingham Formation is overlain by the Vischkuil Formation (Grecula et al., 2003; Sixsmith et al., 2004), and in the Tanqua depocenter by the Tierberg Formation (Hodgson et al., 2006) (Fig 1.3). The argillaceous Vischkuil and Tierberg formations are overlain by the Laingsburg and Skoorsteenberg formations, respectively. These arenaceous formations are in turn overlain by rhythmites and thin muds of the Fort Brown Formation (Laingsburg and Ripon depocenters) and Kookfontein Formation

(Tanqua depocenter) (Johnson et al., 2006). The uppermost formation of the Ecca is the arenaceous Waterford Formation (Catuneanu et al., 2005; Johnson et al., 2006); which in turn is overlain by the first sub-aerial deposits of the Beaufort Group (Rubidge et al., 2000; Johnson et al., 2006).

2.2.2.1 Prince Albert Formation

The Prince Albert Formation is the lowermost stratigraphic unit of the Ecca Group and comprises fine-grained dark-gray shales and graded silts (Visser, 1993). This argillaceous formation conformably overlies the Dwyka diamictites and occasional drop-stones are present within its lower horizons. Irregular carbonate bodies and occasional calcareous or phosphatic concretions are also present more commonly in the uppermost strata. Marine fossils such as *brachiopods*, *cephalopods* and *lamellibranchs*, as well as palaeoniscoid fish and plant remains, are present in the lower units of the formation (McLachlan & Anderson, 1973). Deposition of the Prince Albert Formation occurred in a deep marine setting due to suspension settling of mud. Upwelling of cold water might have caused siliceous and phosphatic beds to form through chemical processes under reducing conditions. This could support the rich marine life during this period. The calcareous nodules and concretions could have been the cause of early diagenetic processes (Johnson et al., 2006).

2.2.2.2 Whitehill Formation

The Whitehill Formation consists mainly of dark to white-weathering carbonaceous shales with occasional pyritic stringers and chert lenses (Cole & McLachlan, 1991; Branch et al., 2007) and ferruginous dolomitic concretions (Johnson et al., 2006). Deposition of this formation occurred in anoxic deep-water, pelagic settling conditions (Cole & McLachlan, 1991). Mudrocks of the Whitehill Formation have a Total Organic Carbon content averaging at 4.5% (Geel et al., 2013). The formation encompasses a rich and diverse palaeontological record including abundant plant fragments, palaeoniscoid fish and the parareptile *Mesosaurus* (Oelofsen, 1987; Branch et al., 2007; Tankard et al., 2009).

2.2.2.3 Collingham Formation

The Collingham Formation conformably overlies the Whitehill Formation with a sharp contact and is characterized by alternating tabular beds of siliceous mudrock and siltstone. It also has interbedded tuff layers that altered to yellow K-bentonite. The Collingham Formation has a distinct marker bed, Matjiesfontein Chert Member, which is laterally continuous across the largest part of the southwestern Main Karoo Basin (Viljoen, 1994; Johnson et al., 2006). Trace fossils are fairly common across the entire formation with variations of trails and grazing patterns (Viljoen, 1992a; Viljoen, 1994). The Collingham Formation is interpreted to have been deposited by distal turbidites (Wickens, 1994).

2.2.2.4 Vischkuil Formation

The Vischkuil Formation (lower Permian) is situated in the Laingsburg depocenter and extends eastward towards the Ripon depocenter (Anderson, 1977; Catuneanu et al., 2005; Johnson et al., 2006; Fildani et al., 2007; van der Merwe et al., 2009). It comprises mainly minor sub-ordinate sand alternating with dark mudrock and siltstone. This formation lacks abundant sandstone layers which distinguishes it from the overlying Laingsburg/Ripon formations. The formation was first named the Lower Ecca Shales by Rogers & Schwarz (1902) for strata which comprised what is today considered the upper part of the Collingham Formation above the Matjiesfontein Chert Member. Theron (1967) used the term Vischkuil Formation to include the Collingham Formation. Later SACS (1980) considered the Collingham Formation and Vischkuil Formation as separate stratigraphic units due to facies changes and the immediate decline in abundance of tuff layers in the Vischkuil Formation. A distinct feature of the Vischkuil Formation is the presence of gravitational slides and slump structures (Wickens, 1994; van der Merwe et al., 2009).

Three distinguishable deformational events have been recognized in the Upper Vischkuil Formation (Viljoen & Wickens, 1992; van der Merwe et al., 2009). Previous work suggests that these mass

transport gravitational slides are indicative of a slope environment and were caused by slope instability (Johnson et al., 2006). However, a recent study by van der Merwe et al. (2011) points out that it is possible to initiate mass transport complexes in basin floor settings by overlying debris flow. It is also suggested (van der Merwe et al., 2010) that the lower Vischkuil is derived from eastern basin infill and represents the distal down-dip deposition of the Puto's Vale Member sandstones of the Eastern Ripon Formation. Palaeocurrent analysis indicates flow towards the W and NW (280° to 300°) for the lower Vischkuil Formation which gradually changes to SE and ENE (80° to 120°) in the upper part of the formation (van der Merwe et al., 2009). This change in palaeocurrent directions and the introduction of Mass Transport Deposits (MTD's), in the form of debrites, changes the sediment input from the eastern side of the basin to the western side (van der Merwe et al., 2009). Deposition of the Vischkuil Formation was terminated by the deposition of large fine-grained sand rich submarine fans of the Laingsburg Formation.

2.2.2.5 Laingsburg Formation

The Laingsburg Formation comprises mostly lithofeldspathic to feldspathic sandstones with alternating silts and shales and is readily distinguishable from the Vischkuil Formation on the greater abundance of sandstone units (Viljoen, 1992b). Calcareous concretions and nodules are common within this formation. Lithological associations show 2nd order upward thickening in the lower part of the Laingsburg Formation and then 2nd order upward fining towards the upper part of the formation.

The depositional environment of this formation is considered to be mid-fan deposition of a prograding sub-marine turbidite fan complex (Wickens, 1994). The Laingsburg succession can be sub-divided into 6 map-able individual fan systems. These are classified as Fan A-F with Fan A displaying the thickest succession of basin floor stacked turbidite sequences varying in thickness between 150.0 – 350.0 m. Fans B-F are the result of base of slope to slope deposition of submarine fans (Wickens, 1994; Grecula et al., 2003; Sixsmith et al., 2004). Fan A consists mostly of tabular sandstone sheets with little evidence of deeply scouring channel fills and levee deposits. Fan B contains thicker beds than Fan A

and is dominated by channel fills and lobe deposits showing a more proximal depositional setting than Fan A (Grecula et al., 2003). Fans C-F have a fining up nature where fan lobes become thinner towards the upper Laingsburg Formation (Sixsmith et al., 2004). Studies show that, even though there are local variations due to channel migration and structural influences, the general trend of sediment transport for the Laingsburg (Grecula et al., 2003; Sixsmith et al., 2004) is towards the E and NE (50° to 90°).

2.2.2.6 Ripon Formation

Relatively little is known about the Ripon Formation and detailed submarine fan architectural analysis is lacking compared to that of the Laingsburg and Tanqua depocenters. The Ripon Formation comprises dark grey lithofeldspathic sandstone, mudrock and occasional rhythmic interbedded mud silt (Johnson & Kingsley, 1993). Sandstone units commonly exhibit a tabular nature and can occasionally show a mottled texture. Fining-upwards sequences from sandstones into mudrocks and rhythmites are common in the upper Ripon Formation (Johnson & Kingsley, 1993). Studies done on the Ripon Formation agree on sediment transport towards the W and NW (260° to 300°) (Kingsley, 1977, 1981; Johnson, 1991).

Originally this formation was referred to as the "Lower Shales and Sandstones" of the Ecca Series by Du Toit (1954). Johnson (1966) suggested the unit be called the Ecca Pass Formation while Ryan (1967) proposed the Upper Arenaceous Formation. Only a few years later the Ripon Formation became the generally accepted name for the unit (Johnson, 1976). Kingsley (1977) then subdivided the Formation into three members: lower Pluto's Vale Member which has abundant sandstone packages and contains minor mudrock and rhythmite units; middle Wonderfontein Member dominated by mudrock and rhythmites with occasional minor sandstone; upper Trumpeters Member which is sandstone rich with alternating layers of sandstone, mudrock and rhythmite showing cyclical repetitions (Johnson et al., 2006). The massive sandstones of the Ripon Formation are the result of sedimentation through high-density turbidity currents and the fine-grained rhythmites and mudrocks were the products of suspension deposition (Lowe, 1982). The lower units of the Ripon Formation are considered

representative of distal outer fan deposition whereas the upper sections of the Ripon Formation have a more proximal inner fan appearance (Kingsley, 1981).

Overall thickness of the Ripon Formation east of 26°E is around 1000.0 m and thins to about 600.0 m west of 26°E. Thinning towards the west is apparent due to the pinch-out of the Upper Trumpeters Member (Johnson & Kingsley, 1993). Conversely, the Pluto's Vale Member increases in thickness from east to west with an average thickness of 200.0 m at 27°E to 600.0 m close to 26°E. According to Kingsley (1977) the Wonderfontein Member gains thickness from the east to the west. The Wonderfontein Member has a thickness of about 100.0 m towards Grahamstown and reaches a thickness of 300.0 m at Jansenville.

2.2.2.7 Fort Brown Formation

The Fort Brown Formation stratigraphically overlies the Laingsburg Formation in the west and Ripon Formation in the east with a gradational conformable contact. It comprises predominantly mudrocks with rhythmically interbedded siltstone and sandstone (Johnson et al., 2006). The formation displays gradual coarsening up of sediments from a mudrock-dominated lower Fort Brown to silt-dominated upper Fort Brown (Sixsmith, 2000; Van Lente, 2004). This coarsening up sedimentation is typical of a delta front propagating into the basin. The depositional environment for the Fort Brown Formation is considered a deep water pro-delta to slope setting (Cole, 1992). The occurrence of deformed units and slumps as well as soft sediment deformation indicates occasional slope instability (Wickens, 1994; Van Lente, 2004). The presence of wave ripples towards the upper Fort Brown and evidence of trace fossils in the form of *cruziana* and *skolithos* confirms a progressive shallowing of water depth (Kingsley, 1977; Johnson et al., 2006).

2.2.2.8 Waterford Formation

Regionally overlying the Fort Brown Formation, the Waterford Formation comprises mainly fine- to medium-grained sandstone with various architectural elements such as distributary channel fills,

crevasse splays and overbank mudstone (Wickens, 1994; Van Lente, 2004). General coarsening up sequences are observed, especially in the upper strata of the formation. The depositional environment for the Waterford Formation is considered a delta front to delta plain setting (Rubidge et al., 2012). The uppermost unit of the Waterford Formation forms the boundary between the sub-aqueous delta front sedimentation and the sub-aerial fluvial sedimentation (Beaufort Group) (Wickens, 1994; Van Lente, 2004; Rubidge et al., 2012).

2.3 U-Pb zircon Geochronology

Radiometric age dating of detrital zircon and other minerals has greatly improved our ability to date certain sedimentary systems. Within the last decade, U-Pb detrital zircon dating has become a useful research tool not only in the determination of maximum age of deposition, but also for determining sediment provenance. Multiple studies have been executed on providing age constraints for the Ecca Group as well as categorizing the different source regions that provided sediment to the southern Karoo Basin. Some recent studies for the Karoo Supergroup include; Nguema-Mve (2005), Fildani et al. (2007), Coney et al. (2007), Fildani et al. (2009), Lanci et al. (2013), Rubidge et al. (2013), McKay et al. (2015) and McKay et al. (2016). Most workers analyzed zircons from the Karoo Supergroup using sensitive high-resolution ion microprobe (SHRIMP) technology (Nguema-Mve, 2005; Fildani et al., 2009; McKay et al., 2015; McKay et al., 2016). Rubidge et al. (2013) used chemical abrasion - thermal ionization mass spectrometry (CA-TIMS) technology, and Coney et al. (2007) analysed only three (3) single zircon grains by means of isotope dilution - thermal ionization mass spectrometry (ID-TIMS).

Most U-Pb zircon analyses were conducted on tuff layers interbedded between mudrocks and fine-grained sandstones of the Ecca and Beaufort Groups with the assumption of collecting co-eruptive ages. Ash fall tuffs were sampled mostly across the southern and central Karoo Basin and stratigraphically from the Lower Ecca to the Upper Beaufort. Most studies found that the zircon ages reveal some complex spectra and may provide some erroneous ages for Karoo strata (Fildani et al., 2007; Coney et al., 2007; Fildani et al., 2009; Rubidge et al., 2013; Lanci et al., 2013).

Radiometric ages on the submarine fan complexes of the Tanqua and Laingsburg depocenters obtained by Fildani et al. (2007) indicate that the Vischkuil Formation and Fan A of the Laingsburg Formation were deposited before the first sand-rich submarine fan of the Skoorsteenberg Formation. An age of ~ 275.0 Ma was determined for the Upper Collingham across both depocenters where Fan A of the Laingsburg Formation yielded ages from ~262.0 Ma (Base of Fan A) to ~255.0 Ma (just below Fan B) and ages ~255.0 Ma were recorded for deposition of the Skoorsteenberg Formation. These ages indicate that both the Tanqua and the Laingsburg depocenters were contemporaneously depositing submarine fans.

Ash fall tuff single zircon grains obtained by Rubidge et al. (2013) and Lanci et al. (2013) for the overlying Beaufort Group yielded ages varying from ~268.0 Ma to ~255.0 Ma. This poses a problematic scenario where the overlying Beaufort Group yields older ages than the underlying Laingsburg and Skoorsteenberg formations of the Ecca Group. This problem was addressed by McKay et al. (2015) who sampled several tuff layers across the southern Karoo Basin, covering the Ecca and Beaufort Groups. The analyzed samples were then compared to previous work (Coney et al., 2007; Fildani et al., 2007; Fildani et al., 2009; Lanci et al., 2013; Rubidge et al., 2013). McKay et al. (2015) observed a period of significant absence of tuff layers within the upper Ecca Group across the southern Karoo Basin (Tanqua, Laingsburg and Ripon depocenters) and correlated it with South-American volcaniclastic strata (Fig 2.4). Tuff layers below the “no tuff” period seem to follow a chronological younging of strata up to the Fort Brown and Waterford formations ranging between ~275.0 Ma and ~250.0 Ma (McKay et al., 2015). Tuff layers above this period exhibited problematic ages and does not show any age trends in stratigraphy. According to McKay et al. (2015), the problematic nature of these grains is based on a few possible scenarios. There also seems to be textural differences between tuff layers below and tuff layers above the “no tuff” period.

Many authors focussed on tuff zircon samples, but only a few used detrital zircon geochronology to determine sediment provenance. Nguema-Mve (2005) suggested three source regions for sediments

deposited into the Tanqua and Laingsburg depocenters. The youngest peak ranges from 270.0 – 290.0 Ma derived from the Choiyoi magmatic arc in northern Patagonia, a 460.0 – 495.0 Ma range is linked to the Arroyo Salado and Famatinian granites as well as the Deseado Massif. The older 545.0 – 620.0 Ma grouping is derived from the Neoproterozoic metamorphic belts of South Africa.

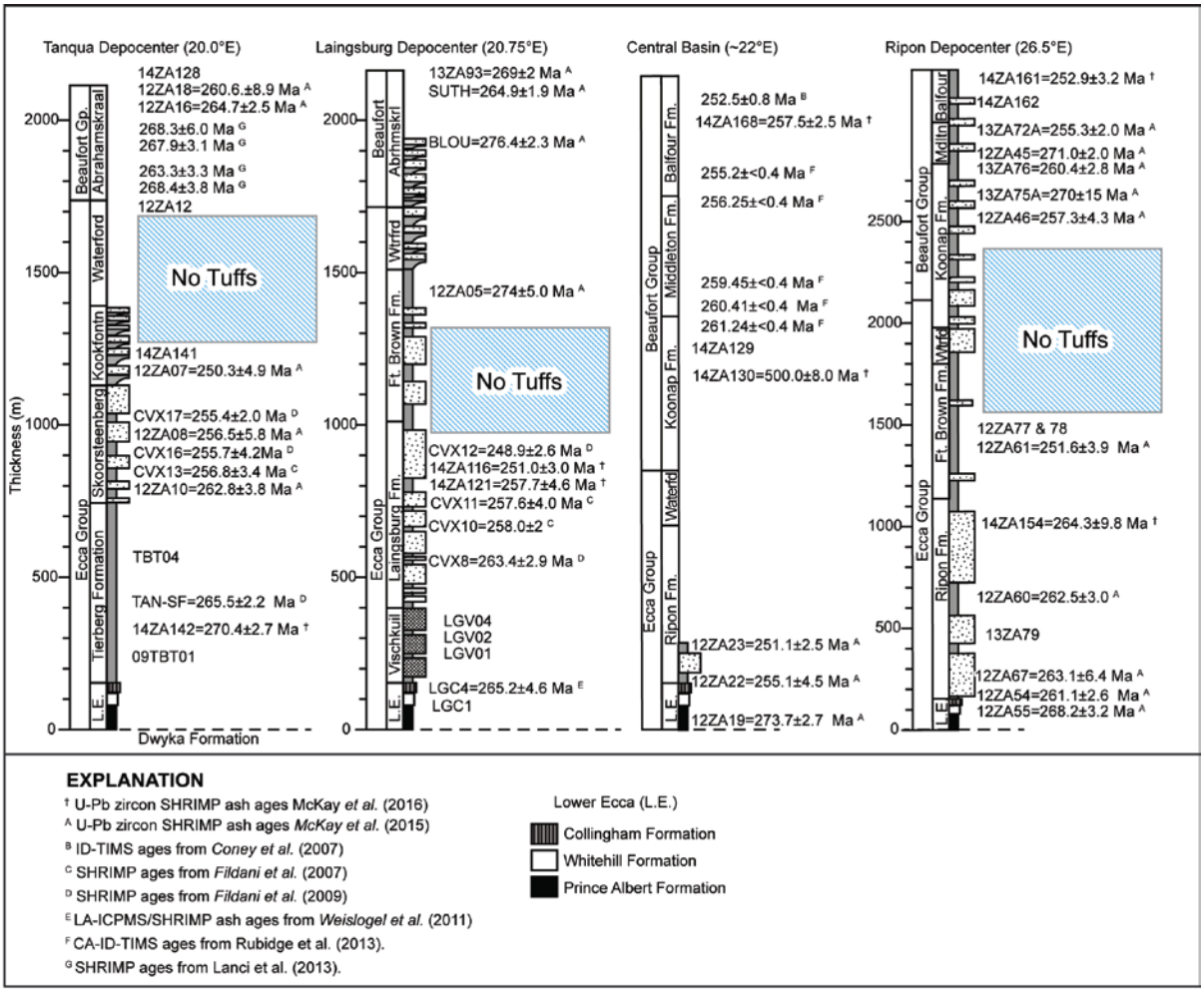

Figure 2.4: Simplified stratigraphy of the Tanqua, Laingsburg and Ripon depocenters. U-Pb zircon dates are presented from several studies and includes data from the Central Basin. Notice the "No Tuffs" zones within each depocenter signifying a period of starvation in volcanic activity. After McKay et al. (2016).

Chapter 3:
Methodology

Chapter 3: Methodology

3.1 Sedimentology

For this study, a modified facies analysis approach was utilized based on the approach developed for reconstructing fluvial deposited sediments by Miall (1977, 1985) to systematically identify repeating and co-occurring depositional packages preserved within the rock record. Miall's original methods have been greatly modified for this study to apply to a deep marine depositional environment. Each sedimentary succession was described at decimeter scale to properly identify upper and lower bounding surfaces, lithological patterns, and sedimentary and biogenic structures to properly assign facies codes. Distinct variation and co-occurring nature of these codes form the basis for defining different facies associations. These facies associations were compared with facies analyses conducted by previous studies on the Ecca Group (Kingsley, 1981; Johnson, 1991; Wickens, 1994; Sixsmith et al., 2004; Hodgson et al., 2006; van der Merwe et al., 2009; Flint et al., 2011).

Facies descriptions and stratigraphic relationships were obtained in-field and used to draft stratigraphic profiles at a number of localities. The study area encompasses folded strata caused by the Cape Fold Belt tectonism and were corrected for during the construction of stratigraphic profiles. The use of a Jacob's staff and Krantz Compass (set with a magnetic declination of -25.14°) made it possible to obtain accurate thickness measurements of the folded sedimentary beds and younging direction were constantly measured against the dip of the strata. All GPS readings were taken by Garmin eTrax 10 GPS set on the WGS 1984 datum. Distinct bounding surfaces and marker beds were walked out to determine lateral extent and facies changes. The marker horizons were defined by laterally extensive (greater than 50.0 km) mudrock units, deformed units (DU) and the Matjiesfontein chert bed within the Collingham Formation. Twelve stratigraphic sections were measured spanning from the upper part of the Collingham Formation to the lower Fort Brown Formation in order to cover the complete deep-water succession and to analyze lateral variation of the different facies and

formations. These stratigraphic sections are spread out across the study area and are strategically chosen to cover the lateral facies changes between the Laingsburg and Ripon depocenters.

The relationships between specific beds are also important for understanding depositional patterns. For this purpose, bounding surfaces were also examined. A 0^{th}-order represents long term settling of sediment without erosion, conversely 4^{th}-order is classified as rapid deposition causing erosive features such as scouring (Reading, 1996).

3.2 Petrography

Discrete analysis of mineralogy, grainsize, texture, sorting and rounding, matrix and cement provides a holistic understanding of the depositional history and source of the rocks (Carozzi, 1993; Readings, 1996; Boggs, 2009). In order to better understand granule scale context, thin sections were produced from key stratigraphic horizons across all three formations. Sixteen thin sections were analysed and described using a Leica thin-section microscope. The samples were chosen due to their stratigraphic position and could provide key evidence for the depositional nature of distinct formations. Sandstone beds were favored during sampling to better observe grain composition and boundaries. Samples were obtained from various horizons and each formation is represented.

Thin sections were observed under PPL (Plain Polarized Light) and XPL (Cross Polarized Light) to identify mineralogy and grain relationships. A 500-grain point count was done on each thin section using a standard point counter set at 0.4 mm intervals (Dickenson et al., 1983). Point count data were then plotted onto QFL diagrams, based on classification schemes from Folk (1974) and Pettijohn (1973), to elucidate compositional variations between samples. A QFL classification scheme of Dickenson et al. (1983) was used to plot data in possible tectonically controlled provenance scenarios.

3.3 U-PB detrital zircon dating

3.3.1 Zircon mineral separation, preparation, and imaging

Eight samples were derived from sandstone units of key stratigraphic intervals throughout the formations studied (Table 1). The first two samples, WK01 and WK-2016-1, were acquired respectively from the Upper Laingsburg Formation and Upper Vischkuil Formation on the farm Zacharias Fontein 135. WK01 was derived from the first very fine-grained sandstone layer within the Upper Vischkuil Formation and WK-2016-1 from the uppermost sandstone of the Laingsburg Formation just underlying the contact between the Laingsburg Formation and the Fort Brown Formation. The third and fourth samples, KG06 and KG-2016-1, were obtained from Groot Tygerberg 102 representing the Lower Ripon Formation and Upper Vischkuil Formation. The sample collected from the Vischkuil Formation, KG-2016-1, is also stratigraphically from the same horizon as sample WK01. KG06 was taken from a prominent sandstone situated at the base of the Pluto's Vale Member also at Groot Tygerberg 102.

The fifth sample, N12-2016-1, was obtained from outcrop exposure at the N12 road cutting and represent the upper Laingsburg Formation. The sixth and seventh samples were collected from Klipfontein 174 (OM01 and OM06) and both samples are from the Ripon Formation. OM01 was acquired from the lowermost sandstone unit of the Pluto's Vale Member and is stratigraphically about 2m above the contact with the Collingham Formation while OM06 was from a sandstone lens situated in the upper Wonderfontein Member. The last sample was collected from Minnies Kraal 112 (MK-2016-4) and is stratigraphically the highest sample obtained of the Ripon Formation. MK-2016-4 represents the last sandstone bed of the Trumpeters Member just before the contact between the Ripon Formation and the Fort Brown Formation.

All samples were prepared and analyzed at the Central Analytical Facility (CAF) of the University of Stellenbosch. Bulk rock samples were initially processed via jaw crushing and disk mill to obtain a maximum fragment size of 2.0 mm. Clays were liberated via hand washing and removed from the

sample. The washed material was sent through a panner through which heavier material were manually separated from the lighter fraction. The heavy minerals were then processed via magnetic separation by the traditional Frantz Magnetic Separator with an isodynamic vibrator. Magnetic intensity was staggered from 0.8 to 1.4 amps. Thereafter, the samples were processed in Tetra bromoethane (TBE) heavy liquid with a density of 2.96. Separated heavy minerals were then washed and dried.

Table 3: List of detrital zircon samples used for LA-ICPMS analysis.

Sample	Stratigraphic horizon	Farm Name	Latitude	Longitude
WK01	Middle Vischkuil Fm	Zacharias Fontein 135	S 33.21093°	E 22.05490°
WK-2016-1	Upper Laingsburg Fm	Zacharias Fontein 135	S 33.20867°	E 22.05218°
KG06	Middle Pluto's Vale M	Groot Tygerberg 102	S 33.12811°	E 22.34262°
KG-2016-1	Lower Vischkuil Fm	Groot Tygerberg 102	S 33.12910°	E 22.34383°
N12-2016-1	Upper Laingsburg Fm	N12 Road Cutting	S 33.11820°	E 22.53867°
OM01	Lower Pluto's Vale M	Klipfontein 174	S 33.28221°	E 22.77908°
OM06	Middle Wonderfontein M	Klipfontein 174	S 33.28428°	E 22.77593°
MK-2016-4	Upper Trumpeters M	Minnies Kraal 112	S 33.21683°	E 22.82622°

From each sample 150 to 250 zircon grains were handpicked and mounted. For Mount SW1, four samples were placed and then molded into an epoxy. The epoxy consisted of SpeciFix Resin and SpeciFix-40 curing agent. The set mount was then polished on the zircon holding platform to expose the crystals and remove irregularities. Polishing was done on a MD-Dac Satin Woven Acetate Polishing Cloth (3.0 µm) using a DiaPro-Dac3 Suspension for 10 min and then on a MD-Nap Synthetic Short Nap Polishing Cloth (1.0 µm) using a DiaPro-Nap B1 Suspension for 10 min. Mount SW2, which consists of five samples, was prepared in the same manner.

Samples were loaded in a Zeiss MERLIN Field Emission Scanning Electron Microscope at the Electron Microbeam Unit of Stellenbosch University's Central Analytical Facility. Prior to loading the samples, the polished mounts were coated with a thin (~10.0 µm thick) layer of gold, using an Edwards S150A Gold Sputter Coater. Beam conditions during the analysis on the Zeiss MERLIN were set at 20 kV accelerating voltage, 11nA probe current and maintaining a working distance of 9.5 mm. For the

purposes of this study only two forms of images were produced, the Back Scattered Electron images and Cathodoluminescence images. To generate Backscattered Electron (BSE) images for each sample a Zeiss 5-diode Back Scattered Electron (BSE) Detector (Zeiss NTS BSD) and Zeiss Smart SEM software were used. To produce the Cathodoluminescence (CL) images each sample was imaged using a CL detector (Zeiss CL) and Zeiss Smart SEM software.

3.3.2 Laser Ablation – Inductively Coupled Plasma Mass Spectrometry (LA-ICPMS)

All zircon U–Pb age data were obtained at the Central Analytical Facility, Stellenbosch University, by laser ablation - single collector - magnetic sectorfield - inductively coupled plasma - mass spectrometry (LA-SF-ICP-MS). This methodology employs a Thermo Finnigan Element2 mass spectrometer coupled to an ASI Resolution SE-S155 excimer laser ablation system. A spot diameter of 25.0 µm and a crater depth of approximately 10.0 -15.0 µm by conducting single spot analysis. Ablation time was set to 15 secs with a 15-sec wash-out delay. For the purpose of this study, 2.54 cm round mounts were employed. The methods used for analysis and data processing are similar to those described by Frei & Gerdes (2009). For quality control, the Plesovice (Sláma et al., 2008) and M127 (Nasdala et al., 2008; Mattinson, 2010) zircon reference materials were analysed, and the results were consistently in accurate agreement with the published ID-TIMS ages. For calibration and reference purposes, a primary standard, GJ-1 (Jackson et al., 2004), was analysed throughout the procedure. Raw data from the analysis was processed using Iolite's (extension in IgorPro) data reduction scheme (DRS) to correct for downhole fractionation (Hellstrom et al., 2008; Paton et al., 2010). Full analytical details and the results for all quality control materials analysed are presented in Table 1. Calculation of concordia ages and plotting of concordia diagrams were performed using Isoplot/Ex 4.15 (Ludwig, 2003). Representative numerical results for the analyses are given in the results section. All grains are presented at a 2-sigma error. Table 2 summarizes the specifications for detrital zircon analysis on this study's samples.

Table 4: LA-SF-ICP-MS U-Th-Pb dating methodology CAF, Stellenbosch University

Laboratory & Sample Preparation	
Laboratory name	Central Analytical Facility, Stellenbosch University
Sample type / mineral	Detrital zircons
Sample preparation	Conventional mineral separation, zircon: 2.54 cm resin mount and in-situ in thin section, 1 µm polish to finish
Imaging	CL MERLIN FE-SEM, 11 nA, working distance 9.5 mm
Laser ablation system	
Make, Model & type	Resonetics Resolution ME-S155, ArF Excimer ATL Atlex
Ablation cell & volume	Laurin Technology S155 dual volume cell
Laser wavelength	193 nm
Pulse width	< 5 ns
Fluence	2.0 J/cm^{-2} (measured with external energy meter above sample cell)
Repetition rate	9 Hz zircon
Spot size	25 µm
Sampling mode / pattern	25 µm single spot analyses
Cell carrier gas	100% He, Ar and N_2 make-up gases combined into Nylon 10 tubing
Pre-ablation laser warm-up (background collection)	3 cleaning shots followed by 15 seconds background collection
Ablation duration	15 seconds
Wash-out delay	15 seconds
Cell carrier gas flows	325 ml/min He
ICP-MS Instrument	
Make, Model & type	Thermo Finnigan Element2 single collector HR-SF-ICP-MS
Sample introduction	Via Nylon 10 tubing
RF power	1350 W
Make-up gas flow	920 ml/min Ar & 4 ml/min N_2
Detection system	Single collector secondary electron multiplier
Masses measured	202, 204, 206, 207, 208, 232, 233, 235, 238
Integration time per peak	4 ms
Total integration time per reading	0.1 sec *(represents the time resolution of the data)*
Sensitivity	30000 cps/ppm Pb
Dead time	6 ns
Data Processing	
Gas blank	15 second on-peak
Calibration strategy	GJ-1 used as primary reference material, Plešovice & M127 used as secondary reference materials (Quality Control)
Reference Material info	GJ-1 (Jackson et al. 2004), Plešovice (Sláma et al. 2008), M127 (Nasdala et al. 2008; Mattinson 2010)
Data processing package used / Correction for LIEF	Iolite data reduction software was used to process data
Mass discrimination	Standard-sample bracketing with $^{207}Pb/^{206}Pb$ and $^{206}Pb/^{238}U$ normalized to reference material GJ-1
Common-Pb correction, composition and uncertainty	204-method, Stacey & Kramers (1975) composition at the projected age of the mineral, 5% uncertainty assigned
Uncertainty level & propagation	Ages are quoted at 2-sigma absolute, propagation is by quadratic addition. Reproducibility and age uncertainty of reference material and common-Pb composition uncertainty are propagated.
Quality control / Validation	M127: Concordia age = 528±6 Ma (2s, MSWD = 1.2) Plešovice: Concordia age = 340±2 Ma (2s, MSWD = 1.03)

3.3.3 Grain age determination

Various methodologies exist for the determination of the maximum age of deposition based on the youngest detrital zircon signature. Due to the deep marine environmental setting, zircon grains from this study may exhibit a broad range of sources. Therefore, this study utilized six different methods to statistically determine the maximum depositional age for each sample (Dickenson & Gehrels, 2009; Lawton & Bradford, 2011; Robinson et al., 2012; Tucker et al., 2013). The methods for determining maximum depositional age include: 1) youngest single grain age (YSG), 2) youngest graphical detrital zircon age (YPP), 3) youngest detrital zircon age (YDZ), 4) weighted mean average (YC2σ), 5) weighted average and 6) TuffZirc age extractor. Other workers have conducted a comparative study on these various methods, focusing on obtaining the most robust youngest maximum depositional age from a statistical group of youngest detrital zircon ages (Dickenson & Gehrels, 2009; Lawton & Bradford, 2011; Robinson et al., 2012; Tucker et al., 2013).

The youngest single grain (YSG) method is based on extracting the youngest zircon age present in a suite of detrital zircon grains. The youngest graphical zircon age (YPP) utilizes the age probability plot constructed in ISOPLOT (Ludwig, 2009) and extracts the youngest peak of clustered zircon grain (Detrital Zircon>3) ages within a population (Dickenson & Gehrels, 2009). The youngest detrital zircon age (YDZ) is an algorithm in ISOPLOT (Ludwig, 2009) determining the youngest statistical subset of a population of zircons through the utilization of a Monte Carlo analysis. The weighted mean average at 2 sigma (YC2σ) incorporates the external error in determining the average of the youngest grains within a population and is derived using AGE PICK (Dickenson & Gehrels, 2009). For this study, the three (3) youngest grains of each sample was used with this algorithm. Another algorithm in ISOPLOT (Ludwig, 2009) was utilized to determine an inverse variance-weighted average within a population of grains including the ten (10) youngest grains within each sample. The last approach was based on the TuffZirc algorithm that mathematically ascertains the youngest coherent population of zircons based

on the loss and inheritance of Lead (Pb) including its error (Ludwig, 2009). The 10 youngest grains were used for this method.

Chapter 4:
Results

Chapter 4: Results

4.1 Facies Analysis

This study identified twelve genetically related and repeating facies (Table 3), which were documented to co-occur in repeating groups referred to as facies associations. Seven such facies associations were observed (Table 4). A detailed description of each facies association is provided together with an interpretation of the depositional nature. Minor variations do occur within a single facies association, yet overall similarities remain within all representations of each specific facies association. All colour codes are based on the GSA Munsell rock colour chart (2009) and bounding surfaces are identified based on Vail et al. (1977) which was later revised by Miall (2010) (Table 5). Bounding surfaces vary from 0^{th}- to 4^{th}-order which represent magnitude of erosion and rate of deposition.

Table 3: Table showing facies codes based on lithofacies, grainsize and sedimentary features. Modified from Miall (1977, 1985).

Facies Code	Lithofacies	Sedimentary Structures	Interpretation
Sm	sand, very fine to medium	massive bedded	rapid fall-out of suspension, no traction
Sh	sand, very fine to medium	horizontal lamination, parting or stream lineation	planar bed flow (upper flow regime)
Scr	sand, very fine to medium	current ripple cross laminae	traction transport (lower flow regime)
Sch	sand, very fine to medium	chaotic convolute beds	slump deposits, debrite, MTC
Sdw	sand, very fine to medium	soft-sediment deformation	rapid deposition, water-saturated sediments
Ssc	sand, very fine to medium	scour marks	rapid deposition, strong current, traction
Fl	silt, mud	fine lamination	low energy settling or waning deposits
Fm	silt, mud	massive bedded	low energy settling or waning deposits
Fch	silt, mud, clay	chaotic convolute laminae	slump deposits, debrite, MTC
Frip	silt, mud, clay	rip-up clasts	erosional base (high energy)
Fcr	silt, mud	current ripple cross laminae	channel or current (lower flow regime)
Fis	silt, mud, clay	thin interbedded sheets	waxing and wayning flow, low energy settling

Table 4: Facies associations based on lithofacies and a combination of facies codes. A basic interpretation is also given for each association. Modified from Miall (2010).

Facies	Facies Associations	Facies Codes	Comments	Sediment Size	Lithofacies	Interpretation of Depositional evironment
	**FA1:** Inter-laminated hemipelagic Silt and Shale	Fl, Fis, Fm Fcr	Fine interbedded layers no more than 20cm thick, fining upwards	clay to c silt 3.9µm - 31µm	Hemi-pelagic shale and silty mudstone	Low energy suspension settling of hemi-pelagic material
	**FA2:** Thin-bedded Sandstone	Sm, Scr, Sh, Sdw, Ssc, Frip	Thin beds less than 1m, sharp lower bounding surface, scour marks present, debrite	c silt to f sand 31µm - 250µm	Sandstone/Greywacke	Deposition from turbidity current (Distal)
	**FA3:** Thick-bedded Sandstone	Sm, Sh, Ssc, Frip,	Mostly massive, sharp lower bounding surface with occasional load casts, beds between 1-3m, debrite	vf to m sand 125µm - 500µm	fine- to medium grained sandstone	Rapid deposition from turbidity current (channel or proximal lobe)
	**FA4:** Chaotic Mudrock	Sch, Fch, Fl	Mixing of rock types, sheath folds and chaotic deposition	clay to vf sand 3.9µm - 125µm	Sandstone, siltstone and mudstone	Mass transport complex caused by slope instability
	**FA5:** Silliceous Siltstone	Fis, Fl, Fm	Regular thickness between 10-30cm, dominant chert cement	clay to c silt 3.9µm - 31µm	Silliceous siltstone/mudrock	Low energy, very fine grained turbidite deposition on abyssal plain
	**FA6:** Finely inter-bedded Sand and Mud	Scr, Fcr, Sh, Fl, Sdw	Rhythmite, regularly alternating layers of 2-10cm, current ripple cross-laminae fairly common	clay to f sand 2.5µm - 250µm	Fine sandstone and mudrock interbedded	Overbank deposits, Distal pro-deltaic to slope deposits
	**FA7:** Tuffaceous Mudrock	Fm, Fl	Very fine volcanic ash, yellowish, fine pencil weathering	clay to vf silt 0.5µm - 31µm	Tuffaceous siltstone/mudrock	Volcanic ash suspension settling with hemi-pelagic material

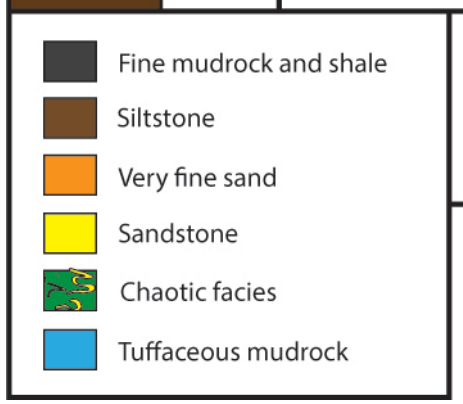

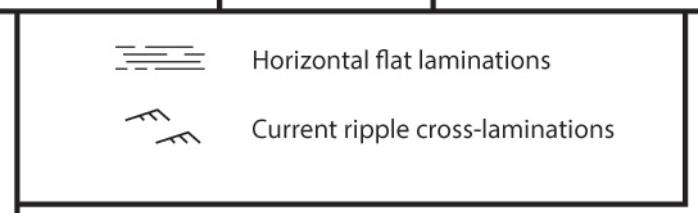

Table 5: Table indicating orders of bounding surfaces. 0^{th}-order bounding surfaces indicates suspension settling with no erosive features and occurs over a long period of time. 4^{th}-order surfaces represent highly erosive surfaces with rapid deposition. Modified from Miall (2010).

Rank of bounding surfaces	Characteristics of bounding surfaces	Depositional unit	Time scale of processes (yrs.)
0th -order	Lamination surface	Lamina	10^{-6}
1st -order	Set bounding surface	Ripple/Tabular (microform)	10^{-5} - 10^{-4}
2nd -order	Co-set bounding surface	Bed (mesoform)	10^{-2} - 10^{-1}
3rd -order	Convex-up macroform top minor channel scour	Macroform (channels architect)	10^{2}- 10^{3}
4th -order	Sharp erosional minor scour	Bed (macroform)	100 - 10^{1}

4.1.1 Facies Association 1 (FA1): Interlaminated siltstone and shale

Description:

This argillaceous facies association (Fig 4.1 A) commonly occurs in the Vischkuil, Laingsburg and Ripon formations, although relative abundance of FA1 within each formation differs. Identified facies codes in descending order of abundance include Fl, Fis, Fm and Fcr. This facies association exhibits a weathered dark grey (5YR 2/1) to unweathered black colour (N2) (Munsell). FA1 tends to weather negatively and fluctuates between platy and pencil weathering (size of weathered pieces varies between 2.0 cm and 10.0 cm depending on the grainsize of the rock).

Both upper and lower bounding surfaces are identified as 1^{st}-order and can exhibit normal grading from the lower to the upper bounding surface. Individual units are very thinly bedded (3.0 - 4.0 cm) to thinly laminated (0.5 - 3.0 cm) and are laterally continuous across outcrop, although highly variable (up to 100.0 km). FA1 commonly exhibits massive (Fm) or flat laminated (Fl), yet rare occurrences of 2^{nd}-order wavy bounding surfaces or current ripple laminations (Fcr) are observed. Bedded units are

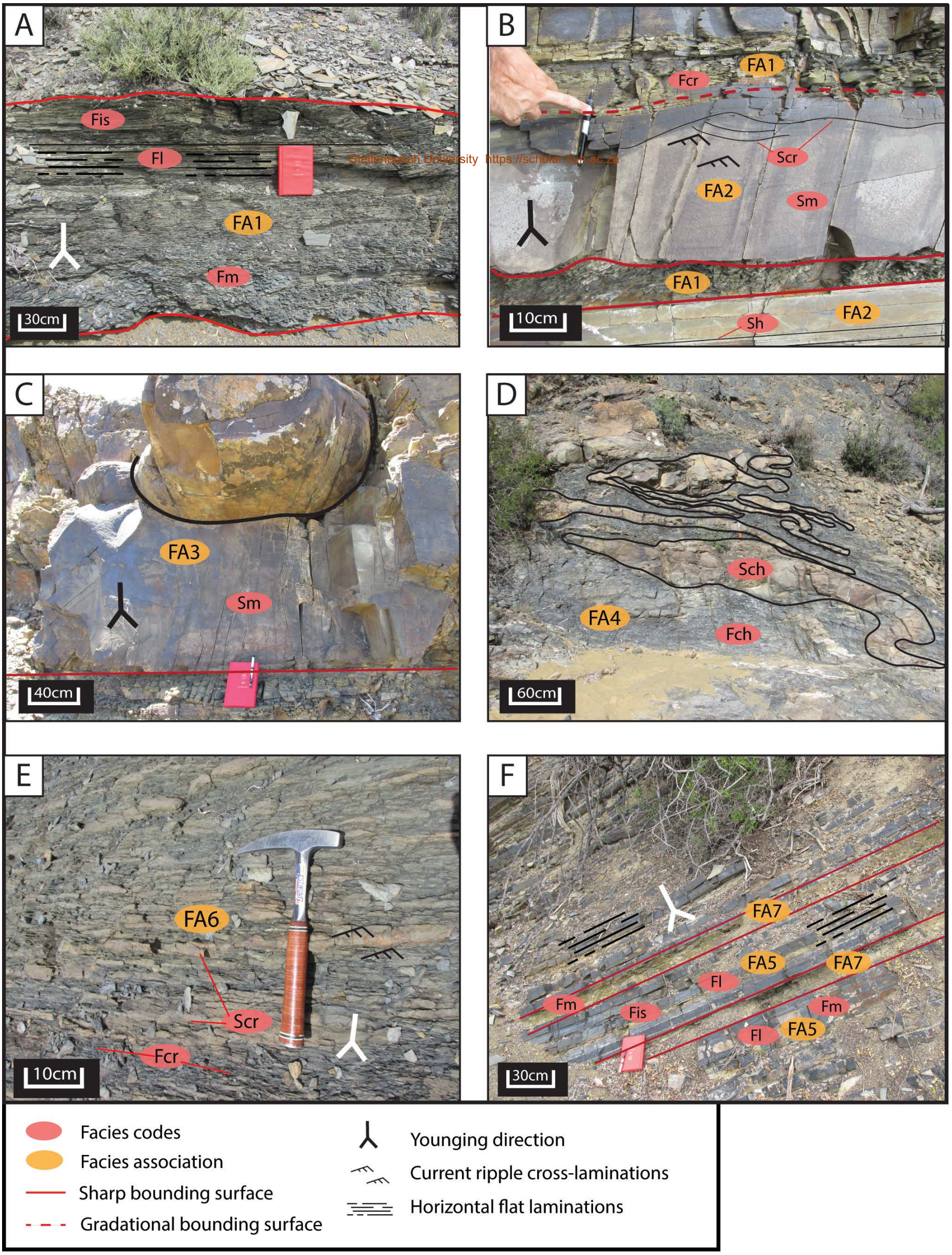

Figure 4.1: A) FA1 showing flat, finely-laminated layers of silt and shale. B) FA2 with ripple laminations close to the upper bounding surface and no internal sedimentary features close to the lower bounding surface. FA2 is interbedded with FA1. C) FA3 showing a massively bedded sandstone unit with an accentuated large-scale concretion. D) FA4 with slumped units of sandstone and mudstone. Deformation of sandstone units clearly visible. E) FA6, finely interbedded sandstone and mudrock rhythmite showing ripple laminae. F) FA5 interbedded with FA7 in the Colllingham Formation. FA7 exhibits a yellowish colour due to the abundance of volcanic ash.

characterized by silt and clay-size material (3.9 µm to 31.0 µm), whereas thinly-laminated units commonly consist of muds and clays (0.06 µm to 3.9 µm). Grading is commonly normal, but minor occurrences of reverse grading are observed. Rare occurrences of trace fossils may be present in the form of multiple epichnial grooves and horizontal burrows (*Cruziana* and *Nereites*). Trace fossils found closely fits descriptions of *Scolicia* and *Isopodichnus* described by Anderson (1974) in similar facies occurrences elsewhere in the basin. A few variations are found, but the most common are thin horizontal *Scolicia* grooves (1.0 - 2.0 mm in diameter) which occur as randomly orientated paths with no fixed movement direction (Fig 4.2 A). The second most occurring trace fossils are shallow wide (up to 1.0 cm) *Isopodichnus* epichnial grooves occasionally showing traction marks and maintain more directional pathways (Fig 4.2 B). These grooves can also exhibit menisci along the edges.

Interpretation:

This facies association was deposited by suspension settling of fine material during periods of low energy input into the basin as seen by the abundance of very fine-silt and clay sediments with mainly flat laminations (Fl). Environmentally, FA1 can be found in a number of settings, but the widespread depositional nature and lack of sedimentary features suggests a deep-marine or -lake environment. Within a deep basin setting the rate of sediment settling can be particularly low, because of extended periods of starved conditions (Stow et al., 1996; Arnott, 2010). These conditions increase bio-activity which ultimately leads to the preservation of trace fossils. The abundance of *Nereites* and occasional occurrence of *Cruziana* indicates abyssal plain conditions and supports low settling rates and starved periods. These starved periods can be short-lived, being interrupted by rapid deposition from turbidity currents, or long-lasting events forming thick packages of FA1 (Andersson & Worden, 2004). Occasionally, current flow can produce ripple cross-laminae, but quiet conditions and slight variation in size and composition of settling material mostly leads to horizontal flat laminations and thinly-bedded sheets as seen by the occurrence of 1st-order bounding surfaces. FA1 is commonly identified in most facies analyses done in the southern Karoo Basin by previous workers (Kingsley, 1981; Johnson, 1991; Grecula et al., 2003; Sixsmith et al., 2004; van der Merwe et al., 2009).

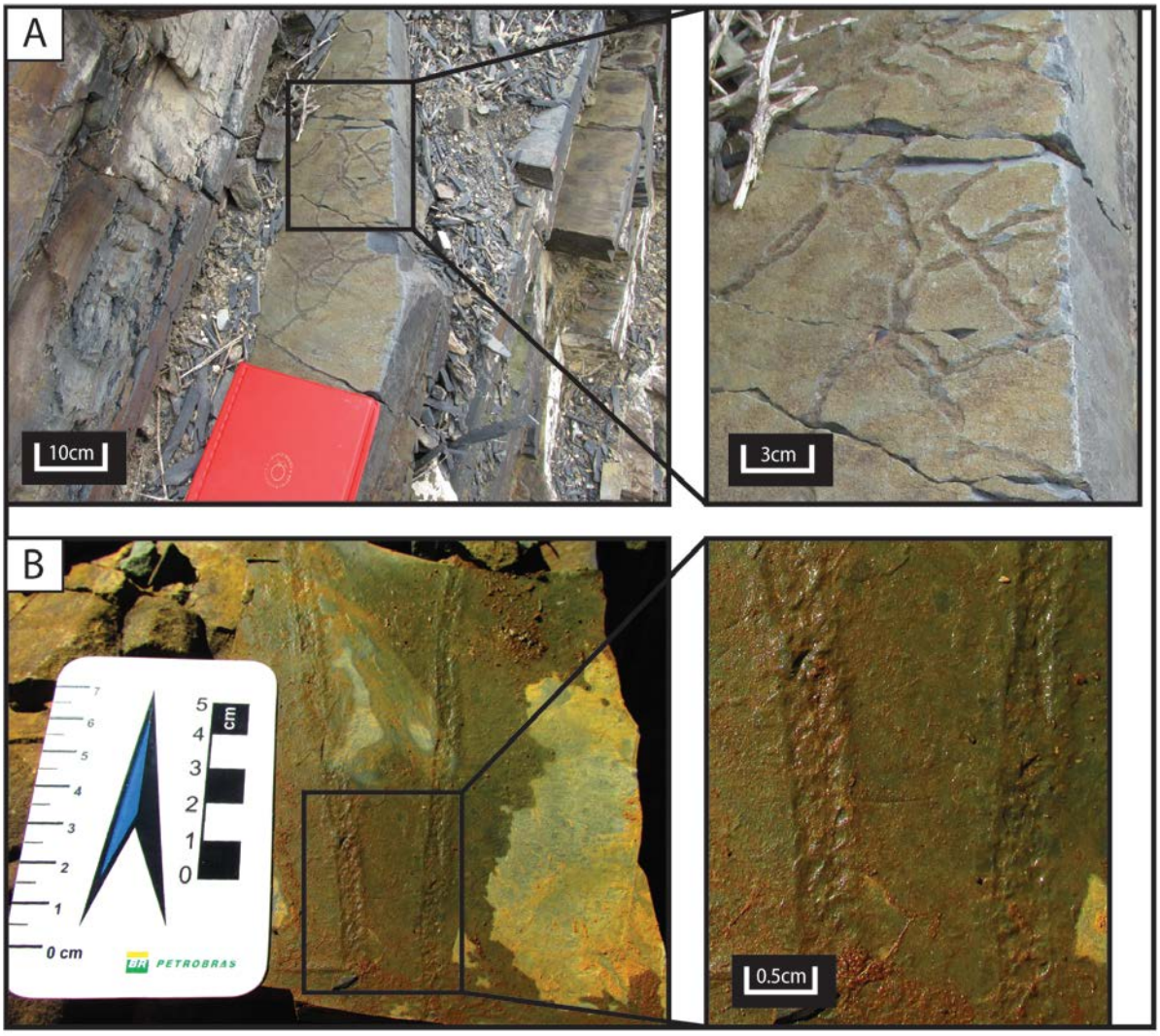

Figure 4.2: A) Trace fossils in the form of epichnial grooves (*Scolicia*) found in FA1, notice the conjugate patterns created by the pathways. They occur on the bedding plain of a siltstone bed. B) Two individual pathways of *Isopodichnus* maintaining the same direction within FA1. Both have distinct lateral bulges due to sediment being compressed to the side of the trails. Very small traction marks are observed within each trail.

4.1.2 Facies Association 2 (FA2): Thin-bedded sandstone

Description:

Beds are commonly thicker than 10.0 cm and do not exceed 1.0 m, therefor defined as thin-bedded sandstone. Ordinarily, beds of FA2 exhibit massive bedding (Sm), but current ripple laminae (Scr) (Fig 4.1 B), horizontal flat laminae (Sh) and dewatering structures (Sdw) are present. In rare instances climbing ripple laminae are also present (Fig 4.3 A). FA2 can vary from greyish brown to moderate brown (both unweathered and weathered), 5Y 3/2 to 5YR 3/4 (Munsell). Lower bounding surfaces are often 2^{nd}- to 4^{th}-order and can preserve sole marks (Ssc) such as groove and flute casts (Fig 4.3 C). Dewatering features can be visible (Fig 4.4 C). Clay clasts may also occur as rip-up clasts (Frip) within the bed. Upper bounding surfaces occasionally show wavy laminae and are 1^{st}- to 2^{nd}-order. Individual beds can have a lateral continuity of up to 10.0 km, with a few isolated beds exhibiting a lenticular geometry laterally not exceeding 5.0 m. FA2 comprises fine-grained sandstone to coarse-siltstone (0.03 mm to 0.25mm).

Interpretation:

This study has identified that the thin-bedded sandstone sheets (FA2) represent deposition from low density turbidity currents into the basin, commonly building the distal ends of turbidite fans (Sixsmith et al., 2004). Scour marks are induced by strong currents and commonly associated with massive beds (Stow et al., 1996; Arnott, 2010). Occasionally, this provides a good transport mechanism to deposit terrestrial material such as plant fragments and leaves, as well as fine-grained clasts assimilated during progression of the currents over semi-consolidated mud stratum. Beds displaying less lateral continuation can depict minor channeling within distal lobe migration. The presence of climbing ripples indicates rapid fall-out from suspension of fine- to very fine-sand during critical to super-critical flow velocity (Southard, 1991). The variance in climbing angle indicates different rates of suspension fall-out and bedload velocity (Jobe et al., 2012). The combination of Scr and Sh represents the Tc and Td divisions of the Bouma Sequence (Bouma, 1962).

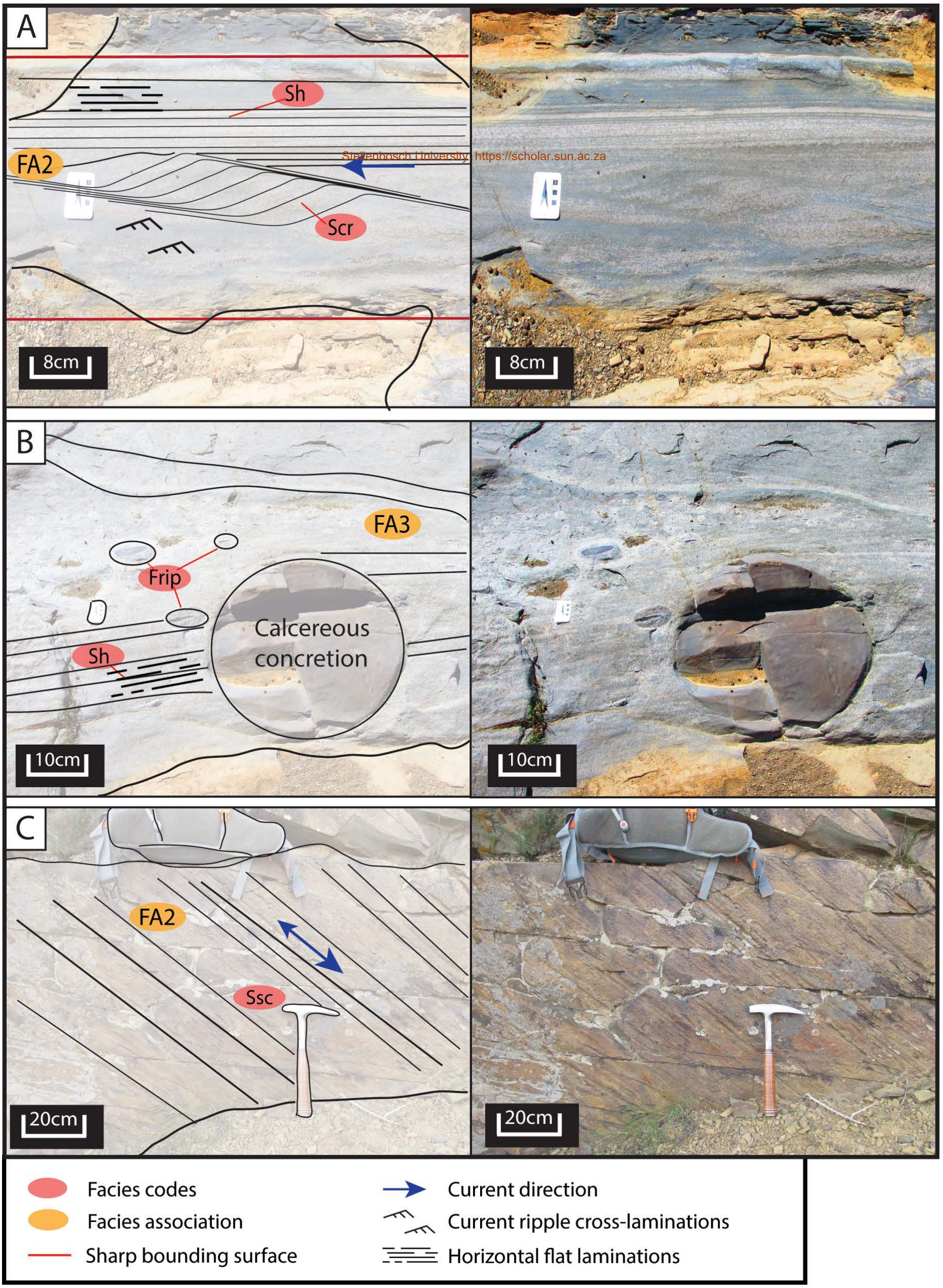

Figure 4.3: A) FA2 with climbing ripples directly overlain by flat laminations. Current direction indicated by arrow. B) FA3 containing calcareous nodular concretions. Clay rip-up clasts are present towards the lower bounding surface of the bed. C) View is looking onto the sole of a FA2 bed with groove casts. Current orientation can be in either direction parallel to the groove casts. Lines indicates orientation of groove casts.

4.1.3 Facies Association 3 (FA3): Thick-bedded sandstone

Description:

This facies association consists mainly of thick-bedded sandstones which exceed 1.0 m in thickness and can extend to about 3.0 m in thickness. It is not uncommon for these beds to amalgamate and form thicker packages. Most beds of FA3 are massively bedded (Sm) (Fig 4.1 C) containing little to no internal sedimentary features, apart from flat laminations (Sh) at a few localities. Included in these sandstones are rip-up clay clasts (Frip) and calcareous nodules and concretions (Fig 4.3 B). Some clasts are preserved within these concretions. FA3 occurs in colours varying from moderate brown (weathered) to greyish brown (unweathered), 5YR 4/4, 5Y 3/2 and 5YR 3/4 (Munsell).

The lower bounding surface is very erosive and sharp (3rd- to 4th-order) with groove and load casts (Ssc) readily present. At many instances, the upper bounding surface grades into finer sediments showing 1st- to 2nd-order bounding surfaces. Most beds can extend laterally for up to 5.0 km kilometers, but in a few places, have a lateral extent of only a few hundred meters. Beds generally consist of fine- to medium-grained sand (0.12 mm to 0.5 mm). The rip-up clay clasts rarely occur towards the base of these beds. In most beds, clay clasts can be observed towards the middle and towards the upper bounding surface occasionally co-occurring with plant fragments.

Interpretation:

Deposition from high-density turbulent flow is required to produce thick packages of sandstone in a deep basin setting (Stow et al., 1996; Arnott, 2010). The massive nature, grainsize, normal grading and thickness of FA3 represents the base of a typical Bouma Sequence (known as the Ta section) (Bouma, 1962) assigned to sand-rich turbidites. In the case of beds with very minor lateral continuity, it is possible that these constitute channel-fills caused by channel erosion into substrate. Loading occurs due to rapid deposition with occasional scour marks initiated by the strong current produced during a turbidity event (Arnott, 2010). Clay clasts ripped up by the turbulent flow of the current appears to have been rafted by the matrix allowing the clasts to be preserved in the center or close to the upper bounding surface of a FA3 bed. Calcareous nodules and concretions, in some cases, appear to be

formed through diagenetic processes by the nucleation of some of these clasts and is also generally observed in the center or close to the upper bounding surface of these beds (Sixsmith et al., 2004). FA3 represents more proximal deposition of turbidite fans due to the abundance of sandy sediments and tabular to channelized lobe migration patterns.

4.1.4 Facies Association 4 (FA4): Chaotic mudrock

Description:
This facies association is mostly found in the Vischkuil and Ripon formations. The dominant feature of FA4 (Fig 4.1 D) is the presence of chaotic depositional features such as convolute laminations and dewatering structures in very fine deformed mudstone (Fch) (Fig 4.4 A) as well as occasional deformed strata of fine- to medium-grained sandstone (Sch) (Fig 4.4 E). Slump structures include chaotic laminae and convolution of finer material and sheath folding of coarser material. Occasionally localized horizontal flat laminations (Fl) occur.

The lower bounding surface may show detachment and erosive features (4^{th}-order) whereas the upper bounding surface is gradational. Slumped deformed strata can extend laterally for up to 50.0 km and the thickness of slump packages can vary from 1.0 m to 30.0 m. Detachment blocks are also present in the larger units of FA4. This facies association rarely preserves any primary internal sedimentary features such as ripple laminae. Grainsize can vary from very fine-silt (3.9 µm) to fine-sand (125.0 µm). Two types of FA4 have been identified; sand-rich facies (Type-1) and sand-poor facies (Type-2). Type-1 is commonly recognized by more than 40% very fine- to fine-sand (63.0 µm to 125.0 µm) in the form of sandstone layers or sandy matrix within FA4. Type-2 is dominated by silt and mud-rich sediments (<31.0 µm) showing convolute laminations. The presence of large blocks is observed in some Type-2 FA4 deposits (Fig 4.4 D). The two types can co-occur, but Type-2 is dominant in the Ripon Formation, whereas Type-1 is commonly found in the Vischkuil Formation and occasionally in the upper Wonderfontein Member of the Ripon Formation.

Interpretation:

Slope instability is a common occurrence in slope to deep basin settings (Arnott, 2010) where slight disturbance of sediments positioned at an angle can cause these sediments to slump down into the basin (Mason et al., 2002; Frey-Martinez et al., 2005; Moscardelli & Wood, 2008). Sediments of FA4 were likely semi-consolidated and exhibit ductile deformation due to their waterlogged state during emplacement. Mass transport complexes (MTC's) are indications of events of mass-wasting processes on instable water-saturated muddy submarine slope environments (van der Merwe et al., 2009), but can also be induced on the basin floor by overlying debris flows (van der Merwe et al., 2010). The combination of Type-1 facies and the occasional presence of overlying debritic material support a distinct occurrence of debrite induced deformation. The abundance of thin deformed sandstone within Type-1 indicates a setting where substrate included thin bedded sandstone sheets. The abundant fine-grained material of Type-2 suggests slope instability during periods of starvation on the slope to basin floor, while sediments build up on the shelf. Detachment of large blocks suggests semi-consolidated to consolidated sediments rapidly initiated by mass transport. Slump deposits can provide ample evidence for instable slope conditions and events leading to MTC's.

4.1.5 Facies Association 5 (FA5): Siliceous Siltstone

Description:

FA5 (Fig 4.1 F) is most abundantly present in the Collingham and lower Vischkuil formations. Internal sedimentary features are not commonly observed and most units are massively bedded (Fm); only occasional evidence of horizontal flat laminations (Fl) are present. Little variance is seen between weathered and unweathered outcrop with regards to colour, maintaining a dusky brown 5YR 2/2 hue. The upper and lower bounding surfaces of FA5 are mostly sharp 2nd-order with occasional normal grading visible. Beds of FA5 is generally no thicker than 30.0 cm and are laterally extensive reaching tens of kilometers as thinly interbedded sheets (Fis). FA5 varies in grainsize from very fine-silt (3.9 µm) to coarse-silt (31.0 µm), but consists a large proportion of chert cement. Trace fossils in FA5 are abundant and occur on bedding surfaces as epichnial grooves and burrows with the most common

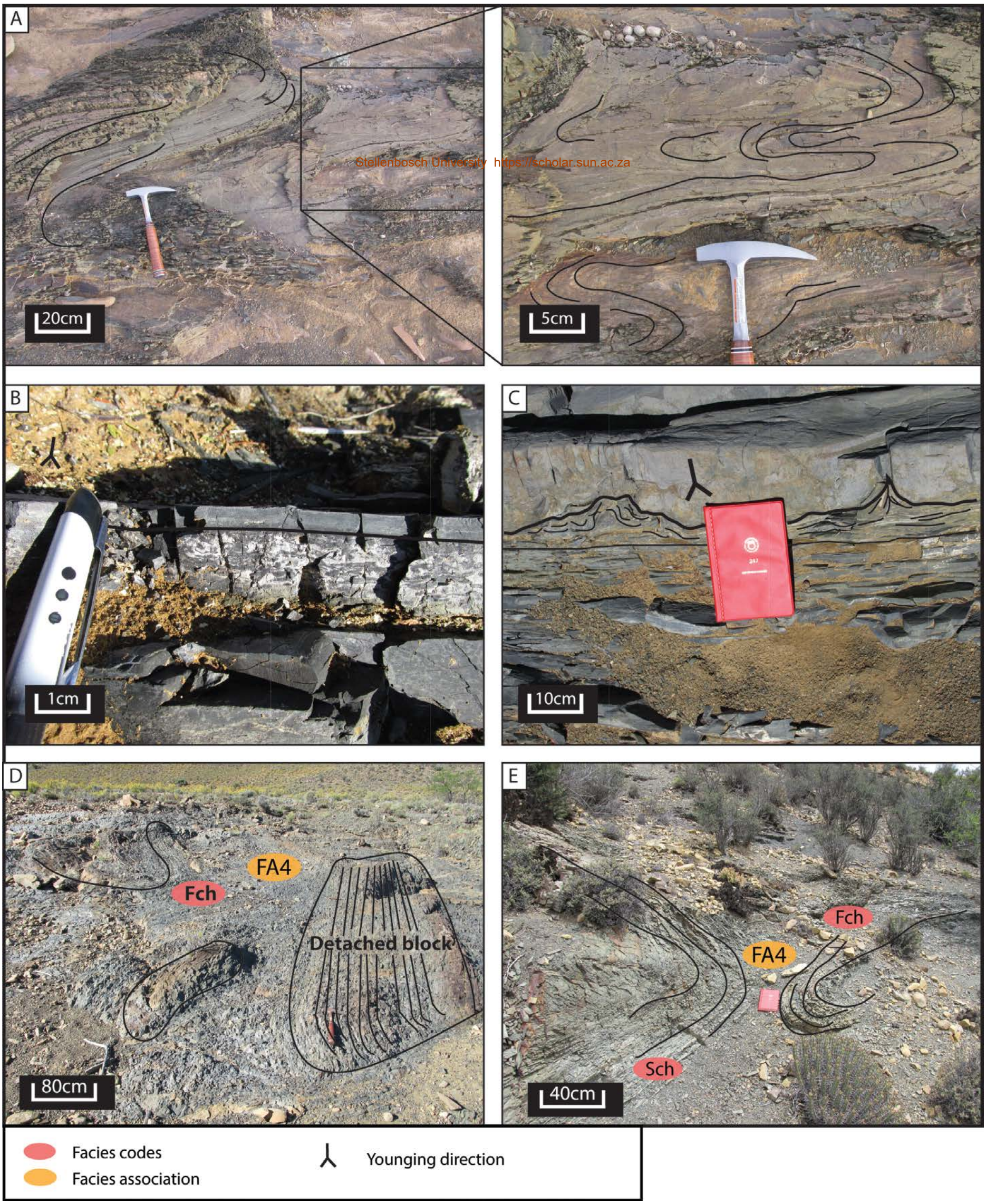

Figure 4.4: A) Chaotic convolute laminations in a Type-2 deformed strata. The dominant lithofacies is mudrock to fine-siltstone. B) very fine layer of micro soft-sediment deformation. Notice the horizontal fine-grained layer to the top with a chaotic mix of mud and sand as an underlying layer. C) Soft-sediment deformation caused by the overlying sandstone forming convolute laminations to occur at the upper bounding surface of the mudrock. Load features are commonly observed at the base of the sandstone. D) Type-2 FA4 with entire detached blocks of FA6 still maintaining its thinly bedded heterolithic nature. These blocks occur within fine-grained chaotic mud. E) Sheath folds within Type-2 FA4.

being thin, randomly orientated, grooves (smaller than 1.0 mm in diameter). These grooves commonly create semi-conjugate patterns and are from the *Nereites* assemblage (Fig 4.2 A).

Interpretation:
This siliceous facies association signifies a calm, low energy depositional environment with evidence of higher silica content (Johnson et al., 2006). FA5 favors abyssal plain benthic conditions and rarely indicates current influences. The widespread extent of thinly bedded sheets indicates that conditions were consistent throughout the basin plain with minimal basin-floor topography. The calm conditions also helped provide a stable environment for organisms to thrive (Anderson, 1974). The lack of coarser-grained material implies a more distal deposition of material away from any submarine fan influences.

4.1.6 Facies Association 6 (FA6): Finely interbedded sand and mud

Description:
This facies association (Fig 4.1 E) consists of heterogenic regularly alternating layers of sandstone and mudstone. The common facies codes observed in FA6 are Scr, Fcr, Sh, Fl and Sdw. FA6 exhibits sharp lower and upper bounding surfaces of 1st- to 2nd-order and do not seem to show erosional features. Wavy bedding is fairly common within FA6 between bounding surfaces of sandstone and mudrock. Layers vary between laminae (2.0 cm) and bed scale (10.0 cm) portraying a regular thickness between alternating sheets.

A distinct moderate brown (5YR 4/4) colour is observed in weathered and unweathered layers of the sandstone lithology, while the mudrock commonly exhibits a brownish grey (5YR 4/1) weathered and brownish black (5YR 2/1) unweathered colour. Current ripple laminae (Scr and Fcr) are dominant in FA6 and displays regular fluctuations in current direction as well as flow energy. These ripples commonly display a low climbing angle (<5°). The dewatering features (Sdw) vary from mostly slight convolution between laminae to rare occurrences of dewatering pipes. Occasionally ripples are

present on the upper surfaces of sandstones. The grainsize varies between fine-sand (250.0 µm) to very fine-silt and clay (2.5 µm).

Interpretation:
The heterolithic nature of FA6 suggests regular fluctuations in depositional energy. The ripple cross-laminae with a low climbing angle together with the thin bedded nature of these layers indicates slow moving low volume flows that represents the distal setting of overbank deposits. These flows can be widespread depending on the nature of the channelized turbidity current (Sixsmith et al., 2004, Jobe et al., 2012). The high concentration of fine-sand and constant thickness of alternating layers suggests a proximal fan setting with constant input from overbank flows.

4.1.7 Facies Association 7 (FA7): Tuffaceous mudrock

Description:
FA7 is typically limited to the Collingham Formation and is rarely observed within the Ripon, Laingsburg and Vischkuil formations (Fig 4.1 F). Occasionally horizontal flat laminations (fl) occur; little to no internal structures are preserved leaving FA7 massively bedded (Fm), but highly susceptible to weathering. Bounding surfaces present a gradational nature but can display a sharp upper bounding surface subject to the overlying unit (1st- to 2nd-order). The lower bounding surface are more commonly sharp. The most distinctive feature of FA7 is the presence of fine glassy volcanic ash shards (observed under a hand-lens) and K-Bentonite (Potassium Bentonite) composition. This composition gives FA7 a distinct yellowy orange colour (10YR 6/6, unweathered), but a dark yellowish brown (10YR 4/2, weathered) colour. FA7 exhibits pencil weathering with very fine shards no longer than 2.0 cm. Layers are generally of laminae scale (1.0 - 3.0 cm), but in some cases layers can preserve thicknesses of 20.0 cm. In-field these layers mostly occur as thin sheets. Grainsize varies between clay (0.5 µm) to coarse-silt (31.0 µm) with most grains being clay (0.5 µm) to very fine-silt (4.0 µm).

Interpretation:
The fine material and lack of internal sedimentary features of FA7 is the result of very low energy deposition caused by suspension settling (Stow et al., 1996; Arnott, 2010). The presence of volcanic

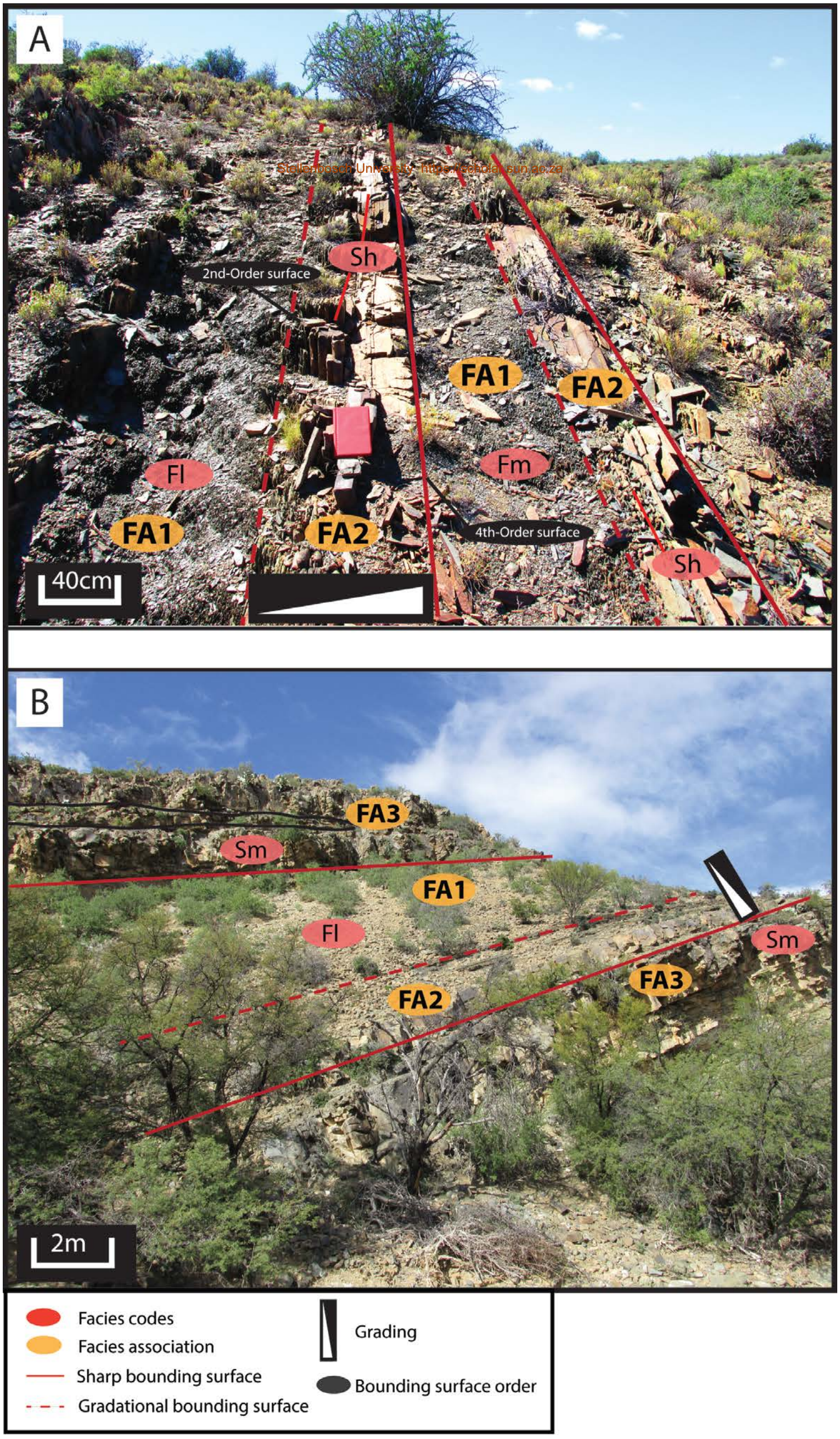

Figure 4.5: A) FA1 interbedded with FA2. Normal grading is present within FA2 with a sharp lower bounding surface. Upper part of the stratigraphic succession is on the left. B) Association of FA1,2 and 3 with a fining-up depositional nature. FA3 exhibits occasional channelling within amalgamated beds.

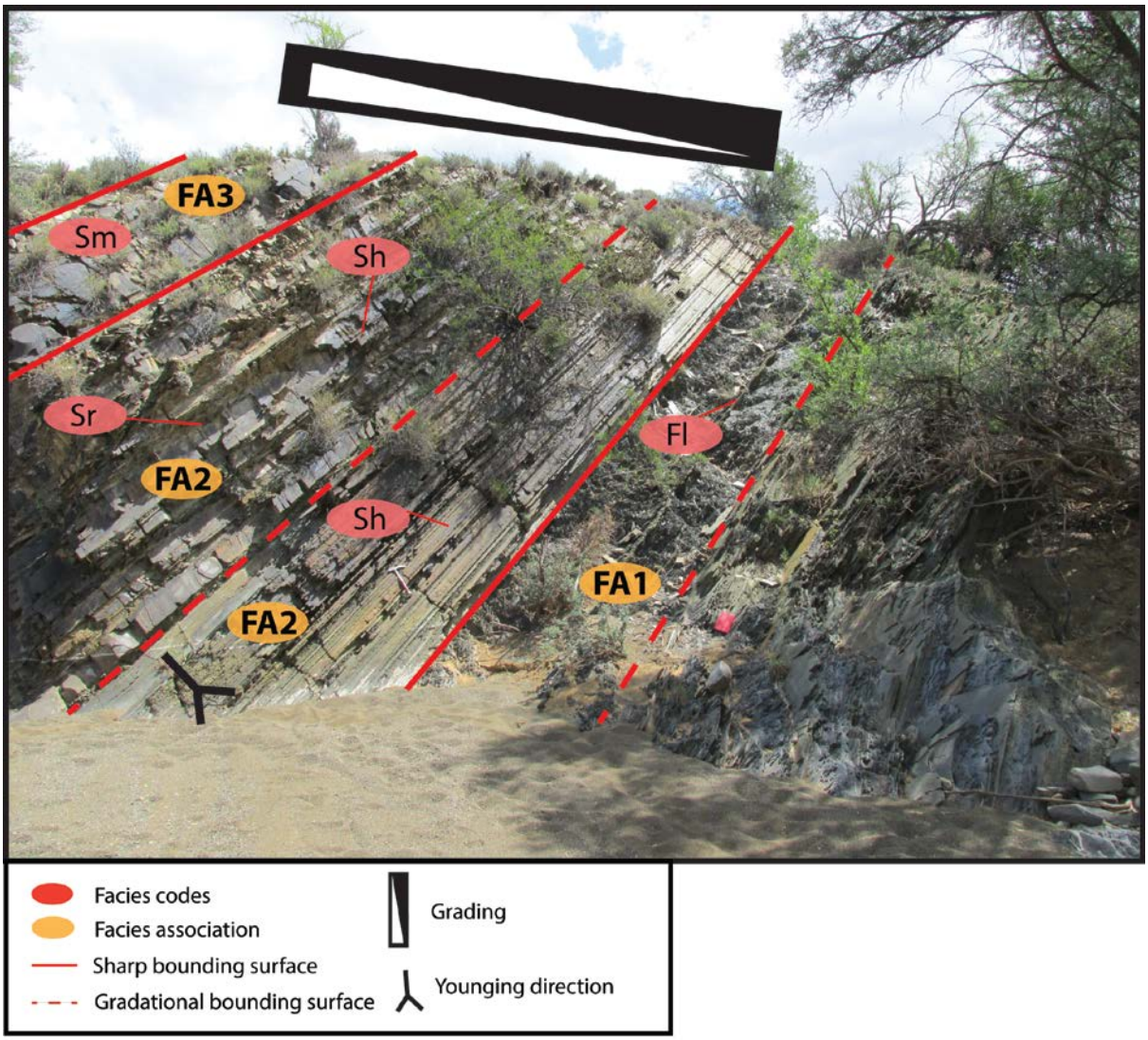

Figure 4.6: Interbedded units of FA1 and FA2 showing a reverse grading to a thicker unit of FA3. The sedimentary features grade form flat laminated to current ripple laminae.

ash provides evidence of volcanic activity occurring during, or just prior to deposition of FA7 (Viljoen, 2004). Due to the fine-grained nature of FA7, the volcanic ash likely settled on the basin floor with pelagic material in periods of calm conditions (Fildani et al., 2007). The occurrence of this facies association in discrete horizons makes it evident that the volcanic activity was restricted to short periods.

4.2 Sedimentary Petrography

Sixteen thin-sections from different stratigraphic units were prepared and studied (Fig 4.7) (Table 6). One sample was obtained from the Vischkuil Formation, three samples from the Laingsburg Formation and twelve samples from the Ripon Formation. Samples do not exceed a grainsize of 0.5 mm (medium-sand). Common mineral grains for all samples are mono-crystalline quartz, plagioclase feldspar, K-feldspar, micro-crystalline quartz (chert) as well as minor mica minerals, iron-oxides, and occasional zircons.

4.2.1 Vischkuil Formation

4.2.1.1 WK01

A sample of a silty to very fine-grained sandstone was collected from the Vischkuil Formation (Fig 4.8 C). Grainsize ranges from 0.03 mm to 0.2 mm and grains are generally angular and moderately sorted. Grains and cement are of equal proportions, each constituting 35% of the sample with matrix representing about 30%. Alterations include sericite on the K-feldspars as well as calcitized plagioclase feldspars. Perthitic textures are also visible in K-feldspars. 59% of feldspars are plagioclase and 41% are K-feldspar. Lithic fragments are also fairly common in the form of poly-crystalline quartz, sedimentary fragments and occasional volcanic fragments. This sample has QFL ratio of 17:49:34. Authigenic quartz are generally present as a constituent of the cement. The most common cement type is sparitic calcite with minor chert also visible.

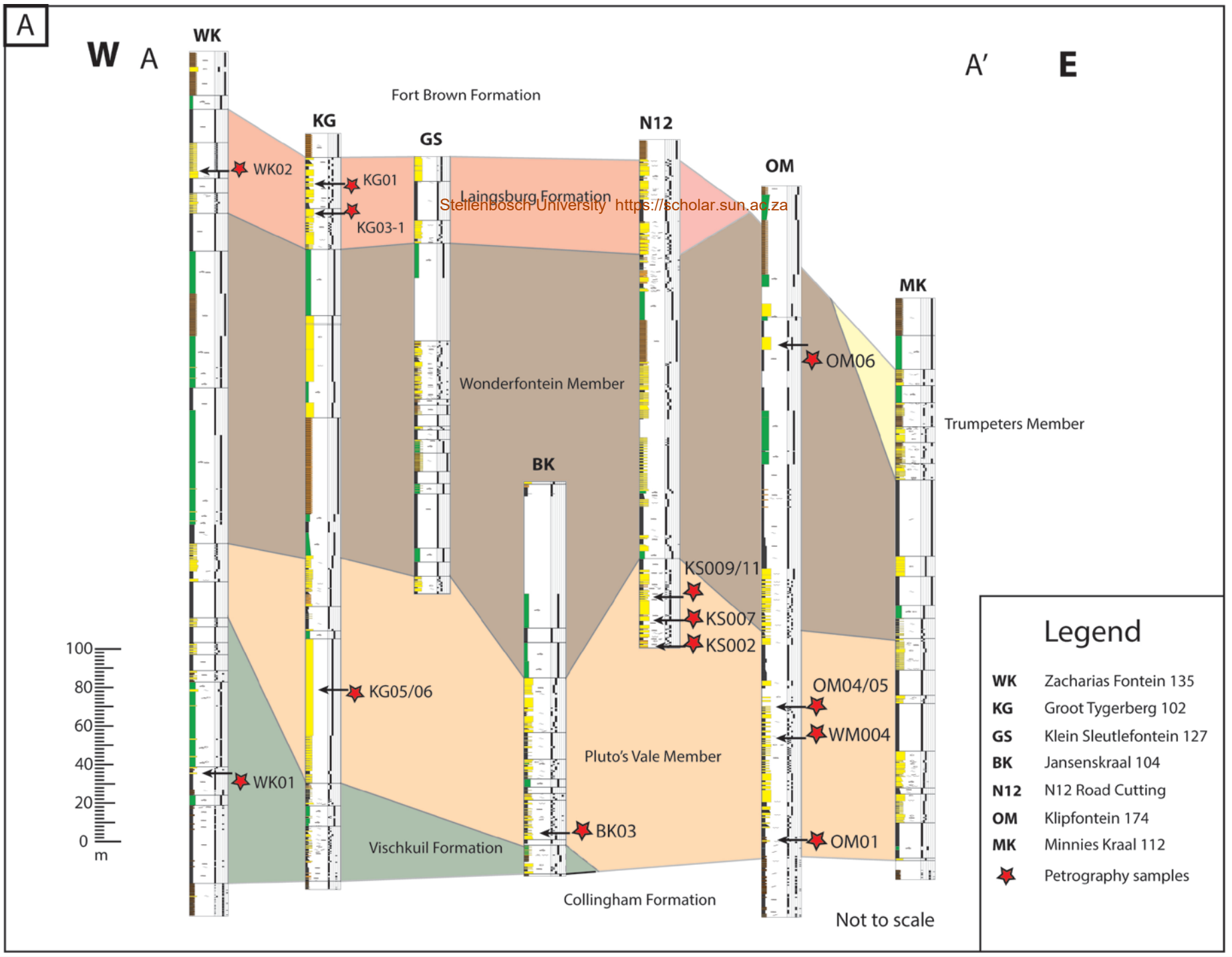

Figure 4.7: Stratigraphic sections (horizontally not to scale) showing the position of each sample used for petrographic studies.

Table 6: Geographic location and stratigraphic position of each sample used for sediment petrography.

Sample	Stratigraphic horizon	Farm Name	Latitude	Longitude
WK01	Middle Vischkuil Fm	Zacharias Fontein 135	S 33.21093°	E 22.05490°
KG01	Upper Laingsburg Fm	Groot Tygerberg 102	S 33.11350°	E 22.35134°
KG03-1	Lower Laingsburg Fm	Groot Tygerberg 102	S 33.09889°	E 22.36170°
WK02	Lower Laingsburg Fm	Zacharias Fontein 135	S 33.20856°	E 22.05337°
OM01	Lower Pluto's Vale M	Klipfontein 174	S 33.28221°	E 22.77908°
BK03	Lower Pluto's Vale M	Jansenskraal 104	S 33.11663°	E 22.40402°
WM004	Middle Pluto's Vale M	Minnies Kraal 112	S 33.27987°	E 22.76554°
OM04	Middle Pluto's Vale M	Klipfontein 174	S 33.28345°	E 22.78037°
OM05	Middle Pluto's Vale M	Klipfontein 174	S 33.28345°	E 22.78032°
KG05	Middle Pluto's Vale M	Groot Tygerberg 102	S 33.12811°	E 22.34262°
KG06	Middle Pluto's Vale M	Groot Tygerberg 102	S 33.12811°	E 22.34262°
KS002	Upper Pluto's Vale M	N12 Road Cutting	S 33.12350°	E 22.53835°
KS007	Upper Pluto's Vale M	N12 Road Cutting	S 33.12148°	E 22.53840°
KS009	Upper Pluto's Vale M	N12 Road Cutting	S 33.12125°	E 22.53838°
KS011	Upper Pluto's Vale M	N12 Road Cutting	S 33.12125°	E 22.53838°
OM06	Upper Wonderfontein M	Klipfontein 174	S 33.28428°	E 22.77593°

4.2.2 Laingsburg Formation

4.2.2.2 KG01 and KG03-1

KG01 was obtained from the upper units of the Laingsburg Formation and KG03-1 stratigraphically slightly lower in the Laingsburg Formation (Fig 4.9). Grains vary in size ranging from 0.3 mm to 0.05 mm. Sorting is moderate to poor. Grains also show very angular boundaries, but larger grains appear rounded and exhibits some reworking. The sample comprises 20% muddy matrix with only 15% of the sample occupied by cement. Lithic fragments consist mainly of sedimentary and poly-crystalline quartz. With no apparent pore spaces within sample KG01, the grains contribute to 65% of the visible sample. 27% of feldspars are plagioclase whereas 73% are K-feldspar. Sample KG01 has a QFL ratio of 30:48:23. Matrix is dominated by detrital material, but shows some pseudo-matrix features. The dominant cement present is calcite, mostly in the form of micrite.

About 60% of sample KG03-1 comprises grains and matrix makes up 25 %. The cement represents 15% with no pore spaces visible. 20% of the feldspars are plagioclase and 80% are K-feldspar. The QFL ratio for sample KG03-1 is 32:40:29. Cement consists mostly of fine calcite and grains do not exhibit much alteration.

4.2.2.1 WK02

This sample is from the lowermost stratigraphic unit of the Laingsburg Formation (Fig 4.8 A). It has a grainsize of 0.45 - 0.2 mm, making it fine- to medium-sand. Grains are angular and samples are moderately to poorly sorted. 55% of the sample is made up of grains while 30% is a mixture of detrital and pseudo-matrix and 15% authigenic cement. No pore spaces were observed. Grains are not as altered as WK01, but occasional calcitization of plagioclase feldspars are visible. 27% of feldspars in this sample are plagioclase and 73% are K-feldspars. A point count generated a QFL ratio of 25:40:36. The main cement present is calcite and chlorite (glauconite) with minor chert cement.

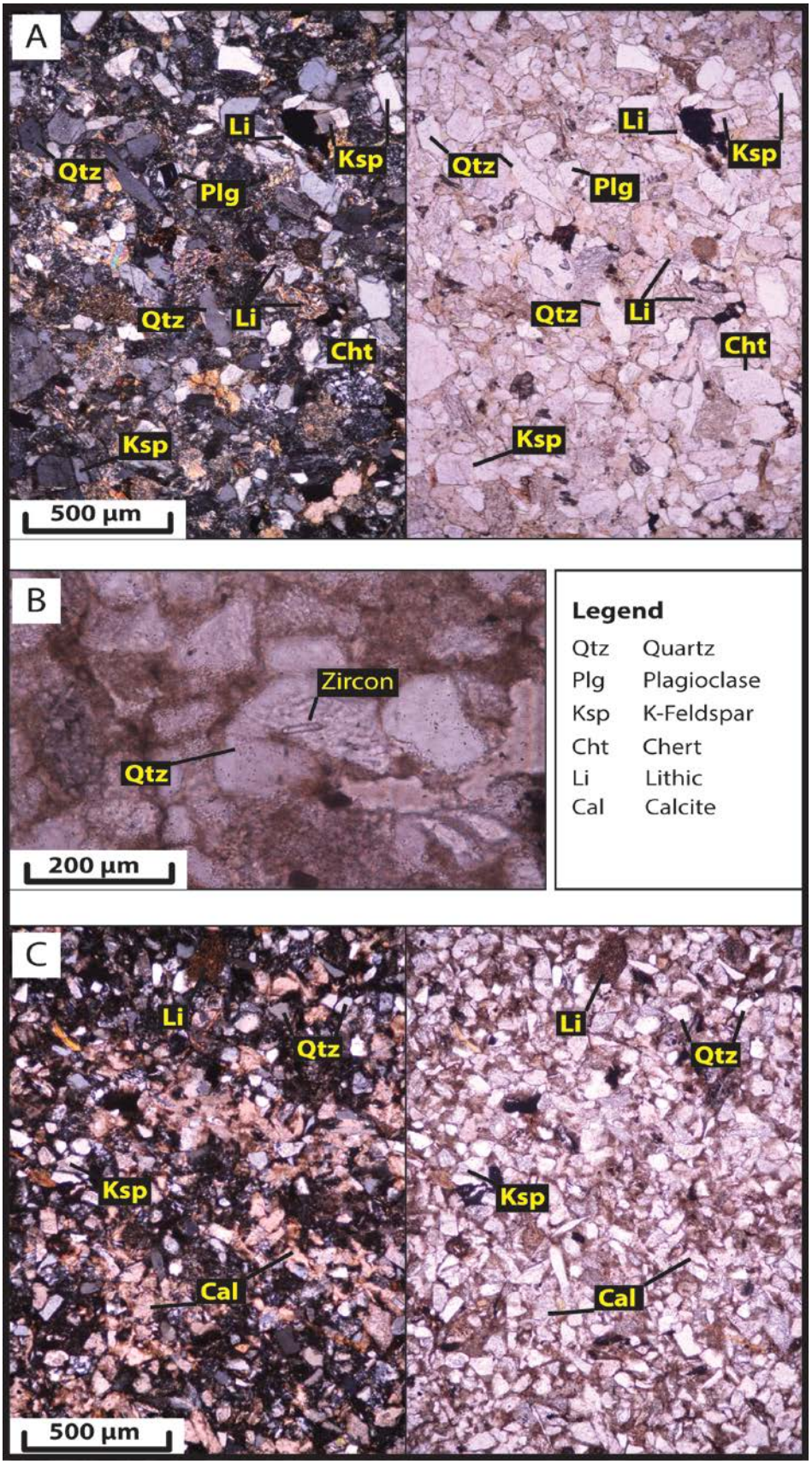

Figure 4.8: Sandstone samples WK01 and WK02. A) Sample WK02 from Laingsburg Formation under XPL and PPL. Fine- to medium-sand grainsize showing alteration of occasional K-feldspar grains. K-feldspar more abundant. B) Euhedral Zircon crystal encased in a Quartz grain from Sample WK01 under PPL. C) Sample WK01 from Vischkuil Formation under XPL and PPL. Finer-grained sediments with high level of alteration. Calcite overgrowth of feldspars common.

4.2.3 Ripon Formation

4.2.3.6 OM01

Sample OM01 is from a sandstone from the lower Ripon Formation (Pluto's Vale Member) with grainsize varying between 0.35 mm and 0.1 mm (very fine- to medium-sand). Grains are sub-angular to angular and are moderately to poorly sorted. About 55% of the sample comprises grains with 35% matrix and 10% cement. Feldspar grains are highly altered to sericite. Only 9% of the feldspars in this sample are plagioclase and 91% are K-feldspar. The point count showed a ratio of 11:44:45. The cement is made up of calcite and minor chert. The sample contains a calcite separation growth vein 0.5 mm thick and a minor quartz vein 0.3 mm thick. The calcite separation growth vein comprises euhedral sparite crystals.

4.2.3.2 BK03

This sample is obtained from a calcareous concretion from the lowermost Ripon Formation and is dominated by secondary sparite cement. Grains constitute 35% of the observable sample and vary in size from 0.45 mm to 0.15 mm (fine- to medium-sand). Grains are angular to very angular and contribute to the sample being moderate to poorly sorted. The cement comprises 38% of the sample and is occasionally introduced as calcite separation growth veins. 27% of the sample consists of very fine-grained matrix. 49% of the total feldspars are plagioclase and 51% are K-feldspar. The QFL ratio is 22:34:44.

4.2.3.9 WM004

This sample represents a sandstone unit from the lower Ripon Formation (Pluto's Vale Member) (Fig 4.10 A). Grains are between 0.5 mm and 0.1 mm (medium-sand to very fine-sand) and are sub-angular. The sample is moderately to poorly sorted. About 70% of the sample consists of grains while 20% consists of matrix. The cement is predominantly calcite and comprises 7% of the sample while pore spaces constitute 3%. Alteration of plagioclase feldspars are visible in the form of calcitization (Fig 4.10

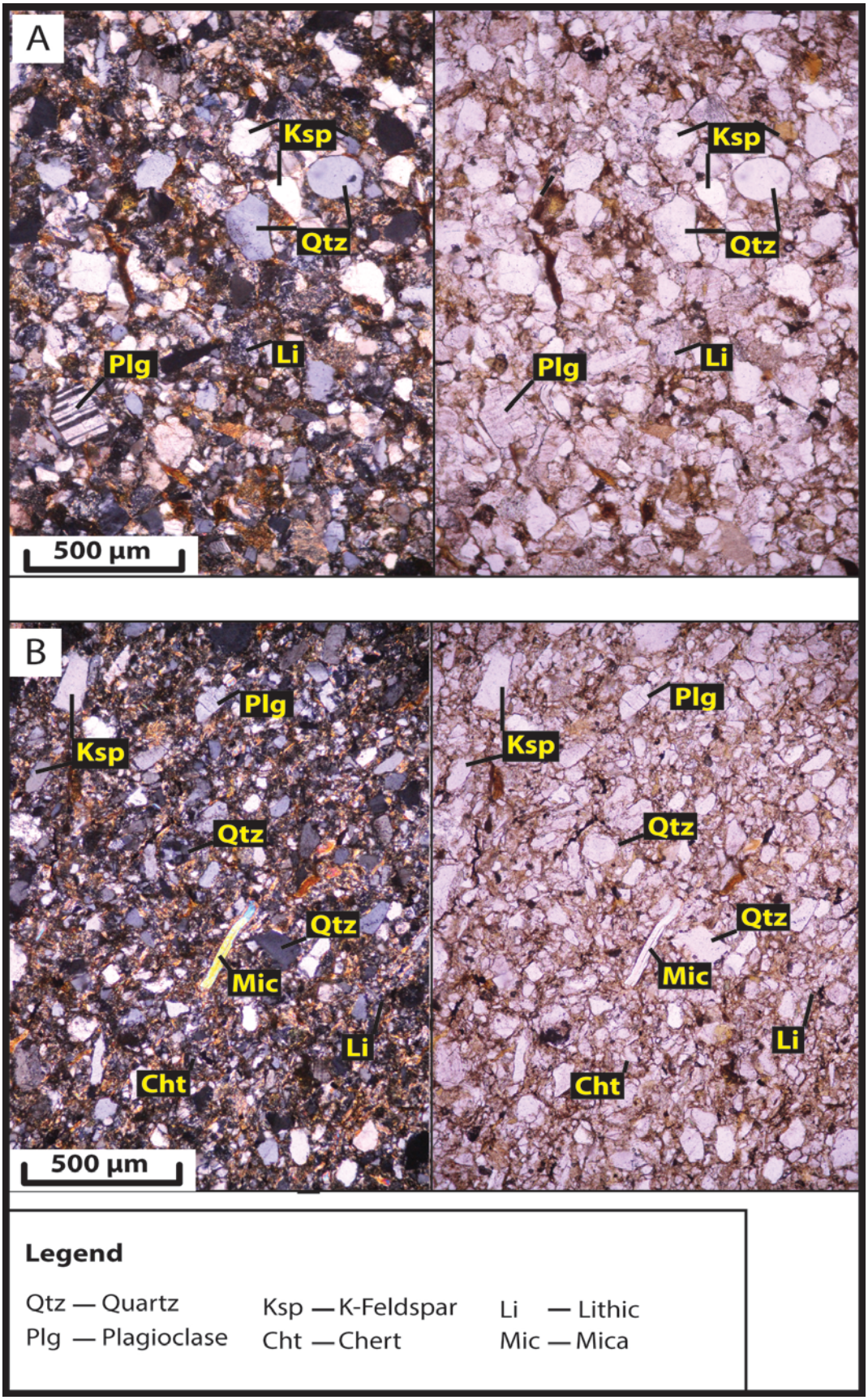

Figure 4.9: Sandstone Samples KG01 and KG03-1. A) Sample KG01 showing fine- to medium-grained sand under XPL and PPL. Sub-angular to angular plagioclase feldspar with sub-rounded quartz grains. Abundant feldspars. B) Sample KG03-1 with muscovite grain and abundant quartz and feldspar grains under XPL and PPL.

B). 60% of the feldspars are plagioclase and 40% are K-feldspar. The sample has a QFL ratio of 16:36:48. A 1.0 mm thick calcite separation growth vein is present in the thin section which consists of sparitic calcite crystals with occasional hexagonal grown quartz crystals (Fig 4.10 C).

4.2.3.7 OM04 and OM05

Sample OM04 is from a debrite layer overlying a sandstone (represented by sample OM05) in the lower Ripon Formation. Grains vary between 0.5 mm (medium-sand) and 0.1 mm (very fine-sand) and are angular to sub-rounded. Both samples have a moderate to poorly sorted nature. Grains in sample OM04 represent 75% of the sample while the matrix comprises 20% and cement 5%. Pore spaces are rare, contributing about 1% of the sample. Sample OM04 contains clay clasts no larger than 2.0 mm which show a flattened elongate geometry. The clay clasts consist of 60% matrix and 40% grains. Grains within the clay clasts do not exceed 0.05 mm in size (medium-silt and smaller). Some grains underwent micritization. 52% of feldspar is plagioclase and 48% K-feldspar. The QFL ratio for sample OM04 is 18:29:54. The cement is dominated by micritic calcite.

For sample OM05, grains comprise about 40%, the cement is about 35%, and matrix 25% of the sample. 41% of the feldspars are plagioclase and 59% are K-feldspar. The QFL ratio of sample OM05 is 13:44:43 as per point count. Sparite occurs within the primary porosity while the micrite cement seems to have a preferred orientation/foliation. Alteration of grains also favor this preferred orientation.

4.2.3.1 KG05 and KG06

Samples KG05 and KG06 are from a thick sandstone package within the Wonderfontein Member (Ripon Formation) and have a grainsize varying between 0.4 mm and 0.05 mm (coarse-silt to medium-sand). Grains are generally sub-angular to angular and exhibit a moderate to poor sorting. On millimeter scale, the samples have a mottled texture where blotched areas contain less altered mud and can be around 4.0 to 5.0 mm. Sample KG05 comprises 5% cement, 25% is a mixture of authigenic

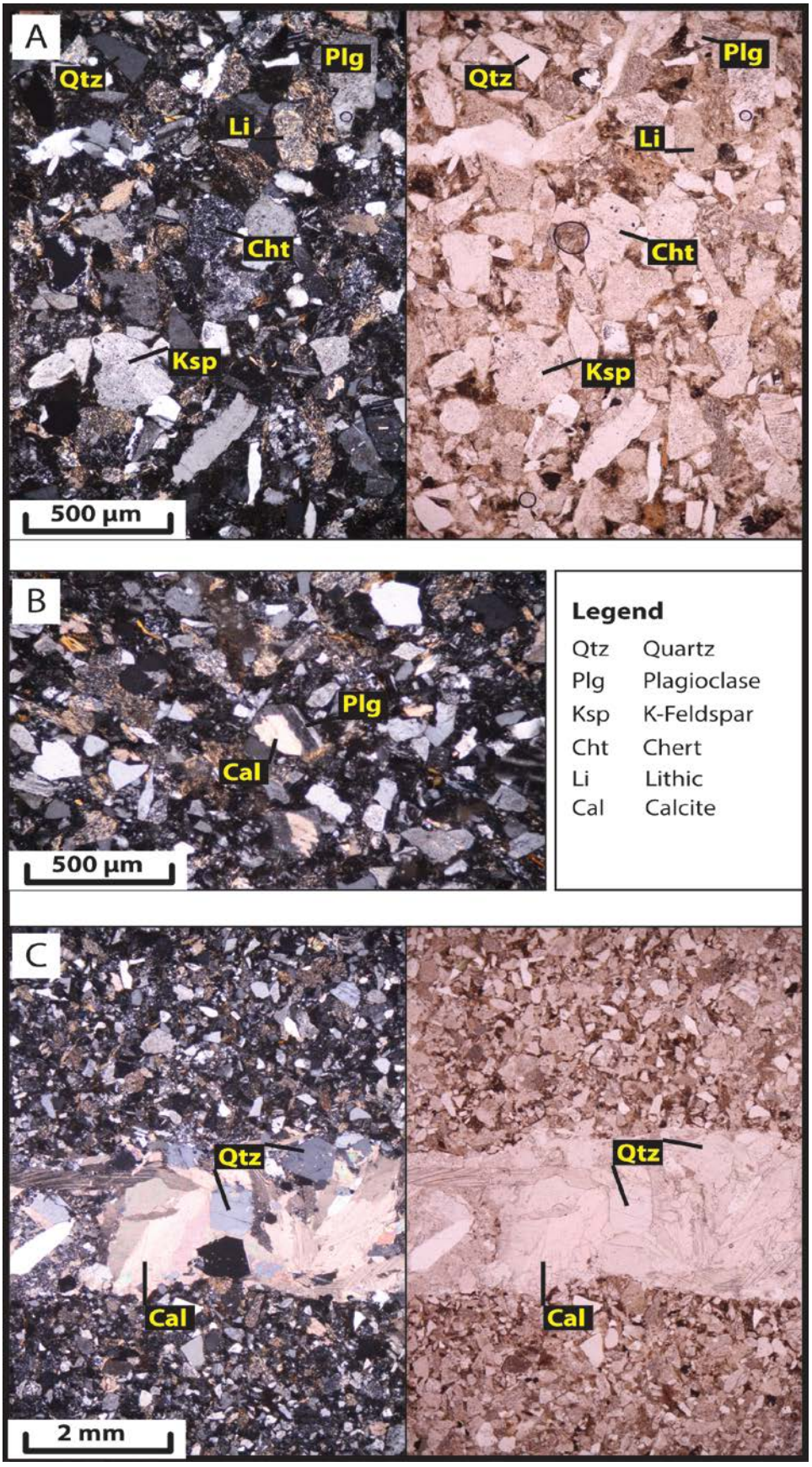

Figure 4.10: Sandstone sample WM004. A) Fine- to medium-grained sand showing sub-angular grains under XPL and PPL. B) Calcite overgrowth on a Plagioclase feldspar under XPL. C) Calcite vein containing large mosaic calcite crystals and hexagonal euhedral Quartz crystals under XPL and PPL.

and detrital matrix. With no pore spaces visible, the grains make up 70% of the sample. 31% of feldspars are plagioclase and 69% are K-feldspar. The QFL ratio for sample KG05 is 14:49:37. The cement, consisting mostly of calcite, is present in a micritic nature.

In sample KG06 grains constitute 68%, with 25% of the sample comprising matrix. 39% of the feldspar is plagioclase and 61% is K-feldspar. The QFL ratio for sample KG06 is 15:45:40. The cement amounts to 7% of the sample and comprises minor calcite and chert.

4.2.3.3 KS002

KS002 is a very fine-grained, finely laminated shale from the lower Ripon Formation exposed in N12 road cuttings (Fig 4.11). Grains are no larger than 7.8 µm (very fine-silt). Larger grains appear angular and variation in grainsize suggests a moderately sorted nature. Calcite replacement of clay is common and shadows the laminae (Fig 4.11 A). The calcitized zones exhibit a mottled texture with spots no larger than 0.1 mm (Fig 4.11 B). A QFL classification of this sample was not applicable due to more than 75% of the sample consisting of matrix and therefore classifying the sample as a mudrock.

4.2.3.4 KS007 and KS009

KS007 is from a sandstone unit in the lower Ripon Formation exposed along the N12 with grainsize varying between very fine-sand and medium-sand (0.3 mm - 0.1 mm). KS009 is from a sandstone horizon slightly higher up in stratigraphy than KS007. Both samples are poorly sorted with sub-angular finer grains and sub-rounded coarser grains. In sample KS007, grains constitute about 73% while the fine-grained matrix amounts to 22%. Biotite is a common accessory mineral and about 30% of grains are altered to sericite and calcite. 58% of the total feldspar are plagioclase and 42% are K-feldspar. The QFL ratio for KS007 is 23:32:45. Cement is rare (5 - 10%) and consists mostly of calcite and chert. The cement of sample KS009 also consists of some chlorite (glauconitic).

Sample KS009 consists about 60% of grains while the matrix only takes up about 30% of the visible

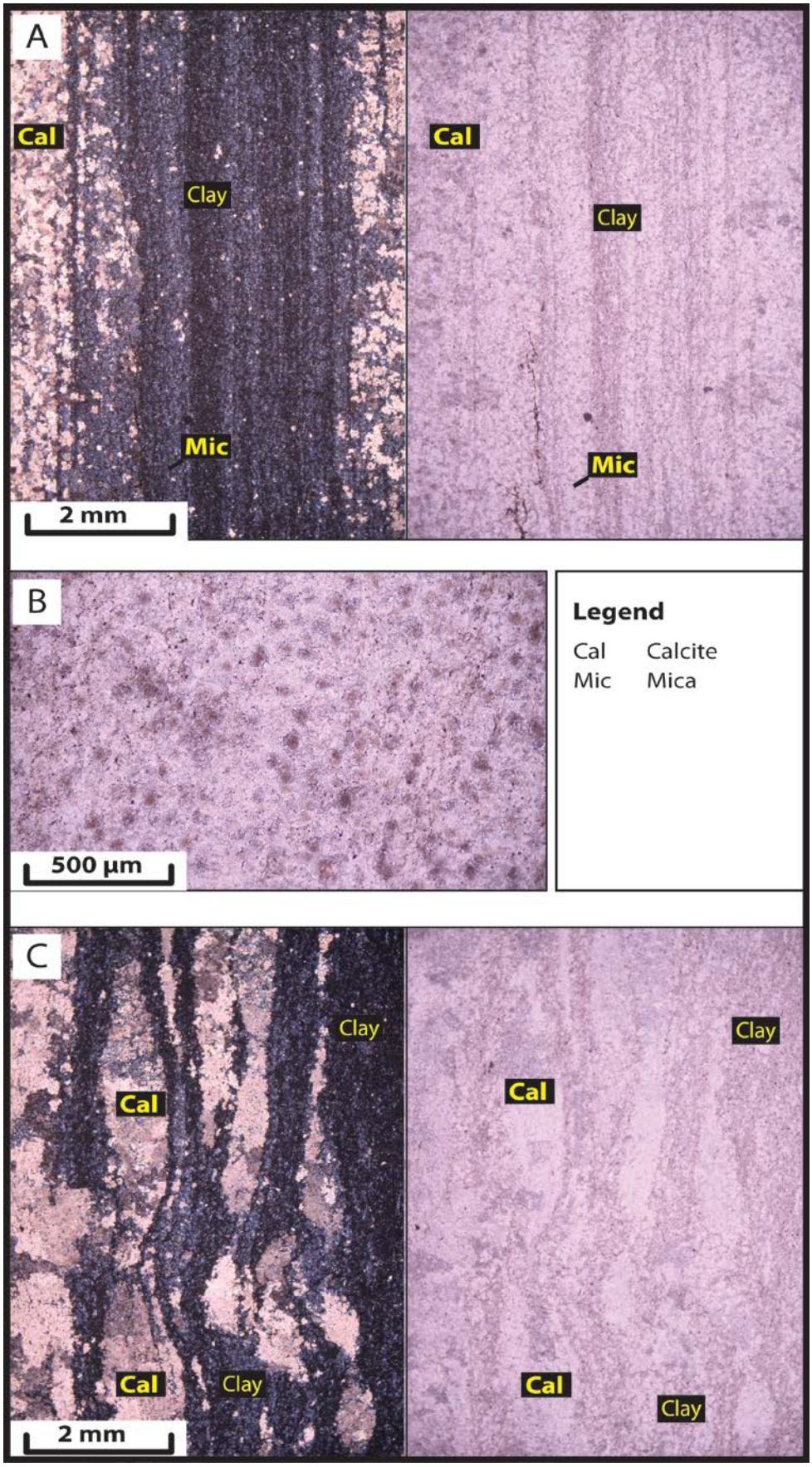

Figure 4.11: Shale Sample KS002. A) Fine lamination of mud rich layers and calcitized mud-poor layers under XPL and PPL. B) Mottled texture of calcitized layers under PPL. C) Micro rippling occurring within fine laminations under XPL and PPL.

sample. It appears that most grains remain unaltered. 51% of the feldspars in this sample are plagioclase and 49% are K-feldspar. The QFL ratio for sample KS009 is 14:41:45.

4.2.3.5 KS011

This sample is from a clay clast-rich debrite and the grains surrounding the clast are very fine- to medium-sand in size (0.45 mm - 0.1 mm) (Fig 4.12 A). The finer grains show sub-angular to angular grain boundaries while the larger grains exhibit bit more sub-rounded grain boundaries. 60% of the sample consists of grains. The matrix amounts to 25% of the sample and 15% is represented by calcite cement. The clay clasts are mostly 1.5 mm long. The clasts comprise mainly fine-grained material dominated by organic rich clay and micritic mud. The clay clasts indicate some micro dewatering structures as the clay and mud escapes in a preferred orientation due to early compaction (Fig 4.12 C). It seems that more than 50% of all clay clasts observed under the microscope exhibit this dewatering feature. Feldspars in this sample are equally divided between plagioclase and K-feldspar. Point count shows a QFL ratio of 12:38:50.

4.2.3.8 OM06

This sample is from the Wonderfontein Member of the Ripon Formation (Fig 4.13). Grains are less than 0.5 mm and are sub-angular to angular. This sample is moderately to poorly sorted and is dominated by 40% calcite cement. The grains constitute 35% and matrix 25% of the sample. 57% of the feldspar is plagioclase while 43% is K-feldspar. Point count illustrates a QFL ratio of 23:35:42. The sample shows millimeter scale bioturbation with slightly larger grains within these vertical burrows (Fig 4.13 C).

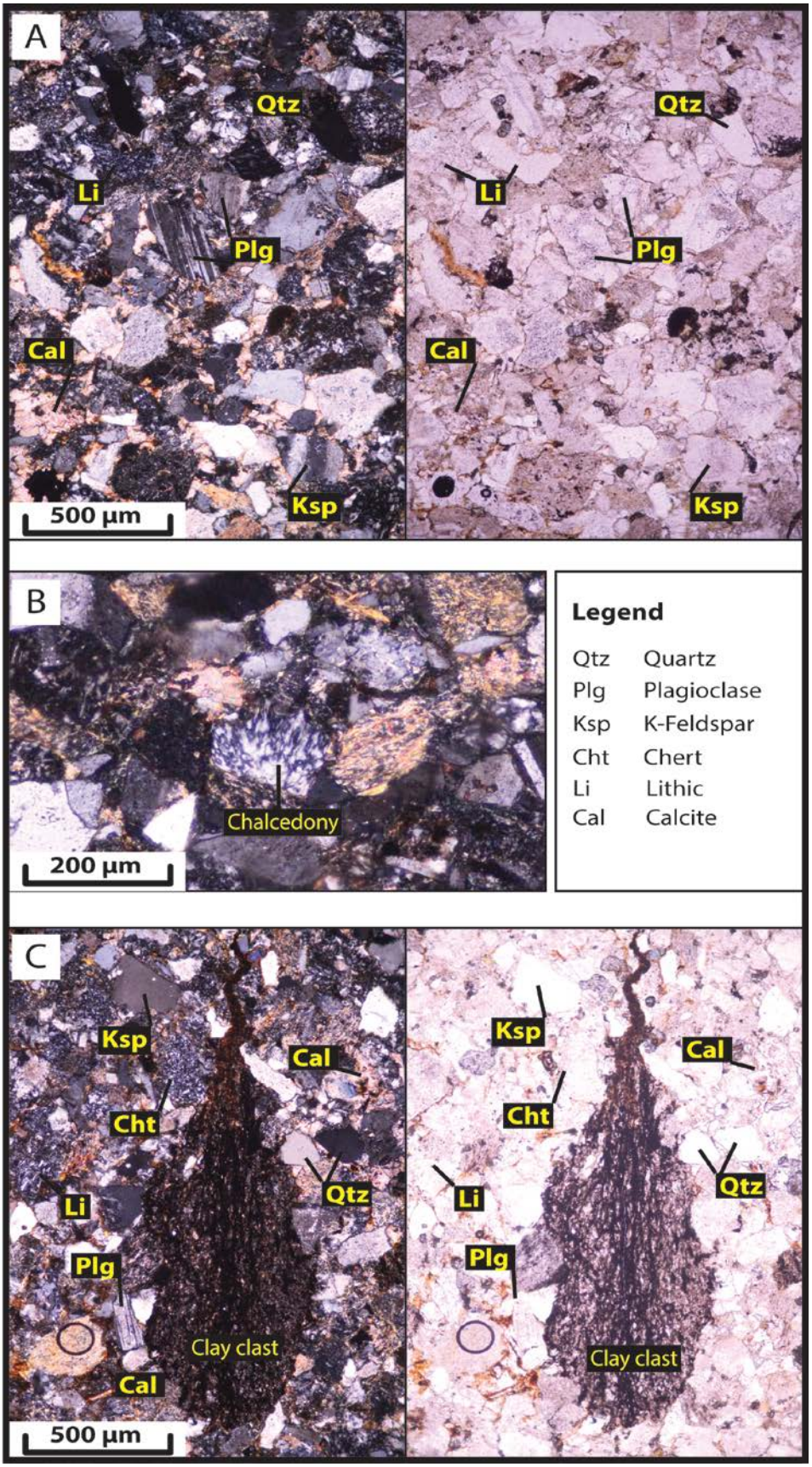

Figure 4.12: Sandstone sample KS011. A) Fine- to medium-grained sand showing calcite overgrowth of Plagioclase feldspars and a common occurrence of chert and Sedimentary Lithic fragments under XPL and PPL. B) Chalcedony grain surrounded by altered lithic fragments under XPL. C) A large clay clast with orientated dewatering feature under XPL and PPL.

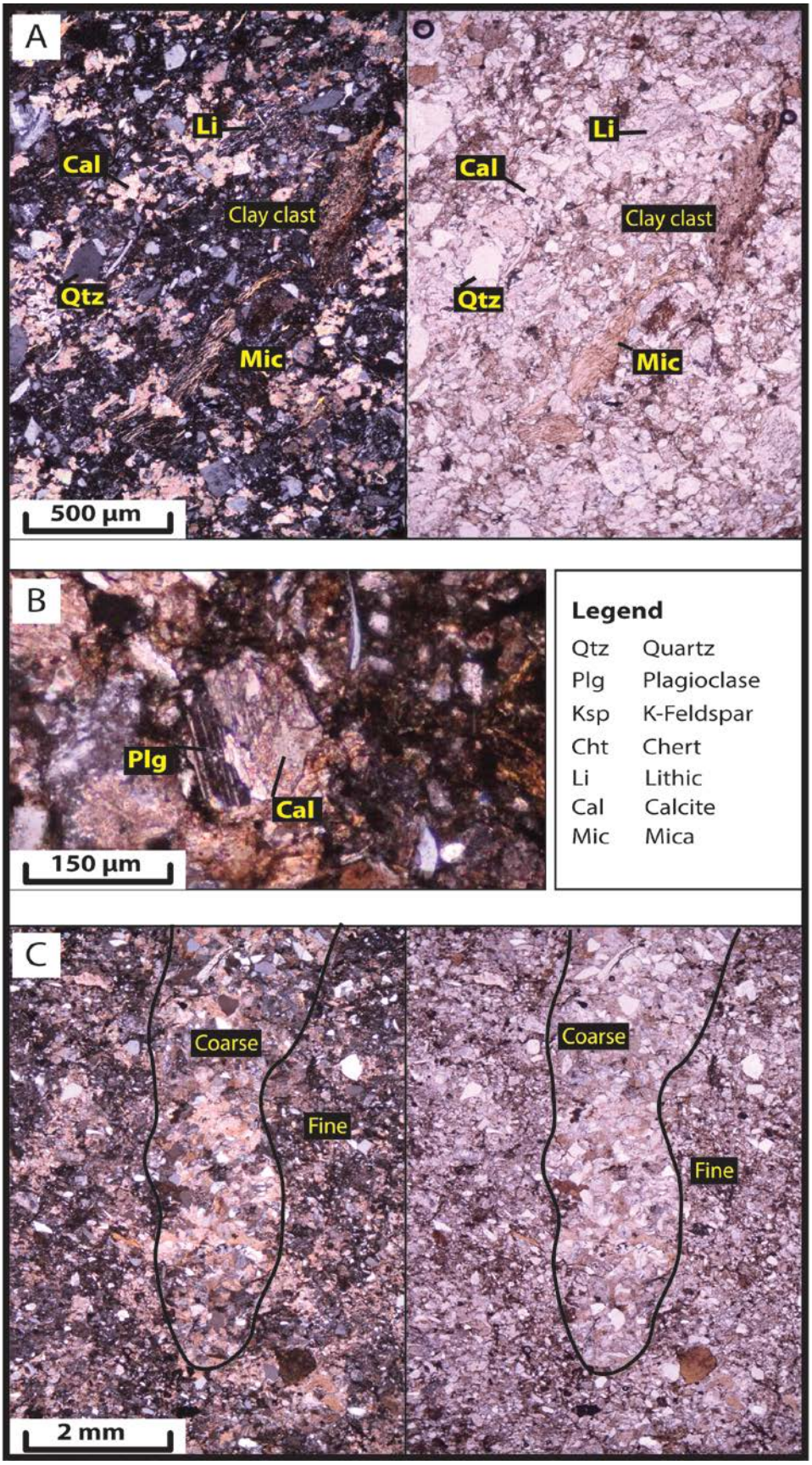

Figure 4.13: Sandstone sample OM06. A) Orientated clay clast and Mica minerals under XPL and PPL. Calcite and Lithic fragments abundant. B) Plagioclase feldspar with calcite overgrowth under XPL. C) Tubular burrow containing coarser-grained material surrounded by very fine-sand under XPL and PPL.

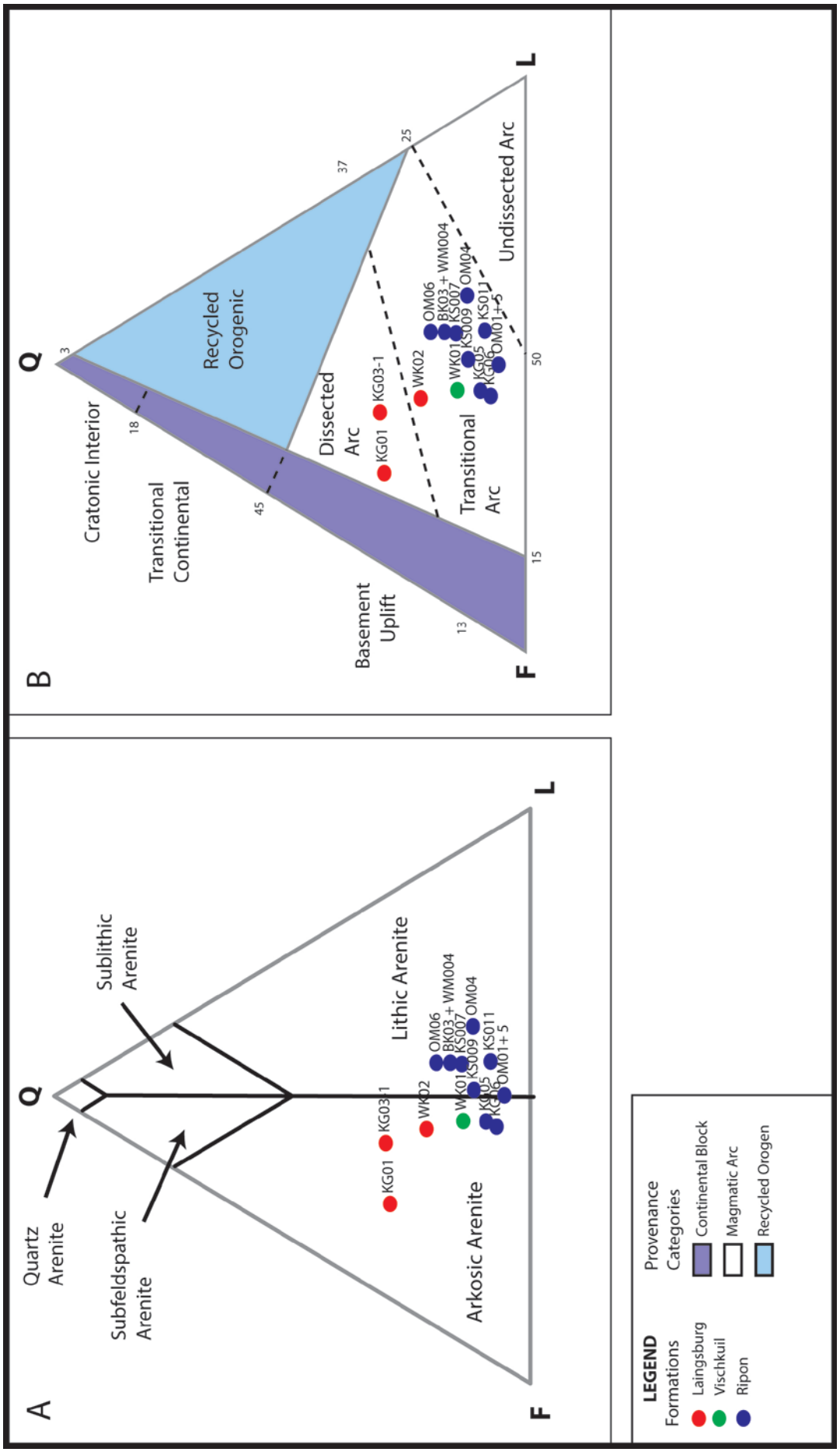

Figure 4.14: A) Ternary QFL classification scheme after Pettijohn (1973) with plotted samples of formations. B) Ternary provenance classification scheme after Dickinson et al. (1983) with plotted samples of formations showing a transitional to dissected arc provenance.

4.2.4 Discussion

The source, transport and depositional history of sediments are locked in their size, geometry and concentration of grain composition. The implications of this petrographic study provide insight into the depositional history and source of the sediment. In general, this petrographic study provided similar results to previous work (Kingsley, 1977; Viljoen, 1992; Viljoen & Wickens, 1992; Johnson & Kingsley, 1993; Wickens, 1994; Van Lente, 2004).

This study shows that the Ripon Formation is ultralithofeldspathic and is in agreement with prior studies done by Kingsley (1977) and Johnson (1991) (Fig 4.14 A). All samples obtained from the Ripon Formation are starved of quartz grains and show a general increase in lithic fragments compared to the Laingsburg Formation. The upper units of the Ripon Formation show a similar composition to the lower units. Samples from the Ripon Formation also exhibit a slight decrease in K-feldspar to plagioclase compared to what is observed in the Laingsburg Formation. The general grainsize of sandstones from the Ripon Formation is between 0.5 µm and 0.1 µm. Due to the fine-grained nature of the Vischkuil Formation only one sample (WK01) was analyzed and this closely resembles the composition of the Pluto's Vale Member (Ripon Formation).

Samples obtained from the Laingsburg Formation (WK02, KG01 and KG03-1) exhibit a feldspathic litharenite composition with a notable increase in quartz grains (around 30%) (Fig 4.14 A). The overall grainsize of the Laingsburg Formation is between 0.45 µm and 0.05 µm, making it slightly finer-grained than the Ripon Formation. A study by Van Lente (2004) focused on providing a chemostratigraphic correlation between the Tanqua and Laingsburg depocenters. This study by Van Lente (2004) undertook petrographic analysis on the middle Ecca Group of both depocenters and found that rocks of the Laingsburg depocenter (Laingsburg and Vischkuil formations) are lithofeldspathic to feldspathic. The Vischkuil Formation, however, exhibits less quartz than the Laingsburg Formation (Fig 4.15 A).

Although samples of the Laingsburg and Vischkuil formations from this study are generally lower in quartz than data presented by Van Lente (2004), the overall trend differences between the Laingsburg and Ripon depocenters are apparent. Based on the ternary diagram constructed by Dickens et al. (1984), the variation in QFL ratios suggest a dissected arc source for sediments in the Laingsburg depocenter and a transitional arc setting for the Ripon depocenter sediments (Fig 4.14 B).

All samples show very little to no porosity due to primary burial compaction as well as cementation such as chert, calcite and occasional chlorite within remaining pore spaces. Primary compaction can also be seen by the preferred orientation of clay clasts showing micro dewatering escape features. This would indicate fairly rapid deposition and burial of sand, which included fine clay clasts, exerting pressure on these clay fragments with a high water-content (Schieber, 2016).

The overall abundance of feldspar minerals, suggest rapid erosion and deposition of nearby hinterland sediments. However, sediments are moderately sorted and the grainsize is generally medium-sand and finer, suggesting a longer travel distance (Reading, 1996). Geochemical data from several studies, including Van Lente (2004), suggests that sediments are derived from a source further than the adjacent Cape Supergroup. Van Lente (2004) proposed that the relatively high latitude provide a colder climate which inhibits the chemical breakdown and weathering of fragile minerals such as feldspars, thus supporting the abundance of feldspars within the sediments (Reading, 1996).

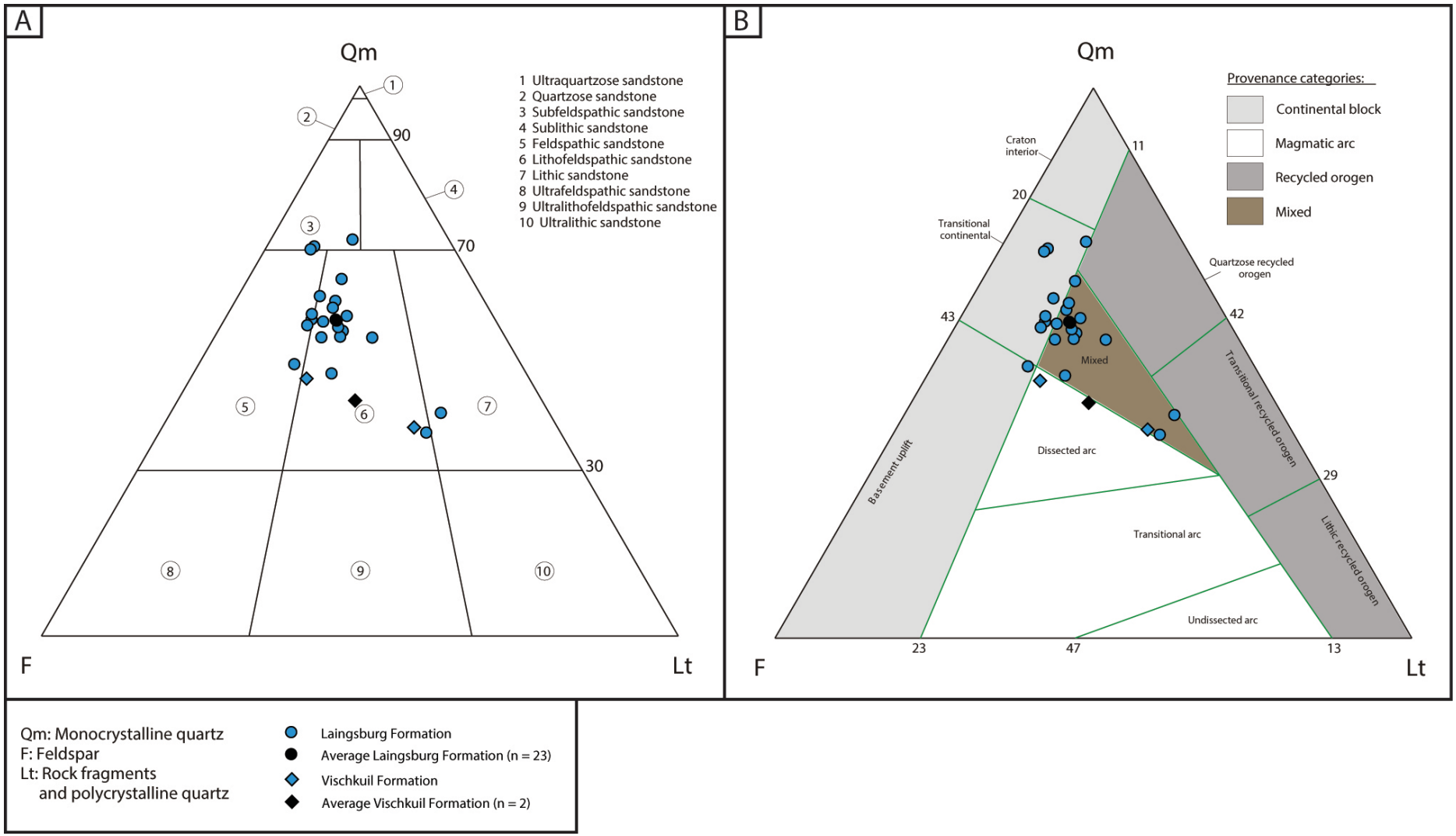

Figure 4.15: QFLt ternary diagrams of samples obtained from the Laingsburg and Vischkuil formations by Van Lente (2004). A) Sandstone classification (method after Johnson (1976) and Johnson (1991)). B) QFLt ternary diagram showing the provenance categories after Dickinson et al. (1983). All Laingsburg Formation and Vischkuil Formation samples from Van Lente (2004) exhibit a variation between dissected arc, mixed and transitional continental provenances.

4.3 Stratigraphy

Twelve stratigraphic sections were measured from the upper Collingham Formation to the base of the Fort Brown Formation. By combining lithofacies as well as facies and architectural analysis, a set of lithostratigraphic units and marker beds were identified, defined and correlated. This was achieved by constructing stratigraphic sections at key areas. These key areas and stratigraphic sections were named after the farm on which they are situated (Fig 1.6). These are from west to east:

- Zacharias Fontein 135 (WK)
- Klein Sleutlefontein 127 (GS)
- Groot Tygerberg 102 (KG)
- Jansenskraal 104 (BK)
- N12 road cutting
- Klipfontein 174 (OM)
- Minnies Kraal 112 (MK)

The mudrock units, consisting mostly of FA1 (Facies Association 1) hemi-pelagic material representing periods of suspension settling, are used as base markers for the construction of this facies-based stratigraphic framework. Mudrock units generally preserve finely flat laminated layers occasionally showing ripple laminae. Key mudrock units thicker than 10.0 m have been identified and correlated across the study area within specific formations.

The deformed units (DU) are represented by chaotic deposition and syn-depositional deformed strata comprising FA4 (Facies Association 4). Two types of deformed units have been identified. Type-1 is described as chaotic folded FA4 with more than 30 % sandstone incorporated within the folded facies and can be overlain by a fine layer of debrite containing clay clasts and plant fragments. Type-2 generally contains less than 30% sandstone and is dominated by folded and chaotic mudrock occasionally exhibiting detached blocks of FA1 (finely-interlaminated shale) and FA6 (rhythmite).

These units can vary in thickness from 20.0 m to 60.0 m and are observed in various stratigraphic horizons. Type-1 is commonly found towards the upper units of the Vischkuil Formation and Type-2 is abundant in the Wonderfontein Member of the Ripon Formation. The lateral continuity of these units is generally widespread and can extend up to 80.0 km.

On occasion FA2 and FA3 are overlain by a fine layer of debrite (Fig 4.16 D, F). These debrite deposits consist of fine clay clasts and plant fragments (Fig 4.16 A, B) in a mud-matrix dominated, poorly sorted sandy mudrock. In a few instances, the plant remains may consist of complete *Glossopteris* leaves ranging from 4.0 cm to 40.0 cm in length (Fig 4.16 C, E).

4.3.1 Collingham Formation

In the study area, the Collingham Formation regionally underlies the Vischkuil Formation to the west of the N12 towards the Laingsburg depocenter, and the Ripon Formation to the east of the N12. The Collingham Formation's upper bounding surface is consistently sharp with the overlying units. Only the upper section of the Collingham Formation was examined and documented for the purpose of this study (Fig 4.17). The Collingham Formation predominantly consists of finely interbedded FA5 (Facies Association 5) siliceous siltstone (averaging 0.1 - 0.2 m) and FA7 (Facies Association 7) volcanic ash-fall layers with occasional thin (0.1 m) FA1 layers. A regionally mappable white chert bed (Matjiesfontein Chert), averaging 0.2 - 0.6 m in thickness, is present within the lower Collingham Formation (Viljoen, 1994).

4.3.2 Vischkuil Formation

The Vischkuil Formation directly overlies the Collingham Formation west of the N12 and is defined by the lack of FA7 tuff beds as well as an increase in FA1 hemi-pelagic muds (Fig 4.17). The Vischkuil Formation's sharp lower bounding surface forms a conformable contact with the underlying Collingham Formation. According to van der Merwe et al. (2009) the Vischkuil Formation can be subdivided into a lower Vischkuil and an upper Vischkuil. The lower Vischkuil consists of interbedded

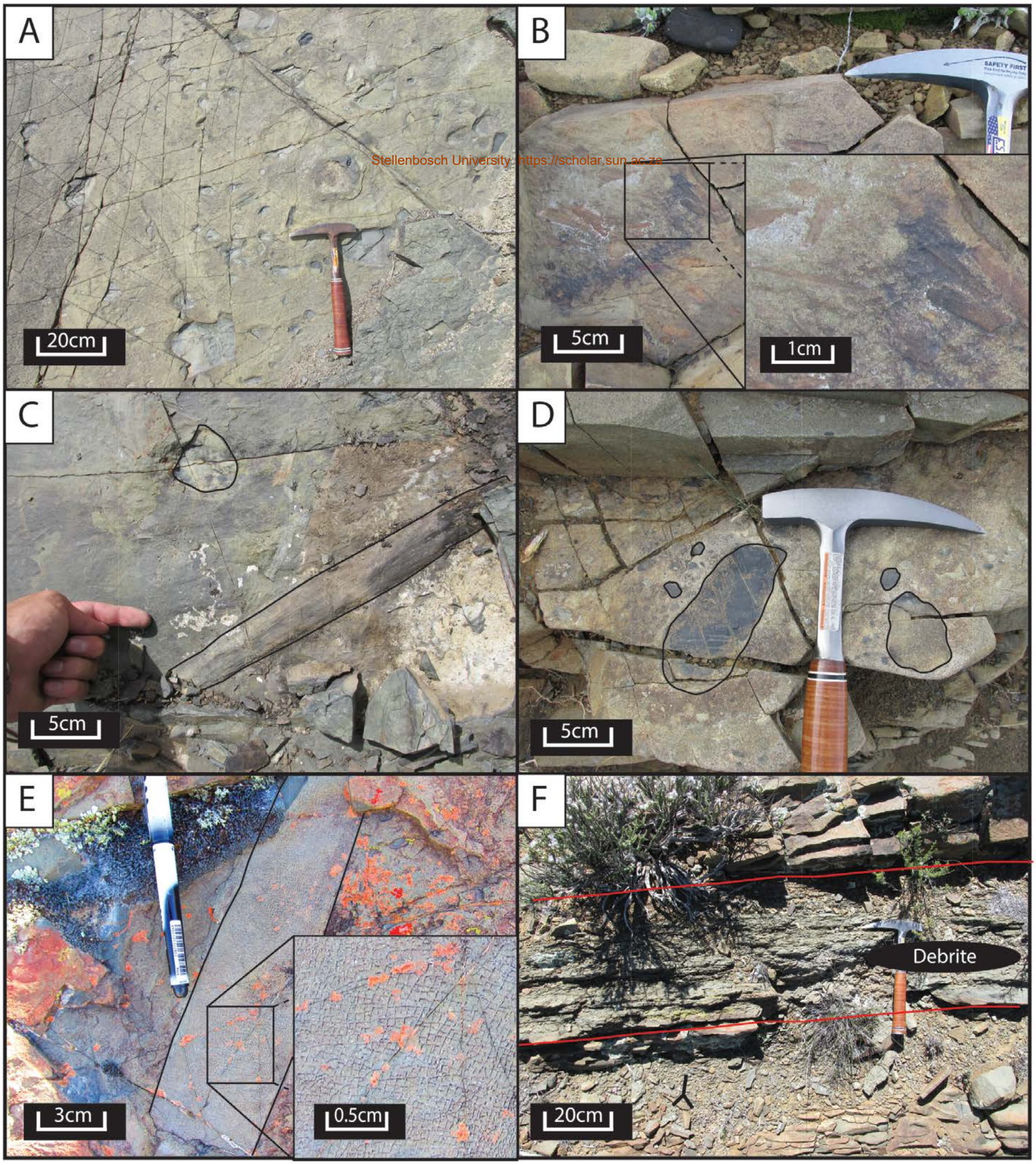

Figure 4.16: A) Upper bedding plain surface of a FA2 bed containing debrite material. Multiple clay clasts in various orientations are visible. The occurrence of plant fragments is also common. B) Plant fragments occur on the upper bedding plane. C) a large Glossopteris leaf observed along with clay clasts on the same bedding plane as figure A. D) Clay clasts of various sizes co-occurs. E) Glossopteris leaf on upper bedding surface. Notice the box-work veining of the leaf's cell structure. F) Debrite depositional layer about 40cm to 50cm thick grading normally, but followed by a gradual increase of sandstone.

FA1 hemi-pelagic material and FA5 siliceous siltstone and is generally un-deformed. In the study area, the lower Vischkuil is present only at Zacharias Fontein 135 (WK). Here it has a thickness of about 40.0 m and dramatically pinches out toward the east at Groot Tygerberg 102 (KG).

The upper Vischkuil is defined by the presence of Type-1 deformed strata and interbedded siltstone, mudrock and minor very fine-grained sandstone units. The dominant facies in the upper Vischkuil are FA4, FA5 and FA1. van der Merwe et al. (2009) described three distinct deformation units (DU1, DU2 and DU3) within the upper Vischkuil Formation which are mostly present in the western side of the study area. On the farm Zacharias Fontein 135 (WK) only the upper two deformed units were identified; the middle deformed unit 2 (DU2) and the upper deformed unit 3 (DU3). From here the upper Vischkuil Formation thins laterally eastward from 100.0 m thickness at Zacharias Fontein 135 (WK) to 20.0 m at Jansenskraal 104 (BK) and pinches out east of this farm. At Groot Tygerberg 102 (KG) and Jansenskraal 104 (BK), east of Zacharias Fontein 135 (WK), only the upper DU3 is present which decreases to a thickness of 8.0 m at the farm Jansenskraal 104 (BK).

4.3.3 Ripon Formation

4.3.3.1 Pluto's Vale Member

The Pluto's Vale Member is the lowest stratigraphic member of the Ripon Formation. The basal unit of the Pluto's Vale Member has a sharp lower bounding surface overlying the Collingham Formation east of the N12 and a less definable formation boundary overlying the Vischkuil Formation west of the N12. The Pluto's Vale Member can be divided into a lower and upper section, both comprising interbedded FA1, FA2 and occasional FA3 beds with a mottled texture. The upper and lower sections of the Pluto's Vale Member are divided by the Pluto's Vale mudrock unit (PV-mud). This unit comprises finely laminated (0.05 m) FA1 with rare FA2 sandstone beds (0.4 - 0.6 m) and maintains its average thickness of 20.0 m across the study area, but increases in thickness to about 70.0 m at Minnies Kraal 112 (MK) on the eastern side of the study area. The PV-mudrock unit exhibits a gradational lower

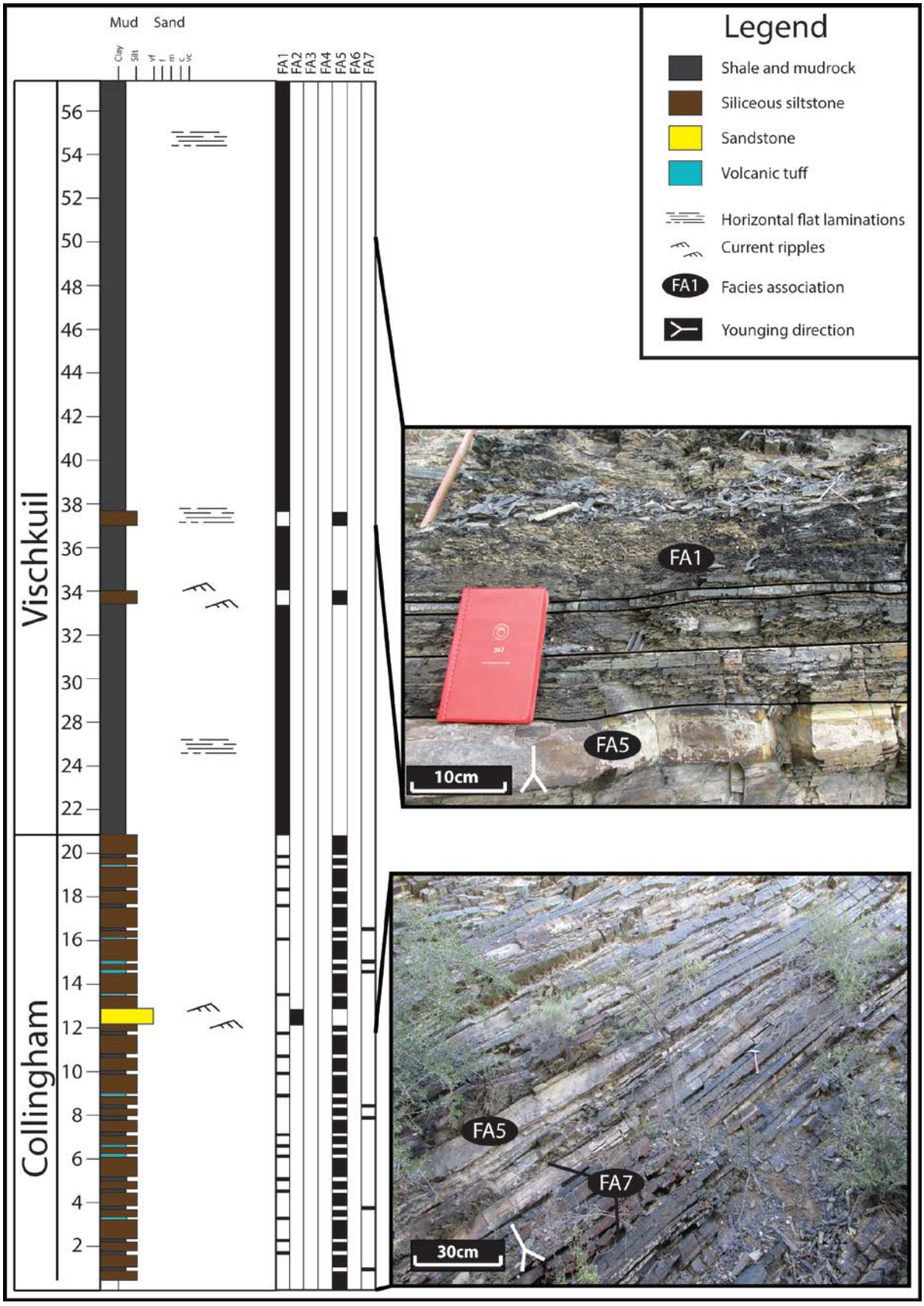

Figure 4.17: Statigraphic section at Zacharias Fontein 135 (WK) showing characteristics of the Collingham Formation as well as the boundary between the Collingham Formation and lower Vischkuil Formation.

bounding surface and a sharp upper bounding surface with the lowermost sandstone unit of the Upper Pluto's Vale.

The Lower Pluto's Vale unit contains an amalgamated sandstone package between 16.0 m and 20.0 m thick comprising FA3. This sandstone unit extends laterally towards the west where it pinches out just west of the N12. In the Lower Pluto's Vale, at Groot Tygerberg 102 (KG), a channelized sandstone unit with no internal sedimentary features is present about 14.0 m above DU2 of the Vischkuil Formation and directly underlying the PV-mud (Fig 4.18). This sandstone is named the Kaaimansgat Sandstone after the farm house. The Kaaimansgat Sandstone has a large lenticular geometry with a maximum thickness of about 45.0 m and lenses do not exceed 200.0 m in lateral extent, occurring on the same stratigraphic horizon (Fig 4.19). The Upper Pluto's Vale is on average between 20.0 m and 30.0 m thick and grades into the overlying Wonderfontein Member. The entire Pluto's Vale Member thins towards the West with an E-W trend exhibiting an overall thickness of 90.0 m at WK. It merges with the Vischkuil Formation until it becomes indistinguishable to the west of Zacharias Fontein 135 (WK).

4.3.3.2 Wonderfontein Member

The Wonderfontein Member of the Ripon Formation almost entirely comprises finely interlaminated (0.1 - 1.5 cm) FA1 and FA4 Type-2 deformed strata with minor rhythmite (FA6). The Wonderfontein Member overlies the Pluto's Vale Member across the study area and its boundary is defined by the first major (greater than 5.0 m in thickness) FA1 or FA4 mudrock above the Upper Pluto's Vale Sandstones. Two Type-2 deformed units are present; the lower Deformed Unit A (DU-A) and upper Deformed Unit B (DU-B). DU-A only occurs west of the N12 and thins into irregular slivers of about 10.0 m thick deformed strata towards BK in the east. At WK, in the west of the study area, the thickness of DU-A is 70.0 m.

DU-B is laterally extensive across the study area and occurs stratigraphically about 10.0 m above the base of the Wonderfontein Member east of the N12. West of the N12 the thickness of DU-B increases

to 60.0 m and the unit directly underlies the Laingsburg Formation. Large lenticular sandstone units (maximum thickness of 30.0 m) occur at KG, GS and BK with a lateral extent not exceeding 500.0 m (Fig 4.20) and are associated with FA4 and FA6.

4.3.3.3 Trumpeters Member

The uppermost Trumpeters Member of the Ripon Formation is not laterally continuous across the study area and is limited only to the east of the N12 at MK. The Trumpeters Member overlies the Wonderfontein Member at MK and is overlain by a gradual conformable contact with the base of the Fort Brown Formation. It consists of three cyclic normally grading sandstone units (Lower Unit 1, Middle Unit 2 and Upper Unit 3), each comprising interbedded FA3, FA2 and FA1. Unit 2 exhibits minor FA6 rhythmite deposition grading normally. Unit 3 forms a sharp lower bounding surface with FA5 beds. The Trumpeters Member has a thickness of about 40.0 m, extends eastward beyond the town of Willowmore, but pinches out west of MK and is not present at OM.

4.3.4 Laingsburg Formation

Sharply overlying the Wonderfontein Member west of the N12, the Laingsburg Formation consists of two sandstone units divided by a mudrock unit. The sandstone units have a general upward fining nature consisting of interbedded layers of FA2 and amalgamated beds of FA3 (Fig 4.21). The mudrock unit is dominated by FA1 and varies in thickness from 4.0 m to 20.0 m. Both sandstone units are interpreted to primarily preserve the T_a to T_e sections of the Bouma Sequence (Bouma, 1962). The upper sandstone unit of the Laingsburg Formation grades normally upwards into the Fort Brown Formation forming a conformable formation boundary. An overall thickness of about 50.0 m for the Laingsburg Formation is maintained on the western side of the study area, from the town of Prince Albert towards the N12. The entire formation pinches out just east of the N12 where the Fort Brown Formation directly overlies the middle Wonderfontein Member of the Ripon Formation.

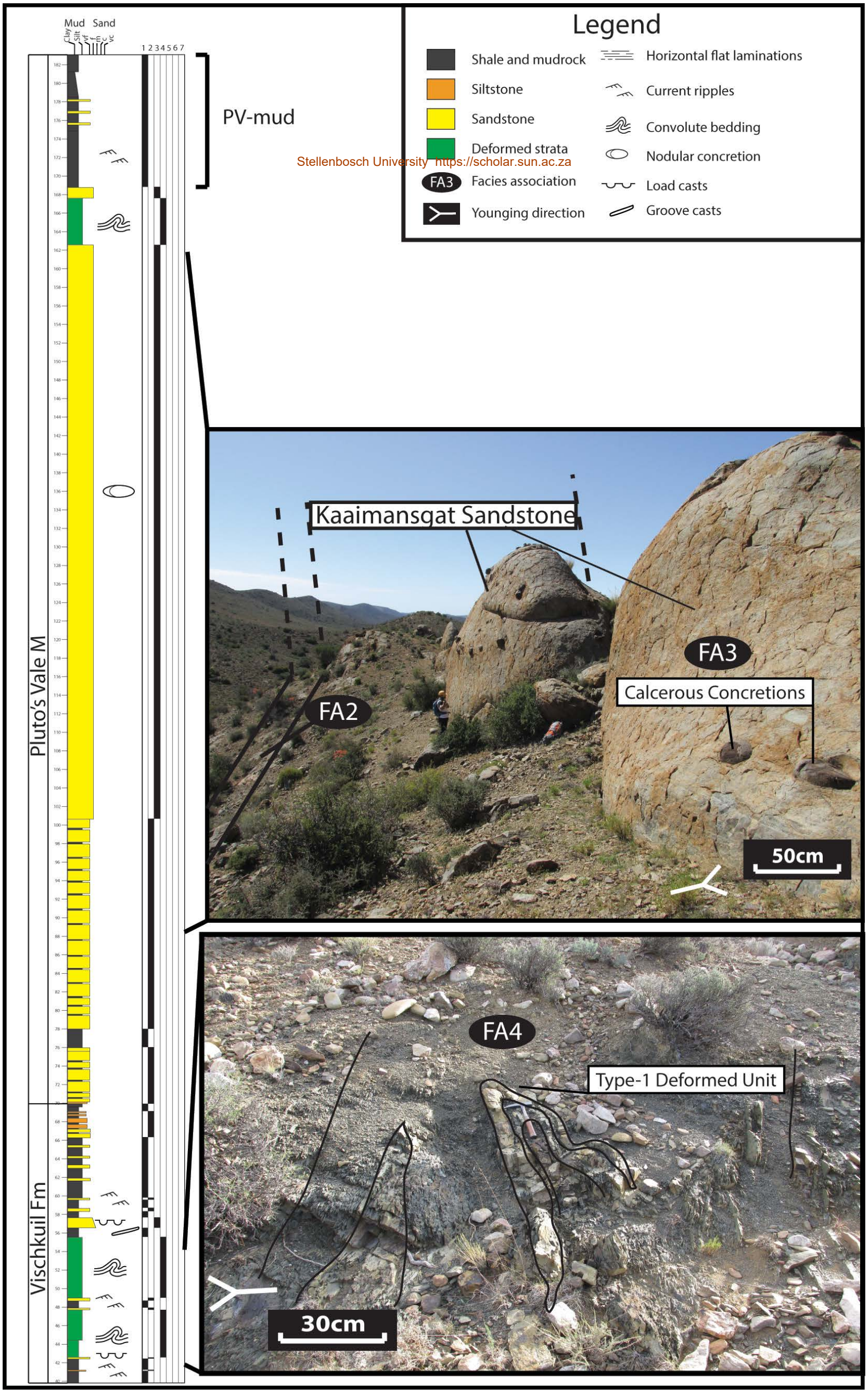

Figure 4.18: Stratigraphic section of Groot Tygerberg 102 (KG) showing the placement of the Kaaimansgat Sandstone Unit overlying the Vischkuil Formation and underlying the Pluto's Vale Mudrock (PV-mud) marker.

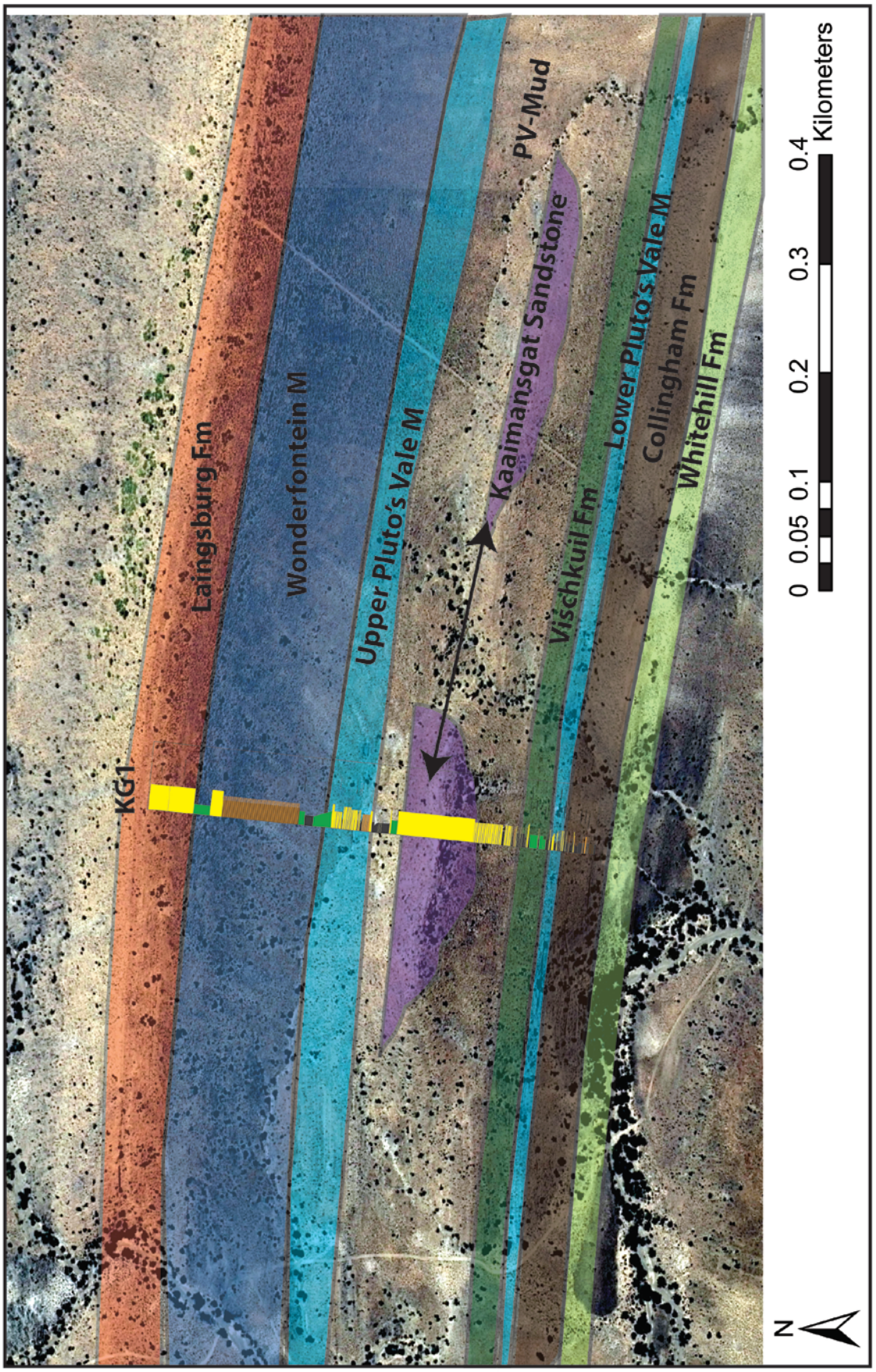

Figure 4.19: Geographic location of profile KG1 showing the position and lateral continuity of the Kaaimansgat Sandstone (Purple).

4.3.5 Fort Brown Formation

The Fort Brown Formation regionally overlies the upper units of the Laingsburg Formation in the west of the study area and the Ripon Formation to the east. The lowermost section of the Fort Brown Formation was observed for the purposes of this study. The formation boundary is distinct from the underlying units with a notable increase in FA6 rhythmites, although the lower bounding surface of the Fort Brown Formation is gradational and conformable. Lenticular sandstone units are rare. FA1 is almost entirely absent and Type-2 deformed strata are occasionally preserved comprising FA4. It is common to find entire detached blocks of FA6 within the Fort Brown Formation. Detachment points and decollement surfaces have been identified and blocks can show a variation in size.

Figure 4.20: Stratigraphic section of the upper Wonderfontein Member showing the lateral edge of the channelized lobe complex at Klein Sleutelfontein 127. Notice the fining up nature of the sandstone units interbedded with FA6 deposits.

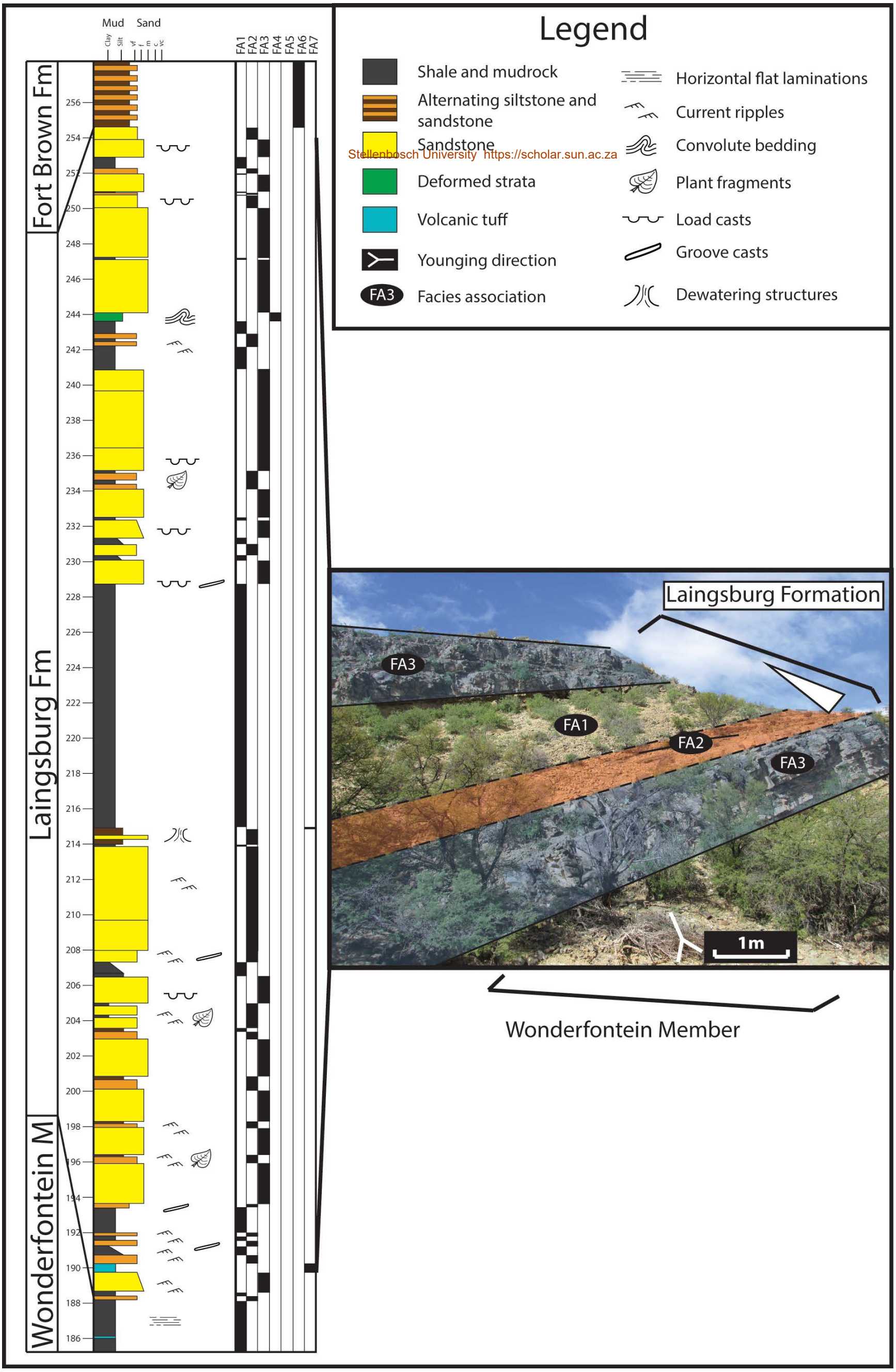

Figure 4.21: Stratigraphic section of the N12 road cutting showing the formation boundary between the Wonderfontein Member of the Ripon Formation and the Laingsburg Formation. The Laingsburg Formation directly underlies the Fort Brown Formation.

4.3.6 Facies Correlation

The distribution of facies across the study area is widely variable as far as thickness is concerned, but certain trends are observed (Fig 4.22). The Collingham Formation maintains a constant laterally continuous interbedded nature of shales and siliceous siltstones (FA5, FA7 and FA1), with FA5 being the dominant facies association within the Collingham Formation. The Vischkuil Formation, overlying the Collingham Formation to the west of the N12, is marked by the dramatic decrease of tuffaceous mudrock (FA7) and increase of sandstone (FA4). To the east of the N12 the Pluto's Vale Member of the Ripon Formation also exhibits a dramatic decrease of tuffaceous mudrock (FA7) suggesting a termination in volcanic activity, but is marked by the deposition of sandstones directly overlying the Collingham Formation.

The Pluto's Vale Member can be divided into the Lower Pluto's Vale and the Upper Pluto's Vale. The sandstone dominated Lower Pluto's Vale Member extends laterally towards the west at Groot Tygerberg 102 (KG) where it becomes more lenticular. The Upper Pluto's Vale Member is laterally continuous throughout the study area, but possibly pinches out west of the town of Prince Albert. It is unclear where this pinch-out occurs as it is not within the study area. The shale dominated PV-mud dividing the Upper and Lower Pluto's Vale Members is also laterally continuous and also extends west of Prince Albert.

The overlying Wonderfontein Member (dominated by shales and chaotic facies with minor occurrences of rhythmite) is also present throughout the study area. It is unclear whether the Wonderfontein Member pinches out or merges with the Vischkuil and Laingsburg formations west of Prince Albert as it is also not within the study area. Within the Wonderfontein Member, isolated channelized sandstone units are present and have restricted lateral continuity. These are commonly associated with rhythmites and occasionally show slumped features. The upper Trumpeters Member of the Ripon Formation is present only on the eastern side of the study area. This member is dominated by cyclic deposition of Interbedded sandstones and shales with minor rhythmites present.

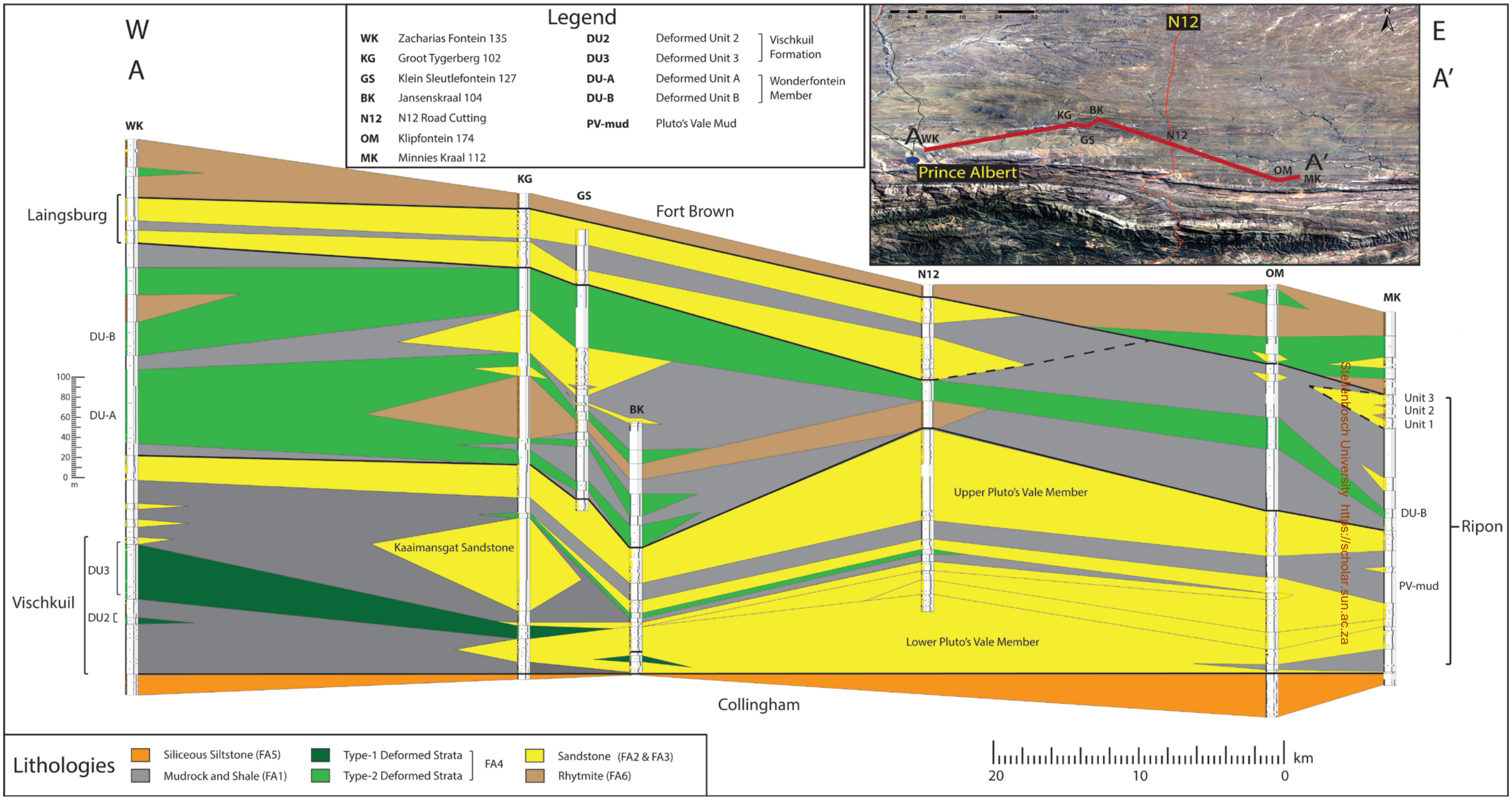

Figure 4.22: Correlation panel in cross-sectional view of the dominant facies and marker units across the study area from West (A) to East (A'). The Collingham Formation forms the baseline for the correlation panel and the Fort Brown Formation forms the upper boundary. The Lower Pluto's Vale Member merges with the Vischkuil Formation at KG.

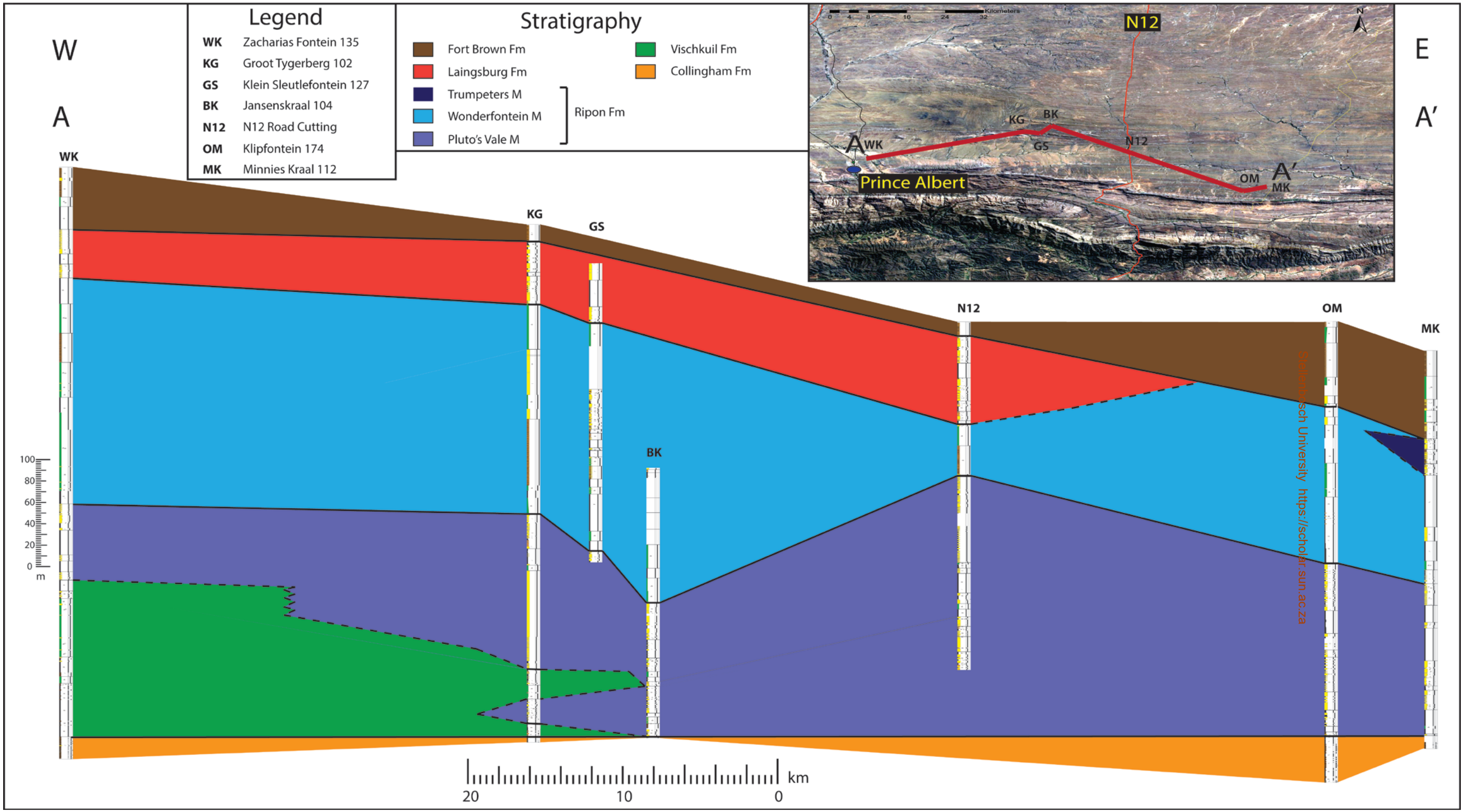

Figure 4.23: Correlation panel in cross-sectional view of the stratigraphic units (formations and members) across the study area from the West (A) to the East (A').

The sandstone beds dramatically pinch out west of Minnies Kraal 112 (MK) where shales of the Wonderfontein Member dominate. West of the N12 the Wonderfontein Member is overlain by sandstone and shale turbidite beds of the Laingsburg Formation.

The Laingsburg Formation comprises two sandstone units dominated by which are separated by an argillaceous unit. There is a notable decrease in chaotic facies deposits in this formation compared to the underlying Wonderfontein Member. The Laingsburg Formation extends eastward and pinches out just east of the N12. The overlying Fort Brown Formation is dominated by rhythmites and shows a dramatic decrease in larger sandstone beds. Sporadic occurrences of chaotic deposition are present. The Fort Brown Formation overlies the Laingsburg Formation west of the N12, the Wonderfontein Member east of the N12 and the Trumpeters Member east of MK.

4.3.7 Stratigraphic Correlation

The overall stratigraphic and geographic placement of the Vischkuil, Laingsburg and Ripon formations exhibits an interfingering nature within the study area (Figure 4.23), while the underlying Collingham Formation and the overlying Fort Brown Formation are laterally continuous. The Collingham Formation is the lowermost stratigraphic unit researched for this study and has a sharp upper bounding surface with the overlying units. West of the N12 the Collingham Formation is directly overlain by the mudrock, siltstone and deformed units of the Vischkuil Formation, which in turn thins and pinches out towards the east. Directly overlying the Collingham Formation to the east of the N12 is the lowermost Pluto's Vale Member of the Ripon Formation. The Pluto's Vale Member thins towards the west and continues laterally west of the town of Prince Albert where it directly overlies the Vischkuil Formation until it possibly dissipates (Johnson et al., 2006).

Regionally the Pluto's Vale Member is overlain by the middle, mud-rich, Wonderfontein Member of the Ripon Formation which seems to extend laterally west of Prince Albert, beyond the bounds of the study area. The upper Trumpeters Member of the Ripon Formation is present only east of the N12

and truncates towards the west. The three sandstone units (lower Unit 1, middle Unit 2 and upper Unit 3) thin westward into the upper mudrocks of the Wonderfontein Member. To the west of the N12 the Wonderfontein Member is directly overlain by the arenaceous Laingsburg Formation with which it has a gradual contact. The Laingsburg Formation, which has its greatest thickness to the west, thins laterally towards the N12 in the east where it pinches out. The overlying Fort Brown Formation extends laterally across the entire study area. It has a gradual contact with the underlying Laingsburg Formation to the west of the N12 and the Wonderfontein Member of the Ripon Formation east of the N12. Further east the Fort Brown Formation overlies the upper Trumpeters Member.

4.3.8 Palaeocurrents

Where possible, palaeocurrents were measured on sole marks and current ripple cross-laminations (Fig 4.24). A total of forty readings were taken across the study area based on outcrop availability (Table 7). Each palaeocurrent reading was taken as a lineation within folded strata and was corrected to its primary horizontal depositional transport direction. This was achieved by plotting the primary bedding strike and dip on a stereo net and rotating the lineation in a small circle around the horizontal axis.

The palaeocurrent readings collected in this study indicates that the Vischkuil Formation (n=9) displays a predominant palaeotransport direction towards the East. Readings close to the town of Prince Albert are slightly more East Southeast, ranging from 90° to 130°, than readings taken towards the fringes of the Vischkuil depositional units at Groot Tygerberg 102 (Fig 4.25 A). This corresponds with the upper Visckuil Formation of the Laingsburg depocenter (van der Merwe et al., 2009).

The lowermost units of the Ripon Formation at the base of the Pluto's Vale Member exhibit a strong West and West Northwest current direction (n=12) (Fig 4.25 B). At Groot Tygerberg 102 (KG) palaeocurrent readings taken from minor siltstones within the PV-mud (n=3) show a sudden change

Table 7: All corrected palaeocurrent readings according to the formation it was obtained from.

Palaeocurrent	Formation/Member	Farm Name
103°	Upper Vischkuil Formation	Groot Tygerberg 102
106°	Upper Vischkuil Formation	Groot Tygerberg 102
76°	Upper Vischkuil Formation	Groot Tygerberg 102
89°	Upper Vischkuil Formation	Groot Tygerberg 102
83°	Upper Vischkuil Formation	Groot Tygerberg 102
93°	Upper Vischkuil Formation	Zacharias Fontein 135
130°	Upper Vischkuil Formation	Zacharias Fontein 135
110°	Upper Vischkuil Formation	Zacharias Fontein 135
112°	Upper Vischkuil Formation	Zacharias Fontein 135
345°	Lower Ripon Formation (Pluto's Vale M)	Jansenskraal 104
346°	Lower Ripon Formation (Pluto's Vale M)	Jansenskraal 104
326°	Lower Ripon Formation (Pluto's Vale M)	Jansenskraal 104
285°	Middle Ripon Formation (Wonderfontein M)	Groot Tygerberg 102
285°	Middle Ripon Formation (Wonderfontein M)	Groot Tygerberg 102
282°	Middle Ripon Formation (Wonderfontein M)	Groot Tygerberg 102
280°	Middle Ripon Formation (Wonderfontein M)	Groot Tygerberg 102
281°	Lower Ripon Formation (Pluto's Vale M)	Groot Tygerberg 102
290°	Lower Ripon Formation (Pluto's Vale M)	Groot Tygerberg 102
260°	Lower Ripon Formation (Pluto's Vale M)	Minnies Kraal 112
285°	Lower Ripon Formation (Pluto's Vale M)	Minnies Kraal 112
285°	Lower Ripon Formation (Pluto's Vale M)	Minnies Kraal 112
286°	Lower Ripon Formation (Pluto's Vale M)	Minnies Kraal 112
282°	Middle Ripon Formation (Wonderfontein M)	N12 Road Cutting
293°	Middle Ripon Formation (Wonderfontein M)	N12 Road Cutting
275°	Middle Ripon Formation (Wonderfontein M)	Klipfontein 174
265°	Middle Ripon Formation (Wonderfontein M)	Klipfontein 174
350°	Middle Ripon Formation (Wonderfontein M)	Klipfontein 174
260°	Lower Ripon Formation (Pluto's Vale M)	Klipfontein 174
260°	Lower Ripon Formation (Pluto's Vale M)	Klipfontein 174
260°	Lower Ripon Formation (Pluto's Vale M)	Zacharias Fontein 135
260°	Lower Ripon Formation (Pluto's Vale M)	Zacharias Fontein 135
250°	Lower Ripon Formation (Pluto's Vale M)	Zacharias Fontein 135
40°	Lower Laingsburg Formation	Klein Sleutelfontein 127
40°	Lower Laingsburg Formation	Klein Sleutelfontein 127
39°	Lower Laingsburg Formation	Klein Sleutelfontein 127
30°	Upper Laingsburg Formation	N12 Road Cutting
90°	Lower Laingsburg Formation	N12 Road Cutting
93°	Lower Laingsburg Formation	N12 Road Cutting
98°	Lower Laingsburg Formation	N12 Road Cutting
30°	Upper Laingsburg Formation	Zacharias Fontein 135

in palaeoflow direction to the North. Channel geometry of the Kaaimansgat sandstone also indicates a Northward channel flow. Higher in the stratigraphic succession at Groot Tygerberg 102, in the upper units of the Wonderfontein Member, a few channelized features are visible exhibiting a North to Northeast transport direction. Towards Klipfontein 174 a few readings also show a palaeoflow to the North within the upper units of the Wonderfontein Member (n=2). The remaining units of the Ripon Formation (n=6) predominantly maintain a West to Northwest palaeoflow direction.

The Laingsburg Formation, which overlies the Wonderfontein Member across the study area, maintains a strong Northeast paleocurrent direction changing slightly more East towards the fringes of the Formation just east of the N12 (n=8) (Fig 4.25 C).

The results of the palaeocurrent analysis indicates an Eastward current direction for the Vischkuil Formation (n=9), a West – West Northwest direction with occasional channeling to the North (n=5) for the Ripon Formation (n=18) and a Northeast direction for the Laingsburg Formation (n=8). Even though these results are preliminary, they do provide additional evidence for stratigraphic separation of these formations.

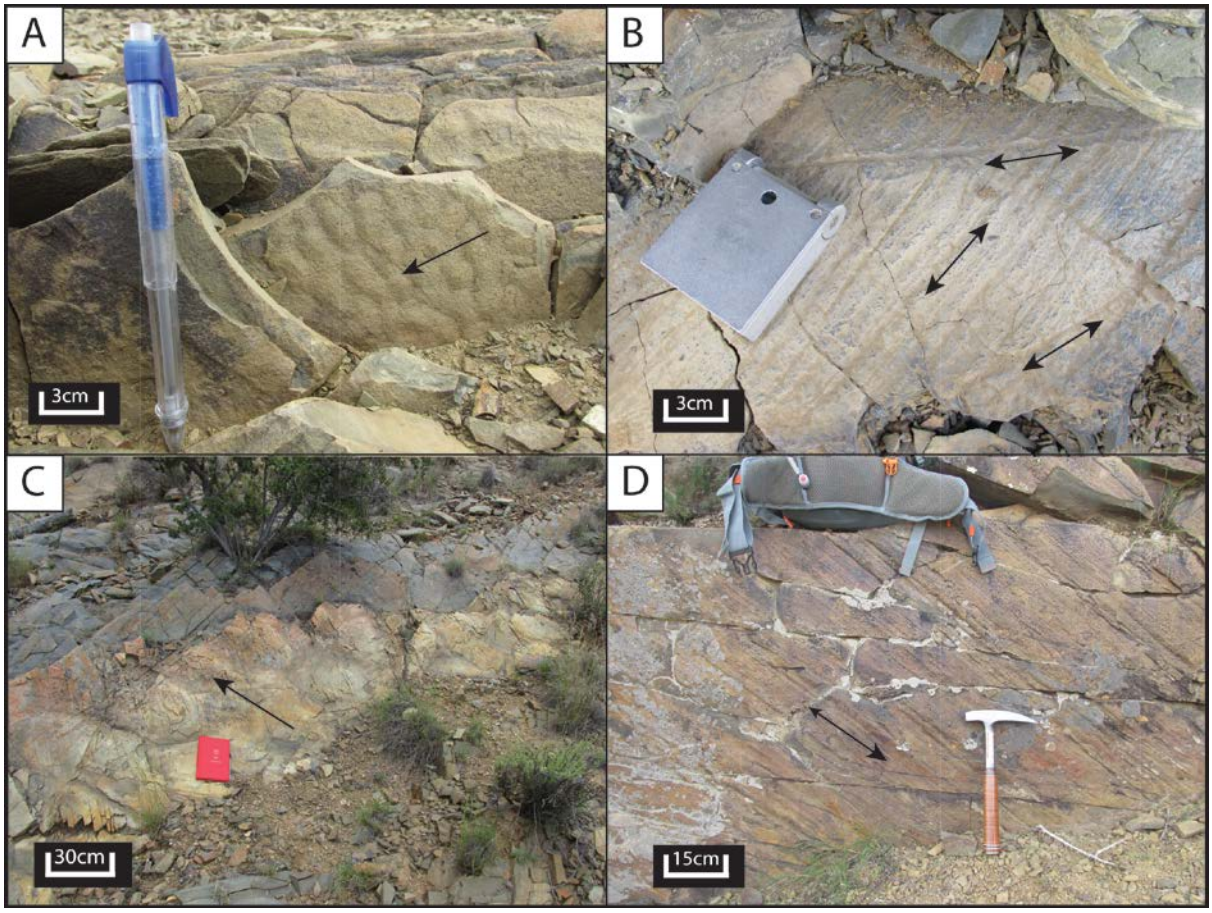

Figure 4.24: A) Small current-ripples on the upper bedding plain of a FA2 bed used to obtain palaeocurrent readings. B) Groove marks with a single dominant current trend. One or two grooves indicate slight variation in flow direction. C) Large 3D ripples on the bedding surface of a FA2 bed. Cross-sectional view of bed indicates linguoid ripple cross-laminations. D) Groove casts on the lower bounding surface of a sandstone bed. Skip and prod marks on this surface favours a stronger indication of current direction towards the one end.

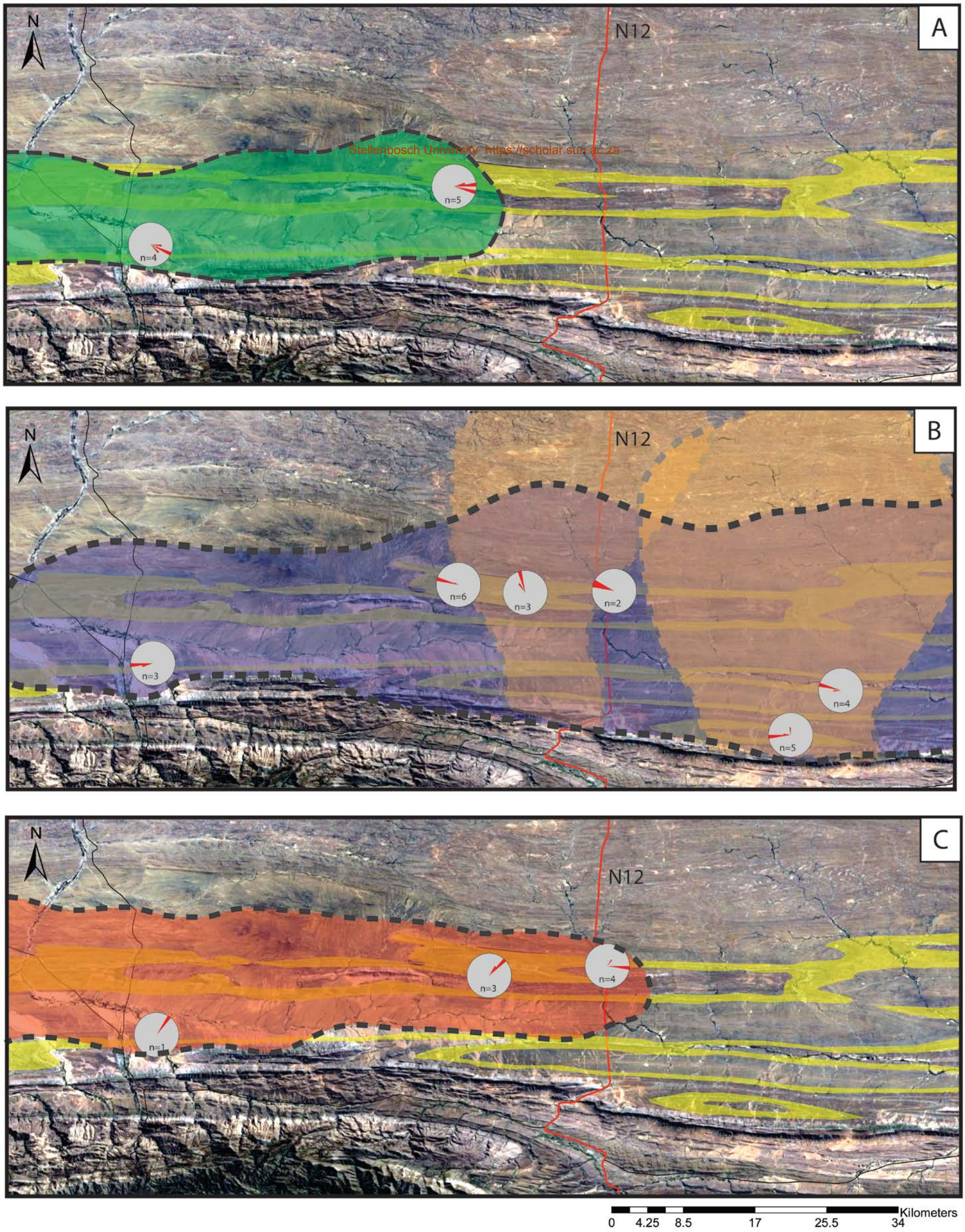

Figure 4.25: A) Geographic distribution of the Visckuil Formation with rose diagrams indicating an E palaeocurrent flow. B) Geographic distribution of the Ripon Formation with an overall W to NW palaeotransport direction also showing the inferred lobe distribution as seen through channelized features and palaeocurrents. C) Geographic distribution of the Laingsburg Formation exhibiting an overall E to NE palaeocurrent flow.

4.4 U-Pb detrital zircon analysis (LA-ICPMS)

Within the study area, eight samples were strategically collected across the range of the Vischkuil, Laingsburg and Ripon formations (Fig 4.26) (Table 8). From these eight samples 987 grains were collected, of which 548 grains could successfully be used within this study (439 grains had a discordance of more than 20%). Discordance greater than 20% could be the result of common lead contamination, lead loss, erroneous readings, and or crystal fractionation (Schoene, 2014). Grains resulting in concordant ages of less than 248.0 Ma are considered to have undergone lead loss.

Table 8: Geographic location and stratigraphic position of each sample used for U/Pb detrital zircon geochronology.

Sample	Stratigraphic horizon	Farm Name	Latitude	Longitude
WK01	Middle Vischkuil Fm	Zacharias Fontein 135	S 33.21093°	E 22.05490°
WK-2016-1	Upper Laingsburg Fm	Zacharias Fontein 135	S 33.20867°	E 22.05218°
KG06	Middle Pluto's Vale M	Groot Tygerberg 102	S 33.12811°	E 22.34262°
KG-2016-1	Lower Vischkuil Fm	Groot Tygerberg 102	S 33.12910°	E 22.34383°
N12-2016-1	Upper Laingsburg Fm	N12 Road Cutting	S 33.11820°	E 22.53867°
OM01	Lower Pluto's Vale M	Klipfontein 174	S 33.28221°	E 22.77908°
OM06	Middle Wonderfontein M	Klipfontein 174	S 33.28428°	E 22.77593°
MK-2016-4	Upper Trumpeters M	Minnies Kraal 112	S 33.21683°	E 22.82622°

Grain populations were determined by groupings of three or more co-temporal grains (n ≥3) (Fig 4.28). All samples show varying morphologies of euhedral, fractured and abraded crystals. Grains vary from elongated crystals with asymmetrical and symmetrical doubly terminating ends to short equal axis crystals with symmetrical doubly terminating ends. The varying morphologies range between S-type and P-type based on Pupin's (1980) Zircon morphology scheme. Growth zoning found in most of the grains are the result of magmatic crystal formation and indicates very little metamorphic influence (Ireland & Williams, 2003). Many of the grains (40%) that yielded an age older than 400.0 Ma exhibit a more abraded nature producing sub-rounded crystals and occasionally exhibit a more metamorphic source due to the irregular internal structure of the grains (Ireland & Williams, 2003).

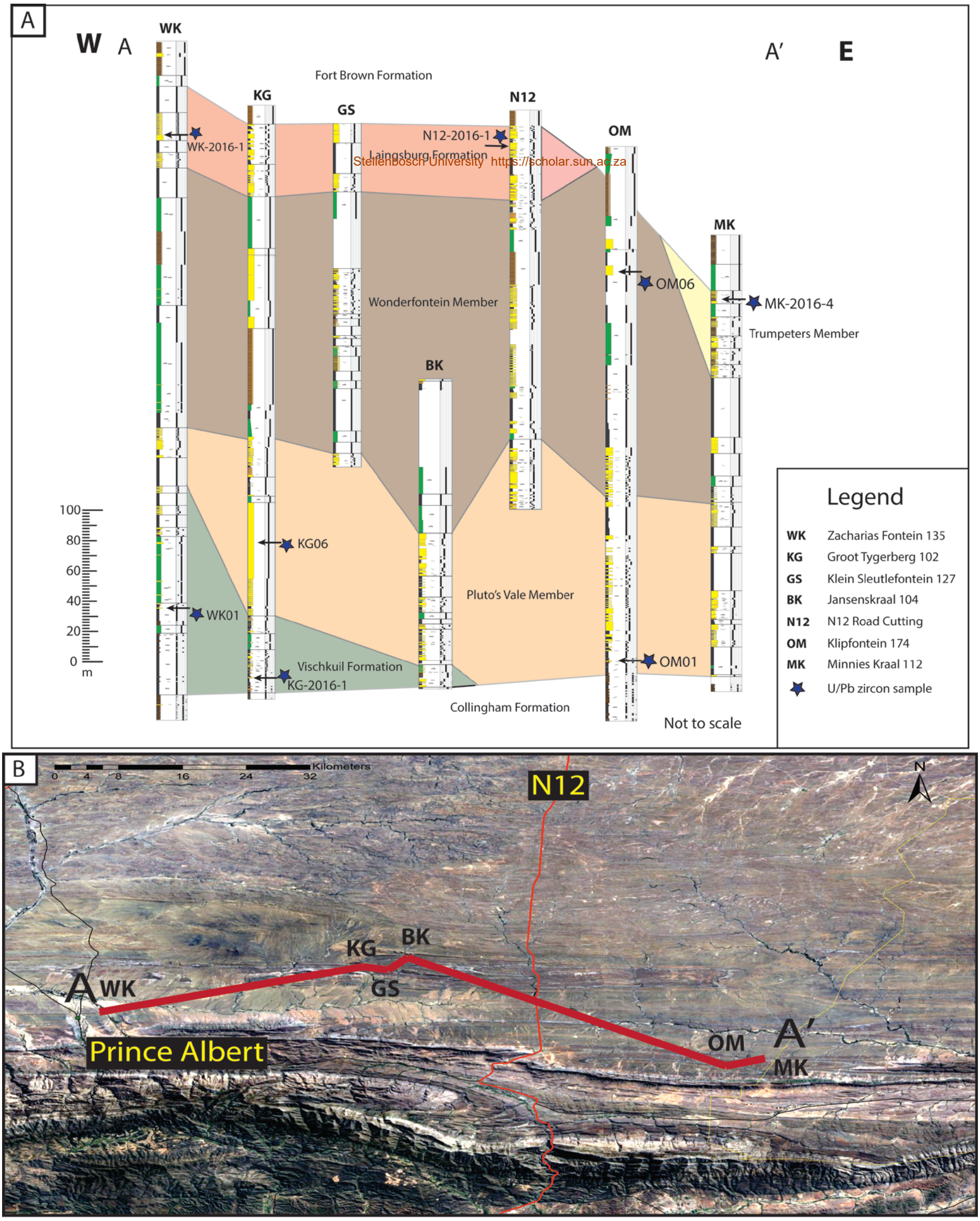

Figure 4.26: A) Stratigraphic sections showing the stratigraphic position of each sample used for U-Pb detrital Zircon analysis. B) Google Earth image showing the geographical position of the stratigraphic sections.

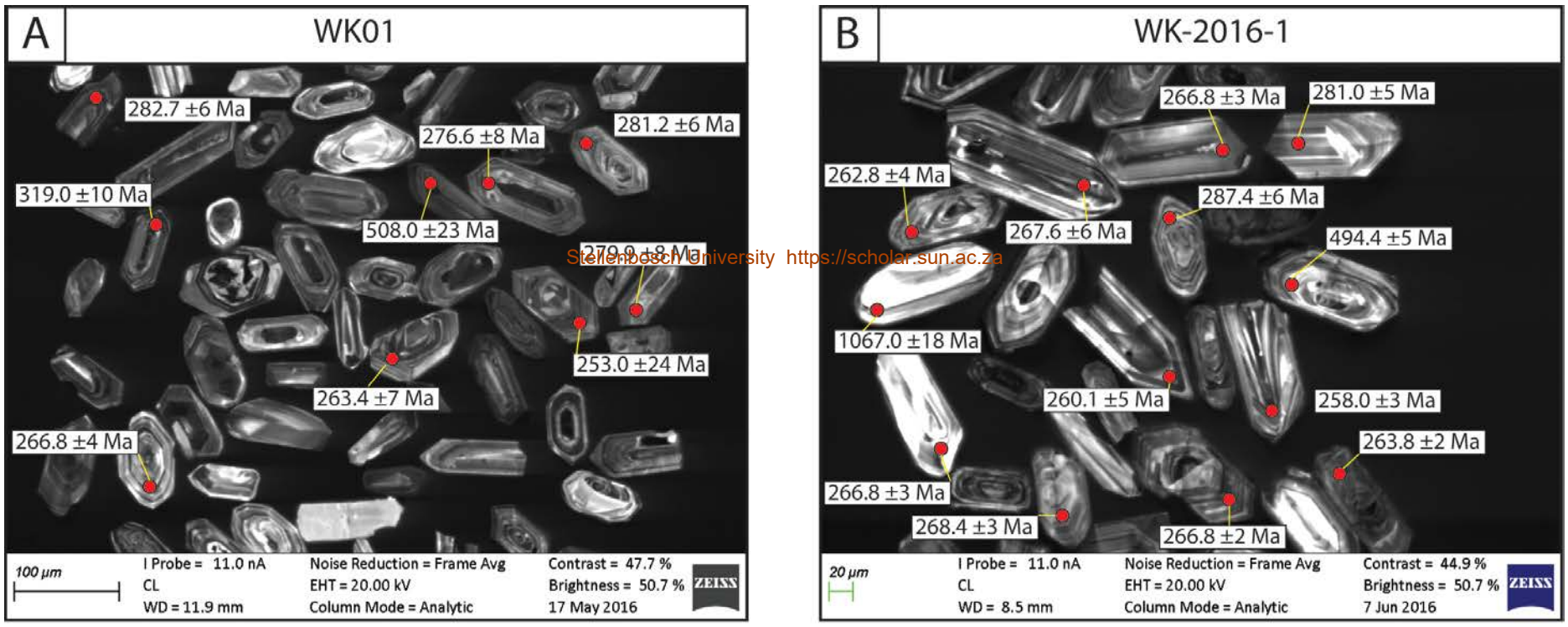

Figure 4.27: A) CL-image of sample WK01. Notice the slightly rounded nature of the older grains. B) CL-image of sample WK-2016-1. The 1Ga grain shows a rounded grain boundary and irregular internal structures. C) CL-image of sample N12-2016-1. Notice the variation in grain morphology between elongated grains and short axis grains. D) Backscatter-image of a single zircon from sample WK-2016-1. Grain shows resetting of the mineral with a new growth pattern around a magmatic core. For this reason, the core was chosen for analysis. E) CL-Image of sample MK-2016-4, different morphologies persist even with grains of nearly similar ages. F) CL-image of sample MK-2016-4.

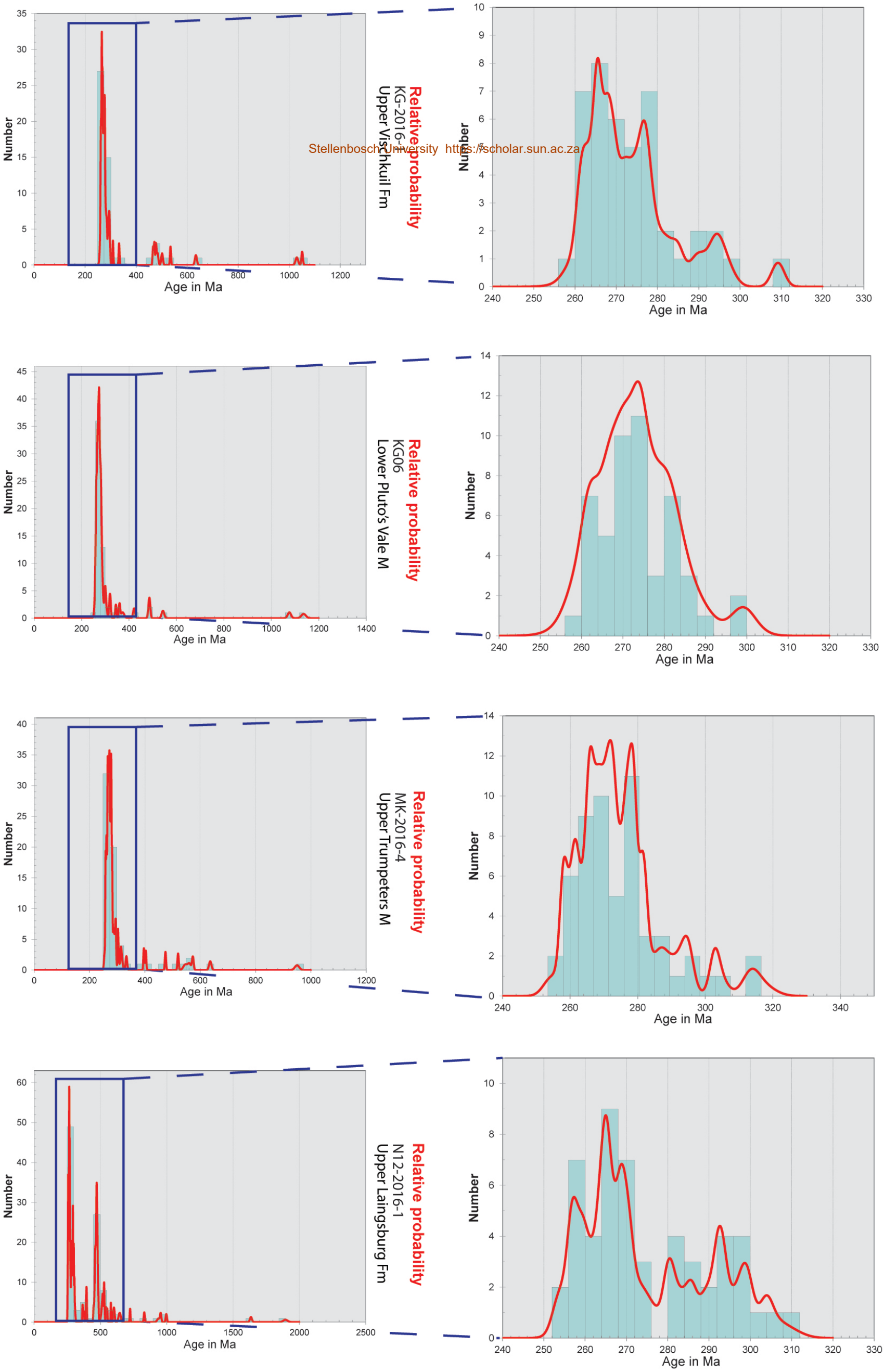

Figure 4.28: Probability density plots of all samples to the age of 2 Ga. Each sample presents a series of peaks which represents a cumulation of a specific zircon grain age. Graphs are plotted in Isoplot with a bin size of 40. Each sample has a major peak between the ages of 250 Ma and 300 Ma.

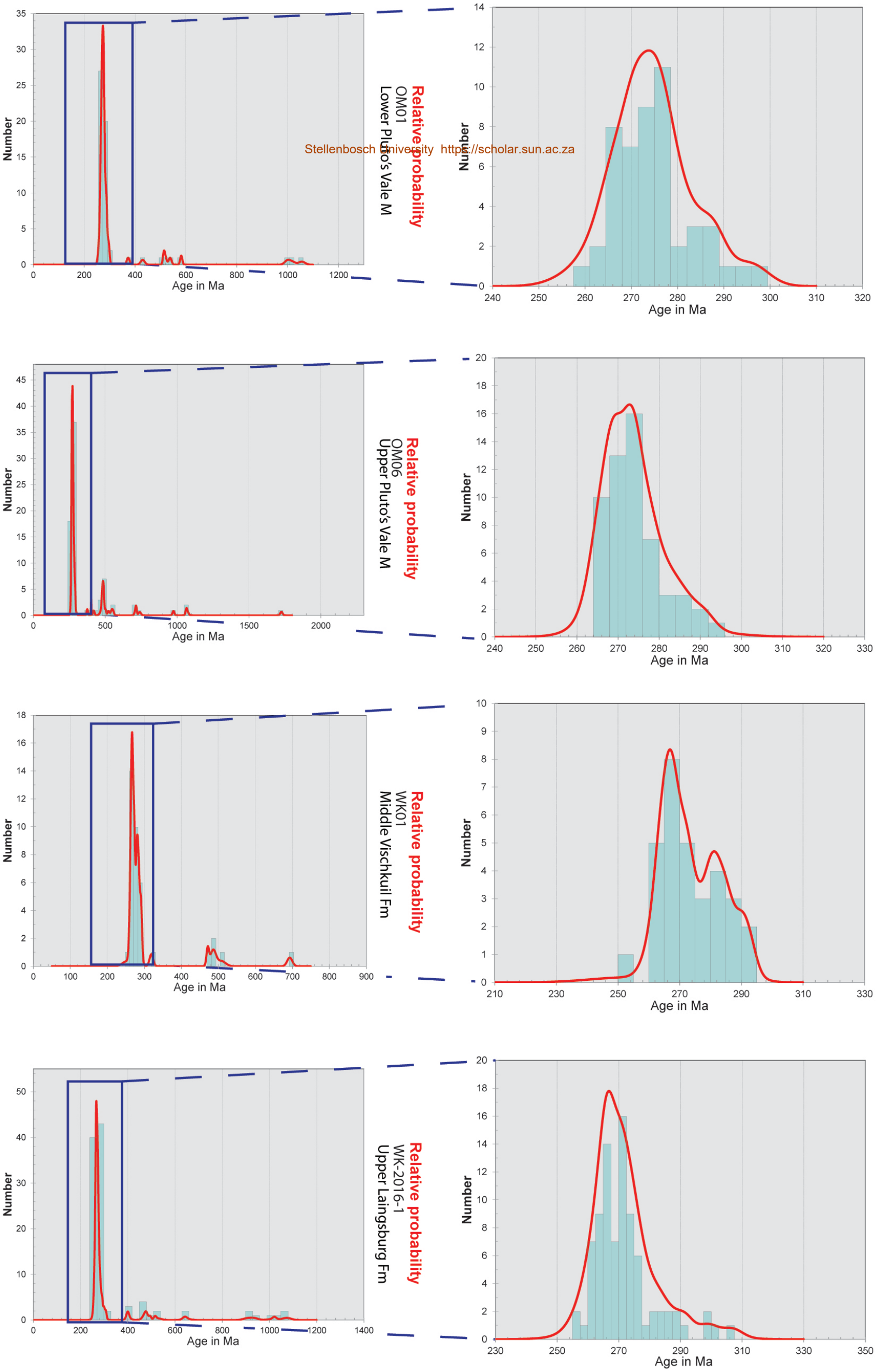

Figure 4.28 (cont.): Probability density plots of all samples to the age of 2 Ga. Each sample presents a series of peaks which represents a cumulation of a specific zircon grain age. Graphs are plotted in Isoplot with a bin size of 40. Each sample has a major peak between the ages of 250 Ma and 300 Ma.

4.4.1 Sample descriptions

4.4.1.1 WK01

About 84% of zircon grains within sample WK01 from the middle of the Vischkuil Formation seem to be magmatic with well-formed growth zonation (Fig 4.27 A). Grains vary in size between 50.0 µm and 100.0 µm with the majority (70%) of grains being around 70.0 µm. From the 60 analysed grains, 38 were concordant with various age populations (64% of sample) (Table 9). 23% of concordant grains were core shots of zircons during ablation, with the rest being rim shots. Two grains (5.3%) were Triassic (<248 Ma), but are considered erroneous due to lead loss. The largest population, 81.6% (n=31) of the sample, is Permian (254.0 Ma - 320.0 Ma) with a sub-ordinate population (7.9%, n=3) around the Ordovician and Cambrian (440.0 Ma - 495.0 Ma) and one older Cambrian grain (508.0 ±23 Ma). A single Neoproterozoic grain (693.0 ±14 Ma) is also present. Out of the Permian population of grains, 23% have a Th/U ratio greater than 1.0 (Th/U>1.0). The following youngest detrital zircon ages were obtained: YSG is 253.0 (±24) Ma; YPP is 266.7 Ma (Fig 4.28); YDZ is 256.3 (+5.7/-5.7) Ma; YC2σ [3] is 262.3 (±10.4) Ma; the weighted average [10] is 265.2 (±1.7); A TuffZirc [10] age of 264.6 (+2.2/-2.1) Ma was determined (Fig 4.29).

4.4.1.2 WK-2016-1

About 81% of grains from sample WK-2016-1 from the upper Laingsburg Formation are magmatic with clear growth patterns, with metamorphic grains not uncommon among grains yielding older ages (Fig 4.27 B, D). The grainsize varies between 80.0 µm and 130.0 µm averaging at 100.0 µm. A total of 170 zircon grains were analysed of which 103 were concordant (60% of sample) (Table 10). 23.3% of the concordant grains were core shots of zircons during ablation, with the rest being rim shots. A large population of grains (81.5%, n=84) are Late Carboniferous to Permian (254.0 Ma - 320.0 Ma) with a minor population (2.9%, n=3) of Devonian age (354.0 Ma - 417.0 Ma). Older zircon populations occur at the Ordovician (440.0 Ma - 495.0 Ma) and Cambrian (495.0 Ma - 545.0 Ma), 4.8% (n=5) and 1.9%

Table 9: U-Pb data for sample WK01. Pb206/U238 is the age.

Sample WK01			RATIOS									AGES [Ma]						Conc.
Analysis	U [ppm][a]	Pb [ppm][a]	Th/U[a]	*206/204*	$^{207}Pb/^{235}U$[b]	2 σ[d]	$^{206}Pb/^{238}U$[b]	2 σ[d]	rho[c]	$^{207}Pb/^{206}Pb$[e]	2 σ[d]	$^{207}Pb/^{235}U$	2 σ	$^{206}Pb/^{238}U$	2 σ	$^{207}Pb/^{206}Pb$	2 σ	%
WK01_31.d	814	663	0.92	2700	0.2490	0.0150	0.0355	0.0013	0.6328	0.0514	0.0046	225	12	224.8	8	250	200	90
WK01_17.d	401	279	0.61	80	0.2650	0.0290	0.0376	0.0028	0.1900	0.0520	0.0062	238	23	238.0	17	260	250	92
WK01_15.d	447	280	0.48	-500	0.2890	0.0400	0.0401	0.0039	0.9089	0.0525	0.0035	257	32	253.0	24	300	150	84
WK01_26.d	176	180	0.93	670	0.2940	0.0240	0.0415	0.0011	0.1432	0.0518	0.0043	261	19	262.2	7	260	170	101
WK01_16.d	414	469	0.87	1600	0.3030	0.0390	0.0417	0.0012	0.2624	0.0530	0.0066	268	30	263.4	7	310	280	85
WK01_9.d	299	303	0.89	800	0.2970	0.0110	0.0417	0.0006	0.0556	0.0514	0.0019	263	9	263.6	4	265	87	99
WK01_5.d	258	304	0.96	-120	0.3050	0.0240	0.0418	0.0013	0.0883	0.0530	0.0048	269	19	264.2	8	300	190	88
WK01_44.d	248	332	1.03	700	0.3040	0.0270	0.0419	0.0009	0.1116	0.0529	0.0050	269	21	264.6	5	290	200	91
WK01_36.d	145	165	0.90	540	0.3000	0.0260	0.0420	0.0012	0.0744	0.0521	0.0046	265	20	265.4	7	260	180	102
WK01_4.d	270	219	0.67	1400	0.2990	0.0190	0.0422	0.0010	0.0293	0.0516	0.0035	265	15	266.6	6	260	140	103
WK01_11.d	225	197	0.77	450	0.3000	0.0120	0.0423	0.0006	0.2214	0.0516	0.0021	266	9	266.8	4	266	88	100
WK01_32.d	245	229	0.74	540	0.3070	0.0200	0.0423	0.0007	0.1776	0.0529	0.0035	271	16	267.0	4	300	140	89
WK01_40.d	249	259	0.87	490	0.3030	0.0140	0.0424	0.0008	0.1440	0.0521	0.0027	268	11	267.7	5	270	110	99
WK01_57.d	259	340	0.93	1700	0.3100	0.0250	0.0426	0.0015	0.5165	0.0529	0.0035	274	19	268.7	9	320	150	84
WK01_35.d	298	614	1.51	-200	0.3030	0.0140	0.0426	0.0009	0.2238	0.0518	0.0029	268	11	269.2	6	270	130	100
WK01_56.d	146	137	0.81	-40	0.3040	0.0340	0.0427	0.0014	0.1313	0.0519	0.0057	268	26	269.2	9	250	220	108
WK01_58.d	225	241	0.88	890	0.3060	0.0150	0.0429	0.0008	0.0255	0.0520	0.0028	271	12	270.5	5	270	110	100
WK01_12.d	254	329	1.05	-370	0.3120	0.0360	0.0432	0.0010	0.2329	0.0528	0.0065	274	28	272.4	6	280	250	97
WK01_46.d	209	166	0.54	-290	0.3090	0.0450	0.0432	0.0006	0.4181	0.0520	0.0075	272	35	272.6	4	250	280	109
WK01_47.d	173	127	0.56	1500	0.3140	0.0370	0.0433	0.0019	0.2222	0.0529	0.0066	276	28	273.0	12	290	250	94
WK01_23.d	206	148	0.50	1600	0.3190	0.0270	0.0438	0.0013	0.0708	0.0532	0.0048	281	21	276.6	8	320	200	86
WK01_34.d	197	191	0.74	400	0.3150	0.0400	0.0439	0.0011	0.3162	0.0522	0.0066	277	31	276.9	7	270	270	103
WK01_14.d	232	338	1.27	500	0.3170	0.0310	0.0444	0.0012	0.2595	0.0522	0.0056	279	24	279.9	8	270	230	104
WK01_53.d	171	104	0.48	560	0.3200	0.0180	0.0445	0.0007	0.1053	0.0524	0.0029	281	14	280.4	4	280	120	100
WK01_24.d	183	262	1.04	-20	0.3200	0.0200	0.0446	0.0009	0.0718	0.0523	0.0032	281	15	281.2	6	320	150	88
WK01_20.d	350	313	0.66	2000	0.3300	0.0200	0.0448	0.0010	0.2524	0.0536	0.0038	289	16	282.7	6	340	160	83
WK01_7.d	301	294	0.86	800	0.3230	0.0160	0.0450	0.0010	0.0532	0.0524	0.0030	284	12	283.7	6	290	120	98
WK01_27.d	358	296	0.58	1900	0.3230	0.0160	0.0453	0.0008	0.2167	0.0520	0.0025	284	12	285.3	5	280	110	102
WK01_37.d	145	167	0.82	800	0.3270	0.0200	0.0455	0.0010	0.2265	0.0522	0.0030	286	15	286.9	6	280	120	102
WK01_55.d	245	312	0.88	1000	0.3270	0.0270	0.0458	0.0018	0.0581	0.0520	0.0047	287	20	289.0	11	260	190	111
WK01_54.d	281	226	0.58	1130	0.3340	0.0160	0.0460	0.0007	0.1303	0.0526	0.0025	292	12	290.2	4	290	100	100
WK01_60.d	241	388	1.13	820	0.3370	0.0140	0.0465	0.0007	0.1777	0.0527	0.0023	294	11	292.8	4	296	92	99
WK01_19.d	263	281	0.73	2000	0.3740	0.0340	0.0507	0.0017	0.1347	0.0540	0.0058	322	25	319.0	10	330	220	97
WK01_43.d	163	174	0.47	800	0.5930	0.0350	0.0759	0.0011	0.0512	0.0568	0.0033	471	22	471.4	7	460	130	102
WK01_39.d	91	162	0.82	0	0.6200	0.0430	0.0782	0.0025	0.4469	0.0579	0.0050	488	26	485.0	15	490	190	99
WK01_45.d	82	43	0.20	140	0.6200	0.0430	0.0785	0.0025	0.1628	0.0576	0.0043	488	27	487.0	15	480	160	101
WK01_22.d	270	274	0.33	3100	0.6520	0.0440	0.0819	0.0039	0.2085	0.0581	0.0021	510	27	508.0	23	531	81	96
WK01_51.d	151	203	0.44	-240	0.9870	0.0360	0.1135	0.0023	0.1622	0.0632	0.0024	696	18	693.0	14	699	82	99

Legend

Triassic | Carboniferous | Silurian | Cambrian | Prefered Age

Permian | Devonian | Ordovician | Proterozoic

Table 10: U-Pb data for sample WK-2016-1. Pb206/U238 is the age.

Sample WK-2016-1			RATIOS										AGES [Ma]						Conc.
Analysis	U [ppm][a]	Pb [ppm][a]	Th/U[a]	206/204	$^{207}Pb/^{235}U^{b}$	2 σ[d]	$^{206}Pb/^{238}U^{b}$	2 σ[d]	rho[c]	$^{207}Pb/^{206}Pb^{c}$	2 σ[d]	$^{207}Pb/^{235}U$	2 σ	$^{206}Pb/^{238}U$	2 σ	$^{207}Pb/^{206}Pb$	2 σ	%
WK1-65	185	139	0.74	144	0.2900	0.0250	0.0406	0.0014	0.2030	0.0519	0.0046	258	20	256.3	9	260	190	99
WK1-78	231	146	0.62	200	0.2890	0.0150	0.0407	0.0007	0.2090	0.0523	0.0028	257	11	257.2	4	270	110	95
WK1-134	273	111	0.36	203	0.2920	0.0110	0.0408	0.0005	0.0626	0.0518	0.0020	260	8	258.0	3	260	80	99
WK1-137	556	415	0.72	560	0.2960	0.0180	0.0412	0.0007	0.1427	0.0522	0.0032	263	14	260.1	5	280	140	93
WK1-79	410	269	0.63	430	0.2940	0.0150	0.0412	0.0009	0.1175	0.0518	0.0027	261	11	260.3	5	260	110	100
WK1-29	451	465	0.88	285	0.2990	0.0097	0.0414	0.0005	0.1919	0.0525	0.0019	265	8	261.5	3	292	79	90
WK1-54	338	268	0.69	880	0.2957	0.0093	0.0415	0.0005	0.1581	0.0518	0.0016	263	7	261.8	3	262	68	100
WK1-101	429	152	0.36	530	0.2970	0.0110	0.0415	0.0007	0.2084	0.0520	0.0018	264	8	262.2	4	275	79	95
WK1-60	296	132	0.44	220	0.2940	0.0190	0.0415	0.0010	0.4620	0.0517	0.0040	262	15	262.4	6	250	160	105
WK1-150	329	164	0.48	338	0.2970	0.0140	0.0416	0.0007	0.3160	0.0518	0.0024	264	11	262.8	4	265	99	99
WK1-128	322	327	0.88	780	0.2965	0.0091	0.0417	0.0005	0.2430	0.0519	0.0016	265	8	263.3	3	265	66	99
WK1-161	436	352	0.71	380	0.3030	0.0120	0.0419	0.0006	0.3540	0.0525	0.0020	269	9.3	264.4	3.5	295	82	90
WK1-133	478	232	0.42	710	0.2985	0.0060	0.0418	0.0004	0.2699	0.0523	0.0012	267	5	263.8	2	287	48	92
WK1-108	179	335	1.67	127	0.2950	0.0140	0.0418	0.0006	0.0655	0.0512	0.0025	265	12	263.9	4	270	110	98
WK1-1	114	56	0.45	16	0.3010	0.0200	0.0418	0.0008	0.1316	0.0523	0.0034	266	15	264.2	5	270	130	98
WK1-73	160	121	0.72	60	0.3000	0.0130	0.0419	0.0006	0.0673	0.0521	0.0023	266	10	264.5	3	269	91	98
WK1-119	229	147	0.58	198	0.3008	0.0083	0.0419	0.0004	0.1378	0.0521	0.0014	266	6	264.8	2	269	58	98
WK1-129	326	392	1.12	400	0.3030	0.0210	0.0419	0.0011	0.2503	0.0527	0.0042	268	16	264.8	7	290	170	91
WK1-83	87	90	0.90	133	0.3020	0.0150	0.0420	0.0005	0.0409	0.0525	0.0026	266	11	265.0	3	268	99	99
WK1-100	186	160	0.81	154	0.3050	0.0140	0.0421	0.0006	0.2293	0.0528	0.0027	269	11	265.8	4	290	100	92
WK1-13	397	251	0.54	185	0.3007	0.0063	0.0421	0.0003	0.1300	0.0519	0.0012	267	5	265.0	2	285	49	100
WK1-167	536	324	0.53	467	0.3011	0.0069	0.0422	0.0004	0.2822	0.0518	0.0011	267	5.4	265.5	2.7	266	49	100
WK1-23	246	189	0.64	147	0.3010	0.0170	0.0421	0.0006	0.1948	0.0520	0.0028	267	13	265.0	4	260	120	102
WK1-43	102	59	0.54	102	0.3030	0.0190	0.0422	0.0006	0.2240	0.0521	0.0031	267	14	266.5	4	270	120	99
WK1-113	283	218	0.70	410	0.3014	0.0064	0.0422	0.0004	0.1918	0.0518	0.0011	267	5	266.6	2	267	46	100
WK1-130	325	305	0.86	490	0.3070	0.0120	0.0423	0.0006	0.0298	0.0528	0.0023	271	10	266.8	4	296	89	90
WK1-136	282	159	0.49	500	0.3020	0.0081	0.0423	0.0004	0.2072	0.0519	0.0014	268	6	266.8	2	285	57	101
WK1-140	100	122	1.05	149	0.2980	0.0140	0.0423	0.0005	0.0506	0.0513	0.0024	263	10	266.8	3	219	90	122
WK1-148	180	236	1.10	194	0.3030	0.0120	0.0423	0.0005	0.1733	0.0520	0.0021	267	9	266.8	3	270	85	99
WK1-51	233	314	1.14	245	0.3030	0.0110	0.0423	0.0005	0.0542	0.0520	0.0019	268	9	266.9	3	269	79	99
WK1-19	135	138	0.88	85	0.3040	0.0100	0.0423	0.0004	0.0983	0.0521	0.0018	268	8	267.2	3	285	70	101
WK1-20	368	262	0.62	236	0.3060	0.0100	0.0424	0.0004	0.0971	0.0526	0.0018	271	8	267.4	3	296	77	90
WK1-107	299	315	1.02	250	0.3070	0.0200	0.0424	0.0015	0.4980	0.0525	0.0028	271	16	267.5	9	300	120	89
WK1-149	246	366	1.39	226	0.3080	0.0200	0.0424	0.0009	0.3033	0.0530	0.0038	272	15	267.6	6	310	150	86
WK1-4	484	347	0.58	126	0.3034	0.0077	0.0424	0.0005	0.1481	0.0519	0.0014	269	6	267.8	3	269	58	100
WK1-138	152	148	0.81	188	0.3040	0.0150	0.0425	0.0005	0.1043	0.0519	0.0026	269	12	268.4	3	280	100	103
WK1-70	391	310	0.71	400	0.3050	0.0140	0.0426	0.0007	0.1427	0.0520	0.0027	270	11	268.6	4	270	110	99
WK1-154	472	242	0.48	500	0.3040	0.0110	0.0426	0.0006	0.3839	0.0518	0.0018	269	9	268.6	3	269	75	100
WK1-39	540	500	0.78	380	0.3050	0.0150	0.0427	0.0008	0.3873	0.0518	0.0023	270	12	269.5	5	270	100	100
WK1-158	163	115	0.56	144	0.3100	0.0120	0.0429	0.0005	0.1929	0.0524	0.0020	273	9.1	270.8	2.9	278	78	97
WK1-38	115	45	0.34	94	0.3110	0.0250	0.0428	0.0012	0.3633	0.0518	0.0040	274	19	270.2	7	250	160	108
WK1-63	550	246	0.42	570	0.3060	0.0130	0.0429	0.0007	0.0939	0.0518	0.0023	271	10	270.5	4	263	96	103
WK1-166	400	350	0.72	50	0.3120	0.0310	0.0430	0.0012	0.3080	0.0526	0.0052	275	24	271.7	7.4	300	210	91
WK1-105	309	220	0.62	168	0.3120	0.0220	0.0429	0.0008	0.0348	0.0528	0.0038	275	17	270.6	5	300	160	90
WK1-7	150	175	0.97	51	0.3082	0.0086	0.0429	0.0004	0.0302	0.0522	0.0015	272	7	270.7	2	289	61	101
WK1-94	371	286	0.65	290	0.3150	0.0170	0.0429	0.0011	0.0111	0.0533	0.0031	278	13	270.8	7	330	130	82
WK1-6	125	121	0.79	43	0.3100	0.0120	0.0430	0.0005	0.0782	0.0524	0.0021	273	10	271.1	3	273	81	99
WK1-118	281	184	0.57	310	0.3078	0.0071	0.0430	0.0003	0.1112	0.0522	0.0013	272	6	271.3	2	274	51	99
WK1-8	293	219	0.67	94	0.3120	0.0110	0.0430	0.0006	0.2462	0.0527	0.0018	275	9	271.6	3	302	75	90
WK1-58	277	275	0.87	480	0.3080	0.0150	0.0430	0.0010	0.0322	0.0520	0.0029	272	12	271.6	6	270	120	101
WK1-124	86	49	0.52	106	0.3130	0.0150	0.0430	0.0007	0.2465	0.0529	0.0025	275	12	271.6	4	330	110	82
WK1-14	220	174	0.70	100	0.3110	0.0190	0.0431	0.0006	0.0302	0.0524	0.0032	274	15	271.8	4	280	120	97
WK1-25	210	94	0.36	140	0.3130	0.0120	0.0431	0.0006	0.0479	0.0529	0.0022	276	10	271.8	4	303	88	90
WK1-32	260	452	1.46	120	0.3110	0.0190	0.0432	0.0008	0.2920	0.0523	0.0033	274	15	272.3	5	280	140	97
WK1-89	255	187	0.70	280	0.3100	0.0130	0.0432	0.0007	0.1575	0.0521	0.0022	273	10	272.4	4	274	88	99
WK1-55	202	128	0.54	330	0.3140	0.0120	0.0432	0.0004	0.0239	0.0528	0.0022	276	10	272.7	3	289	83	94
WK1-170	113	85	0.61	135	0.3130	0.0210	0.0433	0.0009	0.2381	0.0525	0.0034	275	16	273.2	5.6	280	130	98
WK1-2	435	184	0.36	80	0.3104	0.0090	0.0433	0.0005	0.2184	0.0521	0.0015	274	7	273.2	3	273	62	100
WK1-30	216	139	0.58	-50	0.3120	0.0150	0.0433	0.0007	0.0954	0.0523	0.0027	275	12	273.4	4	280	110	98
WK1-127	240	192	0.71	193	0.3120	0.0094	0.0434	0.0004	0.0592	0.0526	0.0018	275	7	273.8	3	289	72	95
WK1-106	264	304	1.11	229	0.3090	0.0130	0.0435	0.0005	0.1792	0.0521	0.0023	273	10	274.2	3	272	95	101
WK1-18	723	886	0.73	460	0.3110	0.0100	0.0435	0.0010	0.2881	0.0519	0.0017	275	8	274.4	6	278	75	99
WK1-16	216	122	0.49	128	0.3150	0.0140	0.0436	0.0008	0.2320	0.0522	0.0019	277	10	274.9	5	271	78	101
WK1-165	183	112	0.51	181	0.3150	0.0260	0.0437	0.0009	0.4676	0.0522	0.0040	277	20	275.7	5.3	270	160	102
WK1-82	158	135	0.72	152	0.3140	0.0110	0.0436	0.0005	0.0169	0.0519	0.0018	276	9	274.9	3	269	76	102
WK1-104	209	163	0.72	170	0.3170	0.0190	0.0436	0.0009	0.3628	0.0525	0.0029	279	15	275.4	6	290	120	95
WK1-31	153	128	0.72	160	0.3220	0.0230	0.0438	0.0011	0.0776	0.0535	0.0041	282	18	276.5	7	320	160	86
WK1-21	269	228	0.70	175	0.3148	0.0091	0.0439	0.0004	0.1099	0.0520	0.0015	277	7	276.7	3	275	63	101
WK1-12	193	113	0.50	85	0.3170	0.0190	0.0439	0.0007	0.0015	0.0525	0.0033	279	15	277.1	4	280	130	99
WK1-36	119	106	0.68	116	0.3160	0.0140	0.0439	0.0007	0.2275	0.0517	0.0023	277	11	277.1	4	271	88	102
WK1-22	122	57	0.41	99	0.3190	0.0160	0.0440	0.0006	0.0044	0.0526	0.0028	279	12	277.8	4	280	110	99
WK1-24	180	152	0.61	134	0.3210	0.0270	0.0444	0.0011	0.2236	0.0523	0.0043	282	20	280.2	7	270	170	104
WK1-147	290	258	0.79	286	0.3190	0.0170	0.0446	0.0009	0.1704	0.0520	0.0029	281	13	281.0	5	270	120	104
WK1-111	106	120	0.99	93	0.3260	0.0220	0.0449	0.0008	0.2214	0.0527	0.0036	285	17	282.8	5	280	140	101
WK1-155	492	201	0.33	790	0.3235	0.0086	0.0449	0.0004	0.2245	0.0524	0.0014	284	7	282.8	3	287	58	99
WK1-122	277	257	0.80	260	0.3300	0.0130	0.0454	0.0006	0.0684	0.0528	0.0022	289	10	286.4	4	298	89	96
WK1-144	304	187	0.55	340	0.3280	0.0260	0.0456	0.0010	0.1942	0.0522	0.0041	287	20	287.4	6	270	170	106
WK1-68	153	216	1.13	166	0.3340	0.0170	0.0458	0.0007	0.0363	0.0531	0.0029	291	13	288.3	5	300	110	96
WK1-168	200	199	0.80	225	0.3390	0.0290	0.0459	0.0012	0.5322	0.0535	0.0039	296	22	289.1	7.5	330	160	88
WK1-164	232	249	0.82	188	0.3337	0.0092	0.0463	0.0004	0.0352	0.0524	0.0015	292	7	291.7	2.4	290	62	101
WK1-169	160	108	0.52	440	0.3420	0.0270	0.0473	0.0017	0.6624	0.0522	0.0034	297	20	298.0	10	280	140	106
WK1-116	206	95	0.38	264	0.3460	0.0120	0.0475	0.0005	0.1110	0.0533	0.0020	303	9	299.2	3	311	76	96
WK1-98	236	256	0.74	470	0.3460	0.0140	0.0478	0.0010	0.1763	0.0526	0.0024	302	10	301.1	6	300	100	100
WK1-126	157	130	0.65	260	0.3560	0.0110	0.0488	0.0005	0.1059	0.0529	0.0017	309	8	307.1	3	307	68	100
WK1-72	302	311	0.44	436	0.4850	0.0180	0.0639	0.0009	0.0053	0.0551	0.0022	401	12	399.5	6	399	91	100
WK1-75	267	43	0.09	160	0.4830	0.0140	0.0641	0.0009	0.2855	0.0549	0.0016	400	10	400.3	6	393	65	102
WK1-69	289	206	0.40	258	0.4910	0.0310	0.0645	0.0019	0.2590	0.0551	0.0030	405	22	403.0	12	410	130	98
WK1-37	71	59	0.45	99	0.5890	0.0440	0.0749	0.0016	0.0856	0.0572	0.0045	467	29	465.6	10	460	170	101
WK1-34	184	125	0.31	260	0.5990	0.0260	0.0759	0.0012	0.2016	0.0573	0.0025	475	17	471.5	7	476	96	99
WK1-9	97	81	0.43	67	0.6060	0.0280	0.0771	0.0011	0.0856	0.0572	0.0027	479	18	478.5	7	460	100	104
WK1-120	292	415	0.68	1000	0.6100	0.0190	0.0771	0.0011	0.2727	0.0573	0.0018	482	12	479.0	6	486	70	99
WK1-148	339	117	0.17	710	0.6260	0.0180	0.0797	0.0008	0.0439	0.0574	0.0017	495	11	494.4	5	491	64	101
WK1-50	218	232	0.49	240	0.6700	0.0200	0.0833	0.0010	0.0084	0.0584	0.0018	520	12	515.6	6	524	67	98
WK1-123	171	143	0.35	380	0.6980	0.0680	0.0859	0.0022	0.2081	0.0589	0.0055	536	40	531.0	13	540	210	98
WK1-67	177	481	1.06	430	0.8840	0.0300	0.1047	0.0015	0.1155	0.0613	0.0022	642	17	641.6	9	633	80	101
WK1-92	88	30	0.10	420	0.8970	0.0560	0.1057	0.0027	0.1699	0.0616	0.0036	648	30	648.0	16	640	130	101
WK1-48	33	33	0.24	134	1.4600	0.1100	0.1504	0.0029	0.0003	0.0704	0.0053	903	44	903.0	16	870	160	104
WK1-26	36	100	0.59	78	1.4900	0.1100	0.1536	0.0034	0.3023	0.0705	0.0053	919	46	921.0	19	950	190	96
WK1-76	135	87	0.19	650	1.5370	0.0540	0.1567	0.0027	0.3615	0.0712	0.0024	943	22	938.0	15	946	70	99
WK1-141	27	96	0.77	140	1.8760	0.0930	0.1801	0.0032	0.2493	0.0755	0.0037	1065	33	1067.0	18	1030	110	104
WK1-131	48	575	2.75	182	1.9030	0.0620	0.1823	0.0029	0.1627	0.0767	0.0027	1081	23	1079.0	16	1083	72	100
WK1-157	197	466	0.51	1420	1.7280	0.0660	0.1704	0.0042	0.2023	0.0736	0.0030	1018	24	1014.0	23	1025	82	99
WK1-163	212	632	0.88	580	1.7410	0.0580	0.1716	0.0014	0.0331	0.0736	0.0023	1023	21	1020.9	8	1025	64	100

Legend

Triassic | Carboniferous | Silurian | Cambrian | Prefered Age

Permian | Devonian | Ordovician | Proterozoic

(n=2) of the sample, respectively. Some pre-Cambrian grains (640.0 Ma - 650.0 Ma and 900.0 Ma - 1040.0 Ma) are also present and occupy 8.7% (n=9) of the sample. 12% of the total Permian grains have a Th/U ratio greater than 1.0 (Th/U>1.0). The following youngest detrital zircon signatures were obtained: YSG is 256.3 (±9) Ma; YPP is 266.4 Ma (Fig 4.28); YDZ is 252.5 (+5.6/-16) Ma; YC2σ [3] is 257.6 (±5.6) Ma; the weighted average [10] is 260.6 (±1.2); A TuffZirc [10] age of 260.9 (+1.5/-3.7) Ma was determined (Fig 4.29).

4.4.1.3 KG06

Overall about 88% of the grains in sample KG06 exhibit a magmatic origin with growth zoning. Grains vary from 60.0 µm to 120.0 µm in size averaging at 90.0 µm. 63 Grains were concordant, with various age populations, from a total of 90 grains (70% of sample) (Table 11). 19.0% of the concordant grains were core shots of zircons during ablation, with the rest being rim shots. Two grains (3.2%) were Triassic (<248 Ma), but are considered erroneous due to lead loss. The dominating population (82.5%, n=52) remains in the Late Carboniferous and Permian (254.0 Ma - 320.0 Ma) with a minor population (6.3%, n=4) of ages across the Carboniferous and Devonian (340.0 Ma - 420.0 Ma). Sub-ordinate clusters also occur at the Cambrian (480.0 Ma - 545.0 Ma) and Meso-Proterozoic (1000.0 Ma - 1200.0 Ma) occupying 4.7% (n=3) and 3.2% (n=2) of the sample respectively. From the total Permian population, 10% has a Th/U ratio greater than 1.0 (Th/U>1.0). The following youngest detrital zircon signatures were obtained: YSG is 258.5 (±6) Ma; YPP is 262.8 Ma (Fig 4.28); YDZ is 250.8 (+8.3/-19) Ma; YC2σ [3] is 259.5 (±9.1) Ma; the weighted average [10] is 261.8 (±1.8); A TuffZirc [10] age of 261.9 (+2.3/-0.9) Ma was determined (Fig 4.29).

4.4.1.4 KG-2016-1

About 85% of the grains in sample KG-2016-1 from the upper Laingsburg Formation are euhedral with fracturing visible and commonly have well-formed growth patterns, suggesting a magmatic origin. Grainsize varies between 50.0 µm and 110.0 µm with the average grainsize of 90.0 µm. A total of 86

Table 11: U-Pb data for sample KG06. Pb206/U238 is the age.

Sample KG06			RATIOS										AGES [Ma]						Conc.
Analysis	U [ppm][a]	Pb [ppm][a]	Th/U[a]	206/204	$^{207}Pb/^{235}U$[b]	2 σ[d]	$^{206}Pb/^{238}U$[b]	2 σ[d]	rho[c]	$^{207}Pb/^{206}Pb$[c]	2 σ[d]	$^{207}Pb/^{235}U$	2 σ	$^{206}Pb/^{238}U$	2 σ	$^{207}Pb/^{206}Pb$	2 σ	%
KG06_50.d	600	461	0.66	2900	0.2500	0.0130	0.0352	0.0006	0.3027	0.0513	0.0024	227	10	222.7	4	250	110	89
KG06_19.d	600	376	0.49	5200	0.2541	0.0078	0.0359	0.0004	0.1347	0.0512	0.0015	230	6	227.2	3	241	66	94
KG06_55.d	391	387	0.80	1500	0.2600	0.0390	0.0393	0.0029	0.6896	0.0515	0.0052	250	31	248.0	18	250	210	99
KG06_75.d	274	199	0.63	3000	0.2930	0.0230	0.0409	0.0009	0.0017	0.0520	0.0044	261	18	258.5	6	270	180	96
KG06_26.d	445	522	0.87	4200	0.2950	0.0150	0.0413	0.0017	0.5063	0.0519	0.0024	262	12	261.0	11	270	100	97
KG06_34.d	69	46	0.56	470	0.3000	0.0320	0.0413	0.0014	0.1683	0.0526	0.0054	264	25	261.1	9	270	200	97
KG06_72.d	142	87	0.55	980	0.2970	0.0290	0.0414	0.0011	0.0123	0.0522	0.0054	262	23	261.4	7	240	200	109
KG06_47.d	266	250	0.79	-60	0.2980	0.0120	0.0414	0.0006	0.2383	0.0519	0.0021	265	10	261.7	4	265	87	99
KG06_90.d	335	140	0.38	990	0.2980	0.0130	0.0415	0.0006	0.0297	0.0527	0.0026	264	10	262.0	4	300	100	87
KG06_4.d	195	92	0.38	1000	0.2960	0.0220	0.0416	0.0011	0.4466	0.0521	0.0048	263	17	262.8	7	250	180	105
KG06_1.d	262	299	0.98	1600	0.2970	0.0210	0.0416	0.0021	0.3341	0.0518	0.0039	264	16	263.0	13	260	170	101
KG06_62.d	256	616	2.46	70	0.3020	0.0210	0.0418	0.0016	0.1421	0.0524	0.0039	268	17	264.1	10	280	160	94
KG06_85.d	145	140	0.83	-90	0.2990	0.0260	0.0419	0.0010	0.1594	0.0517	0.0047	264	20	264.7	6	250	180	106
KG06_64.d	297	409	1.18	1000	0.2980	0.0210	0.0421	0.0009	0.0970	0.0512	0.0038	265	16	265.7	6	230	150	116
KG06_53.d	112	96	0.71	670	0.3020	0.0260	0.0422	0.0010	0.1056	0.0518	0.0044	267	20	266.2	6	250	170	106
KG06_8.d	329	240	0.60	-100	0.3030	0.0230	0.0422	0.0006	0.1468	0.0521	0.0043	268	18	266.4	4	260	170	102
KG06_78.d	103	52	0.46	610	0.3030	0.0210	0.0425	0.0009	0.1846	0.0520	0.0039	268	16	268.0	6	250	150	107
KG06_59.d	336	370	0.86	2400	0.3070	0.0170	0.0426	0.0007	0.0972	0.0521	0.0031	271	13	268.7	4	270	120	100
KG06_9.d	406	327	0.56	210	0.2990	0.0190	0.0426	0.0022	0.5127	0.0512	0.0029	265	15	269.0	14	230	120	117
KG06_21.d	159	151	0.78	640	0.3090	0.0160	0.0428	0.0007	0.0012	0.0524	0.0029	272	12	270.0	4	270	110	100
KG06_86.d	87	69	0.67	520	0.3050	0.0270	0.0429	0.0012	0.0795	0.0519	0.0048	268	21	270.8	8	230	180	118
KG06_76.d	197	110	0.47	600	0.3190	0.0260	0.0430	0.0019	0.0130	0.0537	0.0047	280	20	271.0	11	340	200	80
KG06_10.d	202	298	1.18	1400	0.3080	0.0170	0.0430	0.0010	0.0657	0.0521	0.0029	272	13	271.1	6	270	120	100
KG06_77.d	109	132	1.00	770	0.3140	0.0200	0.0430	0.0009	0.1311	0.0530	0.0034	276	15	271.4	6	290	130	94
KG06_74.d	301	394	0.98	3000	0.3090	0.0230	0.0430	0.0011	0.3568	0.0519	0.0035	273	18	271.5	7	270	150	101
KG06_32.d	326	168	0.44	3500	0.3100	0.0290	0.0431	0.0013	0.1483	0.0519	0.0049	274	23	272.2	8	260	200	105
KG06_43.d	307	134	0.33	2300	0.3140	0.0190	0.0433	0.0011	0.0087	0.0525	0.0037	277	14	273.2	7	290	150	94
KG06_49.d	104	76	0.60	450	0.3130	0.0240	0.0433	0.0011	0.2457	0.0523	0.0038	276	18	273.2	7	270	150	101
KG06_79.d	319	231	0.53	1900	0.3160	0.0240	0.0434	0.0013	0.0724	0.0528	0.0039	279	18	273.6	8	300	160	91
KG06_35.d	282	224	0.64	2600	0.3150	0.0180	0.0434	0.0010	0.3661	0.0523	0.0028	277	14	273.7	6	280	110	98
KG06_73.d	245	146	0.51	500	0.3110	0.0190	0.0434	0.0009	0.0149	0.0518	0.0033	274	14	273.9	6	250	130	110
KG06_17.d	300	231	0.63	2200	0.3120	0.0100	0.0434	0.0005	0.0620	0.0517	0.0017	276	8	274.1	3	272	75	101
KG06_16.d	332	318	0.72	4900	0.3090	0.0160	0.0435	0.0011	0.3581	0.0515	0.0025	273	12	274.4	7	260	110	106
KG06_56.d	193	156	0.60	960	0.3110	0.0150	0.0435	0.0011	0.1152	0.0517	0.0026	275	12	274.8	7	260	110	106
KG06_40.d	189	254	1.10	1000	0.3180	0.0180	0.0437	0.0011	0.2379	0.0525	0.0029	280	14	275.8	7	290	120	95
KG06_33.d	275	132	0.39	-240	0.3120	0.0170	0.0438	0.0010	0.2045	0.0517	0.0033	276	13	276.1	6	250	130	110
KG06_20.d	342	296	0.71	2900	0.3170	0.0140	0.0438	0.0010	0.6356	0.0530	0.0017	279	11	276.6	6	298	77	93
KG06_44.d	297	288	0.75	2900	0.3130	0.0190	0.0440	0.0007	0.1357	0.0514	0.0034	276	14	277.8	5	240	140	116
KG06_87.d	374	428	0.95	1900	0.3220	0.0160	0.0444	0.0007	0.3653	0.0529	0.0023	283	12	280.1	4	311	98	90
KG06_84.d	293	242	0.65	120	0.3160	0.0140	0.0445	0.0006	0.2237	0.0517	0.0025	278	11	280.5	4	260	100	108
KG06_42.d	93	112	0.97	680	0.3230	0.0330	0.0445	0.0015	0.2182	0.0525	0.0053	282	25	280.9	9	270	210	104
KG06_22.d	222	178	0.68	1900	0.3190	0.0360	0.0446	0.0012	0.0439	0.0518	0.0061	280	28	281.5	7	260	240	108
KG06_82.d	233	160	0.59	2200	0.3190	0.0210	0.0447	0.0010	0.2005	0.0517	0.0033	281	17	281.9	6	260	140	108
KG06_41.d	285	466	1.34	3000	0.3210	0.0140	0.0448	0.0007	0.0957	0.0518	0.0023	282	10	282.4	4	262	94	108
KG06_12.d	184	145	0.64	1500	0.3280	0.0190	0.0449	0.0012	0.1375	0.0528	0.0033	287	15	283.4	7	280	120	101
KG06_83.d	163	109	0.49	150	0.3310	0.0270	0.0451	0.0014	0.0078	0.0533	0.0046	289	20	284.4	9	310	180	92
KG06_57.d	336	430	0.97	700	0.3230	0.0140	0.0451	0.0008	0.2134	0.0517	0.0022	284	11	284.6	5	263	93	108
KG06_39.d	117	106	0.61	620	0.3260	0.0290	0.0453	0.0015	0.0431	0.0522	0.0051	286	23	285.9	9	260	200	110
KG06_6.d	187	153	0.68	1700	0.3280	0.0210	0.0459	0.0010	0.4230	0.0529	0.0037	287	16	289.4	6	290	140	100
KG06_60.d	197	161	0.64	2500	0.3430	0.0200	0.0475	0.0012	0.0396	0.0522	0.0034	299	15	298.9	8	270	140	111
KG06_58.d	126	157	0.96	-80	0.3470	0.0240	0.0475	0.0009	0.1988	0.0529	0.0039	302	19	299.2	5	300	160	100
KG06_71.d	329	292	0.75	3700	0.3490	0.0240	0.0481	0.0014	0.5708	0.0528	0.0045	304	18	303.1	8	310	190	98
KG06_66.d	267	270	0.63	2400	0.3740	0.0220	0.0507	0.0011	0.3882	0.0533	0.0028	322	16	318.6	7	330	120	97
KG06_23.d	274	269	0.68	4000	0.3710	0.0230	0.0510	0.0010	0.0380	0.0530	0.0034	319	17	320.6	6	320	140	100
KG06_69.d	595	434	0.41	7100	0.4050	0.0200	0.0549	0.0010	0.3552	0.0532	0.0024	345	14	344.6	6	330	100	104
KG06_54.d	130	112	0.48	1700	0.4300	0.0330	0.0574	0.0010	0.2870	0.0538	0.0040	361	24	359.9	6	340	160	106
KG06_67.d	188	91	0.36	210	0.4510	0.0340	0.0596	0.0024	0.5307	0.0535	0.0025	377	23	373.0	14	380	130	98
KG06_52.d	178	110	0.33	1200	0.5170	0.0250	0.0676	0.0014	0.1746	0.0553	0.0027	422	17	421.4	8	400	110	105
KG06_29.d	184	226	0.56	2400	0.6170	0.0330	0.0781	0.0014	0.2123	0.0570	0.0030	486	20	484.5	8	470	110	103
KG06_89.d	301	177	0.25	1500	0.6180	0.0240	0.0784	0.0012	0.0617	0.0572	0.0023	488	15	486.7	7	493	86	99
KG06_88.d	313	363	0.53	2900	0.7060	0.0280	0.0880	0.0018	0.0717	0.0583	0.0026	542	17	543.0	11	529	97	103
KG06_2.d	376	503	0.24	20000	1.8510	0.0530	0.1517	0.0025	0.5699	0.0752	0.0023	1074	19	1076.0	14	1071	50	100
KG06_36.d	321	716	0.44	1200	2.1590	0.0580	0.1627	0.0034	0.3005	0.0809	0.0021	1168	19	1136.0	19	1218	52	93

Legend

Triassic | Carboniferous | Silurian | Cambrian | Prefered Age

Permian | Devonian | Ordovician | Proterozoic

grains were analysed with 52 grains concordant (60% of sample) (Table 12). 17.3% of the concordant grains were core shots of zircons during ablation, with the rest being rim shots. The majority of the grains (82.7%, n=43) are late Carboniferous and Permian (254.0 Ma - 340.0 Ma). Minor populations occur at the Ordovician (440.0 Ma - 495.0 Ma) and Cambrian (495.0 Ma - 545.0 Ma) occupying 7.7% (n=4) and 3.8% (n=2) of the sample respectively. Only a few grains (5.7%, n=3) are pre-Cambrian (630.0 Ma - 1100.0 Ma). 12% of the total Permian grain population has a Th/U ratio greater than 1.0 (Th/U.1.0). The following youngest detrital zircon signatures obtained are: YSG is 259.4.0 (±4) Ma; YPP is 265.7 Ma (Fig 4.28); YDZ is 259.0 (+4.1/-9.4) Ma; YC2σ [3] is 261.2 (±4.4) Ma; the weighted average [10] is 263.7 (±1.3); A TuffZirc [10] age of 263.5 (+1.5/-2.2) Ma was determined (Fig 4.29).

4.4.1.5 N12-2016-1

78% of zircon grains from sample N12-2016-1 from the upper Laingsburg Formation are magmatic, showing well developed growth zonation (Fig 4.27 C). The grains vary in size between 70.0 µm and 130.0 µm with an average grainsize of 100.0 µm. Out of 170 grains analysed, 104 grains were concordant (61% of sample) (Table 13). 16.3% of the concordant grains were core shots of zircons during ablation, with the rest being rim shots. Although the majority of grains are from the Late Carboniferous and Permian, there is a slight decrease in the total percentage of the Permian grain population (254.0 Ma - 320.0 Ma), 49.0% (n=51) of the sample, and an increase in percentage of the Ordovician grain population (440.0 Ma - 495.0 Ma), 31.7% (n=33) of the sample. There are also minor populations around the Cambrian (495.0 Ma - 545.0 Ma) and Neo-Proterozoic (545.0 Ma - 1000.0 Ma), 7.7% (n=8) and 9.6% (n=10) of the sample respectively. Two older grains are also present at 1635.0 ±15 Ma and 1895.0 ±33 Ma. Of the total Permian grain population, 21% has a Th/U ratio greater than 1.0 (Th/U >1.0). The following youngest detrital zircon signatures were obtained: YSG is 253.4 (±3) Ma; YPP is 257.6 Ma (Fig 4.28); YDZ is 251.3 (+4.2/-9.0) Ma; YC2σ [3] is 255.6 (±4.5) Ma; the weighted average [10] is 257.3 (±1.4); A TuffZirc [10] age of 258.2 (+2.1/-1.7) Ma was determined (Fig 4.29).

Table 12: U-Pb data for sample KG-2016-1. Pb206/U238 is the age.

Sample KG-2016-1			RATIOS									AGES [Ma]						Conc.
Analysis	U [ppm][a]	Pb [ppm][a]	Th/U[a]	*206/204*	$^{207}Pb/^{235}U$[b]	2 σ[d]	$^{206}Pb/^{238}U$[b]	2 σ[d]	rho[c]	$^{207}Pb/^{206}Pb$[b]	2 σ[d]	$^{207}Pb/^{235}U$	2 σ	$^{206}Pb/^{238}U$	2 σ	$^{207}Pb/^{206}Pb$	2 σ	%
KG1-47	267	250	0.78	83	0.2960	0.0110	0.0411	0.0007	0.3478	0.0523	0.0019	263	9	259.4	4	290	80	89
KG1-49	441	220	0.45	150	0.2957	0.0095	0.0414	0.0004	0.2006	0.0518	0.0017	263	7	261.3	2	261	73	100
KG1-73	396	336	0.80	390	0.3030	0.0300	0.0414	0.0014	0.0680	0.0535	0.0055	268	23	261.6	9	330	230	79
KG1-84	725	324	0.43	294	0.3000	0.0110	0.0414	0.0004	0.4410	0.0527	0.0017	266	8	261.6	3	310	75	84
KG1-52	690	304	0.45	306	0.3010	0.0130	0.0416	0.0005	0.1623	0.0527	0.0022	267	10	262.6	3	305	93	86
KG1-12	79	67	0.67	22	0.2990	0.0160	0.0417	0.0005	0.0554	0.0520	0.0027	265	12	263.2	3	260	100	101
KG1-58	666	696	0.62	363	0.3027	0.0092	0.0418	0.0007	0.0451	0.0528	0.0019	268	7	263.7	4	309	80	85
KG1-18	167	181	1.01	51	0.3000	0.0100	0.0418	0.0004	0.0820	0.0524	0.0019	266	8	263.9	3	282	78	94
KG1-30	354	221	0.59	120	0.2975	0.0072	0.0420	0.0003	0.2163	0.0518	0.0013	264	6	264.9	2	263	53	101
KG1-82	311	449	1.03	162	0.2970	0.0140	0.0420	0.0005	0.3796	0.0514	0.0023	264	11	264.9	3	249	95	106
KG1-35	349	212	0.56	112	0.2991	0.0058	0.0420	0.0003	0.1193	0.0517	0.0010	265	5	265.4	2	262	43	101
KG1-27	131	63	0.42	40	0.3010	0.0110	0.0421	0.0004	0.1171	0.0520	0.0018	267	8	265.9	2	268	74	99
KG1-1	314	242	0.66	30	0.3022	0.0083	0.0422	0.0003	0.2178	0.0520	0.0014	268	7	266.2	2	270	58	99
KG1-26	133	98	0.66	34	0.3030	0.0110	0.0423	0.0004	0.0315	0.0521	0.0019	269	8	267.0	2	266	77	100
KG1-86	399	237	0.55	165	0.3022	0.0099	0.0424	0.0004	0.0776	0.0518	0.0017	268	8	267.7	2	263	73	102
KG1-76	425	285	0.59	254	0.3031	0.0058	0.0424	0.0003	0.2214	0.0519	0.0010	269	5	267.8	2	269	41	100
KG1-57	295	187	0.57	135	0.3088	0.0084	0.0426	0.0003	0.0651	0.0527	0.0015	273	7	269.1	2	306	62	88
KG1-74	358	267	0.68	212	0.3045	0.0086	0.0426	0.0004	0.1462	0.0520	0.0015	270	7	269.1	2	273	61	99
KG1-38	144	104	0.61	54	0.3100	0.0170	0.0428	0.0007	0.0556	0.0527	0.0029	273	13	270.4	4	290	120	93
KG1-75	204	102	0.46	127	0.3070	0.0150	0.0429	0.0006	0.1753	0.0521	0.0025	271	12	270.9	4	270	100	100
KG1-5	142	187	0.97	35	0.3150	0.0290	0.0429	0.0008	0.0700	0.0531	0.0050	277	22	271.0	5	300	200	90
KG1-22	680	774	0.54	185	0.3130	0.0200	0.0430	0.0010	0.2473	0.0529	0.0033	276	15	271.1	6	310	140	87
KG1-41	418	293	0.64	224	0.3130	0.0110	0.0431	0.0005	0.0882	0.0528	0.0019	276	8	272.2	3	308	78	88
KG1-61	362	114	0.26	189	0.3090	0.0110	0.0432	0.0008	0.0997	0.0520	0.0017	273	9	272.5	5	276	71	99
KG1-6	294	360	1.02	59	0.3090	0.0130	0.0434	0.0008	0.2377	0.0517	0.0021	273	10	273.6	5	263	93	104
KG1-53	174	123	0.66	79	0.3170	0.0290	0.0434	0.0010	0.4782	0.0532	0.0051	279	23	274.0	6	320	210	86
KG1-70	281	108	0.29	177	0.3130	0.0130	0.0435	0.0005	0.0541	0.0522	0.0023	276	10	274.7	3	278	95	99
KG1-50	120	157	1.08	45	0.3190	0.0150	0.0438	0.0005	0.1252	0.0530	0.0026	280	11	276.3	3	292	98	95
KG1-81	232	225	0.75	133	0.3180	0.0180	0.0438	0.0009	0.1085	0.0528	0.0033	280	14	276.5	5	300	130	92
KG1-37	513	420	0.56	206	0.3170	0.0120	0.0439	0.0006	0.0735	0.0527	0.0023	279	9	276.9	4	294	96	94
KG1-20	206	133	0.56	75	0.3155	0.0087	0.0439	0.0004	0.0513	0.0523	0.0015	278	7	277.0	2	276	65	100
KG1-83	479	293	0.50	225	0.3160	0.0093	0.0440	0.0005	0.4298	0.0521	0.0014	279	7	277.8	3	281	59	99
KG1-33	519	290	0.50	148	0.3200	0.0110	0.0441	0.0007	0.1582	0.0528	0.0018	282	8	278.1	5	314	80	89
KG1-54	273	309	0.92	105	0.3170	0.0180	0.0441	0.0008	0.2867	0.0523	0.0034	279	14	278.0	5	280	130	99
KG1-42	86	64	0.61	34	0.3260	0.0170	0.0447	0.0008	0.4963	0.0526	0.0026	285	13	281.8	5	280	100	101
KG1-3	287	199	0.53	56	0.3230	0.0190	0.0448	0.0005	0.0360	0.0523	0.0031	284	15	282.2	3	290	130	97
KG1-25	158	152	0.81	44	0.3260	0.0120	0.0452	0.0005	0.1055	0.0526	0.0020	286	9	285.0	3	287	78	99
KG1-13	354	526	0.86	98	0.3340	0.0210	0.0459	0.0010	0.1326	0.0531	0.0037	292	16	289.1	6	320	150	90
KG1-28	247	408	1.34	77	0.3300	0.0150	0.0460	0.0006	0.1459	0.0522	0.0023	289	11	289.9	4	277	94	105
KG1-9	258	253	0.79	92	0.3420	0.0150	0.0467	0.0006	0.0173	0.0533	0.0025	298	12	294.1	3	320	99	92
KG1-60	134	135	0.81	56	0.3380	0.0370	0.0467	0.0006	0.1395	0.0526	0.0059	295	28	294.4	4	290	230	102
KG1-39	313	286	0.73	119	0.3420	0.0130	0.0471	0.0007	0.1070	0.0527	0.0022	298	10	296.8	4	302	87	98
KG1-11	116	112	0.66	30	0.3630	0.0150	0.0491	0.0005	0.0581	0.0537	0.0022	313	11	309.2	3	330	88	94
KG1-65	263	203	0.51	164	0.3930	0.0180	0.0531	0.0006	0.1428	0.0537	0.0024	336	13	333.3	4	336	97	99
KG1-51	249	86	0.18	212	0.5850	0.0160	0.0751	0.0007	0.1735	0.0567	0.0016	467	10	466.7	4	466	60	100
KG1-32	126	102	0.39	69	0.5940	0.0170	0.0759	0.0006	0.3170	0.0568	0.0015	474	11	471.8	3	475	62	99
KG1-19	166	212	0.57	124	0.6070	0.0190	0.0770	0.0006	0.0581	0.0573	0.0019	481	12	477.9	4	483	73	99
KG1-71	382	98	0.12	353	0.6200	0.0210	0.0780	0.0011	0.1280	0.0577	0.0020	489	13	483.9	6	512	79	95
KG1-10	81	113	0.61	35	0.6440	0.0260	0.0810	0.0011	0.2282	0.0578	0.0026	504	16	501.9	7	500	100	100
KG1-62	157	725	1.90	158	0.7020	0.0160	0.0865	0.0007	0.1493	0.0587	0.0013	539	9	534.9	4	537	51	100
KG1-77	60	72	0.46	67	0.8690	0.0330	0.1034	0.0013	0.0021	0.0612	0.0023	632	18	634.3	8	614	84	103
KG1-14	132	396	0.70	155	1.7620	0.0390	0.1732	0.0019	0.3643	0.0740	0.0015	1030	14	1030.0	10	1033	41	100
KG1-58	526	727	0.29	870	1.8150	0.0190	0.1771	0.0010	0.2369	0.0745	0.0008	1051	7	1050.9	6	1051	21	100

Legend

Triassic | Carboniferous | Silurian | Cambrian | Prefered Age

Permian | Devonian | Ordovician | Proterozoic

Table 13: U-Pb data for sample N12-2016-1. Pb206/U238 is the age.

Sample N12-2016-1			RATIOS									AGES [Ma]					Conc.
Analysis	U [ppm]*	Pb [ppm]*	Th/U*	206/204	$^{207}Pb/^{235}U$	2 σ	$^{206}Pb/^{238}U$	2 σ	rho	$^{207}Pb/^{206}Pb$	2 σ	$^{207}Pb/^{235}U$	2 σ	$^{206}Pb/^{238}U$	2 σ	$^{207}Pb/^{206}Pb$	2 σ	%
N12-1-20	467	665	0.83	259	0.2869	0.0093	0.0401	0.0005	0.0657	0.0520	0.0018	256	7	253.4	3	270	75	94
N12-1-76	327	416	1.21	160	0.2920	0.0140	0.0406	0.0007	0.1818	0.0522	0.0025	259	11	256.5	4	280	100	92
N12-1-139	262	308	1.09	390	0.2880	0.0084	0.0406	0.0004	0.0405	0.0515	0.0016	256	7	256.8	3	259	66	99
N12-1-151	185	131	0.62	234	0.2865	0.0085	0.0407	0.0004	0.0319	0.0510	0.0015	255	7	256.9	2	229	62	112
N12-1-73	151	132	0.75	137	0.2940	0.0200	0.0408	0.0008	0.0440	0.0523	0.0036	260	16	257.8	5	270	140	95
N12-1-53	79	163	1.87	66	0.2920	0.0180	0.0409	0.0006	0.1547	0.0513	0.0030	258	14	258.5	4	230	120	112
N12-1-93	275	283	0.87	261	0.2910	0.0100	0.0411	0.0004	0.0166	0.0519	0.0020	260	9	259.5	2	257	80	101
N12-1-26	378	319	0.81	216	0.3000	0.0140	0.0411	0.0007	0.3194	0.0530	0.0024	266	11	259.7	5	312	98	83
N12-1-102	430	215	0.51	350	0.3000	0.0240	0.0412	0.0008	0.1049	0.0528	0.0043	266	19	260.2	5	300	180	87
N12-1-124	306	429	1.16	220	0.3000	0.0130	0.0415	0.0005	0.1715	0.0524	0.0022	266	10	262.4	3	284	90	92
N12-1-130	314	312	0.98	710	0.2910	0.0200	0.0416	0.0011	0.2824	0.0508	0.0034	259	16	263.0	7	220	140	120
N12-1-84	590	940	1.05	470	0.2970	0.0160	0.0417	0.0010	0.3858	0.0517	0.0025	263	12	263.2	6	260	100	101
N12-1-87	307	245	0.67	210	0.2980	0.0120	0.0418	0.0005	0.1137	0.0518	0.0021	265	9	264.0	3	262	87	101
N12-1-77	281	135	0.41	310	0.3000	0.0094	0.0418	0.0003	0.1074	0.0520	0.0016	266	7	264.2	2	269	67	98
N12-1-148	236	242	0.84	165	0.3020	0.0100	0.0419	0.0004	0.1194	0.0523	0.0018	267	8	264.4	3	277	73	95
N12-1-13	257	302	0.96	101	0.3010	0.0120	0.0420	0.0005	0.0051	0.0520	0.0019	267	9	265.1	3	270	81	98
N12-1-48	306	336	0.94	210	0.3021	0.0070	0.0420	0.0003	0.1138	0.0522	0.0012	268	6	265.2	2	275	50	96
N12-1-97	136	150	0.91	153	0.3040	0.0120	0.0421	0.0005	0.1730	0.0521	0.0021	268	10	266.0	3	265	84	100
N12-1-43	204	183	0.80	140	0.3030	0.0230	0.0421	0.0015	0.0722	0.0525	0.0050	268	18	266.1	9	280	190	95
N12-1-75	196	188	0.78	193	0.3030	0.0110	0.0422	0.0005	0.2744	0.0521	0.0018	268	8	266.3	3	271	72	98
N12-1-105	252	355	1.31	160	0.3050	0.0130	0.0422	0.0006	0.1582	0.0519	0.0024	270	10	266.7	4	266	99	100
N12-1-85	272	371	1.12	290	0.3050	0.0140	0.0425	0.0006	0.0680	0.0520	0.0025	270	11	268.4	4	270	100	99
N12-1-170	331	375	0.97	292	0.3043	0.0070	0.0426	0.0003	0.1627	0.0519	0.0012	269	5	268.7	2	266	48	101
N12-1-92	433	715	0.93	440	0.3130	0.0150	0.0426	0.0007	0.3072	0.0534	0.0024	276	12	269.0	5	330	100	82
N12-1-107	609	431	0.61	780	0.3040	0.0110	0.0426	0.0005	0.0705	0.0518	0.0019	269	8	269.1	3	267	80	101
N12-1-36	113	134	1.06	64	0.3130	0.0210	0.0426	0.0007	0.3396	0.0532	0.0033	275	16	269.2	4	310	130	87
N12-1-63	327	217	0.58	340	0.3077	0.0088	0.0428	0.0004	0.1098	0.0519	0.0015	272	7	270.4	2	271	61	100
N12-1-4	218	225	0.88	63	0.3055	0.0082	0.0429	0.0004	0.1388	0.0520	0.0015	270	6	270.6	3	266	60	102
N12-1-78	394	342	0.74	670	0.3093	0.0087	0.0433	0.0005	0.0267	0.0519	0.0016	273	7	273.2	3	273	66	100
N12-1-91	426	528	0.82	50	0.3150	0.0260	0.0434	0.0010	0.0744	0.0527	0.0045	277	20	273.5	6	300	190	91
N12-1-45	444	400	0.82	277	0.3170	0.0120	0.0437	0.0006	0.1012	0.0526	0.0021	279	9	275.8	4	294	86	94
N12-1-49	318	233	0.62	290	0.3199	0.0081	0.0444	0.0004	0.0051	0.0523	0.0014	281	6	280.1	3	283	59	99
N12-1-9	781	35	0.02	270	0.3226	0.0074	0.0445	0.0005	0.1810	0.0526	0.0013	284	6	280.6	3	302	53	93
N12-1-14	246	330	0.98	122	0.3270	0.0170	0.0446	0.0008	0.2545	0.0531	0.0027	286	13	281.2	5	310	110	91
N12-1-152	292	239	0.67	410	0.3243	0.0096	0.0450	0.0006	0.1315	0.0524	0.0016	285	7	283.7	4	287	66	99
N12-1-69	205	153	0.67	239	0.3280	0.0230	0.0452	0.0012	0.6177	0.0526	0.0030	287	18	284.7	8	290	120	98
N12-1-101	371	303	0.63	370	0.3281	0.0081	0.0454	0.0004	0.2308	0.0525	0.0013	288	6	285.9	3	291	53	98
N12-1-21	385	503	0.95	350	0.3290	0.0370	0.0455	0.0025	0.4997	0.0523	0.0053	288	28	287.0	16	270	200	106
N12-1-59	227	187	0.66	217	0.3330	0.0150	0.0459	0.0005	0.0168	0.0526	0.0024	290	12	289.0	3	292	98	99
N12-1-153	178	155	0.70	232	0.3370	0.0170	0.0462	0.0006	0.0216	0.0529	0.0027	294	13	291.3	4	300	110	97
N12-1-129	202	327	1.33	380	0.3360	0.0110	0.0464	0.0004	0.1341	0.0527	0.0017	294	8	292.5	3	297	67	98
N12-1-88	168	151	0.74	200	0.3350	0.0140	0.0465	0.0005	0.1358	0.0530	0.0025	295	11	292.7	3	298	99	98
N12-1-132	375	313	0.67	30	0.3367	0.0091	0.0465	0.0004	0.0439	0.0523	0.0014	294	7	292.8	3	295	61	99
N12-1-117	483	258	0.42	500	0.3390	0.0180	0.0467	0.0008	0.0330	0.0527	0.0029	296	13	294.3	5	300	120	98
N12-1-30	419	278	0.54	313	0.3480	0.0170	0.0471	0.0009	0.3132	0.0536	0.0025	303	13	296.7	5	340	100	87
N12-1-162	149	236	1.17	160	0.3460	0.0140	0.0472	0.0006	0.0304	0.0532	0.0023	300	11	297.4	4	310	91	96
N12-1-135	160	127	0.59	170	0.3480	0.0130	0.0475	0.0005	0.1526	0.0534	0.0020	302	10	298.8	3	318	78	94
N12-1-169	168	161	0.71	184	0.3490	0.0140	0.0476	0.0005	0.0547	0.0529	0.0022	303	11	299.7	3	300	86	100
N12-1-61	224	149	0.51	240	0.3540	0.0110	0.0483	0.0005	0.0736	0.0533	0.0018	307	9	303.9	3	312	69	97
N12-1-41	111	298	2.14	93	0.3550	0.0170	0.0483	0.0009	0.2303	0.0534	0.0025	307	13	304.3	6	306	97	99
N12-1-95	106	160	1.08	65	0.3620	0.0310	0.0490	0.0011	0.0153	0.0537	0.0048	312	23	308.4	7	320	180	96
N12-1-24	322	283	0.60	320	0.4370	0.0170	0.0585	0.0008	0.1848	0.0542	0.0021	367	12	366.2	5	362	85	101
N12-1-17	467	466	0.65	215	0.4420	0.0210	0.0598	0.0012	0.1042	0.0537	0.0024	371	15	374.3	7	350	100	107
N12-1-138	325	115	0.24	460	0.4800	0.0150	0.0629	0.0009	0.3197	0.0553	0.0017	398	10	393.4	6	411	67	96
N12-1-127	227	257	0.61	700	0.4770	0.0250	0.0630	0.0013	0.2538	0.0550	0.0028	395	17	393.6	8	400	110	98
N12-1-103	168	186	0.62	550	0.4840	0.0220	0.0634	0.0007	0.1970	0.0553	0.0024	399	15	396.4	4	396	93	100
N12-1-150	79	134	0.82	147	0.5610	0.0250	0.0722	0.0009	0.1157	0.0564	0.0025	449	16	449.1	5	423	90	106
N12-1-74	105	198	1.01	189	0.5770	0.0250	0.0735	0.0011	0.3135	0.0570	0.0024	461	16	457.1	7	467	91	98
N12-1-168	190	206	0.51	369	0.5760	0.0330	0.0737	0.0010	0.1706	0.0567	0.0031	461	21	458.3	6	460	120	100
N12-1-163	208	256	0.69	230	0.5780	0.0380	0.0737	0.0019	0.1861	0.0569	0.0038	462	24	459.0	11	470	160	98
N12-1-110	187	275	0.69	220	0.5840	0.0320	0.0741	0.0013	0.3497	0.0570	0.0029	466	20	460.8	8	470	110	98
N12-1-137	209	289	0.68	310	0.5820	0.0250	0.0742	0.0011	0.1007	0.0570	0.0028	465	16	461.2	6	480	100	96
N12-1-51	207	360	0.88	343	0.5830	0.0200	0.0742	0.0007	0.1939	0.0570	0.0020	465	13	461.6	4	467	75	99
N12-1-125	323	290	0.50	1090	0.5850	0.0360	0.0748	0.0017	0.0054	0.0568	0.0037	467	23	465.0	10	470	150	99
N12-1-158	337	297	0.44	650	0.5880	0.0160	0.0748	0.0008	0.1699	0.0570	0.0014	469	10	465.1	5	479	55	97
N12-1-32	235	55	0.12	237	0.5820	0.0180	0.0748	0.0009	0.1593	0.0565	0.0018	465	12	465.2	6	450	72	103
N12-1-161	249	240	0.46	400	0.5870	0.0140	0.0752	0.0007	0.0548	0.0564	0.0015	468	9	467.6	4	453	58	103
N12-1-10	338	320	0.44	238	0.5940	0.0130	0.0753	0.0007	0.4043	0.0573	0.0012	473	9	467.9	4	492	45	95
N12-1-55	178	182	0.49	380	0.5910	0.0150	0.0758	0.0007	0.0847	0.0566	0.0015	470	9	471.0	4	451	55	104
N12-1-56	332	495	0.73	530	0.6000	0.0110	0.0759	0.0005	0.2721	0.0574	0.0010	476	7	471.3	3	490	40	96
N12-1-120	171	334	0.98	260	0.6000	0.0290	0.0759	0.0009	0.4797	0.0587	0.0037	475	18	471.8	5	500	110	94
N12-1-111	341	146	0.20	430	0.5920	0.0130	0.0760	0.0008	0.2445	0.0565	0.0012	471	8	472.0	5	461	48	102
N12-1-98	128	103	0.37	251	0.5940	0.0210	0.0761	0.0009	0.2109	0.0567	0.0019	472	13	472.7	5	444	74	106
N12-1-90	137	76	0.26	130	0.5960	0.0190	0.0762	0.0008	0.0180	0.0572	0.0020	473	12	473.2	5	471	76	100
N12-1-38	167	261	0.72	207	0.6010	0.0300	0.0763	0.0012	0.0983	0.0571	0.0029	477	19	473.9	7	470	110	101
N12-1-3	193	307	0.70	74	0.6000	0.0380	0.0763	0.0027	0.4753	0.0593	0.0049	476	24	474.0	16	540	170	88
N12-1-25	267	491	0.87	277	0.5970	0.0140	0.0765	0.0012	0.0434	0.0570	0.0012	475	9	475.2	7	477	49	100
N12-1-57	157	225	0.68	271	0.5970	0.0150	0.0767	0.0007	0.1947	0.0565	0.0014	474	10	476.6	4	454	56	105
N12-1-58	104	128	0.57	183	0.6020	0.0220	0.0767	0.0009	0.0303	0.0571	0.0022	477	14	476.6	5	461	82	103
N12-1-16	395	327	0.41	380	0.5970	0.0320	0.0768	0.0014	0.1549	0.0565	0.0030	475	20	476.8	9	460	120	104
N12-1-104	255	185	0.39	1600	0.6060	0.0210	0.0771	0.0011	0.0781	0.0570	0.0019	480	13	478.5	7	482	76	99
N12-1-143	226	375	0.79	590	0.6050	0.0160	0.0772	0.0009	0.3404	0.0574	0.0015	482	11	479.3	5	482	57	99
N12-1-145	197	194	0.43	480	0.6070	0.0160	0.0773	0.0014	0.2900	0.0575	0.0019	483	11	479.8	8	502	68	96
N12-1-79	265	407	0.71	450	0.6160	0.0150	0.0782	0.0007	0.2005	0.0574	0.0013	487	10	485.1	4	493	51	98
N12-1-33	178	330	0.79	216	0.6500	0.0330	0.0818	0.0020	0.0274	0.0577	0.0033	507	20	507.0	12	500	120	101
N12-1-166	145	129	0.42	290	0.6590	0.0330	0.0827	0.0012	0.2397	0.0578	0.0028	512	20	512.3	7	500	110	102
N12-1-121	146	330	1.06	200	0.6630	0.0320	0.0835	0.0008	0.2305	0.0577	0.0028	520	17	516.8	5	520	92	99
N12-1-39	89	143	0.70	152	0.6630	0.0240	0.0840	0.0010	0.2067	0.0572	0.0020	517	14	520.1	6	468	75	111
N12-1-7	183	346	0.78	130	0.6750	0.0200	0.0852	0.0009	0.2279	0.0573	0.0017	523	12	526.9	6	483	66	109
N12-1-42	111	167	0.65	250	0.6790	0.0190	0.0853	0.0008	0.1523	0.0577	0.0016	524	11	527.8	5	500	61	106
N12-1-128	289	346	0.54	230	0.6920	0.0160	0.0857	0.0009	0.1734	0.0589	0.0015	535	10	530.1	6	550	56	96
N12-1-18	168	182	0.46	196	0.7090	0.0190	0.0879	0.0009	0.2667	0.0586	0.0015	543	11	543.3	5	533	58	102
N12-1-5	335	262	0.30	195	0.7270	0.0160	0.0893	0.0009	0.4027	0.0594	0.0014	554	10	551.3	6	572	48	96
N12-1-11	202	337	0.69	197	0.7690	0.0160	0.0940	0.0007	0.1795	0.0592	0.0013	579	9	579.2	4	566	44	102
N12-1-80	285	166	0.24	880	0.8130	0.0310	0.0975	0.0017	0.1696	0.0605	0.0023	604	17	599.6	10	614	84	98
N12-1-47	444	13	0.01	1160	0.8190	0.0200	0.0983	0.0015	0.1347	0.0605	0.0016	607	11	604.1	9	613	58	99
N12-1-82	166	410	0.92	400	0.8670	0.0340	0.1046	0.0023	0.4065	0.0616	0.0022	643	18	641.0	13	640	77	100
N12-1-15	290	201	0.27	280	0.9030	0.0270	0.1062	0.0023	0.1789	0.0628	0.0028	660	20	650.0	13	690	92	94
N12-1-46	109	150	0.42	267	1.0420	0.0330	0.1189	0.0010	0.2298	0.0634	0.0019	723	16	723.9	6	698	68	104
N12-1-34	277	331	0.29	560	1.3510	0.0240	0.1376	0.0014	0.4586	0.0712	0.0012	867	11	831.0	8	957	33	87
N12-1-149	62	91	0.35	17000	1.5300	0.1500	0.1569	0.0037	0.3652	0.0707	0.0078	936	60	939.0	21	910	220	103
N12-1-37	62	134	0.51	195	1.6800	0.0380	0.1673	0.0017	0.1552	0.0730	0.0017	998	14	997.0	10	992	47	101
N12-1-71	53	243	0.65	311	4.0120	0.0940	0.2889	0.0031	0.1924	0.1014	0.0026	1634	19	1635.0	15	1647	44	99
N12-1-108	74	479	0.71	480	5.4800	0.1500	0.3417	0.0069	0.4205	0.1162	0.0027	1896	24	1895.0	33	1898	42	100

Legend

Triassic | Carboniferous | Silurian | Cambrian | Prefered Age

Permian | Devonian | Ordovician | Proterozoic

4.4.1.6 OM01

Zoning can be observed in about 85% of the grains from the lower Pluto's Vale Member, especially grains that yielded ages younger than 400 Ma. The average grainsize is about 80.0 µm with grains ranging from 30.0 µm to 120.0 µm. A total of 90 grains were analysed with only 52 grains concordant (57% of sample) (Table 14). Only 7.7% of the concordant grains were core shots of zircons during ablation. The rest were rim shots. A large proportion of grains (75%, n=39) are from the Permian (254.0 Ma - 320.0 Ma) with a few grains (9.6%, n=5) having a slightly younger Triassic age (< 248.0 Ma). Although presented, these grains most likely represent lead loss and is not considered accurate. There is one Silurian grain (430.0 ±16 Ma) present and a minor population (5.7%, n=3) at the Cambrian (495.0 Ma - 545.0 Ma) with some older Meso-Proterozoic grains (995.0 Ma - 1100.0 Ma) occupying 7.6% (n=4) of the sample. 29% of the total Permian grain population has a Th/U ratio greater than 1.0 (Th/U>1.0). The following youngest detrital zircon signatures were obtained: YSG is 264.3 (±6) Ma; YPP is 273.1 Ma (Fig 4.28); YDZ is 259.4 (+11/-19) Ma; YC2σ [3] is 265.1 (±8.7) Ma; the weighted average [10] is 266.9 (±2.3); A TuffZirc [10] age of 267.8 (+2.2/-2.0) Ma was determined (Fig 4.29).

4.4.1.7 OM06

Zoning is a common occurrence in sample OM06 from the middle Wonderfontein Member, occupying 89% of the total zircon grains. The gain-size varies between 70.0 µm and 120.0 µm with an average of 100.0 µm. A total of 120 grains were analysed with 75 grains concordant (62% of sample) (Table 15). 13.3% of the concordant grains were core shots of zircons during ablation while the rest were rim shots. The majority of grains (68.0%, n=51) are from the Permian (254.0 Ma - 320.0 Ma) with very few (4.0%, n=3) younger Triassic grains (< 248 Ma). Although presented, these grains are considered erroneous due to lead loss. A very small population (4.0%, n=3) of grains is Devonian (354.0 Ma - 420.0 Ma). There is also the occurrence of a population (9.3%, n=7) around the Ordovician and Cambrian (440.0 Ma - 495.0 Ma) as well as 4.0% (n=3) early Cambrian grains (495.0 Ma - 545.0 Ma). A few (9.3%, n=7) older pre-Cambrian grains are also present (550.0 Ma - 1100.0 Ma). There is one very old grain

Table 14: U-Pb data for sample OM01. Pb206/U238 is the age.

Sample OM01			RATIOS									AGES [Ma]						Conc.
Analysis	U [ppm][a]	Pb [ppm][a]	Th/U[a]	206/204	$^{207}Pb/^{235}U$[b]	2 σ[d]	$^{206}Pb/^{238}U$[b]	2 σ[d]	rho[c]	$^{207}Pb/^{204}Pb$[e]	2 σ[d]	$^{207}Pb/^{235}U$	2 σ	$^{206}Pb/^{238}U$	2 σ	$^{207}Pb/^{206}Pb$	2 σ	%
OM01_55.d	312	85	0.31	-3200	0.2450	0.0200	0.0352	0.0011	0.0940	0.0508	0.0050	223	16	223.2	7	220	210	101
OM01_33.d	548	619	1.22	-6300	0.2480	0.0150	0.0353	0.0009	0.6173	0.0508	0.0027	224	12	223.4	5	230	120	97
OM01_47.d	538	285	0.43	-70000	0.2560	0.0170	0.0359	0.0010	0.1065	0.0516	0.0037	231	14	227.5	7	260	160	88
OM01_71.d	641	355	0.40	210	0.2580	0.0130	0.0360	0.0007	0.1288	0.0519	0.0031	233	11	228.2	5	270	130	85
OM01_7.d	900	508	0.45	-14000	0.2620	0.0190	0.0367	0.0010	0.4738	0.0518	0.0031	236	15	232.4	6	270	140	86
OM01_67.d	235	222	0.87	-6700	0.2990	0.0240	0.0419	0.0010	0.2384	0.0520	0.0048	265	19	264.3	6	260	190	102
OM01_31.d	261	137	0.48	-2500	0.3040	0.0190	0.0420	0.0018	0.3106	0.0522	0.0031	269	15	265.0	11	280	130	95
OM01_83.d	170	147	0.77	-12500	0.3030	0.0230	0.0422	0.0012	0.2138	0.0521	0.0041	268	18	266.2	8	270	170	99
OM01_15.d	309	320	0.91	-5300	0.3020	0.0240	0.0422	0.0008	0.2025	0.0518	0.0041	268	19	266.5	5	260	170	103
OM01_12.d	272	161	0.54	-6100	0.3050	0.0290	0.0423	0.0021	0.2886	0.0525	0.0048	270	22	267.0	13	290	200	92
OM01_88.d	208	352	1.52	-26000	0.2990	0.0200	0.0423	0.0016	0.0683	0.0515	0.0040	265	16	267.0	10	250	170	107
OM01_14.d	249	188	0.65	-4900	0.3050	0.0260	0.0424	0.0010	0.1249	0.0523	0.0050	270	20	267.5	6	270	190	99
OM01_21.d	376	266	0.59	-6400	0.3090	0.0170	0.0426	0.0014	0.5279	0.0524	0.0025	273	13	269.2	9	290	110	93
OM01_84.d	138	101	0.62	-4900	0.3080	0.0440	0.0427	0.0015	0.0971	0.0525	0.0082	271	34	269.2	9	250	300	108
OM01_74.d	155	223	1.24	-10	0.3150	0.0250	0.0428	0.0007	0.2874	0.0531	0.0041	276	20	270.3	5	300	160	90
OM01_48.d	306	330	0.91	10	0.3100	0.0170	0.0429	0.0008	0.0332	0.0523	0.0031	273	13	271.0	5	270	120	100
OM01_34.d	224	279	1.07	-3000	0.3070	0.0130	0.0430	0.0008	0.0861	0.0523	0.0026	274	11	271.5	5	280	100	97
OM01_18.d	130	85	0.58	-900	0.3040	0.0250	0.0431	0.0015	0.0152	0.0512	0.0046	269	19	272.1	10	230	190	118
OM01_19.d	228	132	0.47	-2400	0.3080	0.0260	0.0431	0.0011	0.1878	0.0519	0.0048	272	20	271.9	7	250	190	109
OM01_53.d	169	253	1.25	-5500	0.3090	0.0200	0.0431	0.0011	0.1582	0.0518	0.0028	273	16	272.2	7	270	120	101
OM01_60.d	84	149	1.53	-2400	0.3180	0.0330	0.0433	0.0013	0.0129	0.0535	0.0059	277	26	273.4	8	290	220	94
OM01_70.d	177	241	1.08	-4300	0.3100	0.0210	0.0433	0.0010	0.2462	0.0519	0.0035	274	16	273.3	6	250	140	109
OM01_78.d	261	220	0.67	-18000	0.3110	0.0260	0.0435	0.0010	0.2205	0.0520	0.0047	274	20	274.4	6	250	180	110
OM01_81.d	292	396	1.15	-10500	0.3160	0.0140	0.0435	0.0007	0.2848	0.0520	0.0022	278	11	274.7	4	275	93	100
OM01_44.d	82	103	1.09	-1340	0.3190	0.0330	0.0436	0.0013	0.0810	0.0534	0.0056	278	25	275.3	8	280	200	98
OM01_8.d	221	210	0.67	-320	0.3200	0.0270	0.0437	0.0015	0.6072	0.0530	0.0038	281	21	275.5	9	310	160	89
OM01_16.d	299	256	0.65	200	0.3170	0.0280	0.0437	0.0013	0.1275	0.0525	0.0047	279	22	275.5	8	290	200	95
OM01_61.d	173	97	0.50	-4600	0.3160	0.0190	0.0438	0.0010	0.2150	0.0524	0.0031	278	14	276.2	6	270	120	102
OM01_90.d	314	244	0.57	-37000	0.3170	0.0210	0.0434	0.0012	0.1668	0.0529	0.0034	279	16	273.6	7	310	150	88
OM01_82.d	285	220	0.62	-15000	0.3180	0.0160	0.0439	0.0008	0.1441	0.0523	0.0026	280	12	277.2	5	280	110	99
OM01_51.d	290	430	1.19	-13000	0.3220	0.0300	0.0440	0.0014	0.2794	0.0531	0.0049	283	23	277.6	9	310	200	90
OM01_66.d	219	302	1.21	-8100	0.3210	0.0240	0.0441	0.0010	0.2340	0.0528	0.0040	282	19	278.1	6	290	160	96
OM01_3.d	209	285	1.15	-3600	0.3130	0.0290	0.0441	0.0010	0.2177	0.0516	0.0052	276	22	278.4	6	250	210	111
OM01_38.d	152	137	0.72	-800	0.3190	0.0220	0.0441	0.0011	0.1212	0.0527	0.0041	280	17	278.0	7	280	150	99
OM01_72.d	135	126	0.77	-6200	0.3160	0.0290	0.0443	0.0012	0.0410	0.0517	0.0047	278	22	279.6	7	300	210	93
OM01_86.d	132	109	0.66	-6100	0.3220	0.0350	0.0443	0.0012	0.0207	0.0524	0.0056	282	26	279.6	8	270	220	104
OM01_89.d	195	149	0.64	-19000	0.3190	0.0190	0.0449	0.0010	0.0061	0.0515	0.0033	280	15	283.0	6	240	130	118
OM01_77.d	124	82	0.57	-3900	0.3270	0.0350	0.0451	0.0011	0.1160	0.0525	0.0056	286	27	284.2	7	290	220	98
OM01_57.d	340	377	0.84	-140	0.3320	0.0280	0.0453	0.0013	0.0763	0.0531	0.0045	291	21	285.5	8	320	180	89
OM01_29.d	138	125	0.72	-50	0.3310	0.0210	0.0456	0.0010	0.1702	0.0527	0.0037	289	16	287.2	6	290	150	99
OM01_54.d	239	195	0.68	-1200	0.3290	0.0140	0.0457	0.0008	0.0767	0.0524	0.0025	288	11	288.1	5	280	100	103
OM01_75.d	142	182	0.98	-5400	0.3350	0.0190	0.0459	0.0011	0.2467	0.0517	0.0024	292	14	289.4	7	290	120	100
OM01_4.d	164	75	0.33	-2400	0.3440	0.0240	0.0470	0.0011	0.0900	0.0534	0.0041	299	18	295.9	7	320	160	92
OM01_80.d	138	145	0.72	-5800	0.3420	0.0310	0.0471	0.0013	0.2887	0.0525	0.0047	298	24	296.5	8	280	190	106
OM01_30.d	188	184	0.58	-5100	0.5230	0.0530	0.0690	0.0026	0.0700	0.0548	0.0058	427	35	430.0	16	390	220	110
OM01_68.d	94	119	0.53	-2400	0.6630	0.0380	0.0829	0.0013	0.0860	0.0580	0.0036	514	23	513.2	8	490	130	105
OM01_27.d	225	278	0.55	-4400	0.6630	0.0350	0.0839	0.0018	0.0333	0.0572	0.0032	516	21	519.0	11	480	130	108
OM01_62.d	156	111	0.34	-10700	0.7020	0.0440	0.0871	0.0018	0.0078	0.0586	0.0040	538	26	538.0	11	520	140	103
OM01_85.d	287	145	0.21	-40000	0.7720	0.0320	0.0944	0.0014	0.0832	0.0600	0.0032	581	18	581.6	8	590	110	98
OM01_9.d	354	685	0.46	-30000	1.6790	0.0610	0.1675	0.0039	0.4953	0.0729	0.0023	1000	23	998.0	21	1011	64	99
OM01_11.d	65	328	1.23	-4400	1.7400	0.1300	0.1709	0.0045	0.2992	0.0741	0.0063	1020	49	1017.0	25	1020	180	100
OM01_46.d	376	1183	0.80	-48000	1.6420	0.0690	0.1781	0.0047	0.1782	0.0753	0.0032	1080	25	1056.0	25	1073	83	98

Table 15: U-Pb data for sample OM06. Pb206/U238 is the age.

Sample OM06			RATIOS										AGES [Ma]						Conc.
Analysis	U [ppm][a]	Pb [ppm][a]	Th/U[a]	206/204	$^{207}Pb/^{235}U$[b]	2 σ[d]	$^{206}Pb/^{238}U$[b]	2 σ[d]	rho[c]	$^{207}Pb/^{206}Pb$[c]	2 σ[d]		$^{207}Pb/^{235}U$	2 σ	$^{206}Pb/^{238}U$	2 σ	$^{207}Pb/^{206}Pb$	2 σ	%
OM06_111.d	781	481	0.57	6300	0.2450	0.0150	0.0349	0.0006	0.3866	0.0509	0.0029		222	12	221.1	4	230	130	96
OM06_28.d	651	383	0.54	18000	0.2470	0.0160	0.0351	0.0007	0.2086	0.0515	0.0037		223	13	222.0	4	250	150	89
OM06_76.d	577	361	0.54	8900	0.2530	0.0150	0.0356	0.0005	0.0462	0.0516	0.0032		229	12	225.5	3	250	130	90
OM06_66.d	367	226	0.47	6700	0.2970	0.0150	0.0418	0.0007	0.0634	0.0515	0.0028		264	12	264.2	5	250	110	106
OM06_49.d	119	118	0.80	2300	0.3040	0.0270	0.0420	0.0011	0.0799	0.0530	0.0051		268	21	265.2	7	280	180	95
OM06_62.d	246	428	1.54	-120	0.3010	0.0220	0.0420	0.0012	0.2003	0.0524	0.0044		266	17	265.3	7	270	170	98
OM06_107.d	324	513	1.42	1500	0.2990	0.0120	0.0421	0.0009	0.1299	0.0513	0.0021		268	11	265.9	5	242	91	110
OM06_63.d	208	151	0.56	50	0.2980	0.0200	0.0421	0.0009	0.2885	0.0513	0.0033		264	15	266.0	5	240	130	111
OM06_109.d	266	215	0.70	3800	0.3050	0.0150	0.0421	0.0008	0.0300	0.0525	0.0028		269	11	266.0	5	290	110	92
OM06_56.d	282	191	0.54	3200	0.3010	0.0100	0.0422	0.0007	0.1329	0.0522	0.0020		267	8	266.5	4	283	81	94
OM06_25.d	237	216	0.71	19000	0.3080	0.0240	0.0423	0.0017	0.3258	0.0532	0.0040		272	18	267.0	11	320	150	83
OM06_120.d	313	261	0.77	2500	0.3030	0.0140	0.0425	0.0010	0.0423	0.0520	0.0026		269	11	268.0	6	270	110	99
OM06_47.d	269	237	0.76	8700	0.3040	0.0170	0.0425	0.0008	0.0953	0.0522	0.0030		269	13	268.1	5	270	120	99
OM06_112.d	293	323	1.01	3200	0.3040	0.0160	0.0425	0.0013	0.4161	0.0522	0.0038		269	13	268.1	8	280	150	96
OM06_50.d	232	333	1.21	7900	0.3050	0.0130	0.0426	0.0006	0.2959	0.0522	0.0021		270	10	268.6	3	271	86	99
OM06_61.d	205	196	0.78	0	0.3040	0.0180	0.0426	0.0010	0.3052	0.0521	0.0036		269	14	268.8	6	260	140	103
OM06_46.d	306	267	0.72	5500	0.3100	0.0100	0.0426	0.0006	0.1926	0.0528	0.0018		274	8	268.9	3	303	77	89
OM06_21.d	176	178	0.88	14000	0.3080	0.0140	0.0428	0.0008	0.0044	0.0527	0.0026		272	11	270.0	5	300	100	90
OM06_119.d	110	86	0.67	620	0.3090	0.0230	0.0428	0.0011	0.1287	0.0526	0.0041		272	18	270.0	7	270	160	100
OM06_97.d	283	241	0.64	-60	0.3130	0.0240	0.0430	0.0010	0.0151	0.0528	0.0043		276	19	271.1	6	300	170	90
OM06_4.d	313	231	0.59	-39000	0.3090	0.0190	0.0431	0.0010	0.0137	0.0521	0.0034		273	15	271.7	6	270	140	101
OM06_34.d	174	157	0.71	6300	0.3130	0.0240	0.0431	0.0013	0.2709	0.0530	0.0042		276	18	271.9	8	300	170	91
OM06_13.d	192	238	1.14	-30	0.3130	0.0390	0.0430	0.0024	0.3105	0.0533	0.0064		275	29	272.0	15	300	240	91
OM06_29.d	320	205	0.52	10000	0.3080	0.0180	0.0431	0.0010	0.0943	0.0522	0.0034		272	14	272.3	6	280	140	97
OM06_72.d	366	574	1.20	6000	0.3130	0.0300	0.0432	0.0010	0.8308	0.0523	0.0040		275	23	272.3	6	280	160	97
OM06_75.d	291	952	3.42	1200	0.3090	0.0110	0.0432	0.0010	0.4479	0.0519	0.0017		273	9	272.3	6	275	77	99
OM06_22.d	321	218	0.52	28000	0.3140	0.0190	0.0432	0.0009	0.1451	0.0530	0.0032		277	14	272.4	6	310	130	88
OM06_51.d	346	73	0.17	13200	0.3150	0.0150	0.0432	0.0007	0.0014	0.0529	0.0026		277	11	272.8	4	310	110	88
OM06_42.d	298	140	0.37	11600	0.3080	0.0110	0.0432	0.0007	0.0768	0.0521	0.0022		272	9	272.9	4	268	88	102
OM06_11.d	230	50	0.14	300000	0.3130	0.0220	0.0433	0.0018	0.1118	0.0528	0.0046		276	17	273.0	11	300	190	91
OM06_64.d	163	105	0.48	4000	0.3100	0.0230	0.0433	0.0012	0.2508	0.0522	0.0044		273	18	273.0	7	270	180	101
OM06_69.d	182	278	1.14	2400	0.3110	0.0210	0.0433	0.0008	0.1725	0.0518	0.0035		274	16	273.1	5	250	140	109
OM06_1.d	83	284	2.72	10	0.3110	0.0300	0.0433	0.0015	0.0791	0.0523	0.0051		273	23	273.2	9	250	190	109
OM06_41.d	183	106	0.45	7100	0.3110	0.0150	0.0434	0.0007	0.1677	0.0515	0.0023		274	12	274.0	5	270	100	101
OM06_10.d	196	101	0.44	-990000	0.3110	0.0110	0.0435	0.0006	0.0806	0.0521	0.0019		275	9	274.2	4	275	79	100
OM06_84.d	224	158	0.58	2000	0.3130	0.0160	0.0436	0.0011	0.0372	0.0520	0.0029		276	13	275.0	7	270	120	102
OM06_110.d	324	336	0.80	2700	0.3100	0.0240	0.0436	0.0010	0.4172	0.0516	0.0037		274	18	275.0	6	250	150	110
OM06_43.d	145	180	1.10	1800	0.3110	0.0220	0.0436	0.0010	0.2002	0.0520	0.0037		274	17	275.2	6	270	150	102
OM06_9.d	299	756	2.62	70	0.3130	0.0170	0.0438	0.0009	0.2753	0.0519	0.0027		276	13	276.5	5	260	110	106
OM06_8.d	145	369	2.13	-37000	0.3250	0.0250	0.0439	0.0009	0.1388	0.0538	0.0044		284	19	276.8	6	330	170	84
OM06_57.d	170	181	0.83	3800	0.3150	0.0190	0.0440	0.0008	0.0261	0.0521	0.0033		277	15	277.7	5	270	130	103
OM06_6.d	295	250	0.74	-41000	0.3180	0.0170	0.0440	0.0010	0.2191	0.0526	0.0033		280	13	277.8	6	290	130	96
OM06_45.d	183	152	0.70	6900	0.3140	0.0190	0.0441	0.0008	0.0135	0.0519	0.0032		276	15	278.3	5	280	130	99
OM06_99.d	140	137	0.75	0	0.3170	0.0230	0.0442	0.0016	0.1635	0.0521	0.0038		279	17	278.6	10	270	160	103
OM06_18.d	211	146	0.54	-20	0.3180	0.0280	0.0442	0.0008	0.2819	0.0525	0.0049		279	21	278.9	5	280	190	100
OM06_24.d	176	170	0.83	15000	0.3210	0.0220	0.0446	0.0011	0.0849	0.0526	0.0038		282	17	281.5	7	290	150	97
OM06_103.d	230	131	0.40	4000	0.3220	0.0240	0.0447	0.0012	0.0767	0.0524	0.0041		283	18	281.7	7	290	170	97
OM06_39.d	185	111	0.48	1500	0.3230	0.0150	0.0447	0.0007	0.3347	0.0526	0.0023		284	11	282.1	4	294	93	96
OM06_105.d	194	155	0.61	1700	0.3240	0.0160	0.0451	0.0008	0.0607	0.0523	0.0029		284	13	284.2	5	280	120	102
OM06_86.d	208	336	1.17	3500	0.3270	0.0210	0.0454	0.0008	0.0290	0.0523	0.0034		287	16	286.2	5	270	130	106
OM06_88.d	83	62	0.60	1080	0.3280	0.0250	0.0456	0.0012	0.0281	0.0516	0.0039		286	18	287.3	8	250	150	115
OM06_70.d	297	414	1.12	4500	0.3280	0.0250	0.0458	0.0014	0.1120	0.0521	0.0043		288	19	288.5	9	280	170	103
OM06_79.d	196	124	0.44	4400	0.3350	0.0250	0.0462	0.0008	0.3049	0.0523	0.0036		292	19	291.1	5	280	150	104
OM06_3.d	173	142	0.61	-16000	0.3400	0.0280	0.0465	0.0026	0.0225	0.0533	0.0059		297	21	293.0	16	320	240	92
OM06_16.d	954	744	0.43	300	0.4590	0.0250	0.0599	0.0016	0.5892	0.0559	0.0036		383	17	375.1	9	440	140	85
OM06_38.d	577	446	0.33	960	0.5040	0.0190	0.0644	0.0006	0.0711	0.0570	0.0019		414	13	402.2	3	488	73	82
OM06_117.d	215	376	1.14	3500	0.5140	0.0320	0.0673	0.0020	0.2565	0.0558	0.0042		421	22	420.0	12	420	170	100
OM06_85.d	148	175	0.52	5900	0.6080	0.0230	0.0770	0.0012	0.0993	0.0572	0.0024		481	14	478.2	7	478	91	100
OM06_19.d	73	72	0.45	16000	0.6180	0.0400	0.0779	0.0016	0.1661	0.0578	0.0037		485	25	483.3	10	480	140	101
OM06_82.d	138	138	0.46	1700	0.6140	0.0310	0.0780	0.0014	0.0390	0.0571	0.0030		484	19	483.8	8	460	110	105
OM06_32.d	39	138	1.65	1300	0.6270	0.0790	0.0780	0.0027	0.1002	0.0589	0.0076		487	48	484.0	16	450	250	108
OM06_74.d	143	210	0.66	3700	0.6190	0.0230	0.0784	0.0013	0.0269	0.0568	0.0022		488	15	486.4	8	476	90	102
OM06_59.d	126	63	0.20	700	0.6210	0.0360	0.0784	0.0017	0.0514	0.0567	0.0031		489	22	487.0	10	480	130	101
OM06_108.d	174	128	0.32	3600	0.6210	0.0230	0.0791	0.0011	0.3789	0.0568	0.0019		489	15	490.7	7	471	77	104
OM06_58.d	86	2	0.00	3900	0.6510	0.0660	0.0810	0.0018	0.3616	0.0582	0.0055		505	39	502.0	10	480	190	105
OM06_5.d	188	203	0.45	-80000	0.6730	0.0400	0.0845	0.0021	0.0765	0.0579	0.0039		521	24	523.0	13	500	140	105
OM06_15.d	80	113	0.54	34000	0.7180	0.0480	0.0881	0.0024	0.0316	0.0596	0.0044		547	29	544.0	14	540	160	101
OM06_115.d	75	82	0.37	2000	0.7320	0.0480	0.0898	0.0023	0.3153	0.0595	0.0046		555	28	554.0	14	540	170	103
OM06_100.d	387	925	0.75	23000	1.0150	0.0320	0.1165	0.0022	0.7225	0.0631	0.0015		711	16	710.0	13	709	50	100
OM06_44.d	350	155	0.13	31000	1.0240	0.0190	0.1174	0.0015	0.3198	0.0635	0.0012		715	10	715.4	9	721	40	99
OM06_71.d	303	333	0.30	28000	1.0690	0.0500	0.1216	0.0029	0.4669	0.0638	0.0026		738	25	740.0	17	730	86	101
OM06_92.d	87	107	0.27	2400	1.6190	0.0520	0.1632	0.0023	0.2377	0.0716	0.0024		976	20	975.0	13	991	66	98
OM06_14.d	105	253	0.47	24000	1.8570	0.0570	0.1796	0.0021	0.4005	0.0753	0.0028		1064	20	1065.0	12	1061	77	100
OM06_91.d	236	485	0.42	26000	1.8850	0.0600	0.1809	0.0033	0.2068	0.0754	0.0025		1075	21	1072.0	18	1071	67	100
OM06_95.d	129	1298	1.31	12500	4.4800	0.0930	0.3070	0.0032	0.0576	0.1061	0.0026		1726	17	1726.0	16	1728	44	100

Legend

Triassic | Carboniferous | Silurian | Cambrian | Prefered Age

Permian | Devonian | Ordovician | Proterozoic

with an age of 1726.0 ±16 Ma. 27% of the total Permian grain population has a Th/U ratio greater than 1.0 (Th/U>1.0). The following youngest detrital zircon signatures were obtained: YSG is 264.2 (±5) Ma; YPP is 269.2 Ma (Fig 4.28); YDZ is 260.8 (+8.1/-13) Ma; YC2σ [3] is 264.7 (±7.3) Ma; the weighted average [10] is 266.2 (±1.7); A TuffZirc [10] age of 266.0 (+2.0/-0.8) Ma was determined (Fig 4.29).

4.4.1.8 MK-2016-4

About 88% of zircon grains from sample MK-2016-4 from the upper Trumpeters Member show a magmatic source by the presence of zoning (Fig 4.27 E, F). Grains vary between 90.0 µm and 200.0 µm with grains averaging at 120.0 µm. Out of 184 grains that were analysed, only 61 grains were concordant (33% of sample) (Table 16). 13.1% of the concordant grains were core shots of zircons during ablation while the rest were rim shots. A large population of grains (85.2%, n=52) is present from the late Carboniferous and Permian (254.0 Ma - 333.0 Ma) with only 3.2% (n=2) of the grains from the Devonian (354 Ma - 417 Ma). One grain is from the Ordovician with an age of 474.5 ±4 and one grain is from the Cambrian with an age of 520.1 ±5. A few Neo-Proterozoic grains (545.0 Ma - 1000.0 Ma) also occur, occupying 8.2% (n=5) of the sample. Out of the total population of Permian grains, 19% has a Th/U ratio greater than 1.0 (Th/U>1.0). The following youngest detrital zircon signatures were obtained: YSG is 257.8 (±2) Ma; YPP is 258.8 Ma (Fig 4.28); YDZ is 256.3 (+3.6/-5.8) Ma; YC2σ [3] is 258.1 (±4.0) Ma; the weighted average [10] is 261.4 (±2.2); A TuffZirc [10] age of 261.1 (+3.8/-2.8) Ma was determined (Fig 4.29).

4.4.2 Youngest detrital zircon age

Out of the eight samples processed, two were from the Vischkuil Formation, two from the Laingsburg Formation, three from the Ripon Formation (two from the Pluto's Vale Member and one from the Trumpeters Member). By extrapolating an average youngest detrital age signature (the average age between six youngest ages obtained from the six methodologies), a maximum depositional age can be inferred for each formation and, where relevant, its members (Table 17, Fig 4.29). The average

Table 16: U-Pb data for sample MK-2016-4. Pb206/U238 is the age.

Sample MK-2016-4			RATIOS									AGES [Ma]						Conc.
Analysis	U [ppm][a]	Pb [ppm][a]	Th/U[a]	*206/204*	$^{207}Pb/^{235}U$[b]	2 σ[d]	$^{206}Pb/^{238}U$[b]	2 σ[d]	rho[c]	$^{207}Pb/^{206}Pb$[e]	2 σ[d]	$^{207}Pb/^{235}U$	2 σ	$^{206}Pb/^{238}U$	2 σ	$^{207}Pb/^{206}Pb$	2 σ	%
MK4-150	277	160	0.51	180	0.2918	0.0079	0.0408	0.0003	0.0225	0.0519	0.0015	260	6	257.8	2	259	61	100
MK4-177	268	283	0.95	250	0.2922	0.0090	0.0409	0.0004	0.3138	0.0517	0.0015	260	7	258.3	2	256	62	101
MK4-91	190	82	0.36	138	0.2910	0.0140	0.0410	0.0006	0.1853	0.0514	0.0025	259	11	258.9	4	250	100	104
MK4-184	298	486	1.28	330	0.2960	0.0160	0.0411	0.0005	0.2588	0.0519	0.0028	263	13	259.8	3	270	120	96
MK4-39	241	400	1.31	203	0.2950	0.0170	0.0413	0.0005	0.0965	0.0518	0.0031	262	13	260.8	3	260	130	100
MK4-182	470	371	0.67	610	0.2966	0.0076	0.0414	0.0004	0.1194	0.0518	0.0013	264	6	261.4	2	266	58	98
MK4-172	222	264	1.12	273	0.2960	0.0120	0.0414	0.0005	0.0589	0.0518	0.0022	262	10	261.6	3	263	92	99
MK4-162	311	619	1.12	347	0.2958	0.0090	0.0416	0.0004	0.3544	0.0515	0.0015	263	7	262.5	3	249	61	105
MK4-43	264	102	0.33	273	0.3010	0.0100	0.0420	0.0004	0.0127	0.0521	0.0019	266	8	264.9	3	269	76	98
MK4-42	360	265	0.62	510	0.3022	0.0069	0.0421	0.0003	0.1865	0.0519	0.0011	268	5	265.8	2	267	47	100
MK4-38	359	243	0.58	217	0.3050	0.0150	0.0421	0.0006	0.4989	0.0525	0.0021	270	12	265.9	4	298	91	89
MK4-54	181	140	0.70	146	0.3020	0.0150	0.0421	0.0006	0.2106	0.0522	0.0028	269	12	266.0	3	290	120	92
MK4-30	386	401	0.84	305	0.3110	0.0180	0.0422	0.0007	0.0740	0.0534	0.0031	275	14	266.3	5	330	130	81
MK4-144	167	85	0.41	156	0.3030	0.0130	0.0422	0.0007	0.1033	0.0524	0.0023	268	10	266.5	4	300	100	89
MK4-161	221	223	0.83	284	0.2990	0.0170	0.0422	0.0007	0.1627	0.0512	0.0028	265	13	266.6	4	250	120	107
MK4-104	232	165	0.65	180	0.3030	0.0100	0.0422	0.0005	0.0433	0.0522	0.0019	268	8	266.7	3	271	76	98
MK4-149	268	167	0.61	-230	0.3110	0.0610	0.0425	0.0014	0.4289	0.0532	0.0098	274	48	268.3	9	330	410	81
MK4-51	198	123	0.49	182	0.3050	0.0092	0.0425	0.0004	0.0370	0.0520	0.0016	270	7	268.6	2	274	67	98
MK4-28	427	817	1.08	320	0.3070	0.0220	0.0426	0.0010	0.3052	0.0524	0.0043	271	17	269.0	6	280	170	96
MK4-2	551	255	0.41	201	0.3100	0.0120	0.0427	0.0007	0.1861	0.0526	0.0021	274	10	269.8	4	302	90	89
MK4-160	225	328	1.27	260	0.3070	0.0190	0.0428	0.0007	0.1818	0.0521	0.0032	271	15	269.8	4	260	120	104
MK4-84	166	142	0.64	245	0.3180	0.0380	0.0429	0.0011	0.3285	0.0536	0.0061	279	29	270.5	7	320	240	85
MK4-36	205	98	0.43	148	0.3040	0.0180	0.0429	0.0007	0.0174	0.0517	0.0033	269	14	270.6	4	240	120	113
MK4-159	253	227	0.77	258	0.3080	0.0088	0.0430	0.0004	0.0470	0.0520	0.0016	272	7	271.2	2	270	64	100
MK4-183	211	171	0.76	256	0.3070	0.0120	0.0430	0.0006	0.2938	0.0517	0.0019	272	9	271.2	4	261	78	104
MK4-180	323	96	0.21	342	0.3110	0.0140	0.0430	0.0006	0.1135	0.0521	0.0026	274	11	271.6	3	270	110	101
MK4-107	159	175	0.96	118	0.3106	0.0089	0.0432	0.0003	0.0691	0.0522	0.0016	274	7	272.7	2	273	62	100
MK4-81	104	102	0.83	97	0.3130	0.0130	0.0432	0.0004	0.0539	0.0527	0.0022	275	10	272.9	3	276	83	99
MK4-101	247	207	0.75	268	0.3081	0.0099	0.0435	0.0004	0.0474	0.0515	0.0017	272	8	274.4	2	246	71	112
MK4-29	105	78	0.69	87	0.3140	0.0300	0.0438	0.0010	0.1055	0.0518	0.0050	275	23	276.1	6	230	180	120
MK4-108	255	202	0.62	297	0.3164	0.0081	0.0438	0.0004	0.2390	0.0522	0.0014	279	6	276.2	2	278	58	99
MK4-41	327	277	0.72	350	0.3120	0.0190	0.0438	0.0006	0.1340	0.0518	0.0032	276	15	276.5	4	260	140	106
MK4-116	167	145	0.71	174	0.3170	0.0170	0.0439	0.0006	0.0048	0.0523	0.0029	279	13	277.2	4	280	120	99
MK4-20	257	363	1.20	194	0.3190	0.0120	0.0440	0.0004	0.0436	0.0524	0.0021	280	10	277.4	3	288	85	96
MK4-53	240	353	1.14	215	0.3110	0.0120	0.0441	0.0004	0.0548	0.0512	0.0020	274	9	277.9	3	235	82	118
MK4-147	338	211	0.51	454	0.3162	0.0065	0.0441	0.0004	0.2390	0.0521	0.0010	279	5	278.2	2	277	44	100
MK4-8	424	342	0.65	249	0.3151	0.0066	0.0442	0.0003	0.1577	0.0516	0.0011	278	5	278.9	2	257	45	109
MK4-145	63	80	0.98	73	0.3230	0.0220	0.0444	0.0007	0.0137	0.0521	0.0034	282	17	280.1	4	280	140	100
MK4-24	343	675	0.98	365	0.3185	0.0085	0.0446	0.0004	0.2621	0.0516	0.0013	280	7	281.5	3	253	56	111
MK4-137	117	106	0.71	112	0.3220	0.0140	0.0447	0.0006	0.0872	0.0524	0.0024	284	12	281.6	3	290	100	97
MK4-19	407	538	0.85	353	0.3195	0.0069	0.0447	0.0003	0.1854	0.0519	0.0011	281	5	281.8	2	273	48	103
MK4-132	188	215	0.89	150	0.3280	0.0210	0.0454	0.0009	0.5271	0.0526	0.0039	288	16	285.9	6	290	160	99
MK4-97	122	198	1.40	138	0.3230	0.0210	0.0455	0.0008	0.2288	0.0515	0.0033	283	16	286.8	5	240	130	120
MK4-13	172	117	0.60	156	0.3290	0.0160	0.0457	0.0009	0.0838	0.0525	0.0026	289	12	288.2	6	300	110	96
MK4-151	276	95	0.29	299	0.3360	0.0110	0.0464	0.0007	0.5535	0.0525	0.0014	293	8	292.3	5	290	56	101
MK4-3	342	332	0.71	139	0.3390	0.0160	0.0467	0.0008	0.2413	0.0527	0.0027	296	12	294.1	5	300	110	98
MK4-86	214	367	1.28	235	0.3370	0.0130	0.0468	0.0005	0.0648	0.0523	0.0021	294	10	294.9	3	282	85	105
MK4-126	96	54	0.43	117	0.3550	0.0160	0.0481	0.0005	0.1322	0.0537	0.0025	307	12	302.8	3	325	93	93
MK4-1	173	117	0.53	46	0.3530	0.0230	0.0483	0.0008	0.1714	0.0533	0.0037	306	17	304.2	5	310	150	98
MK4-35	192	270	1.02	144	0.3620	0.0140	0.0498	0.0008	0.2686	0.0531	0.0022	313	11	313.5	5	311	88	101
MK4-112	237	264	0.77	380	0.3640	0.0100	0.0503	0.0012	0.2903	0.0531	0.0015	315	8	316.4	8	317	60	100
MK4-155	59	76	0.78	130	0.3930	0.0250	0.0531	0.0009	0.1987	0.0536	0.0033	334	18	333.3	6	310	120	108
MK4-168	233	304	0.71	340	0.4800	0.0140	0.0634	0.0006	0.1221	0.0548	0.0016	397	10	396.4	4	384	65	103
MK4-15	357	141	0.21	510	0.4887	0.0099	0.0646	0.0006	0.0949	0.0549	0.0012	404	7	403.3	4	409	45	99
MK4-80	310	237	0.35	535	0.5980	0.0130	0.0764	0.0007	0.3396	0.0567	0.0012	475	8	474.5	4	469	47	101
MK4-64	494	1097	0.64	940	0.6740	0.0140	0.0840	0.0008	0.1748	0.0584	0.0013	523	9	520.1	5	537	49	97
MK4-70	138	264	0.76	280	0.7120	0.0360	0.0883	0.0024	0.2472	0.0587	0.0037	545	21	546.0	14	540	140	101
MK4-9	234	163	0.33	248	0.7610	0.0410	0.0909	0.0020	0.0838	0.0608	0.0035	574	24	561.0	12	620	130	90
MK4-11	378	1711	1.22	520	0.7600	0.0180	0.0930	0.0010	0.3248	0.0593	0.0013	574	10	573.5	6	572	48	100
MK4-18	77	146	0.62	163	0.8810	0.0520	0.1038	0.0015	0.3068	0.0611	0.0034	638	28	636.4	9	610	120	104
MK4-105	69	398	1.21	310	1.6200	0.1000	0.1588	0.0029	0.0351	0.0739	0.0048	977	40	950.0	16	1020	130	93

Table 17: A summary table showing the youngest detrital zircon results obtained through each of the six methodologies

Analysis		Samples															
		WK01		WK-2016-1		KG06		KG-2016-1		N12-2016-1		OM01		OM06		MK-2016-4	
YSG	Age	253	±24	256.3	±9	258.5	±6	259.4	±4	253.4	±3	264.3	±6	264.2	±5	257.8	±2
YPP	Age	266.7		266.4		262.8		265.7		257.6		273.1		269.2		258.8	
YDZ	Age	256.3		252.5		250.8		259.0		251.3		259.4		260.8		256.3	
	Range	+5.7/-57		+5.6/-16		+8.3/-19		+4.1/-9.4		+4.2/-9.0		+11/-19		+8.1/-13		+3.6/-5.8	
	Confidence	95%		95%		95%		95%		95%		95%		95%		95%	
YC2σ	Final Age	262.3	±10.4 (3.9%)	257.6	±5.6 (2.2%)	259.5	±9.1 (3.5%)	261.2	±4.4 (1.7%)	255.6	±4.5 (1.8%)	265.1	±8.7 (3.3%)	264.7	±7.3 (2.8%)	258.1	±4.0 (1.5%)
	Weighted Mean Age	262.3	±9.9 (3.8%)	257.6	±4.8 (1.9%)	259.5	±8.6 (3.3%)	261.2	±3.3 (1.3%)	255.6	±3.5 (1.4%)	265.1	±8.2 (3.1%)	264.7	±6.7 (2.5%)	258.1	±2.7 (1.1%)
	Systematic Error	1.1		1.1		1.1		1.1		1.1		1.1		1.1		1.1	
	MSWD	0.1		0		0		0.1		0.4		0		0		0	
Weighted Average	Age	265.2	±1.7 (0.7%)	260.6	±1.2 (0.47%)	261.8	±1.8 (0.7%)	263.7	±1.3 (0.5%)	257.9	±1.8 (0.7%)	266.9	±2.3 (0.87%)	266.2	±1.7 (0.63%)	261.4	±2.2 (0.83%)
	Confidence	95%		95%		95%		95%		95%		95%		95%		95%	
	Rejected	0		0		0		0		0		0		0		0	
	MSWD	0.48		1.07		0.3		1.9		2.5		0.23		0.23		6.0	
	Probability	0.89		0.38		0.98		0.041		0.007		0.99		1		0	
TuffZirc	Age	264.6	+2.2/-2.1	260.9	+1.5/-3.7	261.9	+2.3/-0.9	263.5	+1.5/-2.2	258.2	+2.1/-1.7	267.0	+2.2/-2.0	266	+2.0/-0.8	261.1	+3.8/-2.8
	Confidence	96.1%		97.9%		97.9%		97.9%		97.9%		97.9%		97.9%		97.9%	
	Total Coherent grains	9 of 10		10 of 10		10 of 10		10 of 10		10 of 10		10 of 10		10 of 10		10 of 10	

youngest detrital age merely expresses the average age trend between the six methodologies of each sample. Although this method does not provide the actual age of deposition, it is possible to elucidate stratigraphic trends and relative placement of sequences given the youngest maximum age of deposition for specific strata. By knowing the youngest maximum age of deposition for strata, a correlation can be made based on syn-depositional units across the basin and a better understanding of the temporal placement of depositional units can be achieved.

4.4.2.1 Pluto's Vale Member (Ripon Formation)

The oldest samples extracted were from the lower stratigraphic units of the Pluto's Vale Member of the Ripon Formation (OM01 and OM06) and seem to be only slightly older than the Vischkuil Formation. Both samples have a single youngest graphical peak on the probability density plots, but exhibit an older age than the other methods. Sample OM06 is from a stratigraphically higher position than Sample OM01. Sample OM01 has an average youngest detrital zircon of 265.9 Ma and sample OM06 an average youngest detrital zircon of 265.1 Ma. In general, a maximum depositional age for the Pluto's Vale Member can be inferred at 265.4 Ma (Fig 4.29).

4.4.2.2 Vischkuil Formation

Detrital zircon ages for the Vischkuil Formation were obtained from samples WK01 and KG-2016-1. Both samples show two distinct peaks in their respective probability density plots. Sample KG-2016-1 provides a good grouping of the six methodologies, which slightly improves accuracy. Sample WK01 shows a younger YSG and YDZ, but the remaining methodologies have a similar grouping as KG-2016-1. Sample WK01 has an average youngest detrital zircon age of 261.4 Ma and sample KG-2016-1 has an average youngest detrital zircon age of 262.1 Ma, suggesting an overall maximum depositional age of 261.8 Ma (Fig 4.29).

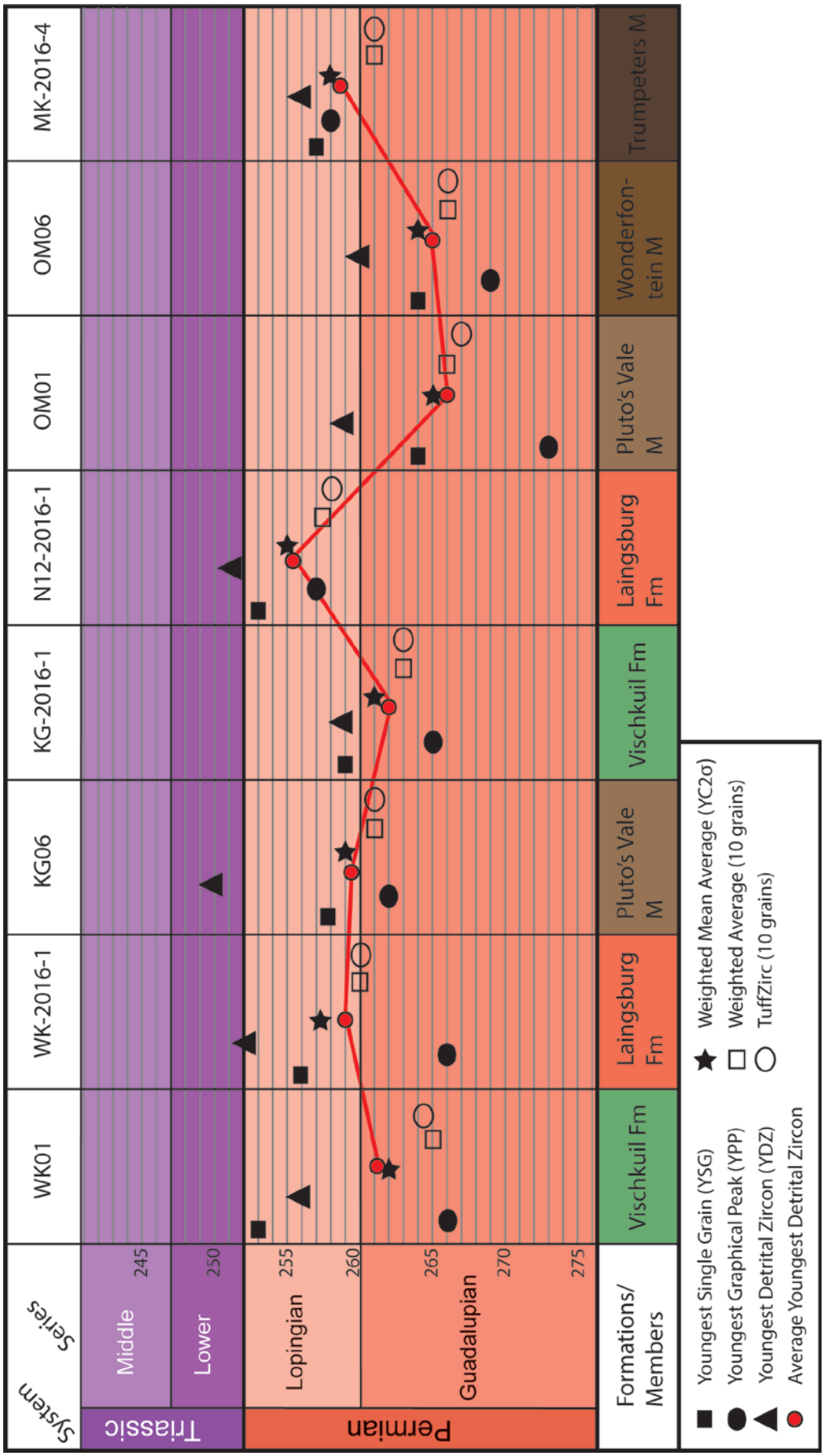

Figure 4.29: A graphical representation of the results obtained through the six youngest detrital zircon methodologies. Notice, the general trend of these methodologies supports the stratigraphic younging of units.

4.4.2.3 Trumpeters Member (Ripon Formation)

The Trumpeters Member of the Ripon Formation is represented only by sample MK-2016-4 and has an average youngest detrital zircon age of 258.9 Ma. Sample MK-2016-4 was obtained from the uppermost unit of the Trumpeters Member within the study area. Multiple peaks are observed within this sample between the ages of 250.0 Ma and 300.0 Ma on its probability density plot with the highest peak situated around 272.0 Ma (Fig 4.29). All six methodologies provide an accurate grouping of youngest detrital zircon ages which temporally correlate with those of the Laingsburg Formation obtained in this study.

4.4.2.4 Laingsburg Formation

The Laingsburg Formation stratigraphically overlies the Vischkuil Formation as well as the Wonderfontein Member of the Ripon Formation and is represented by samples WK-2016-1 and N12-2016-1. Sample WK-2016-1 shows a prominent peak around 271.0 Ma on its probability density plot, whereas sample N12-2016-1 has multiple peaks between the ages of 250.0 Ma and 300.0 Ma. The YPP of sample WK-2016-1 is much older than the general trend of the other methodologies. Sample N12-2016-1 seems to have a much better grouping between the six methodologies, giving it a slightly more accurate average youngest detrital zircon value. Sample WK-2016-1 has an average detrital zircon age of 259.0 Ma while sample N12-2016-1 has an average detrital zircon age of 255.6 Ma. The overall maximum depositional age for the Laingsburg Formation is inferred to be 257.3 Ma (Fig 4.29).

4.4.3 K-S Test

For the purpose of this study the Kolmogorov-Smirnov Test was used to determine the probability of different samples across formations and temporal placement consisting of the same sediment source. If all the samples pass the K-S Test, then this could support a similar source terrain for the Laingsburg/Vischkuil formations as well as the Ripon Formation over time. Each sample was tested against each other and was measured on the probability of similarity (Table 18).

Table 18: A) P-values produced by the K-S Test of all samples. Notice sample N12-2016-1 has no genetic relationship with any of the other samples. B) Therefore, a table showing P-values produced by the K-S Test of all samples excluding sample N12-2016-1 is presented. KG01 = KG-2016-1; MK4 = MK-2016-4; N12-1 = N12-2016-1; WK1 = WK-2016-1

A

K-S P-values using error in the CDF

Samples	OM01	OM06	KG06	WK01	KG01	MK4	N12-1	WK1
OM01		**0.454**	**1.000**	**1.000**	**0.809**	**0.847**	0.000	**0.795**
OM06	**0.454**		**0.215**	**0.573**	**0.825**	**0.409**	0.001	**0.266**
KG06	**1.000**	**0.215**		**1.000**	**0.963**	**1.000**	0.000	**0.757**
WK01	**1.000**	**0.573**	**1.000**		**0.999**	**1.000**	0.000	**0.930**
KG01	**0.809**	**0.825**	**0.963**	**0.999**		**1.000**	0.000	**0.914**
MK4	**0.847**	**0.409**	**1.000**	**1.000**	**1.000**		0.000	**0.791**
N12-1	0.000	0.001	0.000	0.000	0.000	0.000		0.000
WK1	**0.795**	**0.266**	**0.757**	**0.930**	**0.914**	**0.791**	0.000	

B

K-S P-values using error in the CDF

Samples	OM01	OM06	KG06	WK01	KG01	MK4	WK1
OM01		**0.454**	**1.000**	**1.000**	**0.821**	**0.836**	**0.789**
OM06	**0.454**		**0.216**	**0.573**	**0.826**	**0.411**	**0.232**
KG06	**1.000**	**0.216**		**1.000**	**0.963**	**1.000**	**0.737**
WK01	**1.000**	**0.573**	**1.000**		**0.997**	**1.000**	**0.958**
KG01	**0.821**	**0.826**	**0.963**	**0.997**		**1.000**	**0.947**
MK4	**0.836**	**0.411**	**1.000**	**1.000**	**1.000**		**0.684**
WK1	**0.789**	**0.232**	**0.737**	**0.958**	**0.947**	**0.684**	

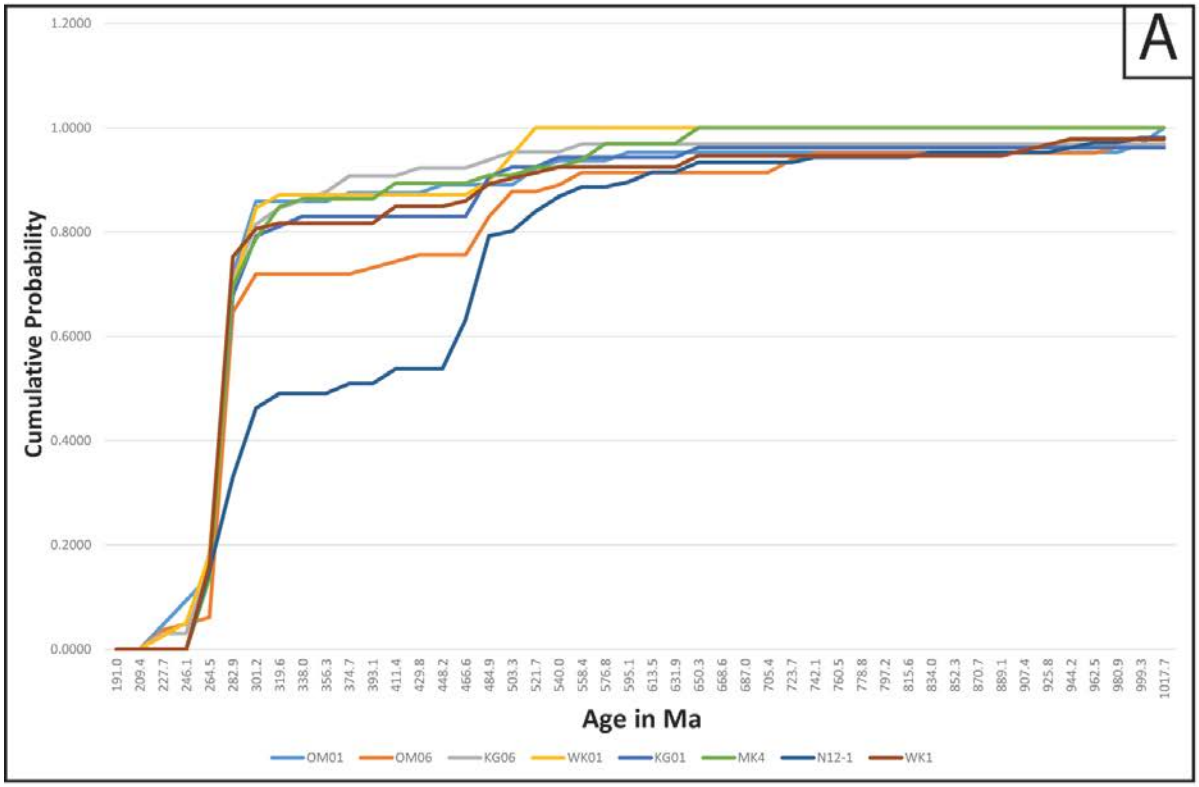

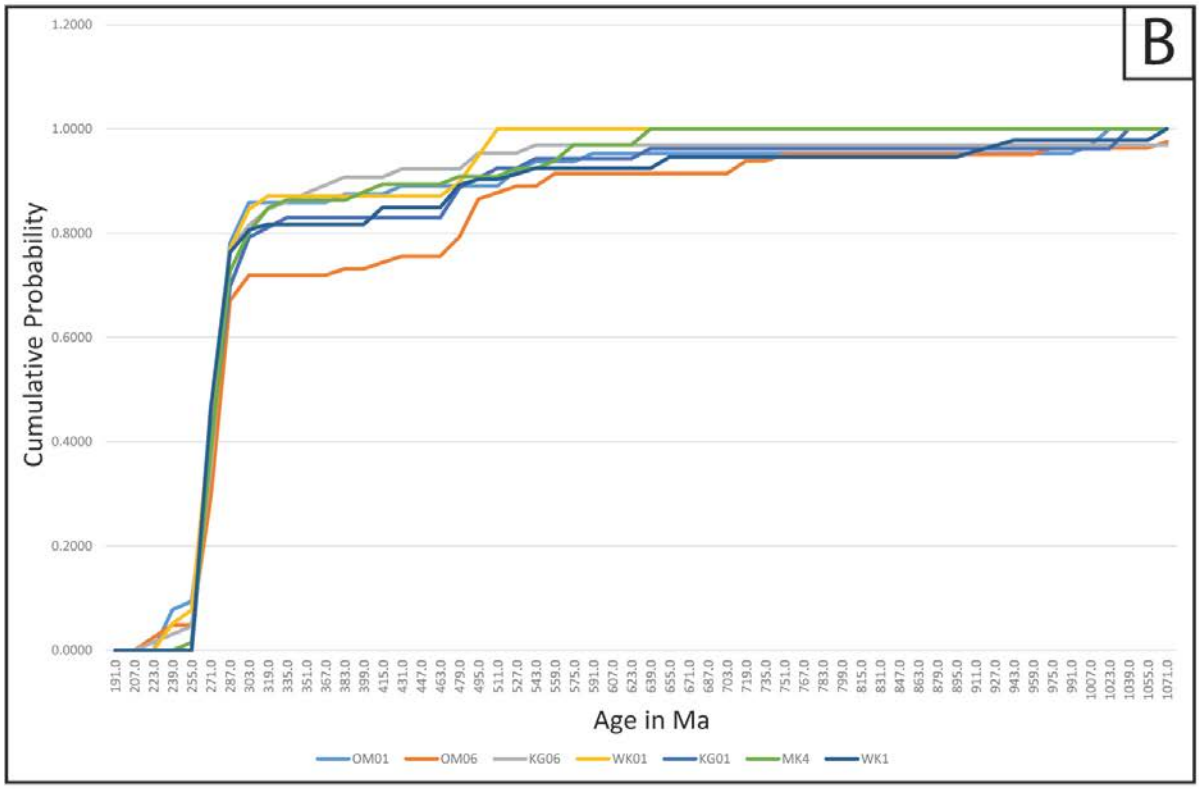

Figure 4.30: A) Cumulative probability plot produces through the K-S Test P-values of all samples. Notice sample N12-2016-1 showing no genetic similarities with other samples between the ages of 264.5 Ma to 631.9 Ma. B) Cumulative probability plot produced through the K-S Test P-values of all samples excluding sample N12-2016-1. KG01 = KG-2016-1; MK4 = MK-2016-4; N12-1 = N12-2016-1; WK1 = WK-2016-1.

All the samples from the Laingsburg, Vischkuil and Ripon formations passed the K-S test moderately to strongly with the exception of sample N12-2016-1. N12-2016-1, which is from the upper Laingsburg Formation, fails the KS-test with all other samples. Therefore, results displayed show all samples including as well as excluding sample N12-2016-1. Sample OM06 (Pluto's Vale Member) passed the K-S Test, but presents the least probable genetic relationship with KG06 (Kaaimansgat sandstone), WK-2016-1 (Laingsburg Formation), MK-2016-4 (Trumpeters Member) and WK01 (Vischkuil Formation) (excluding N12-2016-1). OM06, which was obtained from the upper Pluto's Vale Member moderately fails the K-S Test with OM01 which is taken from the lower Pluto's Vale Member. OM01 passed the K-S Test extremely well with KG06 and WK01. MK-2016-4 also passed the K-S Test very well with KG06, KG01 and WK01.

Cumulative probability plots show that all detrital zircon samples are genetically relatable from the age of 719.0 Ma and older (Fig 4.30). This indicates a near similar source for sediment across the two depocenters. Between the ages of 719.0 Ma and 520.0 Ma all samples seem to show slight variations in their cumulative probability. A larger variety occurs between the ages of 520.0 Ma and 300.0 Ma with samples N12-2016-1 and OM06 diverging the most and showing the least genetic relation to the other samples suggesting possible different sources for the samples. At 264.0 Ma, all samples are genetically near perfect and therefore possibly from the same source.

4.4.4 Detrital Zircon Populations

With all the samples from the three formations (Laingsburg, Vischkuil and Ripon formations) exhibiting a possible similar source history, the detrital zircon population signatures also have near similar age clusters (≥2 grains per cluster).

The detrital zircon age populations extracted from key samples provide a signature for the multiple sources of zircon grains (Fig 4.31). Each sample presents a wide array of age populations, but throughout the samples the age clustering remains similar. The cosmopolitan nature of these grains

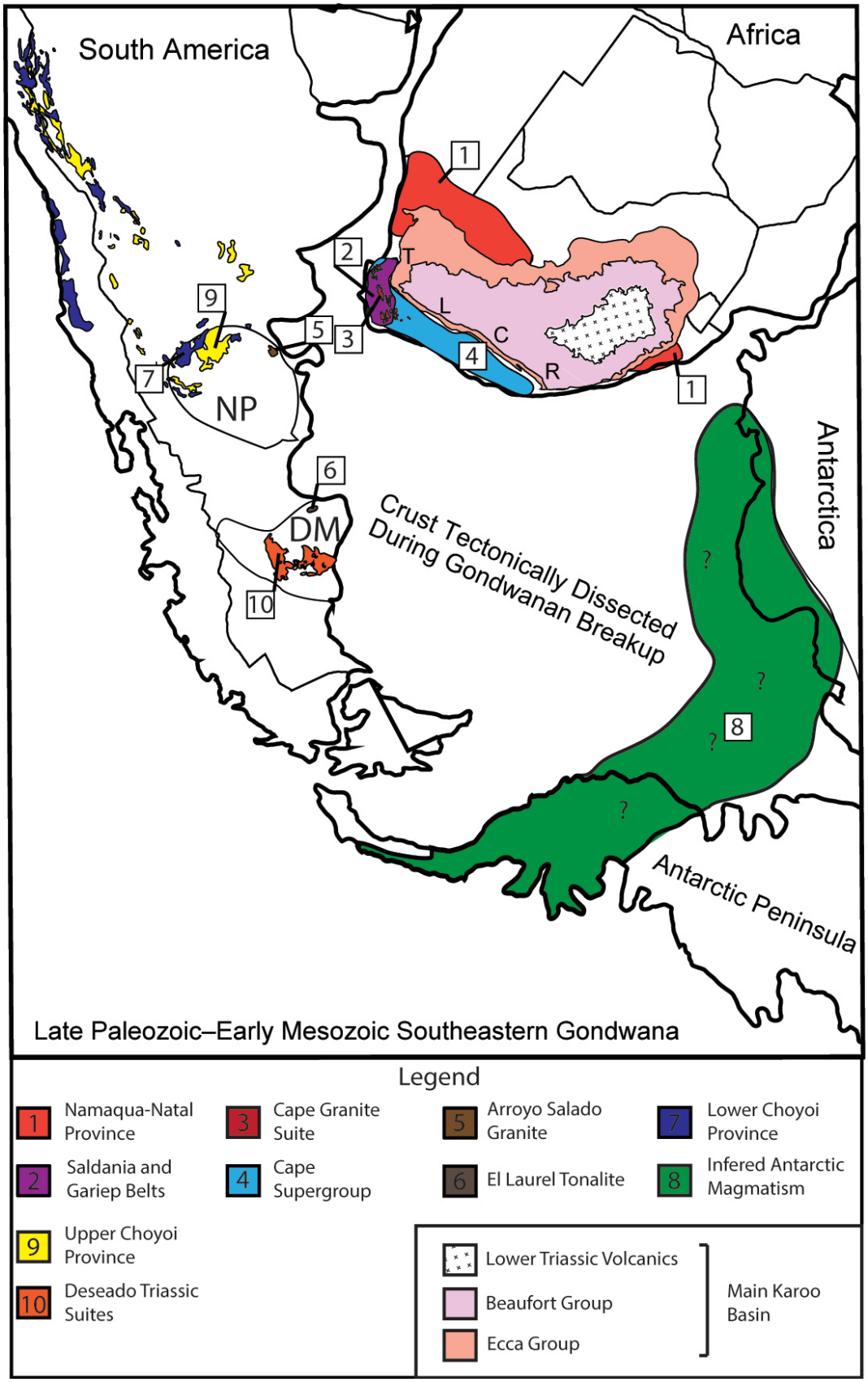

Figure 4.31: Palaeogeographic map of south-eastern Gondwana during the late Palaeozoic to early Mesozoic. All possible source regions for sediment provenance are shown and indicated in the legend. C-Central basin, L-Laingsburg depocenter, R-Ripon depocenter, T-Tanqua depocenter. Data from Da Silva et al. (2000), Pankhurst et al. (2003), Erlington (2006), Pankhurst et al. (2006), McKay et al. (2016). Modified from McKay et al. (2016).

provides for a wide range of weathering and varying morphologies. The oldest Proterozoic grains are most likely inherited from the Namaqua-Natal metamorphic province (Erlington, 2006) which have been recycled through the Neo-Proterozoic Malmesbury Group (Rozendaal et al., 1999) or reworked and recycled through the Cape Supergroup by means of the Cape Fold Belt (Fig 4.32 A, B). The latter seems more unlikely due to the high abundance of feldspar seen in petrographic analysis and the dissected arc composition (Dickens et al., 1984). The Cape Supergroup consists predominantly of quartzite and quartz-rich quartzofeldspathic sandstones (Thamm & Johnson, 2006). With a majority of the Proterozoic grains exhibiting a more abraded rounding texture, a recycled and reworked history is supported. However, the relatively low percentage of grains of these Proterozoic ages suggests that these regions were not major sediment providers for the Ecca Group of the Karoo Basin. The dominant peak of zircon grains around 250.0 Ma and 290.0 Ma suggest that magmatic sources exhibiting these ages are the main provider of sediment into the Karoo Basin.

A less dominant cluster is of Cambrian age (495.0 Ma - 545.0 Ma) (Fig 4.32 C). The most likely source for Cambrian grains is the Cape Granite Suite which is situated adjacent to the southern Main Karoo Basin. These granites have an intrusive age between 550.0 and 510.0 Ma (Da Silva et al., 2000; Scheepers & Armstrong, 2002). Another source for the younger grains between the ages of 460.0 and 480.0 Ma is the Arroyo Salado granite, which is the closest source to the Main Karoo Basin on the Northern Patagonia Massif (Pankhurst et al., 2006) (Fig 4.32 D). The source of Devonian grains is possibly from the Deseado Massif (South America) (Fig 4.32 E). This source comprises mainly of Triassic intrusions, but does have a Devonian tonalitic intrusion, the El Laurel Tonalite (Pankhurst et al., 2003). This plutonic intrusion is situated in the northeast corner of the Deseado Massif and is the closest Devonian source to the southern Main Karoo Basin. The age of the El Laurel Tonalites are synchronous with the population of Devonian grains observed in all samples (354.0 Ma - 417.0 Ma).

The youngest and most prominent age population at the Carboniferous-Permian (320.0 Ma - 254.0 Ma) is a strong indication of a prolonged syn-depositional volcanic event (Fig 4.32 F). With a volcanic

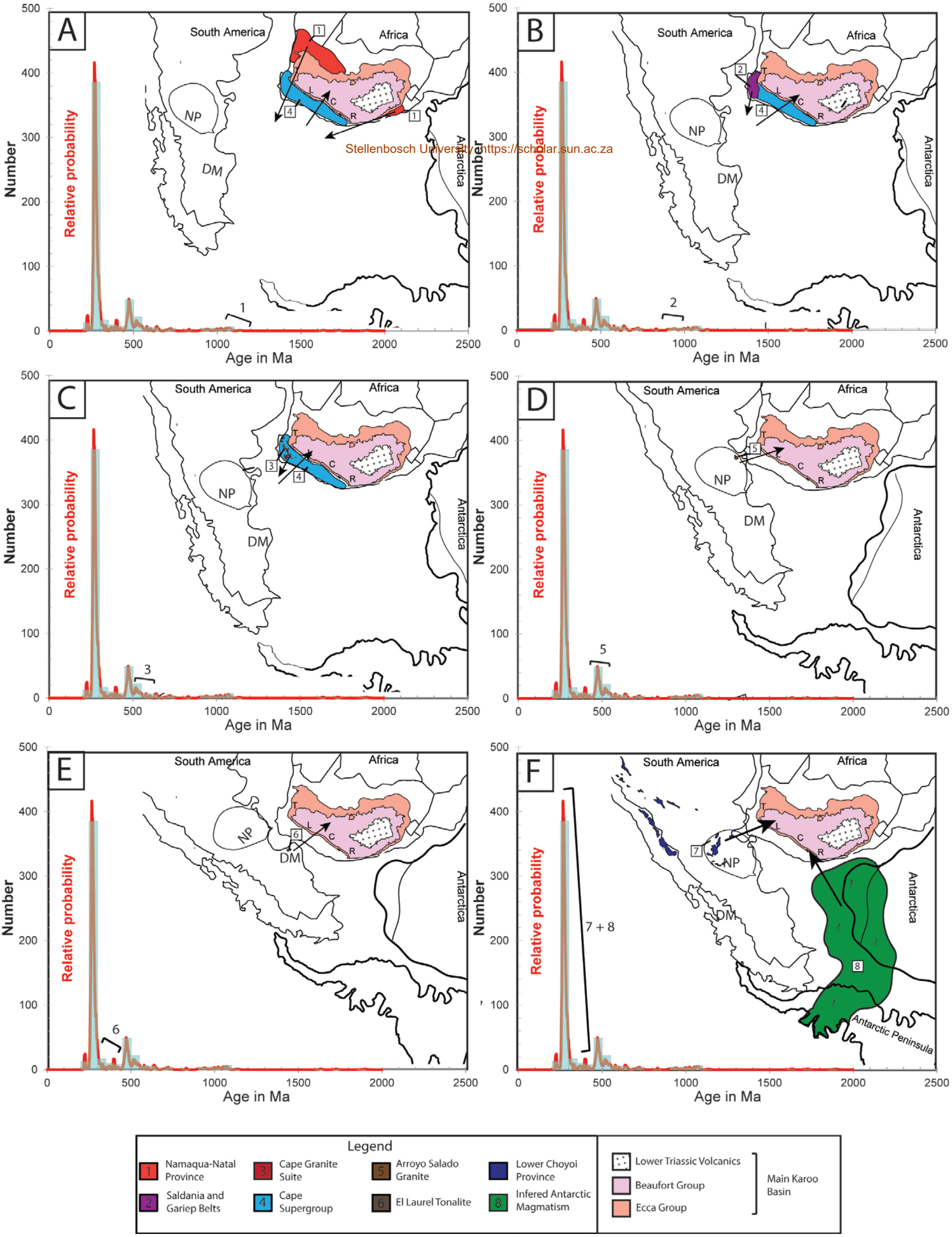

Figure 4.32: Probability density plot of all grain ages from all samples showing the likely source of each peak within the samples. The number indicates the source which supplied sediment. Older Proterozoic grains were likely recycled through the Malmesbury Group or Cape Supergroup.

arc forming south of Gondwana due to subduction of the Panthalassa Plate, a continuous series of eruptions provided volcanic airborne ash which settled in the Karoo Basin. It is generally accepted that the major source for volcanic ash deposition into the basin is the Permian Choiyoi and Triassic Puesto Viejo Suites situated in the Northern Patagonia Massif, South America (Kay et al., 1989; Bangert et al., 1999; Cole, 1992; López-Gamundi & Rossello, 1998; Rocha-Campos et al., 2011).

4.4.5 Discussion

A discrepancy remains between maximum depositional ages presented for the Ecca Group and for the Beaufort Group. A number of studies done on detrital and tuff zircon grains within the Ecca Group, yielded ages showing a progressive younging-up of maximum depositional age from an age of 273.7 ±2.7 Ma at the base of the Ecca Group to 151.1 ±2.5 Ma at the base of a proposed "No Tuffs" zone spanning across the Beaufort-Ecca contact (McKay et al., 2015). Analysis done on samples obtained above the "No Tuffs" zone, within the Beaufort Group, yielded slightly less consistent maximum depositional zircon ages across the southwest and southern Karoo Basin. Ages of the Beaufort Group seem older than the underlying Ecca Group yielding ages of 274 ±5.0 Ma and 261.24 ±<0.4 Ma just above the "No Tuffs" zone.

McKay et al. (2015) suggests that, although multiple scenarios could explain the discrepancy, the most likely interpretation would possibly be that, due to the terrestrial nature of the Beaufort sediments, reworking of older zircon grains into tuff deposits may occur. The possibility that a lack of co-eruptive, terminal phase zircons is likely, might also provide erroneous age constraints on the Beaufort tuffs.

However, the accuracy of the ID-TIMS ages obtained by Rubidge et al. (2013) suggests otherwise and correlates with palaeontological data across the world. The Permian-Triassic extinction event observed in southern China marine palaeontology (Shen et al., 2011) correlates with the end of the *Dicynodon* (now *Daptocephalus*) Assemblage Zone (Rubidge et al., 2013). This contrast in zircon ages is yet to be fully resolved for the Ecca and Beaufort Groups in the southwestern Karoo Basin.

This study focused mainly on detrital zircon populations within clastic sediment of the middle Ecca Group which increases the error margin and can only provide an inferred maximum age of deposition, not a syn-eruptive true age of deposition. Yet, data presented in this study correlate relatively well with previous studies on clastic samples as well as tuff samples (Nguema-Mve, 2005; Fildani et al., 2007; Fildani et al., 2009; McKay et al., 2015). A consistent younging up trend in the maximum depositional age is observed in conformable strata. The older Vischkuil Formation and Pluto's Vale Member yielded ages of 261.8 Ma and 263.4 Ma respectively while the younger Laingsburg Formation and Trumpeters Member yielded ages of 257.3 Ma and 258.9 Ma, respectively.

A recent study by McKay et al. (2016) suggests that zircon grains analyzed from the Northern Patagonia Permian Choiyoi volcanic suite, although temporally similar, does not exhibit similar geochemistry to the grains analyzed in the southern Main Karoo Basin. The Th/U ratio of samples derived from the Lower and Upper Choiyoi province (282.0 Ma - 251.0 Ma) are low (Th/U < 1) with the Triassic Puesto Viejo province (241.0 Ma - 230.0 Ma) yielding higher Th/U ratios (Th/U> 1). However, analysis done on the Antarctic Peninsula, Ellisworth-Whitmore Terrane and the Victoria Group sediments suggest an inferred pre-Triassic extensional backarc magmatism to the south of Antarctica (Riley et al., 2012; Vaughan et al., 2012; Elliot et al., 2014, 2015). Vaughan et al. (2012) suggests that tholeiitic dyke intrusions situated in the Antarctic Peninsula indicates a late Permian to late Triassic magmatic arc known as the Dyer arc. Permian age-correlative zircon grains form these Antarctic Peninsula sediments exhibit a mixture of high (Th/U >1) and low (Th/U<1) Th/U ratios between the ages of 252.0 Ma and 280.0 Ma. Similar Th/U signatures are observed in Karoo tuff zircons from the study by McKay et al. (2016).

Age-dependent Th/U ratios between the ages of 253.0 Ma and 273.0 Ma obtained for this study reflects and correlates with these varying Th/U ratios exhibiting both high (>1) and low (<1) values (Fig 4.33). This suggests that Permian aged zircons are most likely not only derived from the Choiyoi Province, but also from the early magmatic Dyer arc to the southeast of the Karoo Basin close to

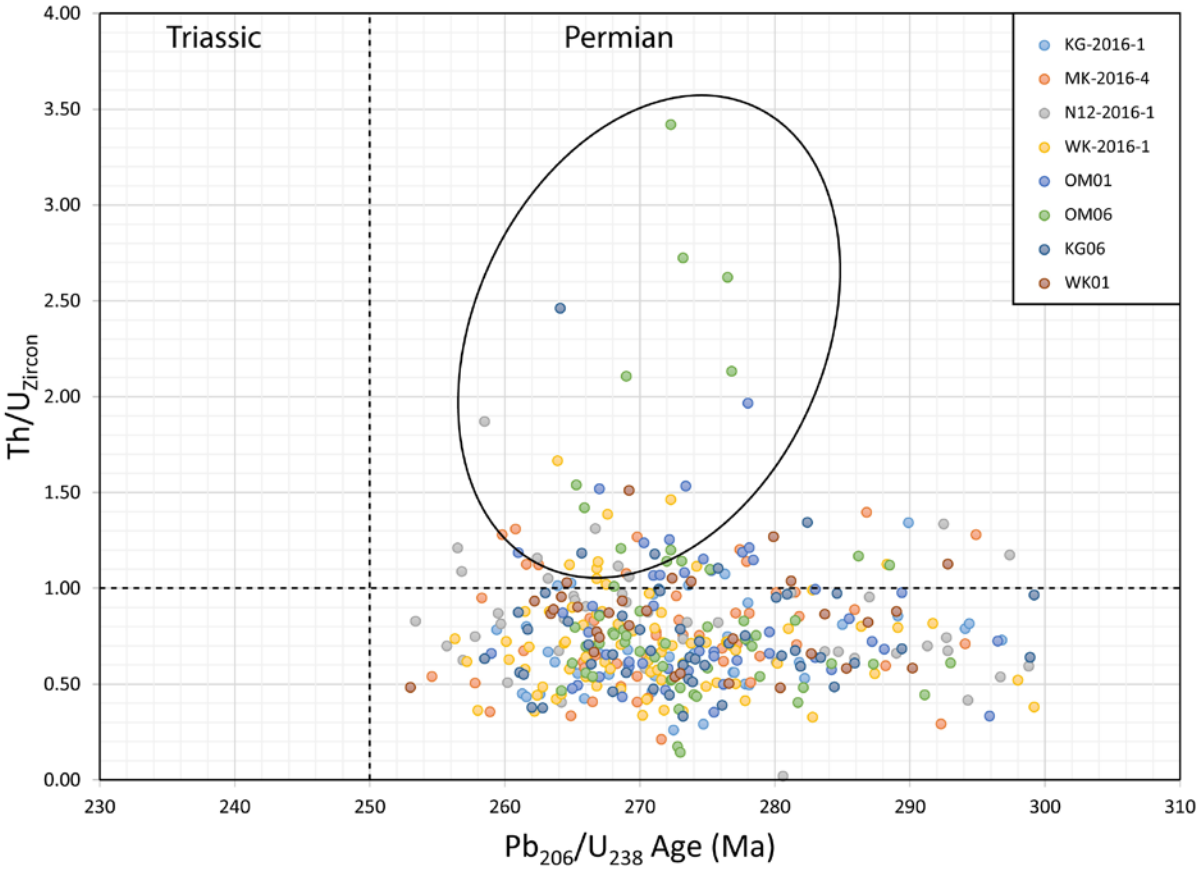

Figure 4.33: Density plot of Th/U ratios against Pb206/U238 ages of grains between the ages of 250 Ma and 300 Ma from all analysed samples. A large amount of grains exhibits a Th/U ratio greater than 1.00 (indicated by circle), although the majority remain between 0.50 and 1.00. Samples OM06 and KG06 presents the highest Th/U ratios (>2.00).

Antarctica. Although not true for all samples, slightly higher concentrations of high Th/U ratios are observed in samples extracted from the Ripon Formation than samples obtained from the Vischkuil This might support the idea that sediments from the southwestern Karoo Basin are derived from the South American volcanic source. Those from the southeastern Karoo Basin were possibly from the Antarctic Dyer magmatic source.

Chapter 5:
Discussion

Chapter 5: Discussion

5.1 Basin development

This multifaceted study sought to better contextualize the mechanisms of sediment emplacement and resolve cryptic stratigraphic relationships in the Lower Ecca, southern Karoo Basin. Thus far, a detailed facies analysis of the Vischkuil, Laingsburg and Ripon formations agrees with previous studies that the Laingsburg (Cole, 1992; Viljoen & Wickens, 1992; Wickens, 1994; van der Merwe et al., 2009) and Ripon formations (Kingsley, 1977; Johnson, 1991) were deposited within basin-floor to slope depositional environments, primarily emplaced by turbidite processes. However, precise stratigraphic relationships, both laterally and vertically, remain unresolved between the Laingsburg and Ripon depocenters. Therefore, in an effort to provide context, this study utilized petrographic analysis and radiometric age dating of detrital minerals coupled with a modified facies and architectural element analysis to elucidate provenance and assist in the characterization of the Vischkuil, Laingsburg and Ripon formations. In this section, more precise resolved stratigraphic correlations between the Laingsburg and Ripon depocenters are presented, and used to re-evaluate the developmental history for the Ecca basin in the southern Karoo during the Guadalupian and Lopingian.

Geochronological data and stratigraphic relationships in the study area indicate that submarine fan building occurred in the Ripon depocenter on the southeastern side of the Karoo Basin at a very early stage and gradually shifted to the west. As a result, the Laingsburg submarine fan complex developed after the Pluto's Vale Member and the Wonderfontein Member of the Ripon Formation were deposited. Similarly, the more westerly positioned Tanqua fan complex is younger than that of the Laingsburg depocenter (Wickens, 1994; Van Lente, 2004; King et al., 2004).

Many early authors suggested that the Cape Fold Belt tectonics was the driver behind initiation of large scale sedimentation into the basin (Hälbich et al., 1983; Cole & McLachlan, 1991; Wickens, 1994; Veevers et al., 1994; Catuneanu et al., 1998). Petrographic studies undertaken for this project confirms

a magmatic source rather than a quartzose sedimentary source as has been previously documented (Wickens, 1994; Van Lente, 2004) and that the Cape Supergroup was not a major source area for the Ecca Group. Despite this, it appears that Cape Fold Belt tectonics influenced basin-floor topography such that subbasins were formed with different depositional pathways into the basin. This dynamic evolution of these subbasins is evident by temporal variation of submarine fan building across the southern Karoo Basin (Wickens 1994; Veevers et al., 1994; Catuneanu et al., 1998).

Deposition of the Collingham Formation, which represents deep-marine conditions, was dominated by abyssal plain suspension settling of fine-grained silts and muds (Viljoen, 1994). The regional scale of distribution of tabular sheets suggests little to no basin floor topography and the maintenance of basin-wide bathyal conditions (Fig 5.1 A). Towards the upper boundary of the Collingham Formation the presence of very fine-grained distal deposits of low density turbidites indicates minor injections of fine material from the low angle slope (van der Merwe et al., 2010). These deposits are also unconfined and no evidence of channeling is present. The rock formations overlying the Collingham Formation were deposited by submarine fan development through high-density turbidity currents which began in the southeastern part of the Karoo Basin and later spread westwards (Fig 5.1 B).

5.1.1 Vischkuil Formation

The Increased input of terrigenous silts and muds distinguishes the Vischkuil Formation from the underlying Collingham Formation. The Vischkuil Formation provides insight into the development of a deep basin-floor setting prior to the onset of increased rates of sediment input by high-density turbidity currents. Laterally continuous sheet-like geometry of the beds, fine-grained sediments (predominantly FA1, with subordinate FA2), and lack of channeling supports a distal deep basin depositional environment (Mutti, 1977; Shanmugam & Walker, 1978; Reading, 1996; Arnott, 2010). Prior studies also conclude that the distally deposited Vischkuil Formation developed on a deep marine abyssal plain with relatively no basin floor topography (Viljoen & Wickens, 1992; Wickens, 1994; van der Merwe et al., 2009).

Petrographic studies show that the sample analyzed from the Vischkuil Formation exhibits a close mineralogical resemblance to that of the Ripon Formation. Geochronology also indicates that the depositional age of the Vischkuil Formation present in the study area is close to the depositional age obtained from the lower Pluto's Vale Member of the Ripon Formation. Although palaeocurrent readings taken from the upper Vischkuil Formation in this study indicates a general E to NE (n=9) flow direction, the lower silt-prone units underlying DU2 and DU3 represents the distal lobe fringes of the lower Pluto's Vale Member. This is suggested by van der Merwe et al. (2010) as a result of palaeocurrent readings taken from the Laingsburg depocenter indicating a westward palaeoflow of the lower Vischkuil Formation, which gradually shifts to an eastward palaeoflow together with the initiation of Mass Transport Complexes (MTC's).

In the western extent of the study area, near Prince Albert, evidence of large Type-1 deformed units are present and are overlain by chaotic mudrock occasionally containing clasts and plant fragments. This occurrence of debritic material indicates the onset of coarser material being supplied to the basin (Posamantier & Walker, 2006). Two of these units are present in the Vischkuil Formation at Prince Albert as deformation units 2 and 3 (DU2 and DU3) (Fig 5.1 C). These arenaceous units merge toward the east with the PV-mud of the Pluto's Vale Member. The lack of thick sandstone beds as well as channel-fills or overbank/levee deposits indicates that deposition of the deformed beds occurred towards the distal fringes of basin-floor fans (Coleman & Prior, 1988; Posamentier & Kolla, 2003; van der Merwe et al., 2009). The general abundance of coarse-silt to very fine-sand coupled with the presence of debritic material overlying the deformed strata indicates similar depositional and post-depositional deformational mechanics for these units to those of the Vischkuil Formation (Laingsburg depocenter) (Viljoen & Wickens, 1992; van der Merwe et al., 2009). The possibility of slides and slumps forming in a basin floor setting is not uncommon as loading of debrites creates shear stresses on the underlying strata, causing it to deform.

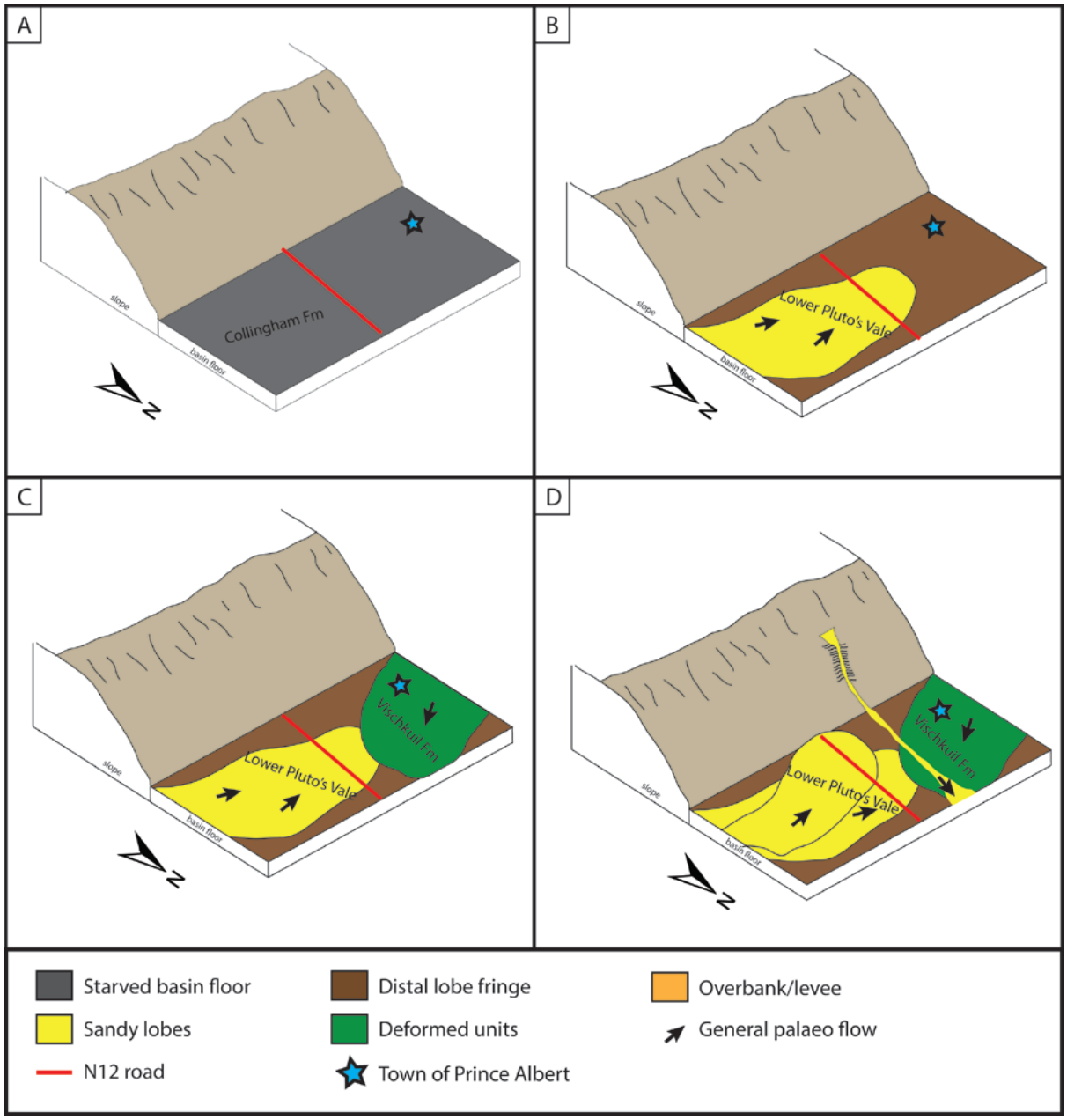

Figure 5.1: Schematic model for the depositional history and basin development in the study area. A) starved conditions on the basin floor, represented by the Collingham Formation. B) Initiation of basin floor fan building in the Ripon depocenter with a fan protruding to the W and NW as well as distal fringes of this fan reaching the Laingsburg depocenter. C) Initiation of sediment input from the west through debrite deposition and deformed strata. D) a second fan builds from the Ripon depocenter as well as a proximal channel migrating from the slope south of the study area.

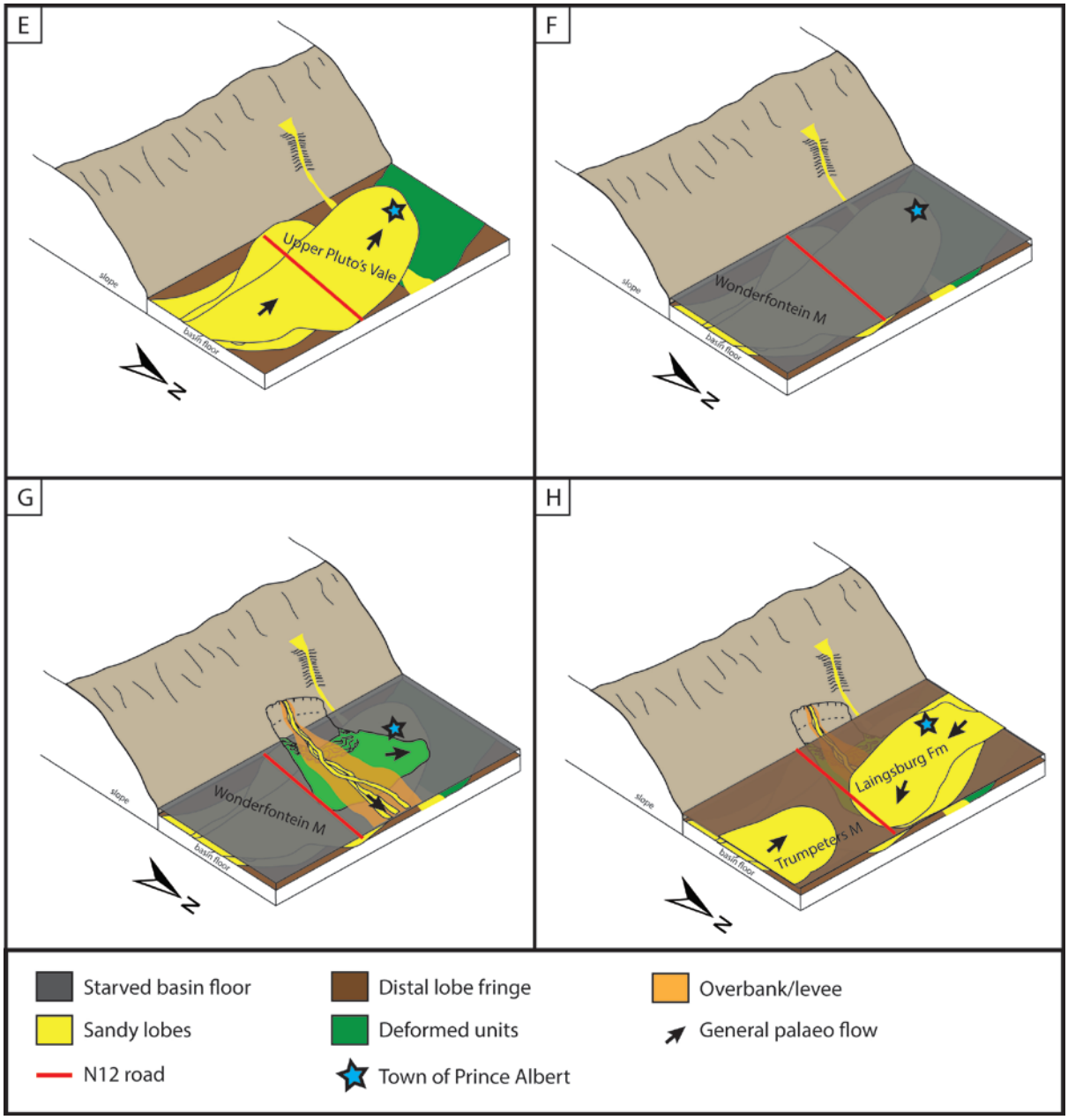

Figure 5.1 (cont.): E) Another fan extends from the Ripon depocenter over these deposits. F) Starvation occurs in this region of the basin causing settling of fine material for an extended period. G) slope instability south of the study area causes MTC's to form as well as the formation of slump scars on the slope. This developed pathway for proximal fan migration to the North with multiple channel structures. Overbank and levee deposits are visible. H) the final stages of distal fan building form the Laingsburg depocenter and the Ripon depocenter before deposition is dominated by slope facies.

5.1.2 Ripon Formation

Deposition of the Pluto's Vale Member (Ripon Formation) marks an abrupt change to higher energy conditions as deposition switches from predominantly suspension settling for the Collingham Formation to rapid turbidite sand deposition. The sandstone beds of the Pluto's Vale Member form an upward thickening succession from thin beds (FA2) to thicker beds (FA3) which indicate a progradational nature of submarine fan development, i.e. evolving from distal lobe sands to mid-fan deposition. Debrites are commonly found at 1st-order upper bounding surfaces of FA2 as well as FA3 sandstone beds higher up in the succession. The lack of FA4 and slumping in this member might indicate a relatively stable slope environment consistently introducing sediments into the basin. Studies done on the Ripon Formation towards Grahamstown suggests a mid- to upper-fan deposition (Kingsley, 1981; Johnson, 1991). Stratigraphic analysis done by Kingsley (1977) shows a gradual increase in fan thickness of the Pluto's Vale Member from Grahamstown (east, 200.0 - 300.0 m thick) towards Jansenville (west, 500.0 m thick). Conversely, in the study area for this project there is a decrease in thickness of the Pluto's Vale Member to about 100.0 m further west, suggesting that the up-dip feeder of the submarine fan is situated southeast of Jansenville.

The lowermost Pluto's Vale, underlying the Pluto's Vale mudrock (PV-mud) forms the mid lobes of a submarine fan protruding from the southeast towards the northwest into the basin based on palaeocurrent readings and abundance of FA2 and FA3 beds. As these lobes pinch out to the west the distal fringes of the Lower Pluto's Vale become the argillaceous Lower Vischkuil Formation (Fig 5.1 C). A second submarine fan, which forms the upper Pluto's Vale Member, overlies the PV-mud with a general thickness of 20.0 - 30.0 m showing a strong westward palaeoflow. This is evident through deposition of tabular FA2 and FA3 beds overlying the PV-mud. The PV-mud represents the inter-fan muds depositing between submarine fans (Andersson & Worden, 2004).

Within the PV-mud the occurrence of channelized sandstones (Kaaimansgat-sandstone) indicates confined channel fill with a northward palaeoflow (Fig 5.1 D). The general lack of lateral accretion and

wide channel margins indicates low sinuosity and high erosive scouring (Johnson et al., 2001). However, the massive nature of the sediments and occurrence of overbank heterolithic deposition (FA6) towards the flanks of these channels might indicate a simple fill of a bypass channel by means of rapid sub-marine avalanche deposition (Grecula et al., 2003; Hodgson et al., 2016). Similar channel-fill deposits were found towards the upper units of the Wonderfontein Member east of the N12.

After deposition of the upper fan of the Pluto's Vale Member the southeastern basin terminated deposition of sand-rich turbidites (Fig 5.1 E, F), while the southwestern basin maintained a prograding nature into proximal fan deposition. Starvation in the southeastern portion of the basin is represented by the Wonderfontein Member. As previously noted the Wonderfontein Member thickens to the west of Grahamstown (300.0 m) and thins further westward to a thickness of 100.0 - 200.0 m within the study area.

The general abundance of FA1 and lack of traction features such as ripple cross-laminae within the middle argillaceous Wonderfontein Member indicates suspension settling of fine material and a general starvation of sediment input. This prolonged period of starvation is not observed within the Laingsburg depocenter and might suggest local basin-floor topographical controls on deposition or local periodic termination of sediment supply from terrestrial sources (Catuneanu et al., 2002).

Although the rocks of the Laingsburg, Tanqua and Ripon depocenters exhibit similar source regions based on detrital zircon signatures, sediment petrography indicates a slight variability in the source material. This variability is seen by the lower quartz composition and higher K-feldspar content in samples from the Ripon depocenter compared to the Laingsburg depocenter. It is apparent that basin-floor topography controlled sub-marine fan migration, but terrestrial conditions may also cause a change in the availability of source sediment along the coastal margin due to lack of fluvio-deltaic migration into the basin (Reading, 1996).

The occurrence of large scale Type-2 deformed strata in the lower units of the Wonderfontein Member indicates MTC's deposited during slope instability (Fig 5.1 G). Debrites are not commonly associated with these Type-2 slumps. MTC's initiated in the slope environment due to instability are known to cause slump scar development (Masson et al, 1998; Frei-Martinez et al., 2005; Moscardelli & Wood, 2008). The evidence of heterolithic overbank/levee deposits truncating the Type-2 deformation units, followed by major channelized amalgamated sandstone beds, indicates a more proximal setting. These channelized sandstones exhibit a N to NNW (n=5) palaeoflow, indicating proximal fan development from south of the study area further west from the well-defined Ripon depocenter. The slump scars created a pathway for sediment to be transported into the basin from the south (Brunt et al., 2012) (Fig 5.1 H). Unfortunately, evidence of the time equivalent up-dip slump scars is not present due to uplift and erosion of the sections south of the Cape Fold Belt. Sediment petrography and geochronology indicates that this system exhibits the same source rock as for the Ripon depocenter. This unit also has an ultralithofeldspathic composition and the zircon age populations coincide with units of the Ripon depocenter.

During the final stages of basin-floor fan building, the Ripon depocenter reintroduced basin-floor fan building providing westward protruding distal fan deposition. This is seen by the upper tabular sandstones (Trumpeters Member) overlying the Wonderfontein Member in the far eastern portion of the study area exhibiting a progradational nature.

The upper Trumpeters Member is not prominent in the study area, being restricted to the east, and represents the distal lobes of a westward propagating submarine fan system. Facies similarities are observed within the deposition of lobes in the Trumpeters Member that correspond to distal sub-marine fan lobe deposition. The Trumpeters Member in the study area commonly exhibits mud-rich sandstones as seen with the abundant dark grey bands within the sandstone units, separating it from the mud-poor sandstones of the Laingsburg Formation.

5.1.3 Laingsburg Formation

This study confirms the presence of the Laingsburg Formation in the study area, which forms the distal fan deposits of the eastward protruding sub-marine fans. The common occurrence of massively bedded FA3 beds and the normal grading of FA3 beds to FA1 laminae supports turbidite fan deposition. The observed facies changes from the generally more argillaceous Vischkuil Formation to the sandstone-rich Laingsburg Formation is gradational, but a distinct boundary is present between the upper Vischkuil Formation distal turbidites and the lowermost Fan A proximal turbidite deposits of the Laingsburg Formation in the Laingsburg depocenter (Wickens, 1994). The Laingsburg Formation is commonly described as a sub-marine fan complex situated on the basin floor to base of slope deep-marine setting.

The very fine- (63.0 µm) to fine-grained (125.0 µm) sand supports a slightly more distal setting. The massive nature of thick-bedded sandstone units and gradational fining up sequences into ripple cross-laminated and flat laminated fine-grained material strongly suggest typical turbidity current influences (Bouma, 1962; Reading, 1996). The feldspathic litharenite composition observed through sediment petrography closely resembling that of the Laingsburg Formation in the Laingsburg depocenter and palaeocurrent readings show a similar E-NE flow direction as readings taken from the Laingsburg depocenter (Wickens, 1994; Sixsmith, 2000; Van Lente, 2004). The cyclic nature of submarine fan deposition for the Laingsburg Formation is observed in the study area as two fining-up cycles of sand-rich lobe deposition, showing a strong E to NE current direction (n=8), divided by a period of fine-grained suspension settling. These units form the Laingsburg Formation is present west of the N12 and thins out just east of the N12. A gradual increase of coarse-grained sediments is observed with the basin floor fan-building units of the Laingsburg Formation (Fig 5.1 H).

The lack of channelized features within the two depositional units observed in the Laingsburg Formation within the study area as well as the tabular widespread sheet-like nature of these sandstone beds support a distal lobe depositional setting (Reading, 1996, Sixsmith, 2004). The general lack of traction flow indicators such as ripple laminations suggests rapid fall-out of suspension. No evidence was observed for the presence of overbank/levee deposits in the study area which supports the lack of channel-fill deposits and therefore a distal lobe setting (Johnson et al., 2001; Sixsmith, 2004). This could also be supported by the thinning of beds towards the east of the N12 until termination of lobe deposition.

Chapter 6:
Conclusion

Chapter 6: Conclusion

The purpose of this study was to provide a detailed account of the sedimentological and stratigraphic variability in the region where the two major southern Karoo Basin depocenters (Laingsburg and Ripon subbasins) meet. This was accomplished by various methods to determine lateral correlation, sediment provenance, and implications on basin development during the Guadalupian and Lopingian. Palaeoenvironmental evolution in the study area exhibits progradational shallowing of the basin-floor and slope depositional setting. As the basin approached the filled-phase, regressive sea-level caused the slope to build into the basin. Temporally, this palaeoenvironmental evolution occurred over a period of about 20 My during the Permian.

By utilizing detailed facies analysis with in-field stratigraphic relationships, a correlation panel across the designated study area was drawn up and the palaeoenvironmental change documented. A provenance study was also conducted by means of sediment petrography and detrital zircon geochronology to obtain the sediment source, history and age. By coupling these results, this study was able to rigorously assess and conceptualize the following conclusions:

- Stratigraphic correlations indicate a strong interfingering relationship between the Laingsburg and Ripon depocenters. The Laingsburg and Vischkuil formations pinch out to the east and the Ripon Formation pinches out to the west.
- Depositional systems along the southern margin of the Karoo Basin, north of the Cape Fold Belt, are much more widespread than initially thought. Evidence of channel-fill deposits indicating migration towards the north suggests an evolution of the depositional system from the Ripon depocenter with sediment feeding from south of the study area. Conversely, this study agrees with Wickens (1994, and references therein), that the Laingsburg depocenter predominantly contained sediments that fed from the west.

- Palaeoenvironmental and basin reconstruction indicates a progressive change from deep marine to base of slope deposition within the regional setting of the basin as well as lateral variations in basin-floor evolution.
- Minor variations in provenance occurred between the two depocenters. The Laingsburg depocenter exhibiting a more feldspathic and quartz-rich source with the possibility of ash-fall being dominantly derived from the Choiyoi igneous province, Northern Patagonia Massif (Kay et al., 1989; Bangert et al., 1999; Cole, 1992; López-Gamundi & Rossello, 1998; Rocha-Campos et al., 2011). The Ripon depocenter is dominated by a slightly more lithic-rich and quartz-poor source with ash-fall predominantly derived from the inferred Antarctic Dyer arc, Antarctic Peninsula (Riley et al., 2012; Vaughan et al., 2012; Elliot et al., 2014, 2015).

The development of the southern Karoo Basin provided several palaeoenvironmental changes over time. The dates provided below were obtained from U/Pb detrital zircon analysis in this study and this may change in the future due more accurate dating methods. The middle Permian, Roadian age (272.0 Ma - 268.0 Ma) (Fig 6.1 A) manifested a change in lithofacies across the southern Karoo Basin. This sudden change in lithofacies from abyssal-plain suspension settling to sandy lobe deposits marked an abrupt change in the shelf deltaic setting and introduced a large amount of sediment into the basin. The distal lobe fringes of low-density turbidites from the Vischkuil Formation were deposited on the abyssal plain and form the distal parts of the more proximal Pluto's Vale Member (Ripon Formation) submarine fans.

During the Wordian age (268.0 Ma - 265.0 Ma) (Fig 6.1 B) the depositional environment in the Ripon depocenter maintained a mid- to distal slope setting, depositing widespread lobes of the Pluto's Vale Member. The palaeoenvironmental setting was on the basin-floor with no visible evidence of slope facies. Widespread slumps from the Laingsburg depocenter were precursors to initiation of submarine fan development in the Laingsburg depocenter which was caused by debritic material deposited rapidly over semi-consolidated, waterlogged strata.

During the Capitanian age (265.0 Ma - 261.0 Ma) (Fig 6.1 C) deposition of the Vischkuil Formation terminated and the depositional setting introduced slope instability and fine-grain suspension settling. Although deposition of coarse material did not occur, the palaeoenvironmental setting was closer to the slope. During the period of sediment starvation in the Ripon depocenter, proximal lobe confined channel-fill occurred within the Wonderfontein Member from a feeder to the south of the study area with a northern flow around 261.0 Ma - 259.0 Ma (Fig 6.1 D). These channel-fills are associated with overbank deposits and were deposited on a base of slope palaeoenvironmental setting. In the Late Permian (259.0 Ma - 254.0 Ma) (Fig 6.1 E), the introduction of mid- to distal submarine fans from west and east of the study area resulted in deposition of the Laingsburg Formation and Trumpeters Member (Ripon Formation) respectively. This formed the last major basin-floor fan setting before a slope environment dominated deposition within the study area.

Progradation of the slope margin along the southern extent of the basin resulted in deposition of slope deposits such as rhythmites and distal delta front sediment becoming more prominent as represented by the overlying Fort Brown Formation (Cole, 1992). The abundance of deformed strata and slumped blocks indicate deposition on the slope environment. These deposits regionally overlie the submarine fans of the Laingsburg and Ripon depocenters, indicating basin-wide progradation.

This study effectively elucidated the cryptic stratigraphy and sedimentology of the Lower Ecca Group east of Prince Albert and provided a better understanding of the inter-relationship between the Laingsburg and Ripon depocenters. Through this, an updated geological map of this area was created to provide a more accurate representation of the Laingsburg, Vischkuil and Ripon formations (Fig 6.2). Enough evidence was obtained to support the presence of two distinct depocenters and this study is an initial attempt to understand the inter-relationship of the Laingsburg and Ripon depocenters and their development.

With sedimentological and stratigraphic analysis still advancing within the southern Main Karoo Basin, this study opens the possibility of integrating more opportunities to decipher the link between

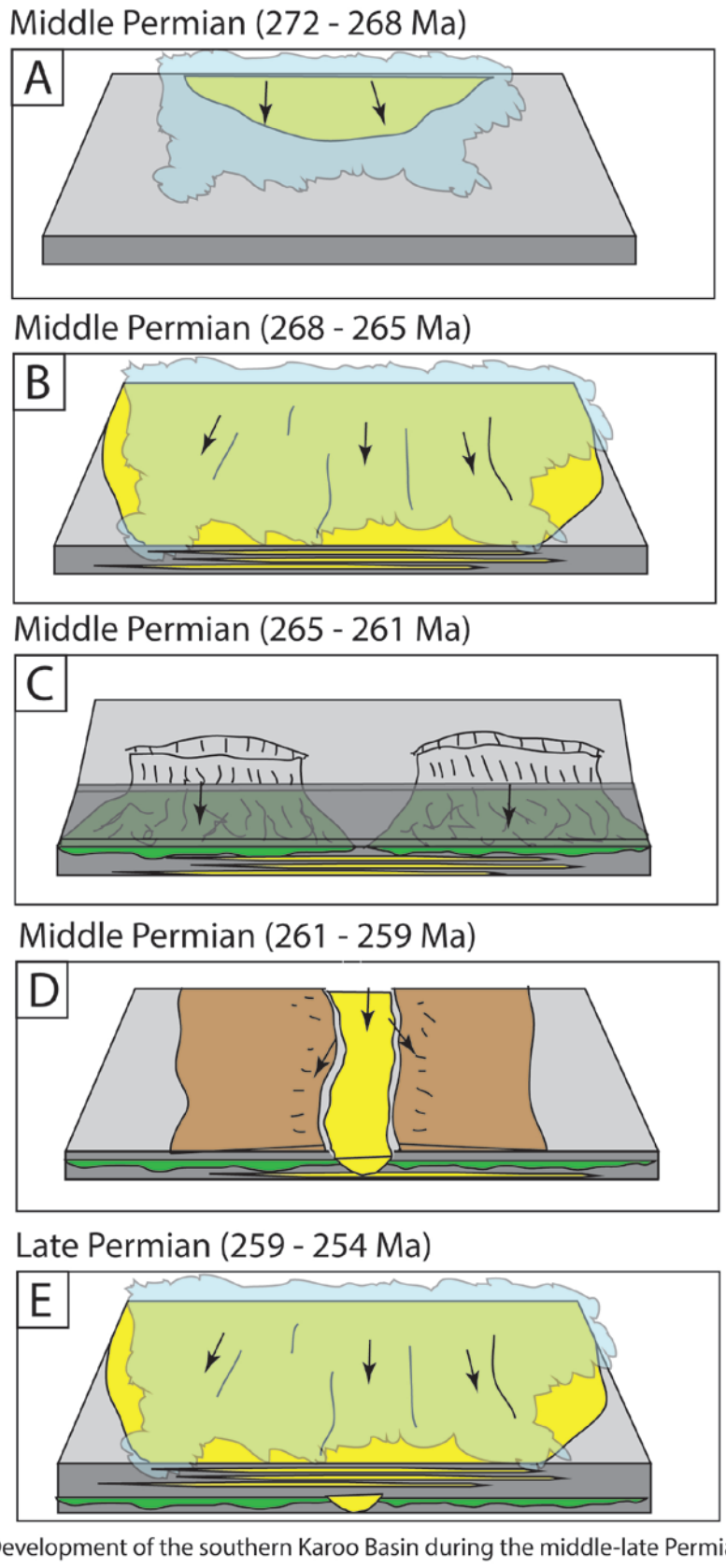

Figure 6.1: A) Distal lobe fringes represented by the Vischkuil Formation and distal lobe deposition of the lower Pluto's Vale Member. B) Mid- to distal submarine fan deposition of the Pluto's Vale Member. C) Slope instability causing slumps with starved conditions on the base of slope represented by the Wonderfontein Member. D) Base of slope confined channels with overbank deposits as observed in the Wonderfontein Member. E) Mid- to distal fan building of the Laingsburg Formation and Trumpeters Member.

the Laingsburg and Ripon depocenters. Through this study, it became apparent that, before this study, little was known about the southern Karoo Basin east of Prince Albert compared to the southwestern portion of the basin. This study forms an attempt at providing a holistic understanding of the link between the two depocenters and delivers a significant contribution in Karoo Basin sedimentological research.

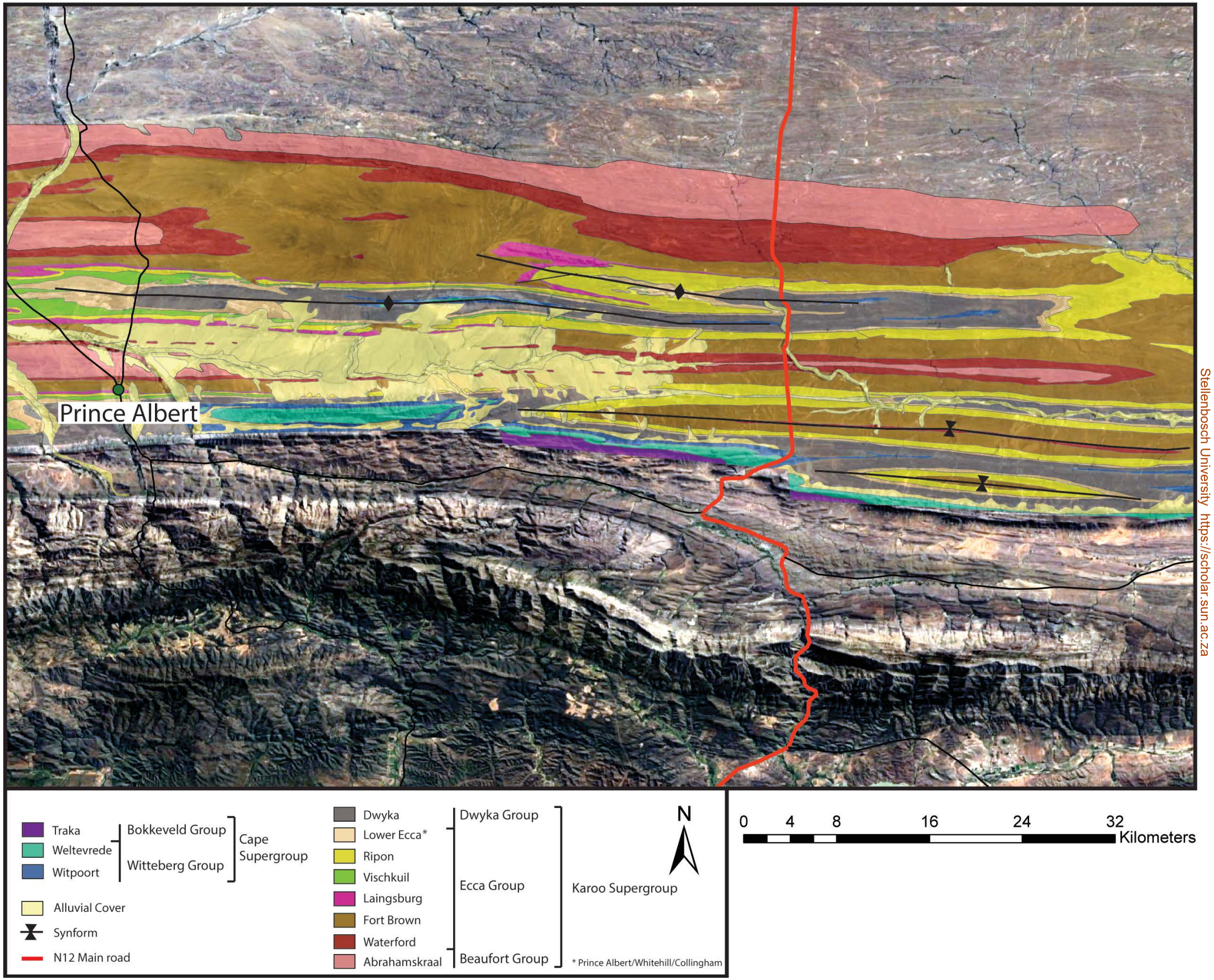

Figure 6.2: Revised geological map of the study area showing the new stratigraphic placement of the Laingsburg, Vischkuil and Ripon formations.

References

Arnott, R. (2010). Deep-Marine Sediments and Sedimentary Systems. *In:* James, N.P. and Dalrymple, R.W. (Eds.), *Facies Models 4* (pp. 295-322). St. John's, Newfoundland & Labrador,

Anderson, A.M. (1974). Arthropod trackways and other trace fossils from the Early Permian lower Karoo Beds of South Africa. Unpublished PhD thesis, University of Witwatersrand, Johannesburg, 172pp.

Andersson, P. O. D., Johansson, A. & Kumpulainen, R. A. (2003). Sm-Nd isotope evidence for the provenance of the Skoorsteenberg Formation, Karoo Supergroup, South Africa. *Journal of African Earth Sciences*, 36, pp. 173-183.

Andersson, P. O. D., & Worden, R. H. (2004). Mudstones of the Tanqua Basin, South Africa: an analysis of lateral and stratigraphic variations within mudstones, and a comparison of mudstones within and between turbidite fans. *Sedimentology,* Volume 51, pp. 479–502.

Andersson, P., Worden, R., Hodgson, D., & Flint, S. (2004). Provenance evolution and chemostratigraphy of a Palaeozoic submarine fan-complex: Tanqua Karoo Basin, South Africa. *Marine and Petroleum Geology,* Issue 21, pp. 555–577.

Bangert, B., Stollhofen, H., Lorenz, V., & Armstrong, R. (1999). The geochronology and significance of ash-fall tuffs in the glaciogenic Carboniferous-Permian Dwyka Group of Namibia and South Africa. *Journal of African Earth Sciences,* 29, pp. 33-49

Barrett, Paul M. (2009) A new basal sauropodomorph dinosaur from the upper Elliot Formation (Lower Jurassic) of South Africa. *Journal of Vertebrate Paleontology*, 29:4, 1032-1045, DOI: 10.1671/039.029.0401

Blignaut, J. J. G., Rossouw, P. J., De Villiers, J., & Russell, H. D. (1948). The geology of the Skoorsteenberg area, Cape Province. Explanation Sheet 166 (Schoorsteenberg). *Geological Survey of South Africa*, 48 pp.

Boggs, S. Jr. (2009). Petrology of Sedimentary Rocks. *Cambridge University Press, (2nd Edition, Cambridge, UK*, 600 pp.

Bouma, A.H. (1962). Sedimentology of some Flysch deposits: A graphic approach to facies interpretation. *Elsevier*, 168 pp.

Bordy, E. M., Hancox, P. J., & Rubidge, B. S. (2004a). Fluvial style variations in the Late Triassic–Early Jurassic Elliot Formation, main Karoo Basin, South Africa. *Journal of African Earth Sciences*, *38*(4), pp. 383-400.

Bordy, E. M., Bumby, A. J., Catuneanu, O., & Eriksson, P. G. (2004b). Advanced early Jurassic termite (Insecta: Isoptera) nests: evidence from the Clarens Formation in the Tuli Basin, southern Africa. *Palaios*, *19*(1), pp. 68-78.

Bordy, E. M., Sztano, O., Rubidge, B. S., & Bumby, A. (2011). Early Triassic vertebrate burrows from the Katberg Formation of the south-western Karoo Basin, South Africa. *Lethaia,* Volume 44, pp. 33-45.

Bordy, E. M., & Abrahams, M. (2016). Geochemistry of the Pronksberg Bentonite of the Upper Elliot Formation (Early Jurassic), Eastern Cape, South Africa. *In*: Linol, B. and de Wit, M. J. (Eds.), *Origin and Evolution of the Cape Mountains and Karoo Basin* (pp. 119-127). Springer International Publishing.

Botha, J., Lee-Thorp, J., & Chinsamy, A. (2005). The palaeoecology of the non-mammalian cynodonts Diademodon and Cynognathus from the Karoo Basin of South Africa using stable light isotope analysis. *Palaeogeography, Palaeoclimatology, Palaeoecology,* Volume 223, pp. 303-316.

Botha-Brink, J., & Smith, R. M. H. (2011) Osteohistology of the Triassic archosauromorphs Prolacerta, Proterosuchus, Euparkeria, and Erythrosuchus from the Karoo Basin of South Africa. *Journal of Vertebrate Paleontology*, 31:6, pp. 1238-1254, DOI: 10.1080/02724634.2011.621797

Branch, T., Ritter, O., Weckmann, U., Sachsenhofer, R. F., & Schilling, F. (2007). The Whitehill Formation - a high conductivity marker horizon in the Karoo Basin. *South African Journal of Geology,* Volume 110, pp. 465-476.

Bräuer, B., Ryberg, T., & Lindeque, A. S. (2007). Shallow seismic velocity structure of the Karoo Basin, South Africa. *South African Journal of Geology,* Volume 110, pp. 439-448.

Brunt, R. L., Hodgson, D. M., Flint, S. S., Pringle, J. K., Di Celma, C., Prélat, A., & Grecula, M. (2013). Confined to unconfined: anatomy of a base of slope succession, Karoo Basin, South Africa. *Marine and Petroleum Geology*, *41*, pp. 206-221.

Cairncross, B., & Cadle, A. B. (1988). Palaeoenvironmental control on coal formation, distribution and quality in the Permian Vryheid Formation, East Witbank Coalfield, South Africa. *International Journal of Coal Geology,* Volume 9, pp. 343-370.

Cairncross, B., Hart, R. J., & Willis, J. P. (1990). Geocheistry and sedimentology of coal seams from the Permian Witbank Coalfield, South Africa; a means of identification. *International Journal of Coal Geology,* Volume 16, pp. 309-325.

Carozzi, A. V. (1993). *Sedimentary Petrography.* 1st ed. New Jersey: PTR Prentice-Hall.

Catuneanu, O. (2002). Sequence stratigraphy of clastic systems: concepts, merits, and pitfalls. *Journal of African Earth Sciences*, *35*(1), pp. 1-43.

Catuneanu, O., Hancox, P.J., & Rubidge, B.S. (1998) Reciprocal flexural behavior and contrasting stratigraphies: a new basin development model for the Karoo retroarc foreland system, South Africa. *Basin Research*, 10(4), pp. 417-439.

Catuneanu, O. (2004). Retroarc foreland systems—evolution through time. *Journal of African Earth Sciences,* Volume 38, pp. 225-242.

Catuneanu, O., Hancox, P., Cairncross, B., & Rubidge, B. (2002). Foredeep submarine fans and forebulge deltas: orogenic off-loading in the underfilled Karoo Basin. *Journal of African Earth Sciences,* Issue 35, pp. 489–502.

Catuneanu, O., Wopfner, H., Eriksson, P. G., Cairncross, B., Rubidge, B. S., Smith, R. M. H., & Hancox, P. J. (2005). The Karoo basins of south-central Africa. *Journal of African Earth Sciences*, *43*(1), pp. 211-253.

Cole, D. I. (1992). Evolution and development of the Karoo Basin. *In:* de Wit, M.J. and Ransome, I.G.D., (Eds.), *Inversion tectonics of the Cape Fold Belt, Karoo and Cretaceous Basins of Southern Africa.* Balkema, Rotterdam, pp. 87-100.

Cole, D.I., & McLachlan, I.R. (1991). Oil potential of the Permian Whitehill Shale Formation in the main Karoo basin, South Africa. *In*: Ulbrich, H. and Rocha, A.C. (Eds.), *Gondwana Seven Proceedings.* Instituto de Geociências, Universidade de Sâo Paolo, Brazil, pp. 379-390.

Coleman, J.M., & Prior, D.B. (1988). Mass wasting on continental margins. *Annual Review of Earth and Planetary Sciences*, 16, pp. 101-119.

Coney, L., Reimold, W. U., Hancox, P. J., Mader, D., Koeberl, C., McDonald, I., Struck, U., Vajda, V., & Kamo, S. L. (2007). Geochemical and mineralogical investigation of the Permian–Triassic boundary in the continental realm of the southern Karoo Basin, South Africa. *Palaeoworld*, *16*(1), pp. 67-104.

Da Silva, L. C., Gresse, P. G., Scheepers, R., McNaughton, N. J., Hartmann, L. A., & Fletcher, I. (2000). U-Pb SHRIMP and Sm-Nd age constraints on the timing and sources of the Pan-African Cape Granite Suite, South Africa. *Journal of African Earth Sciences,* 30 (4), pp. 795 – 815.

De Beer, C. H. (1989). *Structure of the Cape Fold Belt in the Ceres syntaxis* (Doctoral dissertation, Stellenbosch: Stellenbosch University).

DeCelles, P. G., & Giles, K. A. (1996). Foreland basin systems. *Basin Research,* 8, pp. 105-123.

De Wit, M. J., Jeffery, M., Nicolaysen, L. O. N., & Bergh, H. (1988). *Explanatory notes on the Geologic Map of Gondwana*. American Association Petroleum Geology, Tulsa.

De Wit, M. J., & Ransome, I. G. D. (1992). Regional inversion tectonics along the southern margin of Gondwana. *In:* De Wit, M. J. and Ransome, I. G. D. (Eds.)*, Inversion Tectonics of the Cape Fold Belt, Karoo and Cretaceous Basins of Southern Africa*, pp. 15 – 21.

Di Celma, C. N., Brunt, R. L., Hodgson, D. M., Flint, S. S., & Kavanagh, J. P. (2011). Spatial and temporal evolution of a Permian submarine slope channel–levee system, Karoo Basin, South Africa. *Journal of Sedimentary Research*, *81*(8), pp. 579-599.

Dickenson, W.R. (1974). Plate tectonics and sedimentation. *In:* Dickenson, W.R. (Ed.), *Tectonics and Sedimentation.* Special Publication the Society of Economic Palaeontologists and Minerologists, 22, pp. 1-27.

Dickinson, W. R. (1985). Interpreting detrital modes of greywacke and arkose. *Journal of Sedimentary Petrology,* 40, pp. 695 – 707.

Dickinson, W. R., Beard, L. S., Brackenridge, G. R., Erjavec, J. L., Ferguson, R. C., Inman, K. F., Knepp, R. A., Lindberg, F. A., & Ryberg, P. T. (1983). Provenance of North American Phanerozoic sandstones in relation to tectonic setting. *Bulletin of the Geological Society of America,* 94, pp. 222 – 235.

Dickinson, W.R., & Gehrels, G.E. (2009). Use of U-Pb ages of detrital zircons to infer maximum depositional ages of strata: A test against a Colorado Plateau Mesozoic database. *Earth and Planetary Science Letters*, 288(1), pp. 115-125.

Dixon, J. F., Steel, R. J., & Olariu, C. (2012). River-dominated, shelf-edge deltas: delivery of sand across the shelf break in the absence of slope incision. *Sedimentology,* Volume 59, pp. 1133–1157.

Dunn, E. J. (1879). Reports on the coal outcrops of the Camdeboo and Nieuweveld Mountains. *Parliamentary Report. C. G. H*. G37, 31 pp.

Dunn, E. J. (1886). Reports on a supposed extensive deposit of coal underlying the central districts of the Colony. *Parliamentary Report. C. G. H.* G8, 12 pp.

Du Toit, A. L. (1937). *Our wandering continents*. Oliver and Boyd, Edinburgh, 366 pp.

Du Toit, A. L. (1954). *The geology of South Africa*. (Third edition). Oliver and Boyd, 611 pp.

Elliot, D. H., & Johnson, M. (1972). The Gondwanide orogeny: new data from South Africa and the Problem of the Falkland Island. A*bstract Programs, Geological Society of America*, 4, pp. 498-499

Elliot, D. H., & Watts, D. R. (1974). The nature and origin of volcaniclastic material in some Karoo and Beacon rocks. *Transactions of the Geological Society of South Africa*, 77, pp. 109-111

Elliot, D. H., Fanning, C. M., & Laudon, T. S. (2014). The Gondwana plate margin in the Weddell Sea sector: Zircon geochronology of upper Paleozoic (mainly Permian) strata from the Ellsworth Mountains and eastern Ellsworth Land, Antarctica. *Gondwana Research*, doi: 10 .1016/j .gr .2014 .12 .001.

Elliot, D. H., Fanning, C. M., & Hulett, S. R. W. (2015). Age provinces in the Antarctic craton: Evidence from detrital zircons in Permian strata from the Beardmore Glacier region, Antarctica. *Gondwana Research*, v. 28, p. 152–164, doi: 10 .1016 /j .gr .2014 .03 .013.

Ezcurra, M. D., & Butler, R. J. (2015). Taxonomy of the Proterosuchid Archosauriforms (Diapsida: Archosauromorpha) form the earliest Triassic of South Africa, and implications for the early Archosauriform radiation. *Palaeontology,* Volume 58, pp. 141-170.

Fielding, C.R. (2006). Upper flow regime sheets, lenses and scour fills: Extending the range of architectural elements for fluvial sediment bodies. *Sedimentary Geology*, 190(1), pp. 227-240.

Figueiredo, J. J. P., Hodgson, D. M., Flint, S. S., & Kavanagh, J. P. (2010). Depositional environments and sequence stratigraphy of an exhumed Permian mudstone-dominated submarine slope succession, Karoo Basin, South Africa. *Journal of Sedimentary Research,* Volume 80, pp. 97–118.

Fildani, A., Drinkwater, N. J., Weislogel, A., McHargue, T., Hodgson, D. M., & Flint, S. S. (2007). Age controls on the Tanqua and Laingsburg deep-water systems: new insights on the evolution and sedimentary fill of the Karoo basin, South Africa. *Journal of Sedimentary Research*, *77*(11), pp. 901-908.

Fildani, A., Weislogel, A., Drinkwater, N. J., McHargue, T., Tankard, A., Wooden, J., Hodgson, D., & Flint, S. (2009). U-Pb zircon ages from the southwestern Karoo Basin, South Africa—Implications for the Permian-Triassic boundary. *Geology*, *37*(8), pp. 719-722.

Flint, S. A., Hodgson, D. M., Sprague, A. R., Brunt, R. L., van der Merwe, W. C., Figueiredo, J., Prélat, A., Box, D., Di Celma, C., & Kavanagh, J. P. (2011). Depositional architecture and sequence stratigraphy of the Karoo basin floor to shelf edge succession, Laingsburg depocentre, South Africa. *Marine and Petroleum Geology*, *28*(3), pp. 658-674.

Frei, D., & Gerdes, A. (2009). Precise and accurate in situ U–Pb dating of zircon with high sample throughput by automated LA-SF-ICPMS. *Chemical Geology,* 261: pp. 261–270.

Frey-Martinez, J., Cartwright, J., & Hall, B. (2005) 3D seismic interpretation of slump complexes: examples from the continental margin of Israel. *Basin Research*, 17, pp. 83-108.

Geel, C., Schulz, H. M., Booth, P., & Horsfield, B. (2013). Shale gas characteristics of Permian black shales in South Africa: results from recent drilling in the Ecca Group (Eastern Cape). *Energy Procedia*, *40*, pp. 256-265.

Götz, A. E., Beukes, N. J., & De Kock, M. O. (2016). A multidisciplinary approach to decipher the complexity and potential of an unconventional gas resource: The Permian Whitehill Formation (Karoo Basin, South Africa). 3373. Abstract 35th International Geological Congress, Cape Town, South Africa. (http://www.americangeosciences.org/information/igc)

Gradstein, F., Ogg, J., & Smith, A. (2004). A geological time scale: Cambridge, Cambridge University Press, 589 pp.

Grecula, M. (2000). Stratigraphy and architecture of tectonically controlled turbidite systems: Laingsburg Formation, Karoo Basin, South Africa. *Ph.D. thesis*, University of Liverpool, United Kingdom, 291 pp.

Grecula, M., Flint, S. S., Wickens, H. D. V., & Johnson, S. D. (2003). Upward-thickening patterns and lateral continuity of Permian sand-rich turbidite channel fills, Laingsburg Karoo, South Africa. *Sedimentology,* Volume 50, pp. 831–853.

Hälbich, I. W. (1983). A tectogenesis of the Cape Fold Belt (CFB). *In:* Söhnge, A. P. G. and Hälbich, I. W. (Eds.)*, Geodynamics of the Cape Fold Belt. Special Publications of the Geological Society of South Africa,* 12, pp. 165 – 175.

Hancox, P. J., Angielczyk, K. D., & Rubidge, B. S. (2013). Angonisaurus and Shansiodon, dicynodonts (Therapsida, Anomodontia) from subzone C of the Cynognathus Assemblage Zone (Middle Triassic) of South Africa. *Journal of Vertebrate Paleontology*, 33:3, 655-676, DOI: 10.1080/02724634.2013.723551

Hellstrom, J., Paton, C., Woodhead, J., & Hergt, J. (2008). Iolite: Software for spatially resolved LA-(quad and MC) ICPMS analysis*, In:* Sylvester P. (Ed.), Laser Ablation ICP–MS in the Earth Sciences: Current Practices and Outstanding Issues*, pp.* 343–348*, Mineralogical Association of Canada short course series,* Quebec, Canada*.*

Herbert, C., & Compton, J. (2007). Depositional environments of the lower Permian Dwyka diamictite and Prince Albert shale inferred from the geochemistry of early diagenetic concretions, southwest Karoo Basin, South Africa. *Sedimentary Geology,* Volume 194, p. 263–277.

Hobday, D.K. (1973). Middle Ecca deltaic deposits in the Muden-Tugela Ferry area of Natal. *Transactions of the Geological Society of South Africa*, 76, pp. 309-318.

Hodgson, D. M., Flint, S. S., Hodgetts, D., Drinkwater, N. J., Johannessen, E. P., & Luthi, S. M. (2006). Stratigraphic evolution of fine-grained submarine fan systems, Tanqua depocenter, Karoo Basin, South Africa. *Journal of Sedimentary Research*, *76*(1), pp. 20-40.

Hodgson, D. M., Kane, I. A., Flint, S. S., Brunt, R. L., & Ortiz-Karpf, A. (2016). Time-Transgressive Confinement on the Slope and the Progradation of Basin-Floor Fans: Implications for the Sequence Stratigraphy of Deep-Water Deposits. *Journal of Sedimentary Research*, *86*(2), pp. 73-86.

Ingle, M., & Atkinson, D. (2015). Can the circle be squared? An enquiry into shale gas mining in South Africa's Karoo, *Development Southern Africa*, 32:5, pp. 539-554, DOI: 10.1080/0376835X.2015.1044076

Ireland, T. R., & Williams, I. S. (2003). Considerations in zircon geochronology by SIMS. *Reviews in Mineralogy and Geochemistry*, *53*(1), pp. 215-241.

Jackson, S., Pearson, N. J., Griffin, W. L., & Belousova, E. A. (2004). The application of laser ablation – inductively coupled plasma – mass spectrometry to in situ U–Pb zircon geochronology. *Chemical Geology,* 211: pp. 47–69.

Jobe, Z. R., Lowe, D. R., & Morris, W. R. (2012). Climbing-ripple successions in turbidite systems: depositional environments, sedimentation rates and accumulation times. *Sedimentology,* Volume 59, pp. 867–898.

Johnson, M.R., & Kingsley, C.S. (1993). Lithostratigraphy of the Ripon Formation (Ecca Group), including the Pluto's Vale, Wonderfontein and Trumpeters Members. *Lithostratigraphic series South African Committee for Stratigraphy,* 26**,** 8 pp.

Johnson, M. (1991). Sandstone petrography, provenance and plate tectonic setting in Gondwana context of the south-eastern Cape-Karoo Basin. *South African Journal of Geology,* Issue 94, pp. 137-154.

Johnson, M. R., Van Vuuren, C. J., Hegenberger, W. F., Key, R., & Show, U. (1996). Stratigraphy of the Karoo Supergroup in southern Africa: an overview. *Journal of African Earth Sciences*, *23*(1), pp. 3-15.

Johnson, M. R., Van Vuuren, C. J., Visser, J. N. J., Cole, D. I., Wickens, H. D. V., Christie, A. D. M., & Roberts, D. L. (1997). The Foreland Karoo Basin, South Africa. *Sedimentary basins of the world*, *3*, pp. 269-317.

Johnson, M. R., Van Vuuren, C. J., Visser, J. N. J., Cole, D. I., Wickens, H. de V., Christie, A. D. M., Roberts, D. L., & Brandl, G. (2006). Sedimentary Rocks of the Karoo Supergroup. In: M. Johnson, C. Anhaeusser & R. Thomas, eds. *Geology of South Africa.* Johannesburg, Pretoria: Geological Society of South Africa, Council for Geoscience, pp. 461-499.

Johnson, S. D., Flint, S., Hinds, D., & Wickens, H. de V. (2001). Anatomy, geometry and sequence stratigraphy of basin floor to slope turbidite systems, Tanqua Karoo, South Africa. *Sedimentology,* Volume 48, pp. 987-1023.

Johnston, S. T. (2000). The Cape Fold Belt and Syntaxis and the rotated Falkland Islands: dextral transpressional tectonics along the southwest margin of Gondwana. *Journal of African Earth Sciences*, *31*(1), pp. 51-63.

Kay, S. M., Ramos, V. A., Mpodozis, C., & Sruoga, P. (1989). Late Palaeozoic to Jurassic silicic magmatism at the Gondwana margin: analogy to the Middle Proterozoic in North America? *Geology,* 17, pp. 324-328

Kuenen, P. H. (1963). Turbidites in South Africa. *Transactions of the Geological Society of South Africa,* 66, 191 pp.

King, R., Van Lente, B., Potts, G., Hodgson, D. M., Andersson, P. O. D., Worden, R. H., Flint, S. S., & Wickens, H. De V. (2004). Extra-foreland source to turbidite sink in the early Karoo Basin, South Africa. *AAPG Annual Meeting 2004: Embrace the Future, Celebrate the Past Technical Program*.

Kingsley, C.S. (1977). Stratigraphy and sedimentology of the Ecca Group in the Eastern Cape Province, South Africa. Ph.D Thesis (unpubl.), University of Port Elizabeth, 286 pp.

Kingsley, C.S. (1981). A composite submarine fan-delta-fluvial model for the Ecca and lower Beaufort Groups of the Permian age in the eastern Cape Province, South Africa. *Transcript for Geological Society of South Africa,* Issue 84, pp. 27-40.

Lanci, L., Tohver, E., Wilson, A., & Flint, S. (2013). Upper Permian magnetic stratigraphy of the lower Beaufort Group, Karoo Basin. *Earth and Planetary Science Letters,* Issue 375, pp. 123–134.

Lawton, T. F., & Bradford, B. A. (2011). Correlation and provenance of Upper Cretaceous (Campanian) fluvial strata, Utah, USA, from zircon U-Pb geochronology and petrography. *Journal of Sedimentary Research*, 81(7), pp. 495–512.

Lindeque, A., de Wit, M. J., Ryberg, T., Weber, M., & Chevallier, L. (2011). Deep crustal profile across the southern Karoo Basin and Beattie Magnetic Anomaly, South Africa: an integrated interpretation with tectonic implications. *South African Journal of Geology*, *114*(3-4), pp. 265-292.

Lochner, P. A., Schreiner, G. O., & Scholes, R. J. (2016). Strategic Environmental Assessment for shale gas development in South Africa. 5479. Abstract 35th International Geological Congress, Cape Town, South Africa. (http://www.americangeosciences.org/information/igc)

Lock, B.E. (1980). Flat-plate subduction and the Cape Fold Belt of South Africa. *Geology*. 8. pp. 35-39.

López Gamundi, O. R., & Rosselo, E. A. (1998). Basin fill evolution and palaeotectonic patterns along the Samfrau geosyncline: the Sauce Grande basin-Venta, na Fold Belt (Argentina) and Karoo basin-Cape Fold Belt (South Africa) revisited. *Geologische Rundschau,* 86, pp. 819-834.

Ludwig, K. (2003). Isoplot/Ex version 3: a Geochronological toolkit for Microsoft Excel. Geochronology Center, Berkeley.

Ludwig, K.R. (2009). User's Manual for Isoplot 3.70. A Geochronological Toolkit for Microsoft Excel: Berkley Geochronology Centre Special Publication, No.4.

Maré, L., De Kock, M., Cairncross, B., & Mouri, H. (2014). Application of Magnetic Geothermometers in sedimentary basins: an example from the western Karoo Basin, South Africa. *South African journal of Geology,* Volume 117.1, pp. 1-14.

Masson, D. G., Canals, M., Alonso, B., Urgeles, R., & Huhnerbach, V. (1998). The canary debris flow; source area morphology and failure mechanisms. *Sedimentology*, 45, pp. 411-432.

Masson, D. G., Watts, A. B., Gee, M. J. R., Urgeles, R., Mitchell, N. C., Le Bas, T. P., & Canals, M. (2002). Slope failures on the banks of the western Canary Islands. *Earth-Science Reviews*, 57, 1-35.

Mattinson, J. M. (2010). Analysis of the relative decay constants of ^{235}U and ^{238}U by multi-step CA-TIMS measurements of closed-system natural zircon samples. *Chemical Geology,* 275: pp. 186–198.

McKay, M. P., Weislogel, A. L., Fildani, A., Brunt, R. L., Hodgson, D. M., & Flint, S.S. (2015). U-PB zircon tuff geochronology from the Karoo Basin, South Africa: implications of zircon recycling on stratigraphic age controls. *International Geology Review*, 57:4, pp. 393-410, DOI: 10.1080/00206814.2015.1008592.

McKay, M. P., Coble, M. A., Hessler, A. M., Weislogel, A. L., & Fildani, A. (2016). Petrogenesis and provenance of distal volcanic tuffs from the Permian–Triassic Karoo Basin, South Africa: A window into a dissected magmatic province. *Geosphere*, v. 12, no. 1, pp. 1–14, doi:10.1130/GES01215.1.

McLachlan, I. R., & Anderson, A. M. (1973). A review of the evidence for marine conditions in southern Africa during Dwyka times. *Palaeontology of Africa*, 15, pp. 37-64.

Miall, A. D. (1977). A review of the braided river depositional environment. *Earth-Science Reviews*, 13(1), pp. 1-62.

Miall, A. D. (1985). Architectural-element analysis: a new method of facies analysis applied to fluvial deposits. *Earth-Science Reviews*, *22*(4), pp. 261-308.

Miall, A. D. (2010). Architectural-element analysis: a new method of facies analysis applied to fluvial deposits. *Recognition of fluvial depositional systems and their resource potential*, *1*(1), 33 pp.

Moscardelli, L., & Wood, L.J. (2008) New classification system for mass transport complexes in offshore Trinidad. *Basin Research*, 20(1), pp. 73-98.

Mutti, E. (1977). Distinctive thin-bedded turbidite facies and related depositional environments in the Eocene Hecho Group (South-central Pyrenees, Spain). *Sedimentology*, *24*(1), pp. 107-131.

Nasdala, L., Hofmeister, W., Norberg, N., Mattinson, J. M., Corfu, F., Dörr, W., Kamo, S. L., Kennedy, A. K., Kronz, A., Reiners, P. W., Frei, D., Košler, J., Wan, Y., Götze, J., Häger, T., Kröner, A., & Valley, J. W. (2008). Zircon M257–a homogeneous natural reference material for the ion microprobe U-Pb analysis of zircon. *Geostandards and Geoanalytical Research,* 32: pp. 247–265.

Nguema-Mve, O. (2005). Petrology, geochronology and provenance of the Laingsburg and Tanqua Karoo submarine fan systems, Ecca Group, South Africa. Unpublished M. Sc. Thesis, Department of Geology, Geography and Environmental Sciences, University of Stellenbosch, 229 pp.

Nicolas, M., & Rubidge, B. S. (2010). Changes in Permo-Triassic terrestrial tetrapod ecological representation in the Beaufort Group (Karoo Supergroup) of South Africa. *Lethaia,* Volume 43, pp. 45-59.

Oliveira, C. M., Hodgson, D. M., & Flint, S. S. (2011). Distribution of soft-sediment deformation structures in clinoform successions of the Permian Ecca Group, Karoo Basin, South Africa. *Sedimentary Geology,* Volume 235, pp. 314–330.

Oliveira, C. M. M., Hodgson, D. M., & Flint, S. S. (2009). Aseismic controls on in situ soft-sediment deformation processes and products in submarine slope deposits of the Karoo Basin, South Africa. *Sedimentology,* Volume 56, pp. 1201–1225.

Pankhurst, R. J., Rapela, C. W., Fanning, C. M., & Márquez, M. (2006). Gondwanide continental collision and the origin of Patagonia. *Earth-Science Reviews*, *76*(3), pp. 235-257.

Pace, D. W., Gastaldo, R. A., & Neveling, J. (2009). Early Triassic aggradational and degradational landscapes of the Karoo Basin and evidence for climate oscillations following the P–TR event. *Journal of Sedimentary Research,* Volume 79, p. 316–331.

Paton, C., Woodhead, J. D., Hellstrom, J. C., Hergt, J. M., Greig, A., & Maas, R. (2010). Improved laser ablation U-Pb zircon geochronology through robust downhole fractionation correction, *Geochemistry, Geophysics, Geosystems*, 11 , Q0AA06, doi:10.1029/2009GC002618.

Posamentier, H. W., & Kolla, V. (2003). Seismic geomorphology and stratigraphy of depositional elements in deep-water settings. *Journal of Sedimentary Research*, 73, pp. 367-388.

Posamentier, H. W., & Walker, R. G. (2006). Deep-water turbidites and submarine fans. *In:* Posamentier, H.W. and Walker, R.G. (Eds.), Facies Models Revisited. *SEPM Special Publication*. (CD) 84, pp. 399–520.

Prélat, A., Hodgson, D. M., & Flint, S. S. (2009). Evolution, architecture and hierarchy of distributary deep-water deposits: a high-resolution outcrop investigation from the Permian Karoo Basin, South Africa. *Sedimentology,* Issue 56, pp. 2132–2154.

Pupin, J. P. (1980). Zircon and Granite Petrology. *Contributions to Mineralogy and Petrology*, 73, pp. 207-220.

Pysklywec, R. N., & Mitrovica, J. X. (1999). The Role of Subduction-Induced Subsidence in the Evolution of the Karoo Basin. *The Journal of Geology,* Volume 107, pp. 155–164.

Reading, H. G. (1996). Sedimentary Environments, Processes, Facies, and Stratigraphy. *Third Edition, Blackwell Publishing*, 688 pp.

Riley, T. R., Flowerdew, M. J., & Whitehouse, M. J. (2012). U-Pb ion-microprobe zircon geochronology from the basement inliers of eastern Graham Land, Antarctic Peninsula. *Journal of the Geological Society* [London], v. 169, pp. 381–393, doi: 10 .1144 /0016 -76492011 -142.

Roberts, E. M. (2007). Facies architecture and depositional environments of the Upper Cretaceous Kaiparowits Formation, southern Utah. *Sedimentary Geology*, 197(3), pp. 207-233.

Roberts, L. D. (1988). Controls on peat accumulation in the Permian Vryheid Formation in a part of northern Natal, South Africa. *International Journal of Coal Geology,* Volume 9, pp. 315-341.

Robinson, A. C., Ducea, M., & Lapen, T. J. (2012). Detrital zircon and isotopic constraints on the crustal architecture and tectonic evolution of the northern Pamir. *Tectonics,* 31, TC2016.

Rocha-Campos, A. C., Basei, M. A. S., Nutman, A. P., Kleiman, L. E., Varela, R., Llambías, E., Canile, F. M., & Da Rosa, O. D. C. (2011). 30 million years of Permian volcanism recorded in the Choiyoi igneous province (W Argentina) and their source for younger ash fall deposits in the Paraná Basin: SHRIMP U-Pb zircon geochronology evidence. *Gondwana Research*, v. 19, pp. 509–523, doi: 10 .1016 /j .gr .2010 .07 .003.

Rogers, A. W. (1910). Geological survey of parts of the Divisions of Beaufort West, Fraserburg, Victoria West, Sutherland and Laingsburg. *Annual Report of the Geological Commission of the Cape of Good Hope.* 15, pp. 9 – 66.

Rogers, A. W., & Du Toit, A. L. (1903). Geological surveys of parts of the Divisions of Ceres, Sutherland and Calvinia. *Annual Report of the Geological Commission of the Cape of Good Hope*, pp. 25 – 32.

Rogers, A. W., & Schwarz, E. H. L. (1902). Report on a survey of parts of the Beaufort West, Prince Albert, and Sutherland Divisions. *Annual Report of the Geological Commission of the Cape of Good Hope*, pp. 100 – 106.

Rossouw, P. J., Meyer, E. I., Mulder, M. P., & Stocken, C. G. (1964). Die geologie van die Swartberge, die Kangovallei en die omgewing van Prins Albert. K. P. Explan. Sheets 3321B (Gamkapoort) and 3322A (Prince Albert). *Geological Survey of South Africa*, 93 pp.

Rozendaal, A., Gresse, P. G., Scheepers, R., & Le Roux, J. P. (1999). Neoproterozoic to early Cambrian crustal evolution of the Pan-African Saldania Belt, South Africa. *Precambrian Research,* 97, pp. 303-323.

Rubidge, R. N. (1858). Notes on the geology of some parts of South Africa. *Quarterly Journal of the Geological Society (*London) 12, pp. 237–238.

Rubidge, B.S. (Ed.) (1995). Biostratigraphy of the Beaufort Group (Karoo Super Group). *Council for Geoscience*, Pretoria, pp. 1 –45.

Rubidge, B.S. (2013). The roots of early mammals lie in the Karoo: Robert Broom's foundation and subsequent research progress, *Transactions of the Royal Society of South Africa*, 68:1, pp. 41-52, DOI: 10.1080/0035919X.2012.737868

Rubidge, B., Hancox, P., & Catuneanu, O. (2000). Sequence analysis of the Ecca-Beaufort contact in the southern Karoo of South Africa. *South African Journal of Geology,* Volume 103(1), pp. 81-96.

Rubidge, B. S., Hancox, P. J., & Mason, R. (2012). Waterford Formation in the south-eastern Karoo: Implications for basin development. *South African Journal of Science*, 108(3/4), Art. #829, 5 pages. http:// dx.doi.org/10.4102/sajs. v108i3/4.829

Rubidge, B. S., Erwin, D. H., Ramezani, J., Bowring, S. A., & de Klerk, W. J. (2013). High-precision temporal calibration of Late Permian vertebrate biostratigraphy: U-Pb zircon constraints from the Karoo Supergroup, South Africa. *Geology*, *41*(3), pp. 363-366.

Ryan, P. J. (1967). Stratigraphic and Palaeocurrent Analysis of the Ecca Series and Lowermost Beaufort Beds in the Karoo Basin of South Africa: Ph.D. thesis, Univ. of the Witwatersrand, Johannesburg (unpubl.).

Scheepers, R., & Armstrong, R. (2002). New U-Pb SHRIMP zircon ages of the Cape Granite Suite: implications for the magmatic evolution of the Saldania Belt. *South African Journal of Geology,* 105, pp. 241 – 256.

Scheiber-Enslin, S., Webb, S., & Ebbing, J. (2014). Geophysically plumbing the Main Karoo Basin, South Africa. *South African Journal of Geology,* Volume 117.2, pp. 275-300.

Schieber, J. (2016). Experimental testing of the transport-durability of shale lithics and its implications for interpreting the rock record. *Sedimentary Geology*, *331*, pp. 162-169.

Schoene, B. (2014). 4.10-U–Th–Pb Geochronology. *Treatise on geochemistry*, pp. 341-378.

Schwarz, E. H. L. (1897). Geological survey of the Beaufort West District. *Annual report of the Geological Commission of the Cape of Good Hope. for 1896* G81, 12 pp.

Scott, E. D. (1997). Tectonics and sedimentation: the evolution, tectonic influences and correlation of the Tanqua and Laingsburg subbasins, southwest Karoo Basin, South Africa. *Ph.D. thesis (unpublished)*. Louisiana State University, USA.

Shanmugam, G., & Walker, K. R. (1978). Tectonic significance of distal turbidites in the Middle Ordovician Blockhouse and lower Sevier Formations in east Tennessee. *American Journal of Science*, *278*(4), pp. 551-578.

Shen, S. Z., Crowley, J. L., Wang, Y., Bowring, S. A., Erwin, D. H., Sadler, P. M., Cao, C. Q., Rothman, D. H., Henderson, C. M., Ramezani, J., & Zhang, H. (2011). Calibrating the end-Permian mass extinction. *Science*, *334*(6061), pp. 1367-1372.

Sixsmith, P. J. (2000). Stratigraphic development of a Permian turbidite system on a deforming basin floor: turbidite systems: Laingsburg Formation, Karoo Basin, South Africa. *Ph.D. thesis*, University of Liverpool, United Kingdom, 229 pp.

Sixsmith, P., Flint, S., Wickens, H., & Johnson, S. (2004). Anatomy and stratigraphic development of a basin floor turbidite system in the Laingsburg Formation, Main Karoo Basin, South Africa. *Journal of Sedimentary Research,* Volume 74(2), pp. 239–254.

Sláma, J., Košler, J., Condon, D. J., Crowley, J. L., Gerdes, A., Hanchar, J. M., Horstwood, M. S. A., Morris, G. A., Nasdala, L., Norberg, N., Schaltegger, U., Schoene, B., Tubrett, M. N., & Whitehouse, M. J. (2008). Plešovice zircon—a new natural reference material for U–Pb and Hf isotopic microanalysis. *Chemical Geology,* 249: pp. 1–35.

Smith, R. M. H. (1990). A review of stratigraphy and sedimentary environments of the Karoo Basin of South Africa. *Journal of African Earth Sciences,* Volume 10, pp. 117-137.

Spychala, Y., Hodgson, D., Flint, S., & Mountney, N. (2015). Constraining the sedimentology and stratigraphy of submarine intraslope lobe deposits using exhumed examples from the Karoo Basin, South Africa. *Sedimentary Geology,* Volume 322, pp. 67–81.

Stacey, J. S., & Kramers, J. D. (1975). Approximation of Terrestrial Lead Isotope Evolution by a 2-Stage Model. *Earth and Planetary Science Letters 26(2): pp. 207-221.*

Stollhofen, H., Gerschutz, S., Stanistreet, I. G., & Lorenz, V. (1998). Tectonic and volcanic controls on Early Jurassic rift-valley lake deposition during emplacement of Karoo flood basalts, southern Namibia. *Palaeogeography, Palaeoclimatology, Palaeoecology,* Volume 140, pp. 185-215.

Stow, D. A., Readings, H. G., & Collinson, J. D. (1996). Deep seas. *In:* Readings, H.G. (Ed.), *Sedimentary Environments: Processes, Facies and Stratigraphy* (3rd ed., pp. 395-453). Oxford: Blackwell Publishing.

Tankard, A., Welsink, H., Aukes, P., Newton, R., & Stettler, E. (2009). Tectonic evolution of the Cape and Karoo basins of South Africa. *Marine and Petroleum Geology*, *26*(8), pp. 1379-1412.

Terlaky, V., & Arnott, R. W. C. (2014). Matrix-rich and associated matrix-poor sandstones: avulsion splays in slope and basin-floor strata. *Sedimentology*, *61*(5), pp. 1175-1197.

Thamm, A. G., & Johnson, M. R. (2006). The cape supergroup. *The Geology of South Africa, Johannesburg/Council of Geoscience, Pretoria*, pp. 443-457.

Theron, A. C. (1967). The sedimentology of the Koup Subgroup near Laingsburg*. M.Sc. thesis (unpublished)*. University of Stellenbosch, South Africa, 22 pp.

Tucker, R. T. (2014). Stratigraphy, Sedimentation and Age of the Upper Cretaceous Winton Formation, central-western Queensland, Australia: Implications for regional palaeogeography, palaeoenvironments and Gondwanan palaeontology. Ph.D Thesis (Unpubl), James Cook University, Australia, 209 pp.

Tucker, R. T., Roberts, E. M., Hu, Y., Kemp, A. I., & Salisbury, S. W. (2013). Detrital zircon age constraints for the Winton Formation, Queensland: Contextualizing Australia's Late Cretaceous dinosaur faunas. *Gondwana Research, 24*(2), pp. 767-779.

Turner, B. R. (1983). Braidplain deposition of the Upper Triassic Molteno Formation in the main Karoo (Gondwana) Basin, South Africa. *Sedimentology*, *30*(1), pp. 77-89.

Turner, B. R. (1985). Uranium mineralization in the Karoo basin, South Africa. *Economic Geology*, *80*(2), pp. 256-269.

Vail, P. R., Mitchum Jr, R. M., & Thompson III, S. (1977). Seismic stratigraphy and global changes of sea level: Part 3. Relative changes of sea level from Coastal Onlap: section 2. Application of seismic reflection Configuration to Stratigrapic Interpretation.

Van der Merwe, W. C., Flint, S. S., & Hodgson, D. M. (2010). Sequence stratigraphy of an argillaceous, deepwater basin-plain succession: Vischkuil Formation (Permian), Karoo Basin, South Africa. *Marine and Petroleum Geology,* Volume 27, pp. 321–333.

Van der Merwe, W. C., Hodgson, D. M., & Flint, S. S. (2009). Widespread syn-sedimentary deformation on a muddy deep-water basin-floor: theVischkuil Formation (Permian),Karoo Basin,South Africa. *Basin Research,* Volume 21, pp. 389–406.

Van der Merwe, W. C., Hodgson, D. M., & Flint, S. S. (2011). Origin and terminal architecture of a submarine slide: a case study from the Permian Vischkuil Formation, Karoo Basin, South Africa. *Sedimentology,* Volume 58, pp. 2012–2038.

Van Lente, B. (2004). Chemostratigraphic trends and Provenance of the Permian Tanqua and Laingsburg depocentres, southwestern Karoo Basin, South Africa. PhD thesis (unpubl), University of Stellenbosch, 339 pp.

Van Rooyen, D. (2010). Uranium in Beaufort West: implications for the local economy. *Journal for New Generation Sciences*, *8*(1), pp. 321-334.

Varela, R., Basei, M. A. S., Sato, A., Siga, O. Jr., Cingolani, & Sato, K. (1998). Edades isoto´picas Rb/Sr y U/Pb en rocas de Mina Gonzalito y Arroyo Salado, macizo norpatagonico atlantico, Rı´o Negro, Argentina. X Congreso Latinoamericano de Geologı´a Actas, pp. 71–76.

Vaughan, A. P., Leat, P. T., Dean, A. A., & Millar, I. L. (2012). Crustal thickening along the West Antarctic Gondwana margin during mid-Cretaceous deformation of the Triassic intra-oceanic Dyer Arc. *Lithos*, 142, pp. 130-147.

Veevers, J. J., Powell, C., Collinson, J. W., & López-Gamundi, O. R. (1994). Synthesis. *In J.J. Veevers and C. Powell (eds.), Permian-Triassic Pangean Basins and Foldbelts along the Panthalassan Margin of Gondwanaland. Geological Society of America Memoir,* 184, pp. 223 – 279.

Viljoen, J. H. A., & Wickens, H. de V. (1992). Lithostratigraphy of the Vischkuil Formation (Ecca Group). *Lithostratigraphic series South African Committee for Stratigraphy,* 19**,** 7 pp.

Viljoen, J. H. A. (1992a). Lithostratigraphy of the Collingham Formation (Ecca Group), including the Zoute Kloof, Buffels River and Wilgehout River Members and the Matjiesfontein Chert Bed. *Lithostratigraphic series South African Committee for Stratigraphy,* 22**,** 10 pp.

Viljoen, J. H. A. (1992b). Lithostratigraphy of the Laingsburg Formation (Ecca Group). *Lithostratigraphic series South African Committee for Stratigraphy,* 20**,** 7 pp.

Viljoen, J. H. A. (1994). Sedimentology of the Collingham Formation, Karoo Supergroup, South Africa. *Journal of Geology*, 97, pp. 167–183.

Visser, J. N. J. (1979). Changes in sediment transport direction in the Cape-Karoo Basin (Silurian-Triassic) in South Africa. *South African Journal of Science*, 75, pp. 72-75.

Visser, J. N. J. (1983). Glacial-marine sedimentation in the Late Paleozoic Karoo Basin, southern Africa. *In*: Molnia, B.F. (Ed.), *Glacial-marine Sedimentation.* Plenum Publishing Corporation, New York, pp. 667-701.

Visser, J. N. J. (1985). Discussion on "Tectonostratigraphy as applied to analysis of South African Phanerozoic basins", by H. de la R. Winter. *Transactions of the Geological Society of South Africa,* 88, pp. 183 – 185.

Visser, J. N. J. (1986). Lateral lithofacies relationships in the glacigene Dwyka Formation in the western and central parts of the Karoo Basin. *Transactions of the Geological Society of South Africa,* 89, pp. 373 – 383.

Visser, J. N. J. (1989). The Permo-Carboniferous Dwyka Formation of Southern Africa: deposition by a predominantly subpolar marine ice-sheet. *Palaeogeography, Palaeoclimatology, Palaeoecology,* 70, pp. 377 – 391.

Visser, J. N. J. (1990). The age of the late Palaeozoic glacigene deposits in southern Africa. *South African Journal of Geology,* Issue 93, pp. 366-375.

Visser, J. N. J. (1991). Self-destructive collapse of the Permo-Carboniferous marine ice sheet in the Karoo Basin: evidence from the southern Karoo. *South African Journal of Geology,* 94, pp. 255 – 262.

Visser, J. N. J. (1992). Basin tectonics in southwestern Gondwana during the Carboniferous and Permian. *In:* De Wit, M. J. and Ransome, I. G. D. (Eds.)*, Inversion Tectonics of the Cape Fold Belt, Karoo and Cretaceous Basins of Southern Africa*, pp. 109 – 115.

Visser, J. N. J. (1993). Sea-level changes in a back-arc-foreland transition: the late Carboniferous-Permian Karoo Basin of South Africa. *Sedimentary Geology,* Volume 83, pp. 115-131.

Wait, R., & Rossouw, R. (2014). A comparative assessment of the economic benefits from shale gas extraction in the Karoo, South Africa. *Southern African Business Review,* Volume 18, pp. 1-34.

Warren, C. H. (2013). Shale gas in South Africa, *African Security Review*, 22:1, pp. 67-73, DOI: 10.1080/10246029.2013.766443

Weislogel, A., Brunt, R. L., Flint, S., Fildani, A., & Rothfuss, J. (2011). Constraints on deepwater sedimentation in the Karoo Basin, South Africa, from U-Pb Geochronology of the ash interbeds: *AAPG Search and Discover*, Article #90124.

Wickens, H. de V. (1994). Basin floor fan building turbidites of the southwestern Karoo Basin, Ecca Group, South Africa. Unpublished PhD thesis, University of Port Elizabeth, South Africa, 233 pp.

Wickens, H. de V., & Bouma, A. H. (1991). The Tanqua submarine fan complex, Permian Ecca Group, South Africa. *American Association of Petroleum Geologists Bulletin*, Vol. 75, 522 pp.

Winter, H. de la R. (1984). Tectonostratigraphy as applied to analysis of South African Phanerozoic basins. *Transactions of the Geological Society of South Africa* 87, pp. 169 – 179.